UNIVERSITY OF CALIFORNIA SAN DIEGO

Taming and Harnessing the Reactivity of Elusive Main-Group Species

A Dissertation submitted in partial satisfaction of the requirements for the degree of Doctor of Philosophy

in

Chemistry

by

Joseph S Yoon

Committee in charge:

Professor Guy Bertrand, Chair
Professor Daniel Donoghue
Professor Clifford Kubiak
Professor Erik Romero
Professor Palmer Taylor

2024

The Dissertation of Joseph S Yoon is approved, and it is acceptable in quality and form for publication on microfilm and electronically.

University of California San Diego

2024

DEDICATION

Soli Deo Gloria

EPIGRAPH

"If I have a thousand ideas a year, and only one turns out to be good, I am satisfied."

Alfred Nobel

"Fortune favors the prepared mind."

Louis Pasteur

TABLE OF CONTENTS

LIST OF FIGURES

LIST OF ABBREVIATIONS

Å:	Angstrom
ACN:	Acetonitrile
Ad:	Adamantyl
ADAC:	Acyclic diaminocarbene
*a*NHC:	*Abnormal* N-heterocyclic carbene
Ar:	Aromatic ring
BAC:	Bis-aminocyclopropenylidene
BiCAAC:	Bicyclic (alkyl)(amino)carbene
*bz*NHC:	*Benz*imidazol-2-ylidenes
CAAC:	Cyclic (alkyl)(amino)carbene
CAArC:	Cyclic (amino)(aryl)carbene
Cat:	Catalyst
CBA:	Cyclic bent allenes
Cy:	Cyclohexyl
DAC:	*N*,*N*'-diamidocarbene
DCM:	Dichloromethane
DFT:	Density functional theory
DG:	Directing group
Dipp:	2,6-diisopropylphenyl
DME	Dimethoxyethane
DMSO:	Dimethyl sulfoxide
ΔE_{ST}:	Singlet-triplet gap energy
EA	Ethyl acetate
Et:	Ethyl

eV:	Electronvolt
GC-MS:	Gas chromatography mass spectrometry
HBD	Hydrogen bond donor
HEP:	Huynh electronic parameter
HOMO:	Highest occupied molecular orbital
HPLC:	High performance liquid chromatography
HR-MS:	High resolution mass spectrometry
iPr:	*iso*Propyl
IR:	Infrared
KHMDS:	Potassium bis(trimethylsilyl)amide
LDA:	Lithium diisopropylamide
LUMO:	Lowest unoccupied molecular orbital
Me:	Methyl
Mes:	Mesityl
MIC:	Mesoionic carbene
MPAPy	*mono*-acetyl-protected aminoalkylpyridine
N-CBA:	Pyrrolidinyl cyclic bent allenes
NBS	*N*-bromosuccinimide
NHC:	N-heterocyclic carbene
NMR:	Nuclear Magnetic Resonance
Ph:	Phenyl
PIDA	phenyliodine(III) diacetate
ppm:	Parts per million
r.t.:	Room temperature
*t*Bu:	*tert*Butyl

TEP:	Tolman electronic parameter
THF:	Tetrahydrofuran
THT:	Tetrahydrothiophene
TLC:	Thin-layer chromatography
Tol:	Toluene
%Vbur:	Percent buried volume
Xyl:	Xylyl

ACKNOWLEDGEMENTS

Thank you to Prof. Guy Bertrand for exemplifying someone who takes great pride in his work. I appreciate that you say what you mean, and mean what you say. From watching you, I have learned that to excel, I must be my own toughest critic.

Thank you to my committee members Profs. Erik Romero, Clifford Kubiak, Daniel Donoghue, and Palmer Taylor for reading and reviewing this dissertation and for your availability and advice.

Thank you to Rodolphe Jazzar for your helpfulness in chemistry and assistance on my corresponding author paper. It was a pleasure to work and share a desk space with you. I also thank the CNRS staff Dr. Michele Soleilhavoup and Dr. Mohand Melaimi for your chemistry insights. Thanks also to Prof. Jin-Quan Yu for our collaboration on the palladium catalysis project.

Thank you to Dr. François Vermersch – my lab mate, house mate, and best man. You made the first two years of my PhD journey much more enjoyable. Thanks also to Dr. Jan Lorkowski for always having lunch with me. I greatly enjoyed our conversations.

Thank you to all my lab mates from past to present: Dr. Glen Junor, Prof. Jesse Peltier, Dr. Sima Yazdani, Dr. Adam Vianna, Dr. Victor Wang, Dr. Melinda Serrato, Dr. Florian Mulks, Dr. Sonia Bajo, Dr. Sima Yazdani, Dr. Armand Taussat, Dr. Vojtech Docekal, Dr. Jakub Talcib, Dr. Ying Kai Loh, Dr. Marco Passia, Andre Faria-Vieira, Alexis Day, Patrick Yorkgitis, Levan Gojiashvili, and Dr. Mehdi Abdellaoui.

Special thanks to Dr. Anthony Mrse, Dr. Milan Gembicky, and Dr. Su for your expert assistance on NMR spectroscopy, X-ray crystallography, and mass spectrometry, respectively.

I would like to also thank the people who have helped me grow outside of a laboratory context. Thank you, Brian Morehead, my pastor and friend. You have supported me during my

darkest seasons. Thank you, Yann Schrodi, my first chemistry advisor. You were the first to encourage me to pursue a PhD and helped lift me out of addiction while I was under your advisement. Thank you, Travis Wilson, for being a true spiritual brother. Thank you, forever church family, through whom I will always have a home.

Thank you to my mother who raised three challenging kids. I think we can agree that I was the wildest. While I'm sure you are proud of me for growing into the man that I am, I'm even more proud of you for being the wonderful mom that you are.

And most of all, thank you to Bethany, my lovely wife. Lord only knows how a guy like me ended up with the mostest wonderfulest woman in all the worlds. You have encouraged and prayed for me through difficult and uncertain periods. Your excellent cooking skills ensured that I had fuel to keep on going. I thank God for placing you in my life.

Chapter 3 is adapted, in part, from A Carbene-Stabilized Diphosphorus: A Triple-Bonded Diphosphorus (P≡P) and a Bis(phosphinidene) (P-P) Transfer Agent. Yoon, Joseph, Abdellaoui, Mehdi; Gembicky, Milan; Bertrand, Guy. This paper is currently submitted to a journal for review. The dissertation author will be the first author of this paper.

Chapter 4 is an adaptation from Enhancing Substrate-Metal Catalyst Affinity via Hydrogen Bonding: Pd(II)-Catalyzed β-C(sp3)−H Halogenation of Free Carboxylic Acids. Hu, Liang; Meng, Guangrong; Chen, Xiangyang; Yoon, Joseph; Shan, Jing-Ran; Chekshin, Nikita; Strassfeld, Daniel; Sheng, Tao; Zhuang, Zhe; Jazzar, Rodolphe; Bertrand, Guy; Houk, Kenneth; Yu, Jin-Quan, Journal of the American Chemical Society, 2023. The dissertation author was the fourth author on this paper.

VITA

EDUCATION

Doctoral Degree: Organic Chemistry **2020-2024**
University of California, San Diego

Master of Science: Chemistry and Biochemistry **2017-2020**
California State University, Northridge

Bachelor's degree: Chemistry, *magna cum laude* **2012-2016**
California State University, Northridge

PUBLICATIONS and PATENTS

- **Yoon, J.S.**; Abdellaoui, M.; Gembicky, M.; Bertrand, G.* A Carbene-Stabilized Diphosphorus: A Triple-Bonded Diphosphorus (P≡P) and Bis-Phosphinidene (P-P) Transfer Agent. *Submitted for review.*

- Hu, L.; Meng, G.; Chen, X.; **Yoon, J.S.**; Jazzar, R.*; Bertrand, G.*; Yu, J.*; et al. Enhancing Substrate–Metal Catalyst Affinity via Hydrogen Bonding: Pd(II)-Catalyzed β-C(sp3)–H Bromination of Free Carboxylic Acids. *Journal of the American Chemical Society* 2023, *145(30)*, 16297-16304.

    - Featured in *OPR&D* (*Org. Process Res. Dev*. 2023, 27, 9, 1535–1545.)

- **Yoon, J.S.***; Cena, N.; Markarian, C., Schrodi, Y. Olefin Metathesis Catalysts Bearing Hemilabile NHC Ligands: Effect of Remote Torsional Strain on Activity. *Journal of Catalysis* 2023, *421*, 376-383.

- **Yoon, J.S.**; Cena, N.; Schrodi, Y.* Robust Olefin Metathesis Catalyst Bearing a Tridentate Hemilabile NHC Ligand. *Organometallics* 2020, *39(5)*, 631-635.

- "Longer-Lived Ruthenium Olefin Metathesis Catalysts Supported by Hemi-Labile Carbene Ligands" – US Patent No. 20210138444

    - Co-authors: Schrodi, Y.; **Yoon, J.S.**; and Cena, N.

ORAL PRESENTATIONS

- "Tale of two olefin metathesis catalysts: Effect of ligand lability on catalyst performance" *American Chemical Society National Meeting (ACS)* **March 20, 2022**
- "Undergraduate Research Experience for Pre-medical Students" *Health and Medical Professions Preparation Program's Medical Education for Diverse Students Conference (MEDS)* **April 16, 2022**

TEACHING EXPERIENCE

California State University Northridge **2017-2020**
Teaching Associate

- Prepared weekly lectures and demonstrations pertaining to laboratory experiments. Independently created and evaluated exams and laboratory reports.
- Classes taught: Average overall rating: 4.74/5.00 (169 responses)
  - CHEM 101L. General Chemistry I Lab
  - CHEM 102L. General Chemistry II Lab
  - CHEM 104L. Introductory Chemistry II Lab
  - CHEM 235L. Organic Chemistry Lab for Nutritionists
  - CHEM 334L. Organic Chemistry II Lab
  - CHEM 401L. Upper Division Inorganic Chemistry Lab

University of California San Diego **2020-2024**
Head Teaching Assistant

- Contributed to the development of new coursework aimed at tailoring organic chemistry for biology and healthcare majors.
- Instructed weekly classes for chemistry lecture courses fostering a learning environment that encourages critical thinking and complex problem-solving. Arranged class-wide monthly review sessions for 250-300 students.
- Classes taught: Average overall rating: 4.83/5.00 (332 responses)
  - CHEM 6A. General Chemistry I
  - CHEM 40A. Organic Chemistry I
  - CHEM 40A*. Organic Chemistry I *with a Biological Emphasis
  - CHEM 40B. Organic Chemistry II
  - CHEM 40B*. Organic Chemistry II *with a Biological Emphasis
  - CHEM 41B. Organic Chemistry II for Chemistry Majors
  - CHEM 143B. Organic Chemistry Lab

AWARDS AND HONORS

- Deans' Honor List (CSUN) **2016**
- Outstanding TA Award (CSUN) **2019**

- Nyquist Award for Organic Synthesis (CSUN) **2020**
- Teaching Excellence Award for Organic Chemistry (UCSD) **2021**

ABSTRACT OF THE DISSERTATION

Taming and Harnessing the Reactivity of Elusive Main-Group Species

by

Joseph S Yoon

Doctor of Philosophy in Chemistry

University of California San Diego, 2024

Professor Guy Bertrand, Chair

The investigation of elusive species is of great interest to chemists – particularly those comprising groups III-V in the periodic table. What gives these compounds their transient nature is their ferocious reactivity – either within themselves or with other molecules. The work herein focuses on a range of attempts to isolate unstable subvalent species. A library of novel secondary amine scaffolds is employed as electronic and steric stabilizers to pursue this goal. Furthermore, it is demonstrated that the elusive diphosphorus molecule can be stabilized by two small

monosubstituted (amino)carbene ligands – resulting in a species that can act as a diphosphorus surrogate, both as a triple-bonded diphosphorus source, in addition to a bis-phosphinidene. This species also shows promise as a P^- transfer agent. Lastly, transient catalytic intermediates in the palladium-catalyzed C-H activation of free carboxylic acids are characterized, giving insights into the rationale responsible for the enhanced reactivity.

Chapter 1 General Introduction – Singlet Carbenes and Other Elusive Species

1.1 Defying the Octet Rule

One of the fundamental themes taught to students in introductory chemistry courses is the "octet rule." This rule states that atoms tend to bond in such a way that they each have eight electrons in their valence shell, achieving a noble gas configuration. The origins of the octet rule date back to the work of Mendeleev at the end of the 19th century, with further development by Lewis[1] and Langmuir[2] in the beginning of the 20th century. This concept has significantly influenced our understanding of chemical bonding and molecular structure.

Despite the significance of this fundamental chemical principle, modern discoveries have revealed exceptions and limitations to the octet rule. In the year 1900, Moses Gomberg isolated a stable carbon-centered organic radical[3] – a species containing a carbon atom with only 7 valence electrons (Figure 1.1). The stability of this radical stems from its delocalization across the three adjacent aromatic rings. In 1988, Guy Bertrand reported the first isolable singlet carbene – a neutral carbon atom with only six valence electrons.[4] Three years later, Arduengo reported the first crystalline carbene[5] – namely, the N-heterocyclic carbene (NHC). Since these seminal discoveries, carbenes have evolved into a field of their own, making up a diverse and impactful ligand class[6, 7], even acting as organocatalysts themselves.[8,9,10]

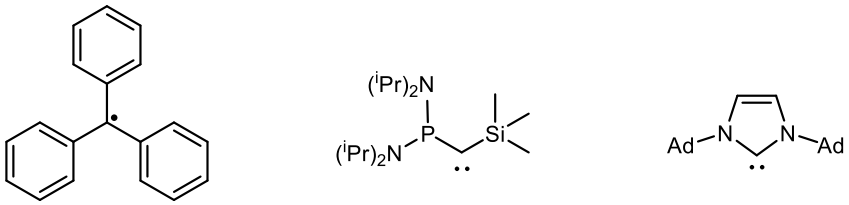

Figure 1.1 – Frontier orbital electronic configurations of triplet and singlet carbenes.

1.1.1 Description of Singlet Carbenes

A carbene is a neutral molecule characterized by a divalent carbon atom with merely six electrons in its valence shell. This carbon atom, bonded to two substituents, contains two non-bonding electrons which can exist in either a singlet (S = 1) or triplet (S = 3) state. The spin multiplicity of the ground state is governed by the orbitals of the carbene center, influenced by the geometry and nature of the substituents. Carbenes can adopt both linear and bent configurations. In the linear arrangement, the central carbon exhibits sp-hybridization, producing two degenerate non-bonding p_x and p_y orbitals (Figure 1.2 – left). These non-bonding electrons, with parallel spins, result in a triplet electronic state. When the angle decreases, the carbon assumes a bent geometry with sp^2-hybridization.

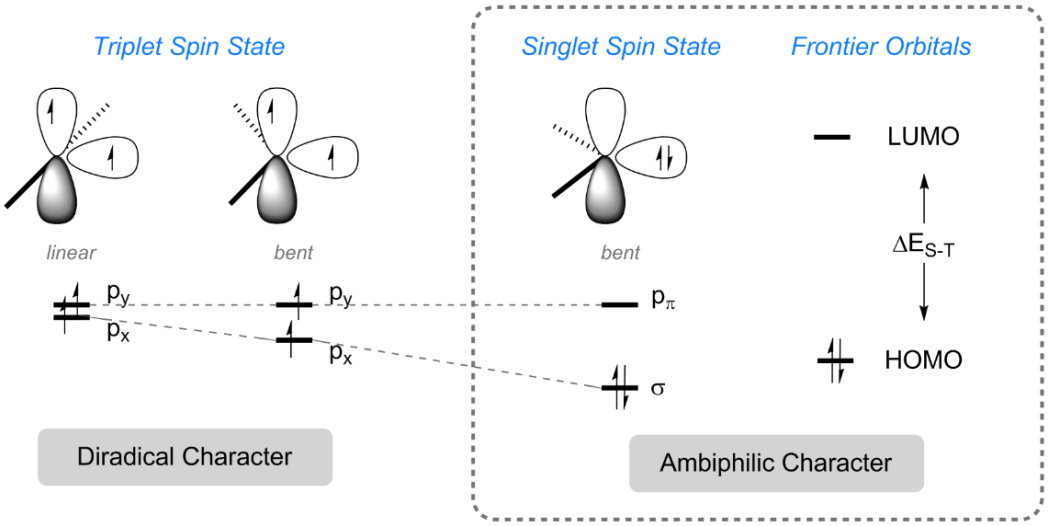

Figure 1.2 – Frontier orbital electronic configurations of triplet and singlet carbenes.

The degenerate orbital (p_x or p_y) perpendicular to the plane defined by the carbene and its substituents remains energetically unchanged. However, the other degenerate orbital gains more s-character, resulting in greater stability and lower energy (Figure 1.2 – right). This modification disrupts the degeneracy, forming two distinct orbitals termed σ and p_π. Typically, these orbitals act as the frontier orbitals of the carbene, representing the highest occupied molecular orbital (HOMO) and the lowest unoccupied molecular orbital (LUMO). The two non-bonding electrons populate the LUMO, resulting in a singlet electronic state. The energy difference between the singlet and triplet states, known as the singlet-triplet gap ($\Delta E_{S\text{-}T}$), gives crucial information about the stability and reactivity of each carbene. Empirical data suggest that carbenes with a $\Delta E_{S\text{-}T}$ exceeding 20 kcal/mol are generally isolable at room temperature.[11] The ground-state spin multiplicity is crucial as it is the largest determining factor of its behavior in chemical transformations. Triplet carbenes predominantly act as diradicals, whereas singlet carbenes, possessing one filled and one vacant orbital, exhibit ambiphilic behavior – akin to that of transition

metals. For the remainder of this manuscript, unless specified otherwise, any discussion on carbenes will be in reference to singlet carbenes.

1.1.2 Stabilization of Carbenes

The successful preparation of stable carbenes hinges on two fundamental principles: kinetic stabilization and thermodynamic stabilization (Figure 1.3). To kinetically stabilize a carbene and thereby hinder its dimerization, the most effective strategy is to enhance the steric bulk of the substituents, particularly around the carbene center. This must be combined with an analysis of the mesomeric and inductive effects of neighboring atoms, which contribute to the electronic stabilization of the frontier orbitals.

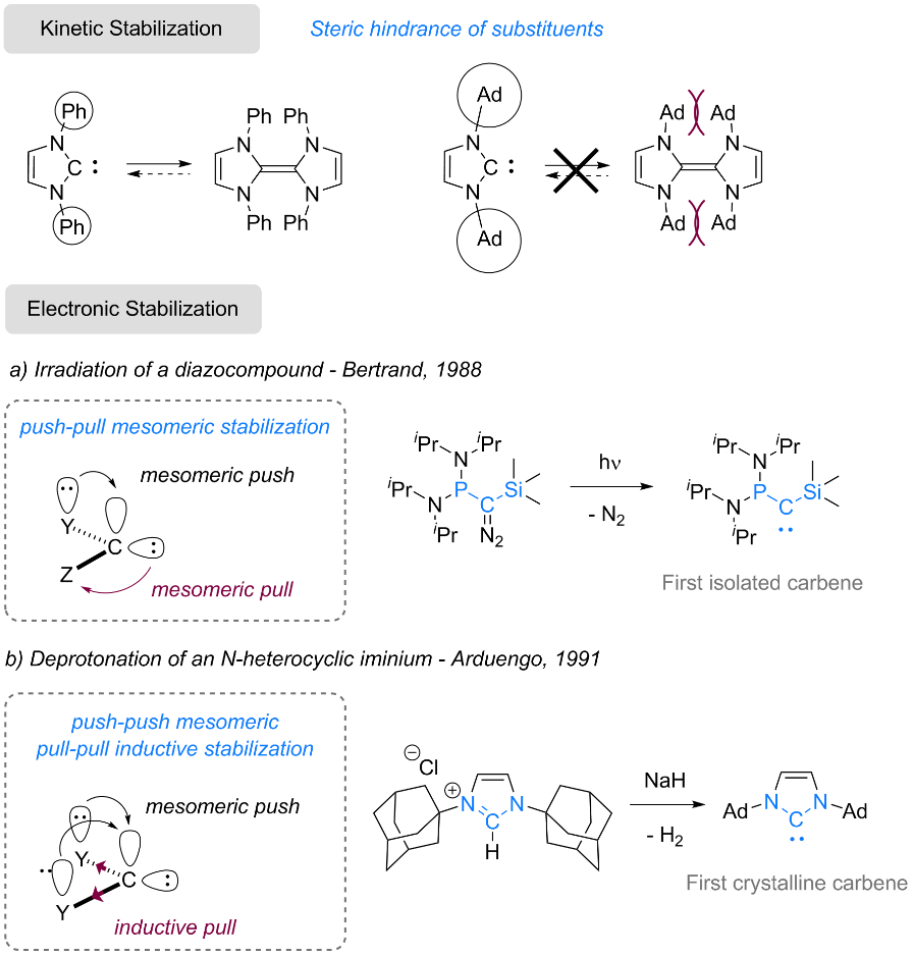

Figure 1.3 – Kinetic and electronic stabilization modes of singlet carbenes. a) The first isolated carbene by Bertrand. b) The first crystalline carbene by Arduengo.

Two primary methods have been used to achieve a thermodynamically stable singlet state. The first method, seen in Bertrand's carbene, involved the so-called "push-pull" effect of the α-substituents. Here, the carbene center is coordinated to a π-donor, in this case a phosphorus heteroatom, which mesomerically stabilizes the vacant p_π orbital, by donating electron density via its lone electron pair. It is also coordinated to a π-accepting silicon atom, which stabilizes the carbene σ lone pair by accepting electron density (Figure 1.3 – a). This strategy led to the observation of the first free carbene, termed the phosphino(silyl)carbene.

The second method utilized two σ-withdrawing and π-donating atoms adjacent to the carbene center. These substituents stabilize the carbene both inductively, by accepting part of the lone pair's electron density due to differences in electronegativity, and mesomerically, by the interaction between the neighboring atoms' lone pairs and the empty p_π orbital. This mode of stabilization, known and the "push-push" mesomeric, "pull-pull" inductive effect, was used by Arduengo and co-workers in 1991 to isolate the first crystalline carbene, namely the N-heterocyclic carbene (Figure 1.2 – b).[12] Arduengo chose amino groups adjacent to the carbene center, similar to Wanzlick's approach, but added substantially bulkier adamantyl substituents for necessary kinetic protection. The nitrogen atoms, being more electronegative than carbon and possessing lone electron pairs, act as σ-acceptors and π-donors, respectively. Since this work, a wide array of stable singlet carbenes have been isolated – most containing at least one phosphorus or nitrogen heteroatom adjacent to the carbene center.

1.1.3 Diversity of Carbenes

The successful isolation and characterization of Bertrand's carbene and Arduengo's NHC marked the advent of a new class of organic compounds. Today, the field of carbene chemistry has expanded significantly, offering a wide array of stable carbenes with diverse steric and electronic properties. This diversity allows chemists to tailor carbenes for specific applications in catalysis, materials science, and organic synthesis (see Section 1.1.4). Besides the aforementioned Bertrand and Arduengo carbenes, some notable types of carbenes include the cyclic (alkyl)(amino)carbene (CAAC), cyclopropenylidene, *anti*-BredtNHC, diamidocarbene (DAC), EndersNHC, mesoionic carbene (MIC), and cyclic bent allene (CBA) (Figure 1.4).

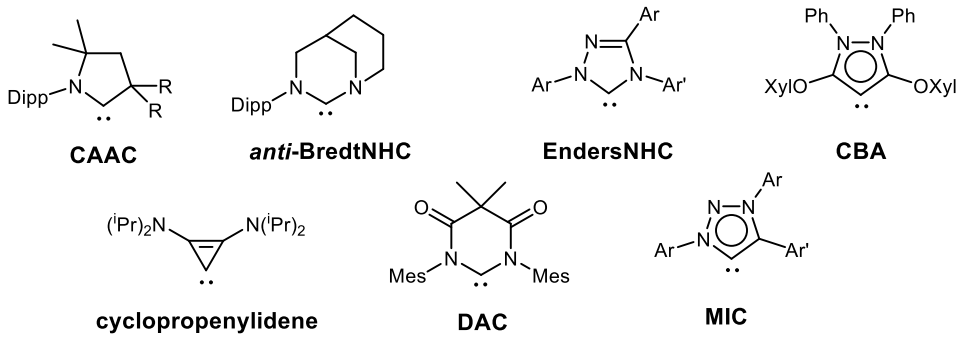

Figure 1.4 – Several examples of notable carbene families.

In recent years, a number of methods have been developed to probe the electronic properties of carbenes. In 2018, Huynh published a review[13] describing the various scales that have emerged to probe the electronic parameters of carbenes. Among these scales are the Tolman Electronic Parameter (TEP), the phenyl-phosphinidene-carbene adduct ^{31}P NMR shift, and selenium-carbene adduct ^{77}Se NMR shift. The TEP has been employed on various carbene-metal-carbonyl complexes to evaluate the carbenes' overall σ-donation strength (Figure 1.5).[14] This is accomplished by comparing the A_1 stretching frequency of the CO ligand in the infrared spectrum for each corresponding complex. A metal center that is more electron-rich will donate greater electron density to the π^* orbital of the CO ligand, thereby lengthening the C-O bond, and lowering the stretching frequency. As a result, carbenes that have stronger σ-donation result in complexes with lower C-O stretch wavenumber.

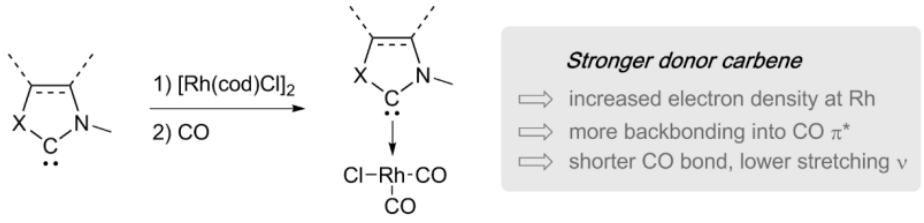

Figure 1.5 – Tolman Electronic Parameter method to gauge carbene σ-donor strength.

In addition to the TEP which measures σ-donation, the π-accepting character of various carbenes can also be quantified by measuring the ^{31}P and ^{77}Se NMR chemical shifts of carbene-phosphinidene[15,16] and carbene-selenium[17] adducts, respectively (Figure 1.6). Carbenes that are more π-accepting give rise to more downfield signals. A series of carbenes and their TEP values is shown in Figure 1.7.

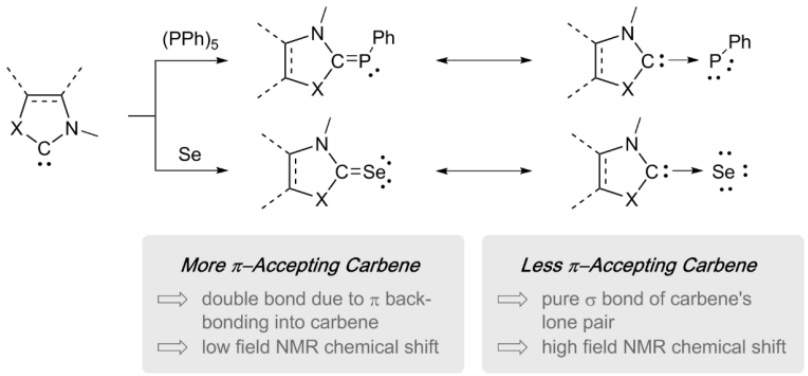

Figure 1.6 – Methods for probing π-accepting ability of carbenes.

Entry	Carbene	^{31}P NMR TEP	Entry	Carbene	^{31}P NMR TEP
1	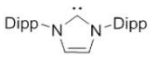	-18.9 2051.5	6	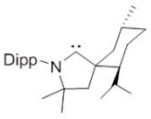	56.2 2042.2
2	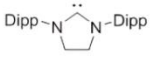	-10.2 2052.2	7	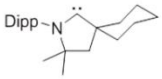	68.9 2048.5
3	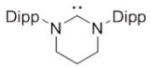	14.8 2044.0			
4	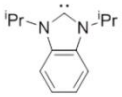	-34.6 2054.0	8	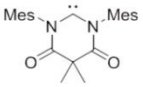	83.0 2055.8
5	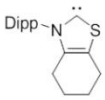	57.0 2054.0	9	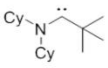	126.3 2043.8

Figure 1.7 – TEP values and ^{31}P NMR shifts of various carbene adducts with metals and phenylphosphinidene, respectively.

1.1.4 Tunability of Carbene Steric Bulk

One of the reasons carbenes have garnered significant attention within the chemistry community is due to their highly adaptable steric properties, which facilitate a wide array of applications. Given that carbenes bear two substituents, a considerable degree of variability can be achieved with regards to the steric environment around the carbene center. The steric environment can be quantified by a metric known as the buried volume parameter ($\%V_{bur}$), introduced by Nolan, Cavallo, and co-workers.[18,19]

In the $\%V_{bur}$ model, a theoretical sphere with a fixed radius of 3.5 Å is centered on a central atom (usually a metal) with the carbene positioned 2 Å away (see Figure 1.8 – left). This parameter reflects the ratio of the volume occupied by the ligand to the total volume of the sphere. As the steric demands of the ligand increase, so does the $\%V_{bur}$. Experimental determination of buried volumes typically relies on X-ray crystallography or theoretical calculations involving free carbenes, carbene-metal complexes, or iminium salt carbene-precursors.

Advancements in computational chemistry have further refined our understanding through tools like SambVca2 (Salerno molecular buried volume calculations), a software developed by Cavallo.[20,21] This tool generated topographic steric maps divided into quadrants, where regions shaded in deeper red indicate heightened steric impact from ligands near the metal center (Figure 1.8 – right). Such visual representations offer detailed 3D insights into the carbene pocket, making this particularly beneficial for studying catalytic processes involving carbene-transition metal complexes. However, interpreting and comparing $\%V_{bur}$ values necessitates caution, as this method relies heavily on the quality of X-ray crystallography data or the computational DFT methods used. Moreover, it's crucial to recognize that these static measurements do not account for the dynamic nature of molecular systems in solution.[22]

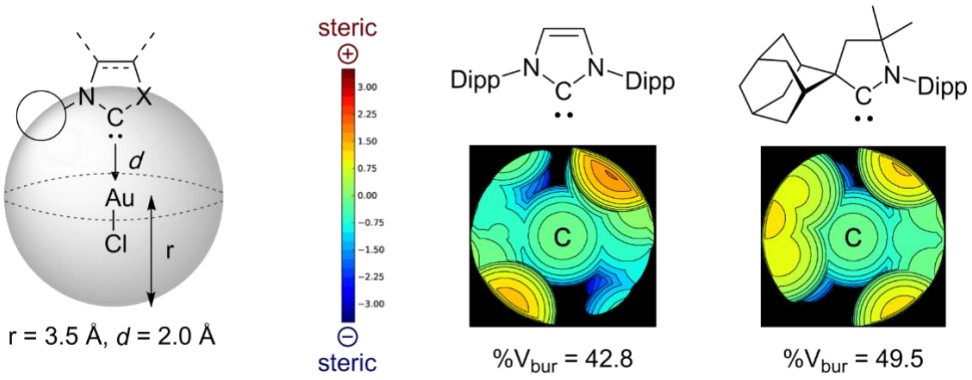

Figure 1.8 – $\%V_{bur}$ model of Nolan and Cavallo and two examples of topographical $\%V_{bur}$ maps.

The $\%V_{bur}$ values for various carbene-AuCl complexes, where the Au-carbene bond is fixed at 2 Å, are depicted in Figure 1.9. Notably, substituting a small isopropyl group (*i*Pr) with a bulkier 2,6-diisopropylphenyl (Dipp) group on the two NHC nitrogen atoms results in an increase of nearly 20% in $\%V_{bur}$. This change arises because larger substituents, such as those in Dipp, provide a dendritic covering around the carbene center. Another factor that increases the $\%V_{bur}$ is the placement of the steric bulk. When the steric bulk is closer to the atom in focus, the atom is so-called "buried" more efficiently in the congested region. Consequently, the $\%V_{bur}$ of NHC-7 is higher than that of NHC-6 and NHC-5, due the flanking Dipp groups being directed closer to the carbene center. Analogously, the $\%V_{bur}$ that is given by ^{menth}CAAC (51.2) is considerably higher than that of the anti-BredtNHC (38.5) where steric protection is only provided to one side of the ligand-sphere. For researchers seeking to maintain the steric environment typical of NHCs while harnessing the electronic properties of CAACs, bicyclic alkyl(amino)carbenes (BICAACs) provide a viable solution. The bridgehead position of the quaternary carbon in BICAACs forces them into a fan-shaped steric configuration akin to NHCs, giving them a similar $\%V_{bur}$ value between 42.1 and 46.5. This exemplifies the remarkable tunability of carbene structures, where subtle modifications can profoundly impact both electronic and steric properties.

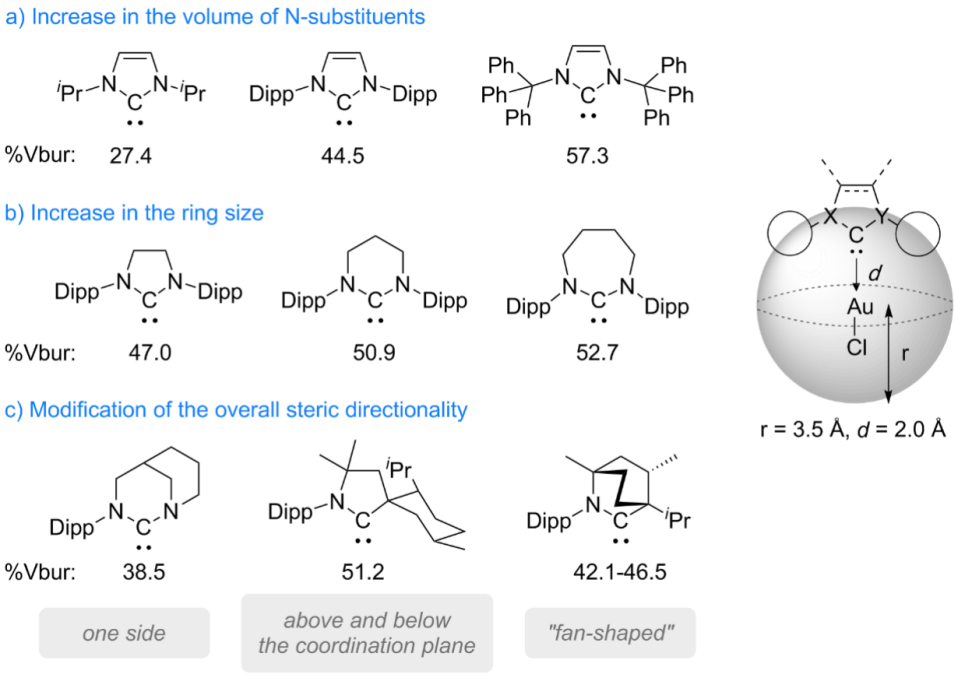

Figure 1.9 – Illustrative examples of influencing the $\%V_{bur}$ of carbene-AuCl complexes.

1.1.5 Major Applications of Carbenes

Initially considered laboratory curiosities, stable singlet carbenes have quickly become indispensable tools in organic, inorganic, and organometallic chemistry. The ground-state electronic structure of singlet carbenes provides a crucial framework for understanding their reactivity. The carbene lone pair imparts nucleophilic character, enabling carbenes to act as σ-donors and coordinate with a wide range of metallic and non-metallic species. The extraordinary strength of these interactions is further enhanced by the vacant p_π orbital, which can accept electron density through back-donation. These features make carbenes excellent transition-metal ligands for use in many catalytic processes.[23] The importance of carbenes was underscored by its role as a ligand in the breakthrough 2nd-generation Grubbs olefin metathesis catalyst (Figure 1.10a) that resulted in the Nobel Prize in Chemistry in 2005.

Carbenes have also been used more recently to stabilize highly reactive species such as metals in unusual oxidation states,[24] persistent radicals,[25,26] and low-valent main group species.[27] Furthermore, they have been shown to exhibit metal-like reactivity due to their energetically accessible frontier orbitals; thus, they can activate small molecular and enthalpically strong bonds such as those in dihydrogen and ammonia[28] (Figure 1.10b).

Beyond these traditional roles, carbenes have found significant applications in materials science, allowing for the functionalization of surfaces, polymers, nanoparticles, and discrete, well-defined clusters.[29] In a recent study, carbenes have been employed in the stabilization and functionalization of graphene to modify its properties.[30] Furthermore, our group has shown that copper-carbene complexes exhibit high photoluminescent quantum yields and short emission lifetimes, making them promising materials for enhancing organic LED performance (Figure 1.10c).[31]

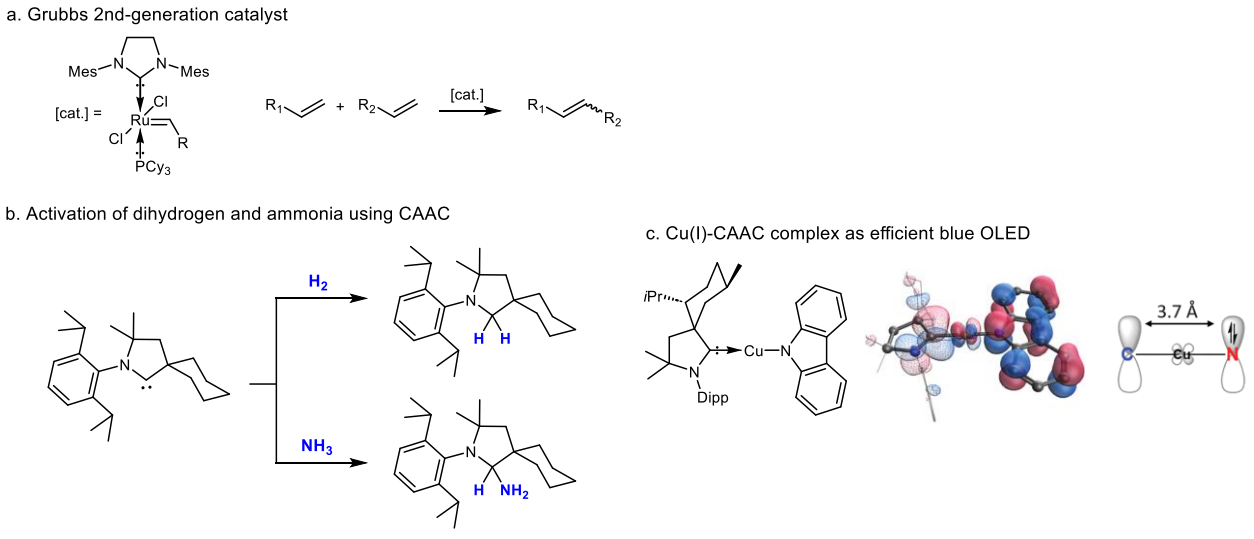

Figure 1.10 – Notable Applications of Carbenes

1.2 Carbene Analogs (e.g. phosphinidenes, nitrenes, and borylenes)

While the field of carbenes has evidently exploded since their first isolation, much less is known about their isolobal group 15 cousins, namely nitrenes and phosphinidenes. The parameters that have been discussed relating to carbenes are also applicable to these species. A notable difference, however, is that singlet nitrenes and phosphinidenes contain one lone pair of electrons, one empty orbital, and only one substituent. The last constraint makes them more difficult to kinetically stabilize than carbenes since one substituent must provide adequate steric protection around the electron-deficient atom. Furthermore, the lack of proper electronic stabilization can lead to an accessible diradical triplet-state with even greater instability. For example, the parent phosphinidene (P-H) has a triplet ground state with a singlet-triplet gap (ΔE_{ST}) of -28 kcal/mol – however, an amino substituent (RP-NH_2) significantly reduces ΔE_{ST} to -1.2 kcal/mol.[32] Despite these challenges, skilled synthetic chemists have achieved the stabilization of such species. The first nitrene was observed at -78 ^{o}C via IR spectroscopy by Dervan in 1978[33] (Figure 1.11). It wasn't until a few decades later, in 2012, that the first crystalline nitrene – namely, the (phosphino)nitrene – was isolated by Bertrand.[34] Remarkably, in the time of writing this paragraph, a publication in *Science* was released by the groups of Hupf and Beckmann reporting the synthesis of the first crystalline *triplet* nitrene.[35] There has only been one instance of a stable phosphinidene, which was isolated by Bertrand in 2016, bearing a phosphino substituent.[36]

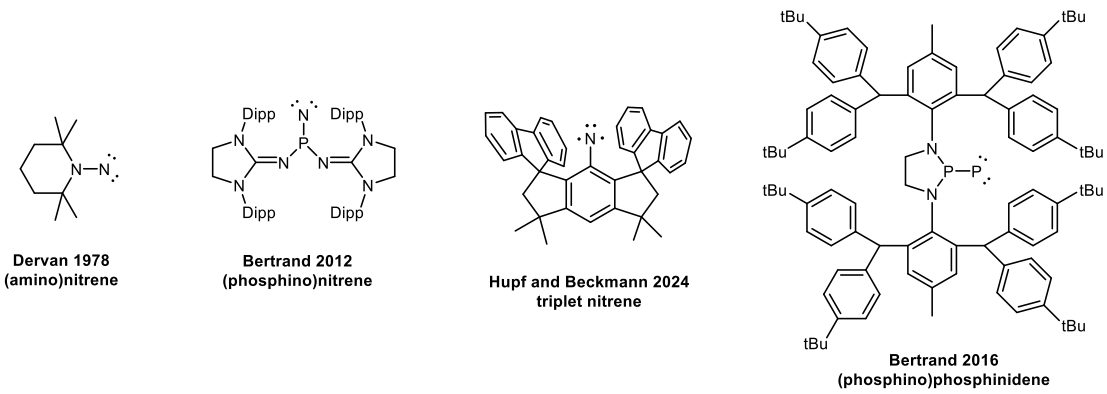

Figure 1.11 – Known examples of nitrenes and phosphinidenes.

Unlike nitrenes and phosphinidenes, borylenes have eluded the synthetic skills of chemists. Theoretical calculations have rendered all borylenes to have a singlet ground state, with ΔE_{ST} ranging from 8 to 79 kcal/mol. Adding a π-donating substituent further increases this gap. While a free borylene has not been isolated, a number of Lewis-base stabilized borylenes have been prepared and studied in depth (Figure 1.12a).[37,38,39] Although the extreme instability of borylenes have rendered their isolation unfeasible, evidence of their formation has been provided via trapping reactions (Figure 1.12b).[40,41] The ferocious nature of borylenes is exemplified in its ability to insert itself into the C-O bond of tetrahydrofuran.

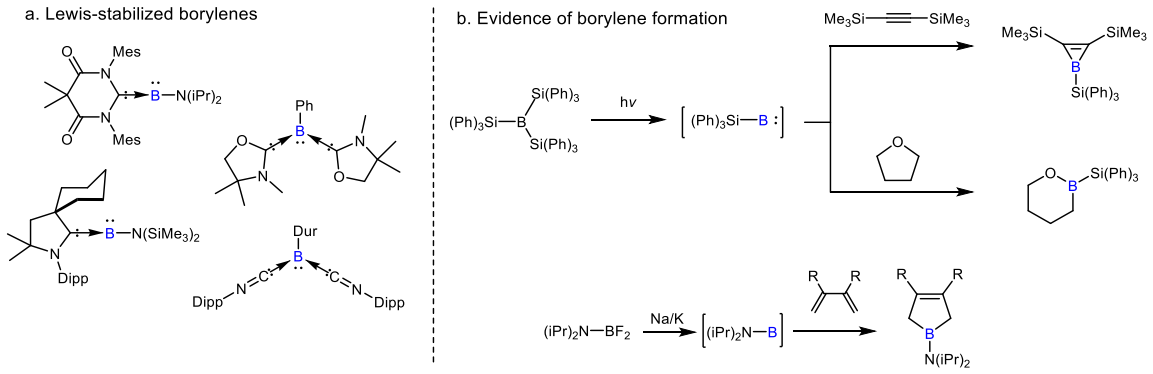

Figure 1.12 – (a) Examples of Lewis base-stabilized borylenes. (b) In-situ formation and trapping of borylene intermediates.

The attempts to isolate analogs of carbenes like phosphinidenes, nitrenes, and borylenes are the focus of Chapter 2 of this dissertation.

1.3 The Chemistry of Diphosphorus

Chapter 3 deals with the elusive species, diphosphorus (P_2). Unlike the previously mentioned elusive species, the instability of P_2 is not due to electron deficiency. Rather, P_2 is unstable due to its low bond-dissociation energy (490 kJ/mol).[42] This contrasts highly with N_2, being the most stable diatomic molecule with a bond enthalpy of 945 kJ/mol[43] – almost double that of P_2. Because of this, the chemical and electronic structural properties of P_2 more closely resemble those of acetylene (HCCH) than those of N_2. When generated, the diphosphorus molecule quickly dimerizes and polymerizes to form white phosphorus (P_4) and red phosphorus, respectively (Figure 1.13 – left). While P_2 itself is highly reactive, it has been widely seen in the coordination sphere of transition-metals, as "tamed" versions (Figure 1.13 – right).[44]

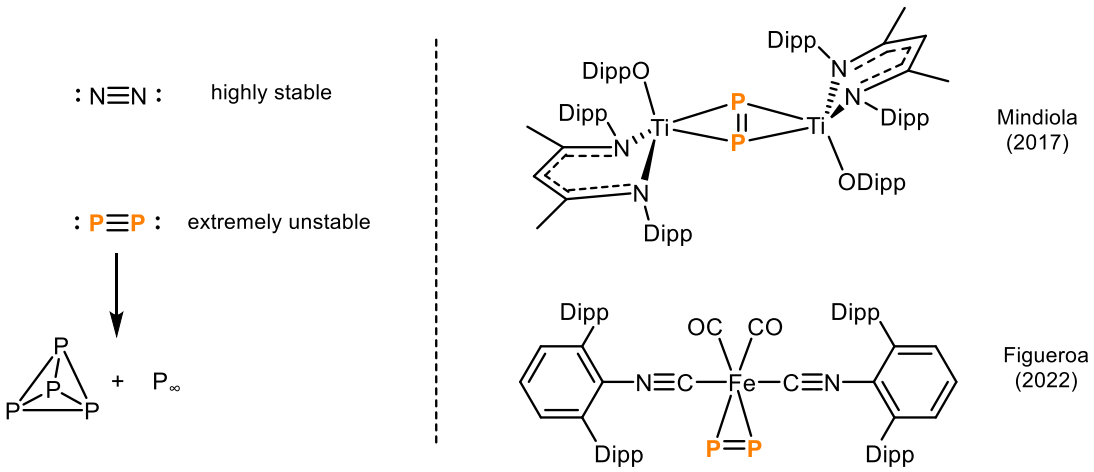

Figure 1.13 – (Left) Difference between N_2 and P_2. (Right) Taming P_2 within the coordination sphere of transition-metals.

Although P_2 fragments have been widely seen in stabilized pockets, less has been explored with respect to the use of P_2 as a reagent. The importance of synthetically useful diphosphorus surrogates cannot be overstated in the field of chemistry. Due to the inherent instability and high reactivity of free P_2, direct utilization in synthetic applications is highly challenging. Consequently, researchers have pursued the development of stable diphosphorus surrogates that can mimic the reactivity of P_2 while offering greater stability and ease of handling. Such compounds are highly desirable to make P_2 synthetically useful. The taming and subsequent transfer of P_2 using small carbene ligands is the focus of Chapter 3 of this dissertation.

1.4 Acknowledgements

I thank Glen P. Junor for the chemical computation of carbenes electronic parameters (HOMO, LUMO, and ΔE_{ST}). Permission to use these data was obtained from Glen P. Junor.

Chapter 2 Bulky Secondary Amine Ligands – Electronic and Steric Stabilizers

The stabilization of main-group (III-V) species bearing a single substituent has been proven to be highly challenging. Among the examples reported in the literature, their lifetimes are extremely short, with only a few being stable in air-free conditions. This chapter describes the development of novel secondary amines featuring an extreme steric bulk profile and unique electronic properties. Subsequently, their functionalization towards stable monocoordinated main-group species is explored.

2.1 Introduction

As predicted by the octet rule, electron-deficient compounds lacking a complete octet are unstable. Whether it is through a reaction with atmospheric oxygen or water, intermolecular dimerization, or a novel reactivity mode, there is an inherent thirst for electron density that needs to be satisfied. Prior to 1988, the reactivity of carbenes could not be well-studied, as they were only postulated as chemical intermediates. Although a general understanding was possible via mechanistic studies of various reactions, a robust and systematic approach was only possible with the isolation of the first carbenes in 1988 and 1991.

Initially, carbenes were considered mere laboratory curiosities with no foreseeable applications. This is quite normal, as this was the case for phosphorus ylides. The first phosphorus ylide was synthesized in 1894 by Michaelis and Gimborn,[45] yet these species did not find practical use until nearly six decades later. It was Wittig and Geissler who reported the now-renowned Wittig reaction (Figure 2.1),[46] a key step in the industrial synthesis of vitamin A. In contrast,

carbenes found relevance in the chemical industry much sooner. By 1995, less than a decade after their first isolation, Herrmann reported the use of NHCs as ancillary ligands in palladium complexes, which promote the catalytic Mizoroki-Heck reaction.[47] Since then, a vast array of metal-carbene complexes have been prepared and employed in various chemical transformations[48] – the most prolific example being the Grubbs 2nd-generation olefin metathesis catalyst.[49] There is no doubt that the pursuit of laboratory curiosities has yielded much fruit in the past, which is the very reason that chemists all over the globe continue at great lengths to attempt to synthesize such exotic species.

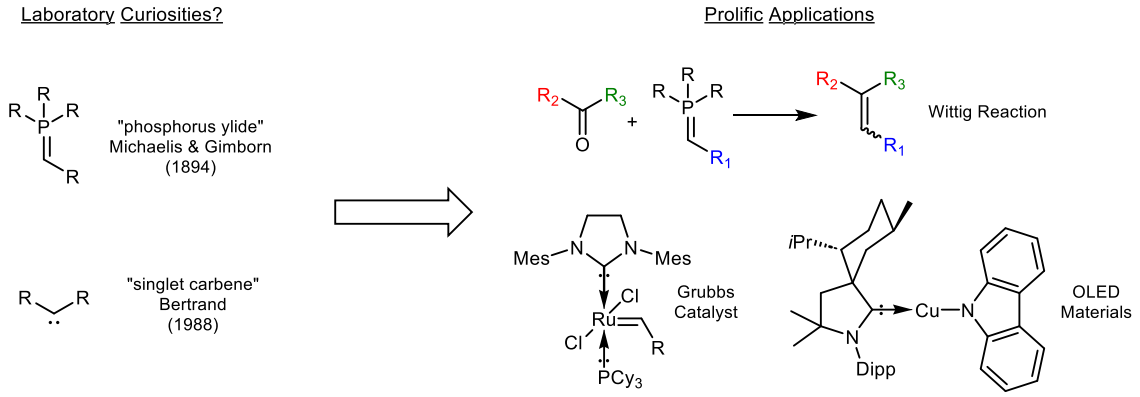

Figure 2.1 – From laboratory curiosities to prolific applications.

There are two major criteria that are necessary for the stabilization of electron-deficient species: electronic stabilization and steric protection. This has been true of nearly all carbenes and their analogs. For decades following the isolation of the first carbene, it was believed that the electronic stabilization of carbenes was possible through the combined effect of *both* substituents working together in a "push-push" or "push-pull (*vide supra*) manner. Since carbenes can bear two substituents (unlike their group III and V analogs), constructing a sterically protected environment necessary to prevent dimerization is less challenging. However, the discovery of the first stable

nitrene and phosphinidene, each bearing only one substituent, suggested that a monosubstituted carbene, bearing only one donor ligand (R(C:)H) could be isolated, provided that R is sufficiently bulky to prevent dimerization. This realization led to the first monosubstituted carbene isolated by our group in 2018, bearing a secondary amino substituent (Figure 2.2).[50] Following this, Hinz reported the isolation of a monosubstituted silylenium cation,[51] also bearing a bulky secondary amine scaffold.

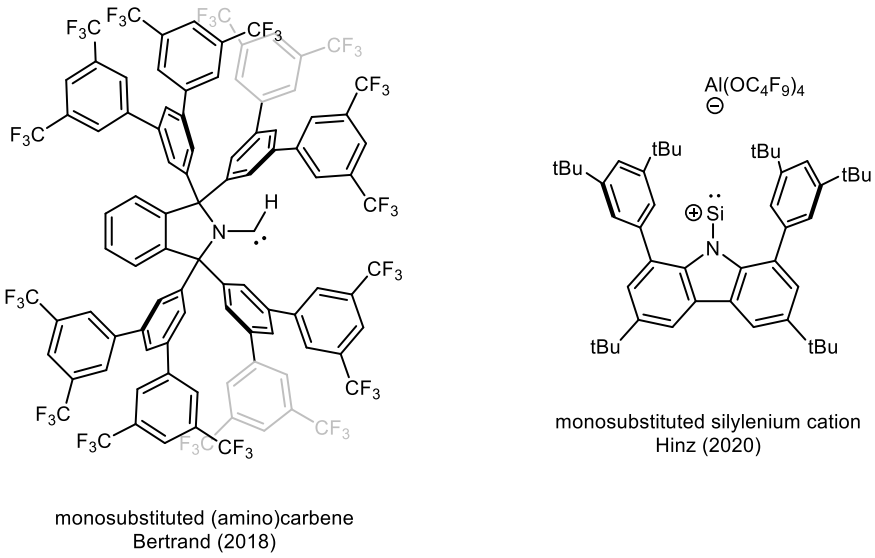

Figure 2.2 – Electron-deficient species stabilized by bulky secondary amines.

Given the scarcity of stable subvalent species (i.e. carbene analogs) reported in the literature, we decided to study the use of secondary amine scaffolds for the preparation of species such as the phosphinidene – specifically an (amino)phosphinidene. Additionally, these extremely bulky secondary amine can be added to the existing library of pre-existing bulky secondary amines, whose uses have been widely explored.[52] While both the (phosphino)phosphinidene and (phosphino)nitrene have been isolated, an amino substituent would present some unique

properties. The incorporation of an amino substituent introduces distinct electronic characteristics that differentiate it from its phosphino counterparts. First, amines are stronger π-donors than phosphines. This leads to a more robust electron-donating effect on the ensuing electron-deficient atom, thereby enhancing overall stability. Furthermore, unlike phosphines, amines lack π-accepting capabilities. The absence of π-acceptance could also lead to greater stability, as the electronic environment of the electron-deficient atom would not be perturbed by back-donation effects that are characteristic of phosphine ligands. Additionally, the nucleophilic nature of amines, as opposed to the electrophilic nature of phosphines, provides an alternative synthetic pathway for the formation of species like phosphinidenes, nitrenes, or borylenes. For instance, secondary amines (unlike secondary phosphines) can be deprotonated with a strong base to make a negatively charged amide anion, which can nucleophilically attack main-group precursors such as EX_3 (E = P or B; X = halogen). This makes secondary amines a suitable precursor to terminal main-group carbene analogs.

Given that the scaffolds presented in Figure 2.2 already have known synthetic protocols, we first used these amines as potential electronic and kinetic stabilizers to electron-deficient species. Additionally, we prepared two novel frameworks to create a library of bulky secondary amine scaffolds, each with their own unique electronic and steric properties. This chapter focuses on the synthesis and characterization of these bulky secondary amines, along with our attempts to stabilize subvalent main-group species using these prepared scaffolds.

2.2 Pyrrolidine-based Scaffold

In our pursuit to stabilize electron-deficient species, we first turned our attention to the benzannulated pyrrolidine-based scaffold, **pyrrol-H** (Figure 2.3) – a well-characterized ligand

developed in our laboratory. This scaffold can also be considered a derivative of isoindoline. This scaffold showcases a robust steric environment, as demonstrated by its ability to kinetically stabilize the monosubstituted carbene. Furthermore, the lone pair of electrons on the amine can mesomerically donate electron density to the electron-deficient atom, thereby attenuating its thirst for electrons. Given its promising properties and its availability, it was a logical choice to explore its potential in stabilizing a phosphinidene.

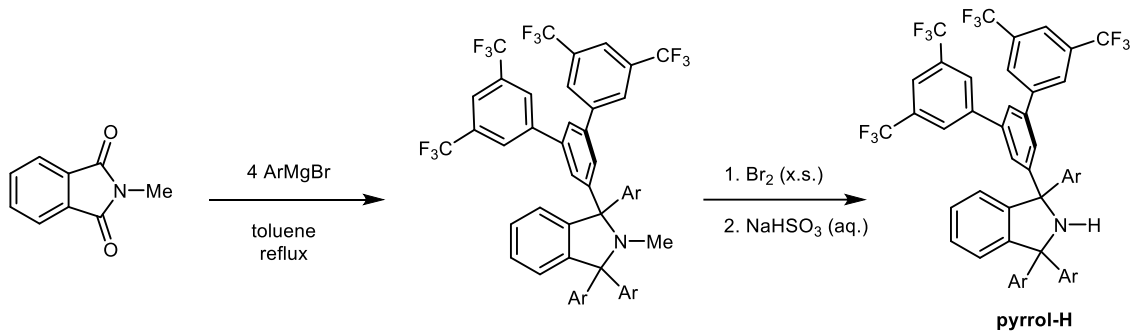

Figure 2.3 – Synthesis of **pyrrol-H** amine from N-methyl phthalimide.

Starting from *N*-methyl phthalimide, the quadruple Grignard reaction using the appropriate bulky Grignard reagent was accomplished by refluxing in toluene. The free amine was obtained by the bromination and subsequent hydrolysis of the methylated precursor to give **pyrrol-H**. With the secondary amine in hand, the next objective was to introduce the phosphorus atom. This was done by deprotonation of the amine using *n*-BuLi at low temperature to give the lithium amide (Figure 2.4). This nucleophile was then reacted *in situ* with phosphorus tribromide at 0 ^{o}C, yielding **pyrrol-PBr$_2$** with a characteristic ^{31}P NMR shift of 143 ppm in DCM. Additional structural elucidation was achieved through X-ray crystallography, revealing an N-P bond distance of 1.673 Å. This bond length is slightly shorter than that of the typical N-P single bond, suggesting a degree of multiple bonding character. The trigonal planar geometry of the nitrogen atom suggests that it

is sp^2 hybridized, indicating that the lone pair is available for mesomeric stablization as it is part of the π-system. Ascertaining from the X-ray structure, it seems that the steric protection is sufficient, as it is highly unlikely that two of these scaffolds can come together to form a P-P bond.

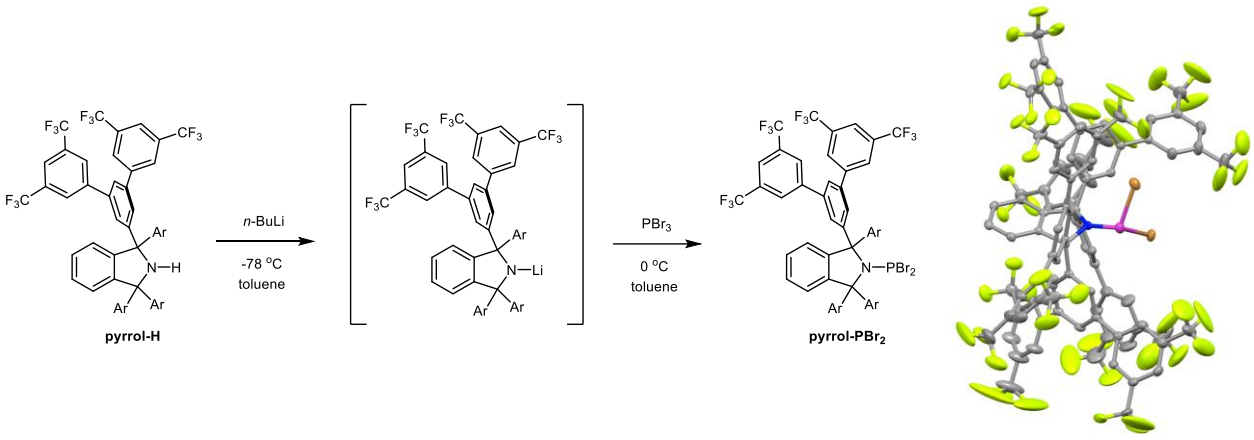

Figure 2.4 – Synthesis of **pyrrol-PBr$_2$** and its X-ray crystal structure (hydrogen atoms are omitted for clarity).

With the phosphorus atom installed, initial reactivity studies were conducted. We quickly found that **pyrrol-PBr$_2$** does not react with elemental sulfur or triethylamine N-oxide to give the corresponding sulfide or oxide. We also found that the anionic oxide of silver oxide (Ag_2O) does not displace the bromide ions.

We then proceeded to the final step in the formation of the phosphinidene – double reduction to eliminate the bromine atoms. While each step following the deprotonation of the amine is sensitive to moisture and air, this final step was conducted with utmost caution, as any trace of water or oxygen would cause rapid hydrolysis or oxidation of the product. The reduction of **pyrrol-PBr$_2$** was accomplished using excess potassium graphite (KC_8) as a reducing agent resulting in the formation of a yellow compound. Analysis of the proton-coupled ^{31}P NMR spectrum revealed a doublet 7.3 ppm with a coupling constant of 151 Hz – indicative of a P-H

bond. The presence of a P-H bond was confirmed by the observation that this signal collapsed into a singlet in the proton-decoupled $^{31}P\{^{1}H\}$ NMR spectrum. This outcome indicates that while the phosphinidene intermediate is likely generated, it readily undergoes intramolecular C-H activation with a nearby aryl C-H bond, leading to the formation of **pyrrol-PH** (Figure 2.5). In attempts to mitigate this issue, we conducted the reduction at a much lower temperature, aiming to slow down the C-H activation and possibly isolate the elusive phosphinidene. Performing the reduction at -78 ^{o}C with KC_8 resulted in the formation of a deep green solution, which we hypothesized contained the phosphinidene. Despite these promising visual cues, low-temperature NMR spectroscopic analysis failed to detect any species other than the starting material and **pyrrol-PH**.

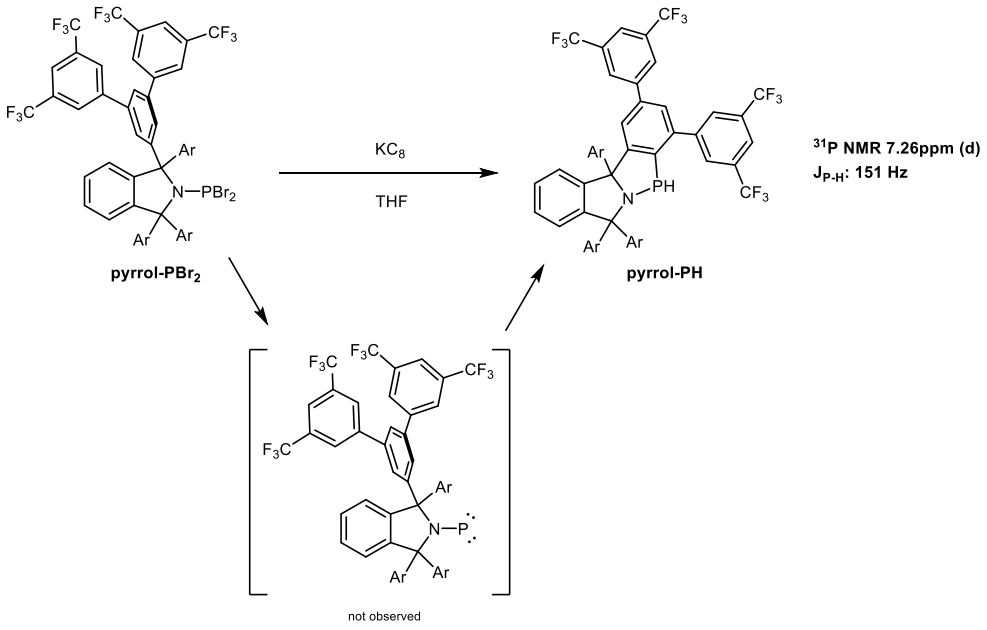

Figure 2.5 – Reduction of **pyrrol-PBr2** and subsequent aryl C-H activation.

We were not too surprised by the activation of the aryl C-H bond, since singlet phosphinidenes are prone to such reactivity. This is especially true if the ensuing product forms a

5- or 6-membered ring, resulting in a greater thermodynamic benefit. Following this result, we moved on to a scaffold based on a carbazole framework.

2.3 Carbazole-based Scaffold

While carbazoles find frequent application in optoelectronics,[53] they had rarely been used for the stabilization of reactive intermediates. [54] This was probably because, until recently, the bulkier carbazolyl compounds featured only tertbutyl, phenyl, mesityl or triisopropylphenyl groups at the 1- and 8-positions. However, in 2019, Hinz reported an extremely bulky carbazole-based scaffold, namely the 1,8-bis(3,5-di-*tert*-butylphenyl)-3,6-di-*tert*-butylcarbazole, **carb-H** (Figure 2.6). This scaffold features a much higher degree of steric protection around the prospective subvalent functional group than the pyrrolidino scaffold. In addition, it allows for stabilizing interactions between the π-systems of the flanking aromatic rings and the subvalent atom, as exemplified by the monosubstituted silylenium cation and other tetrylenium salts which have been isolated using this ligand.[55] Thus **carb-H** was synthesized from the parent carbazole as illustrated in Figure 2.6 with an overall yield of 70% over 4-steps.

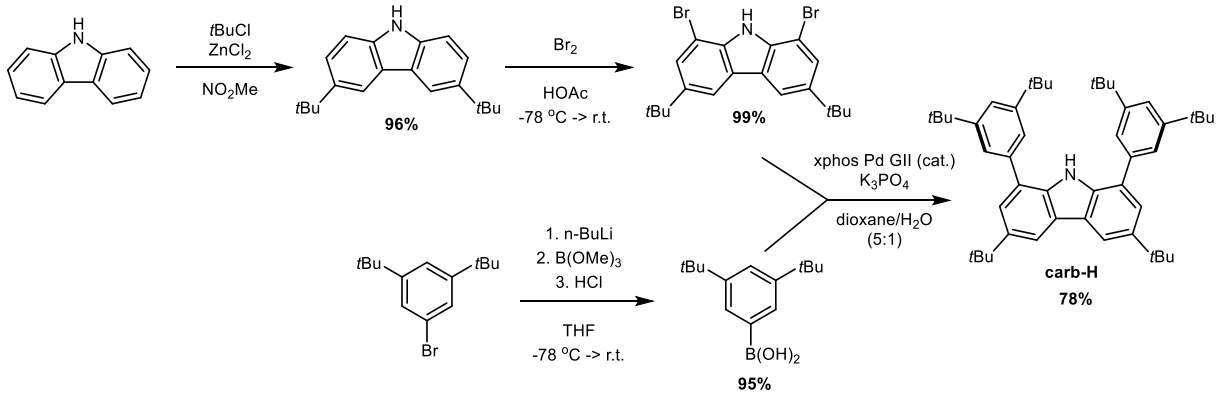

Figure 2.6 – Synthesis of **carb-H**.

With our desired amine in hand, a strong base was need for deprotonation to give the amide. We found that organo-alkali bases such as *n*-butyl lithium, neopentyl lithium, or benzyl potassium worked quite efficiently as they leave behind volatile byproducts. The latter quantitatively gave rise to the potassium amide, **carb-K**, which was more stable than the lithium analogs. We believe that this is due to the significant π-interaction of the bigger potassium ion with the flanking aromatic rings, as shown in the single crystal X-ray structure (Figure 2.7). The average distance between the flanking aromatic ring centroids and the potassium ion was measured to be 3.11 Å – well within the range of a substantial electronic interaction.

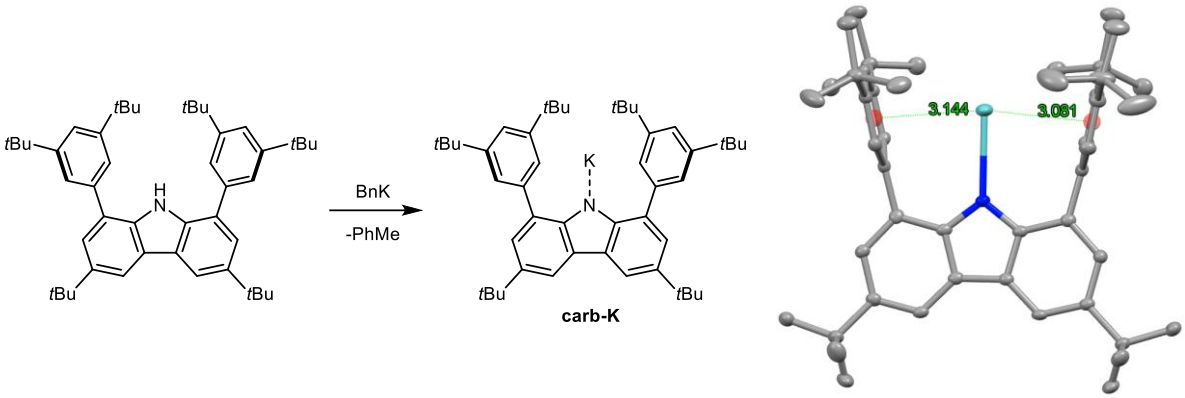

Figure 2.7 – Deprotonation of **carb-H** to give **carb-K** and the aryl centroid to potassium ion distances on the X-ray crystal structure (hydrogen atoms are omitted for clarity).

After the alkali amide nucleophile had been successfully prepared, a chloride metathesis on phosphorus trichloride (PCl_3) was conducted to install the phosphorus functionality in the form of a dichlorophosphine moiety, **carb-PCl$_2$** (Figure 2.8). Note, the amine **carb-H** was not sufficiently nucleophilic enough to react with PCl_3, even in the presence of an external base such as triethylamine. **carb-PCl$_2$** displays a ^{31}P NMR chemical shift of 155 ppm as a singlet – a value expected for such compounds. The single crystal X-ray structure of **carb-PCl$_2$** shows the nitrogen

atom to be pyramidalized, unlike the neutral amine and the potassium adduct. This observation is likely due to the highly congested environment of the -PCl_2 moiety as is evidenced by the "Top View" of the crystal structure. This was an indication that the nitrogen lone pair may not be a great π-donor, since the lone pair must be in an unhybridized p-orbital for it to participate in the π system. Like the **pyrrol-PBr_2**, this dihaloaminophosphine does not react with elemental sulfur to give the corresponding sulfide.

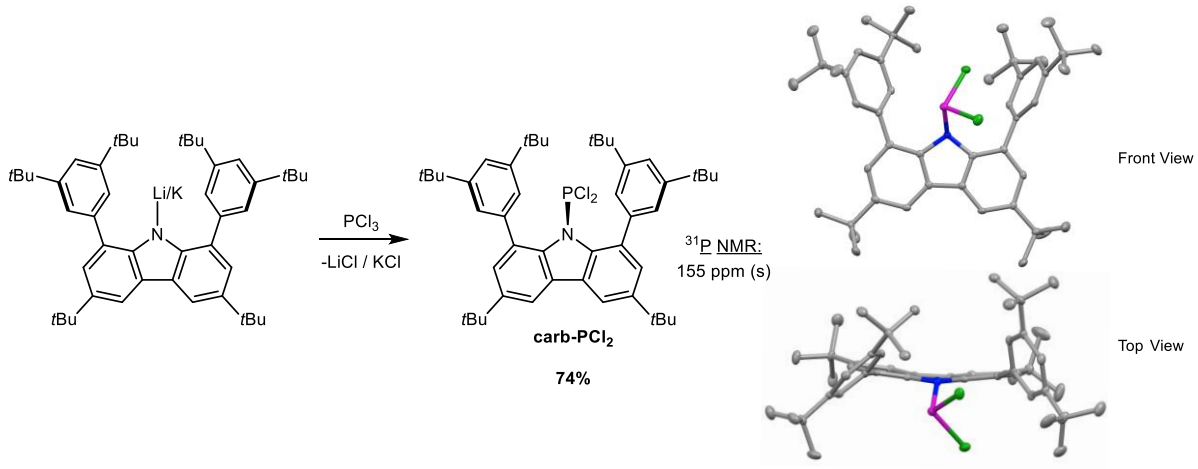

Figure 2.8 – Installation of phosphorus to give **carb-PCl_2** and two orientations of the X-ray crystal structure (hydrogen atoms are omitted for clarity).

With our phosphinidene precursor in hand, we attempted the double reduction to remove two chlorides. Addition of potassium graphite (KC_8) to **carb-PCl_2** resulted in a quick reaction involving the cleavage of the N-P bond to give **carb-K** (Figure 2.9). This unfortunate result was echoed when we tried using the milder Mg(anthracene)$(THF)_3$ complex – an organometallic reducing agent developed by Ramsden in 1965.[56] The use of even milder reducing agents such as zinc or the organic 1,4-bis(trimethylsilyl)-1,4-diaza-2,5-cyclohexadiene[57] did not lead to the phosphinidene, as they were not strong enough to fully reduce the dichlorophosphine. In the case

of the reduction with KC_8, it is difficult to determine whether the cleavage of the N-P bond occurs before or after chlorine abstraction, as the reaction occurs extremely quickly. However, when a substoichiometric amount of KC_8 was used, we could not observe any intermediate species by ^{31}P NMR, which is evidence that the cleavage of the N-P bond likely occurs before the double reduction. Additionally, when the reduction was conducted in the presence of an isocyanide in hopes to trap a possible phosphinidene intermediate, we did not observe the targeted phosphinidene-isocyanide adduct – further evidence that a phosphinidene intermediate is not formed.

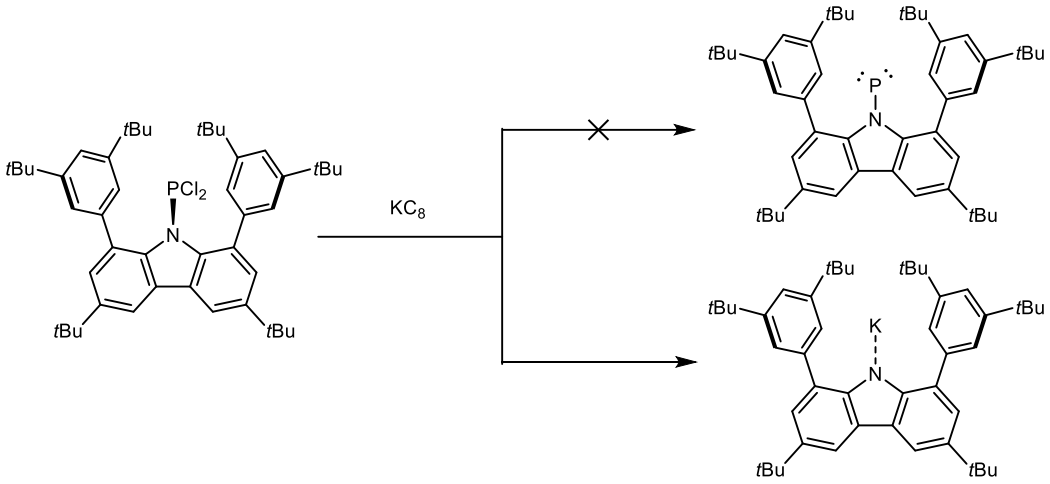

Figure 2.9 – Reduction of **carb-PCl_2** resulting in the cleavage of the N-P bond.

The feeble N-P bond can be rationalized with aromatic theory. The central 5-membered ring of carbazole contains 6 total π-electrons, satisfying the conditions for aromaticity. 4 of these electrons are from the p-orbitals of the sp^2-hybridized carbon atoms, while two of them originate from the nitrogen lone-pair. In order for the nitrogen lone-pair to be donated to the empty orbital on the phosphorus atom, it must be removed from the π-system, resulting in an anti-aromatic system. Consequently, the nitrogen lone-pair is minimally donating, making the N-P bond quite

weak. The weak π-donation is further underscored by the downfield ^{31}P NMR chemical shift of the related dibromo derivative **carb-PBr$_2$** (δ = 164 ppm) compared to **pyrrol-PBr$_2$** (δ = 143 ppm). The dibromoaminophosphine **carb-PBr$_2$** was prepared analogously to **carb-PCl$_2$** with the aim of increasing the lability of the halides. However, even with **carb-PBr$_2$**, the reduction to give a phosphinidene was unsuccessful.

While we did not find success in forming a stable (amino)phosphinidene using this carbazole-based scaffold, our results indicated that the nitrogen lone pair in our next secondary amine scaffold should not be part of an aromatic sextet. Before moving onto a different scaffold, however, we were curious to probe other reactivity modes of **carb-PCl$_2$**. We quickly found that a number of nucleophiles were quite reluctant to displace the chlorides. For example, neither Ag_2O, Na_2O, nor sodium trimethylsilanolate (NaOTMS) produced a reaction even at elevated temperatures. Even sonication of **carb-PCl$_2$** with trimethylsilyl azide in THF/acetonitrile (1:3) at 50 ^oC overnight, gave conversion only to the monosubstituted product as indicated by a new ^{31}P NMR singlet at 123 ppm. Further heating and agitation did not lead to the targeted diazide – which we predicted would extrude three equivalents of dinitrogen to give the phosphinidene. Similar results were obtained using the **carb-PBr$_2$** precursor.

Our results with the carbazole-based scaffold prompted us to explore a new system in which the amine has greater π-donation to strength the N-P bond. Thus, we decided to investigate a framework using phenothiazine as the backbone.

2.4 Phenothiazine-based Scaffold

Phenothiazine consists of a tricyclic system with two benzene rings fused to a central thiazine ring. Unlike the central 5-membered aromatic ring of carbazole, the central ring of

phenothiazine has 6-members and is anti-aromatic. For this reason, the nitrogen and sulfur atoms adopt a pseudo-tetrahedral geometry to avoid a planar structure that would result in anti-aromaticity. As a result, the tricyclic framework is slightly bent on either side of the nitrogen and sulfur atom (Figure 2.10). This "butterfly" shape is thought to be significant to its remarkable and diverse pharmacological activity, establishing it as the core unit for many important drugs.[58] We wondered if the anti-aromatic property of the central ring of phenothiazine would be advantageous in its use for the stabilization of electron-deficient species. In the carbazole system, we observed that the donation from the amine lone pair was minimized due to the anti-aromatic system that results from this donation. In contrast, for phenothiazine, the central ring itself is anti-aromatic with 8 π-electrons and becomes aromatic upon donation of the nitrogen lone pair. Thus, we anticipated a greater degree of mesomeric stabilization from the phenothiazine motif.

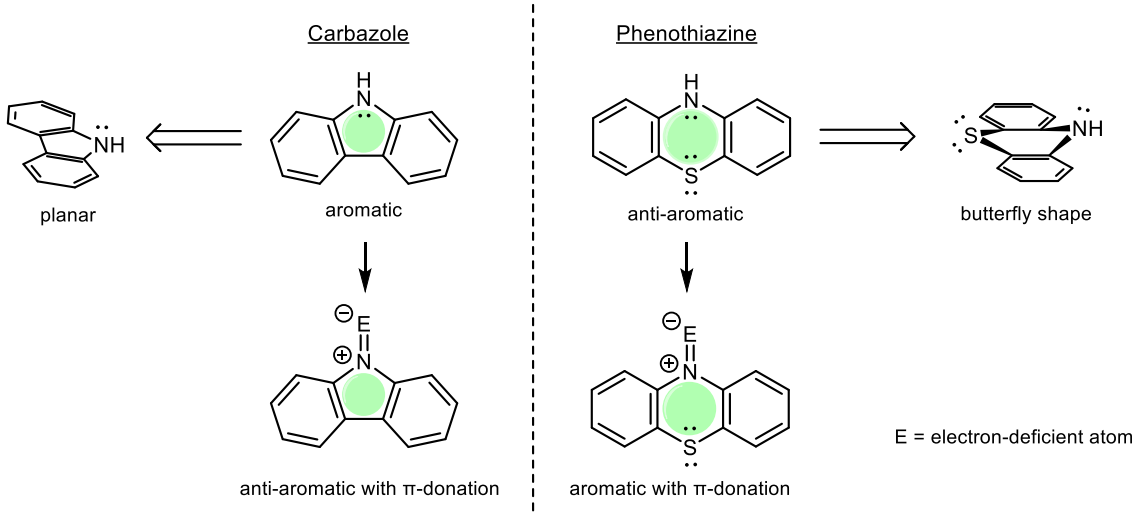

Figure 2.10 – Comparison of aromatic properties and mesomeric donation of amine lone-pair in carbazole versus phenothiazine.

Prompted by this promising theoretical precedent, we proceeded with the synthesis of the sterically bulky derivative of phenothiazine. The first step, namely Friedel-Crafts alkylation,

proved to be the most challenging. We later realized that this difficulty arose from the incompatibility of phenothiazine with Lewis acids/oxidants such as aluminum trichloride, which is a key ingredient for electrophilic aromatic substitution reactions. Despite the challenges, we successfully synthesized the targeted bulky phenothiazine derivative, **phenthz-H**, in low yield, utilizing a synthetic pathway analogous to the previous scaffold (Figure 2.11).

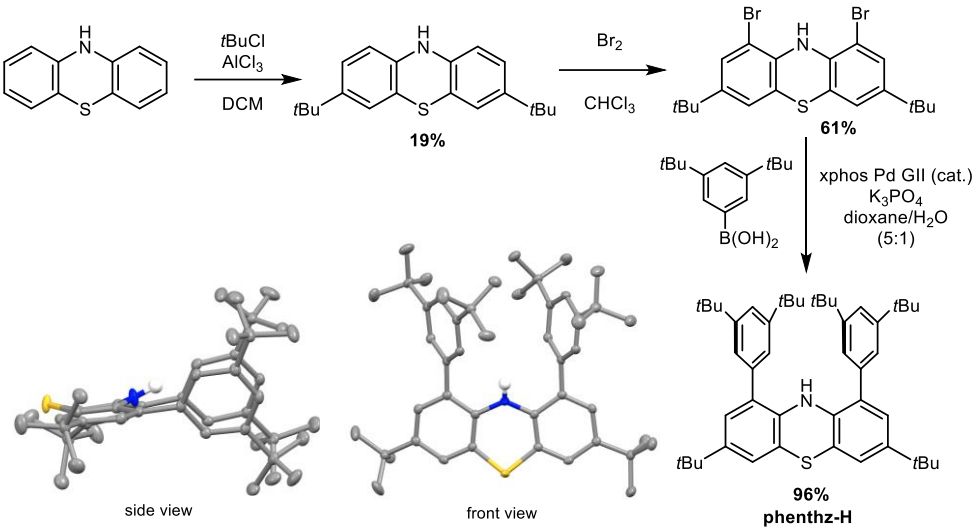

Figure 2.11 – Synthesis of **phenthz-H** and two perspectives of the X-ray crystal structure (hydrogen atoms except N-H are omitted for clarity).

Deprotonation of the amine using KHMDS led to rapid crystallization of the potassium adduct **phenthz-K** (Figure 2.12). Analysis of the X-ray crystal structure revealed that the large potassium ion was coordinated by both the nitrogen and sulfur atoms. This finding suggested that the placement of other electron-deficient atoms, such as a boron, could also benefit from the donation of electron density from a sulfur lone-pair.

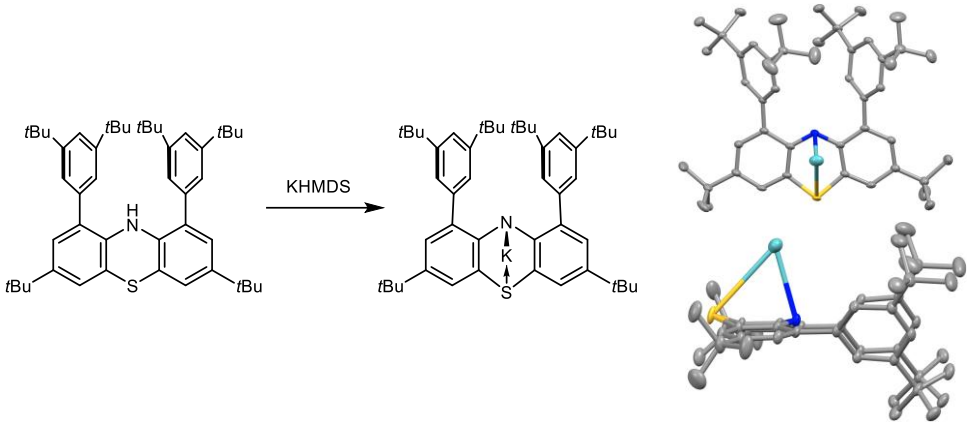

Figure 2.12 – Deprotonation of **phenthz-H** and two perspectives of the X-ray crystal structure (hydrogen atoms are omitted for clarity).

We next investigated the addition of electrophiles to the amine. Although the potassium adduct seemed to be a suitable precursor, the coordination by both the nitrogen and sulfur atoms rendered it quite unreactive. Therefore, we decided to form the anionic amide by *in situ* deprotonation of **phenthz-H** using *n*-butyllithium. The first electron-deficient species we targeted using this scaffold was the borylene. Given the substantial atomic radius of boron, we reasoned that there would be greater stabilization from the sulfur lone pair. We attempted to install boron using boron trichloride as the source of boron. Instead of forming the dichloroboron adduct, however, a deep purple species was obtained. This was reminiscent of the oxidized byproduct that was repeatedly observed during the Friedel-Crafts alkylation step using aluminum trichloride. The same result was obtained when we skipped the deprotonation of the amine and directly reacted **phenthz-H** with boron trichloride. A dive into the literature revealed that phenothiazine and its derivatives form sulfur-centered radicals when subjected to oxidizing conditions,[59] explaining why our system was incompatible with oxidants and Lewis acids.

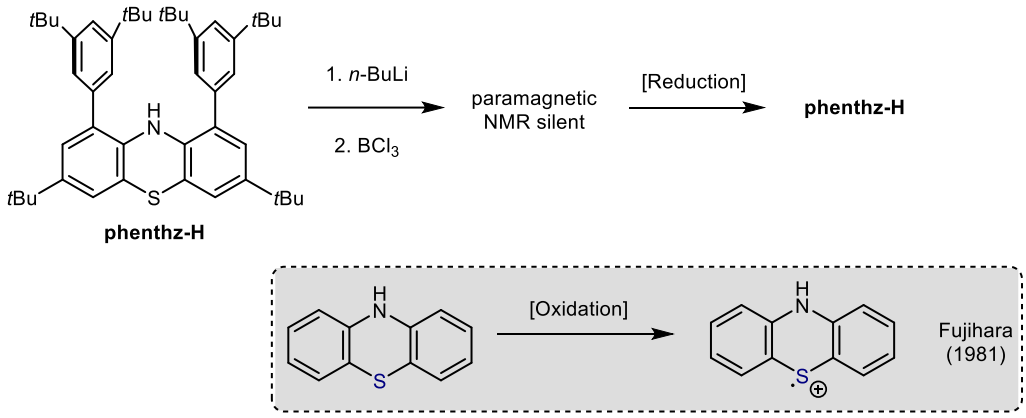

Figure 2.13 – Attempted addition of boron trichloride gives a paramagnetic species which can be reduced to the starting **phenthz-H**. Literature precedent for the oxidation of phenothiazine.

We were curious to determine if our nucleophile would react with less oxidizing electrophiles. Addition of methyl triflate to the deprotonated **phenthz-H** cleanly yielded the *N*-methylated product. Encouraged by this result, we wondered if we could form the hydrazine from **phenthz-H**. We found that monochloramine (NH_2Cl), an electrophilic amine, did not react with the deprotonated amide. In attempts to nitrosylate the amine, we reacted **phenthz-H** with isoamyl nitrite. At room temperature, no reaction occurred; however, upon heating **phenthz-H** in the presence of a large excess of isoamyl nitrite in THF, we observed the disappearance of starting material and the appearance of two new species – both exhibiting broad signals in the ^{1}H NMR spectrum. We speculated that these species might be a product of nitrosylation, along with a further oxidized byproduct. To investigate this possibility, excess diisobutyl aluminum hydride (DIBAL-H) was added to the mixture in attempts to reduce the suspected nitrosyl group to the hydrazine. This reaction was accompanied by vigorous bubbling – indicating the release of hydrogen gas. Unfortunately, however, the ^{1}H and ^{13}C NMR spectra revealed only the presence of **phenthz-H**.

Although the synthesis of this scaffold was successful and the physical properties aligned with our goals, the incompatibility with Lewis acids rendered it to be a poor candidate for the

pursuit of electron-deficient species. Thus, we shifted our attention to a similar scaffold where the sulfur atom was replaced by an alkyl group – namely, an acridine derivative.

2.5 Acridine-based Scaffold

[Note: The full name of 9,9-dimethyl-9,10-dihydroacridine will be simply referred to as "acridine."]

Acridine, like phenothiazine, is comprised of three fused 6-membered rings featuring a central nitrogen-heterocycle. One of the key differences between the two, however, is that the central ring of acridine is non-aromatic, whereas phenothiazine contains an anti-aromatic central ring (as discussed in the previous section). Therefore, the strength of the donation from the nitrogen lone pair is similar to that of diphenylamine. Consequently, acridine does not exhibit the butterfly effect that is seen in phenothiazine, as all three fused rings lie in the same plane.

To synthesize the sterically bulky acridine derivative, we started from commercial 9,9-dimethyl-9,10-dihydroacridine. Conducting the Friedel-Crafts alkylation in DCM using aluminum trichloride as the Lewis acid catalyst gave a yield of 28%. However, switching the catalyst to zinc dichloride and using nitromethane as the solvent improved the yield to 92% (Figure 2.14). The bromination step also proved to be quite tricky as the electron-rich nature of this scaffold led to over-bromination. To mitigate this, the milder *N*-bromosuccinimide (NBS) was selected as the brominating agent, and care was taken to prevent excess addition. It was also crucial to monitor the reaction by TLC so that the reaction was stopped before degradation occurred. Fortunately, the desired dibrominated product was easily distinguished from the mono-brominated product since the latter absorbs both 254 and 365 nm light, whereas the former only absorbs 254 nm light.

Finally, a Suzuki coupling reaction with the proper aryl boronic acid gave the desired bulky amine **acrdn-H** (Figure 2.14) with an overall yield of 44.3%.

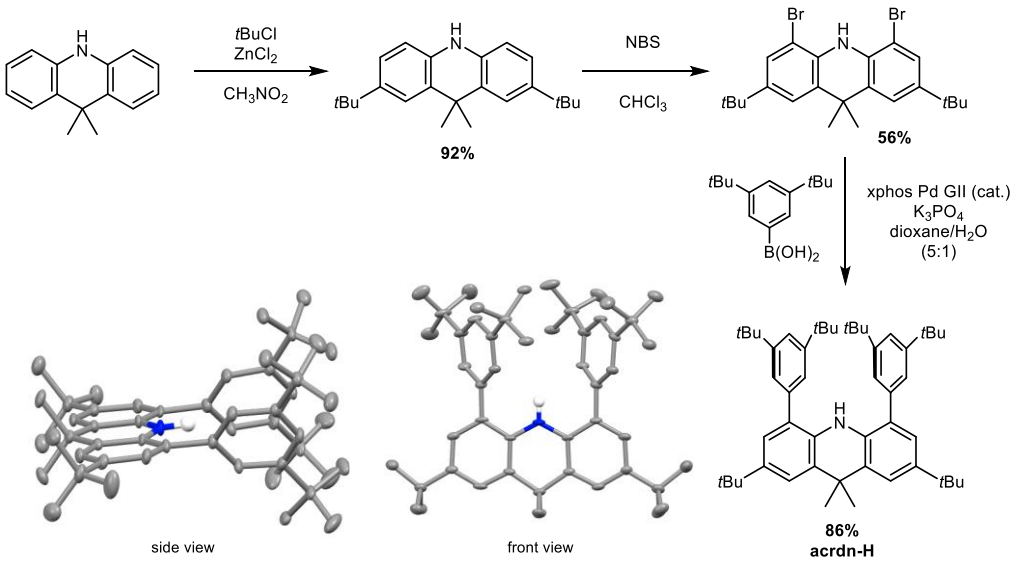

Figure 2.14 – Synthesis of **acrdn-H** and two perspectives of the X-ray crystal structure (hydrogen atoms except N-H are omitted for clarity).

One key feature that was gleaned from the X-ray crystal structure of **acrdn-H** is that the three rings of the acridine backbone are coplanar – contrary to the butterfly shape that the was adopted by **phenthz-H**. We believed this to be advantageous to the stabilization of an electron-deficient atom, as it would be more protected resting in the pocket of steric bulk. However, DFT calculations predicted that the placement of π-accepting moieties (e.g. -B, -BX_2, -P, -PX_2, -N) would lead to the previously seen butterfly structure of the backbone, inducing the pyramidalization of the amine. Since such an effect would cause the electron-deficient atom to pucker out the pocket of steric bulk, we were cognizant that this may be a potential pitfall.

The first electrophile that we added to the deprotonated **acrdn-H** was boron trichloride (Figure 2.15). This gave the borylene precursor **acrdn-BCl_2** with a characteristic singlet at 33 ppm

in the ^{11}B NMR spectrum. Initially, we were surprised to see two singlets in the ^{1}H NMR each integrating to 3H. However, considering the DFT calculations that predicted this species would adopt a butterfly structure, it became apparent to us that the two methyl groups in the acridine backbone are expected to be inequivalent.

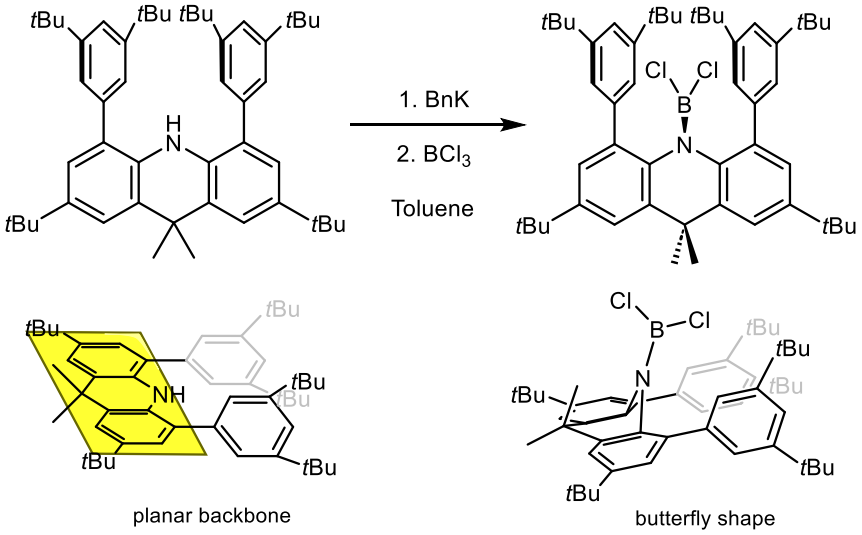

Figure 2.15 – Installation of a boron moiety to give **acrdn-BCl$_2$**. The product exhibits a "butterfly" conformation of the tricyclic backbone.

With the **acrdn-BCl$_2$** adduct in hand, we proceeded in the reduction to prepare the targeted borylene. The addition of KC_8 in diethyl ether led to the evolution of a deep red supernatant solution which was filtered, giving a new species by ^{11}B NMR as a broad signal at -11 ppm. GC-MS analysis under air-free conditions revealed that the mass of the major species corresponded to the loss of two chlorine atoms. Finally, rapid crystallization in ether occurred at -38 ^{o}C, allowing us to unambiguously determine the structure by X-ray crystallography to be the C-H activated borylene product, **acrdn-BH$_2$K** (Figure 2.16). While the first hydride clearly comes from aryl C-H activation of one of the flanking aromatic rings, the source of the second hydride can only be from

the ether solvent. In 1996, Power similarly demonstrated that the reduction of 2,6-$Mes_2C_6H_3BCl_2$ with KC_8 gives a product resulting from aryl C-C activation followed by hydride abstraction from the solvent.[60] The ^{11}B NMR chemical shift of -15 ppm in Power's example is in close agreement with our result.

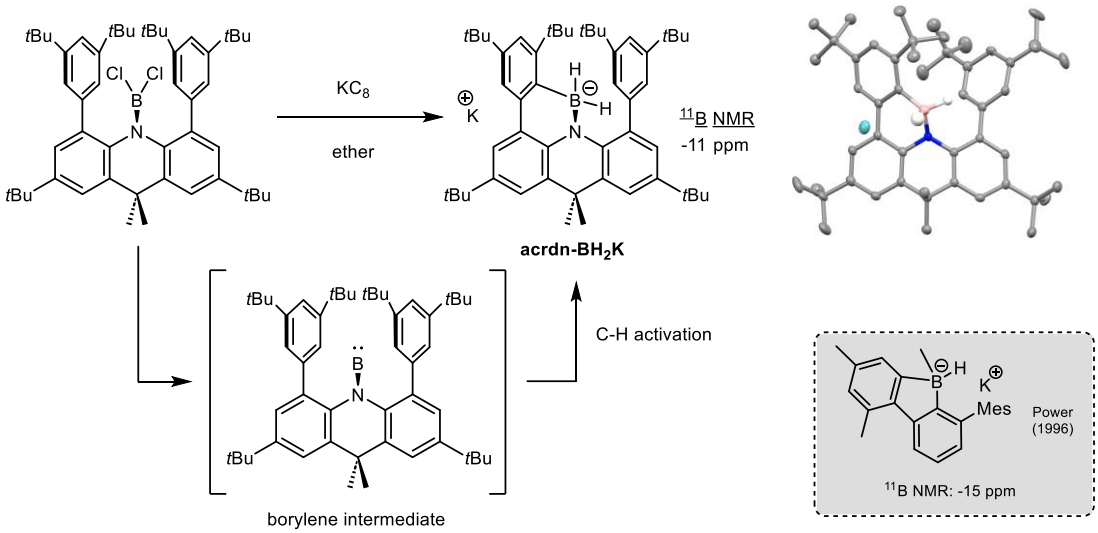

Figure 2.16 – Reduction of **acrdn-BCl_2** to give **acrdn-BH_2K** and X-ray crystal structure (hydrogen atoms except BH_2 are omitted for clarity).

The formation of **acrdn-BH_2K** is strong evidence that a borylene intermediate is formed. *Meta*-terphenyl borylenes and borylene surrogates are well-documented for their ability to undergo C-H and C-C activation of alkanes, alkenes, and arenes.[61,62,63] While we anticipated this possibility for the **acrdn-H** scaffold, the DFT-predicted butterfly effect suggested that the boron atom would perhaps be directed away from the nearby C-C and C-H bonds enough to evade their activation.

We wondered if we could intercept the decomposition of the intermediate borylene by adding a trapping agent, such as 2,3-dimethylbutadiene – the one used by Maringele to trap *i*Pr_2NB.[64] When we repeated the reduction of **acrdn-BCl_2** in the presence of 2,3-

dimethylbutadiene, we found that the rate of intramolecular C-H activation is too fast, making the transient borylene too short-lived to be trapped. This, however, was not too surprising since intramolecular reactions are known to occur much faster than intermolecular reactions.

Although the borylene was not a suitable target using this scaffold, we probed other reactivity modes using this motif. In attempts to add a nitrosyl moiety to the amine, we added excess isoamyl nitrite to **acrdn-H** in toluene (Figure 2.17). At room temperature, no reaction occurred. However, heating the solution to 70 ^{o}C overnight resulted in the clean formation of a new compound. Analysis of the ^{1}H and ^{13}C NMR spectra revealed a desymmetrization of the arene signals, along with a key signal in the carbonyl region of the ^{13}C NMR spectrum at 186 ppm. X-ray crystallographic analysis of the product revealed that the starting material underwent oxidative cleavage of one of the backbone *tert*-butyl fragments to give an asymmetric *p*-benzoquinonimine motif, **acrdn-N-O**. Such a reaction has literature precedent, as diphenylamine is known to undergo oxidation to give *N*-phenyl-*p*-benzoquinonimine,[65,66,67] which also contains a carbonyl signal in the ^{13}C NMR spectrum at 187 ppm. This result showed that even without functionalization of the amine, the aromatic backbone of **acrdn-H** can be oxidized.

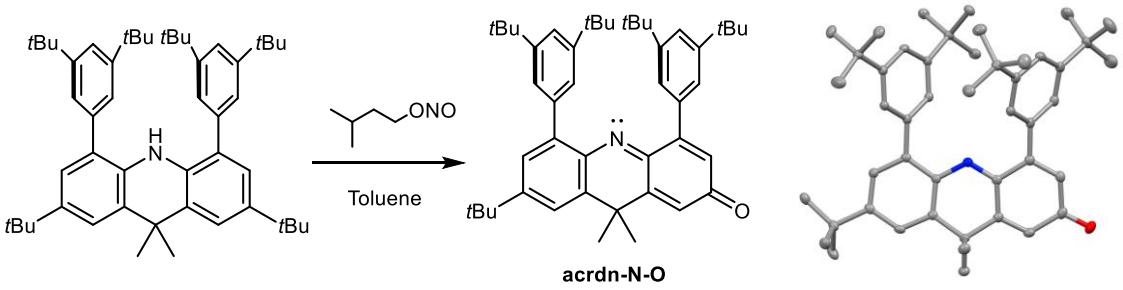

Figure 2.17 – Oxidative cleavage of a *tert*-butyl group to give **acrdn-N-O** and the X-ray crystal structure (hydrogen atoms are omitted for clarity).

We next wondered if **acrdn-H** would be suitable in stabilizing a carbon-based electrophile. A chloroiminium functionality was a desirable target, being a potential precursor to a range of novel species. For example, simple deprotonation of a chloroiminium salt would give the previously unknown chlorocarbene. Furthermore, subsequent chloride abstraction would afford a monocoordinated carbocation – the isoelectronic carbon-equivalent of a borylene. DFT calculations from our group have predicted such a species to have a singlet ground state (ΔE_{ST} = 39.9 kcal/mol). In pursuit of this new goal, various attempts at installing a carbon moiety were unsuccessful. For example, addition of methyl formate and ethyl formate to the deprotonated **acrdn-H** led to simple re-protonation, as the amide is a strong base. Other methods such as the addition of formaldehyde, carbon monoxide, acetic formic anhydride, and chloroform/KO^{t}Bu were also futile, as the protonated amine starting material was repeatedly obtained.

The most promising carbonylation candidate was carbon dioxide. Reaction of the deprotonated **acrdn-H** with CO_2 resulted in the formation of the carbamate, which was protonated to give **acdrn-CO_2H** (Figure 2.18). Unfortunately, efforts to reduce the carbamic acid to the formamide or the hemi-aminal were unsuccessful, as carbamate derivatives are prone to decarboxylation. The pseudo-dimeric nature of **acrdn-CO_2H** reveals the manner in which dimerization would occur given that a species such as a chlorocarbene could be stabilized by this scaffold. However, dimerization of a chlorocarbene to give an alkene would be less likely as it requires the two scaffolds to be brought even closer together than observed in **acrdn-CO_2H** – making it less likely for dimerization to occur.

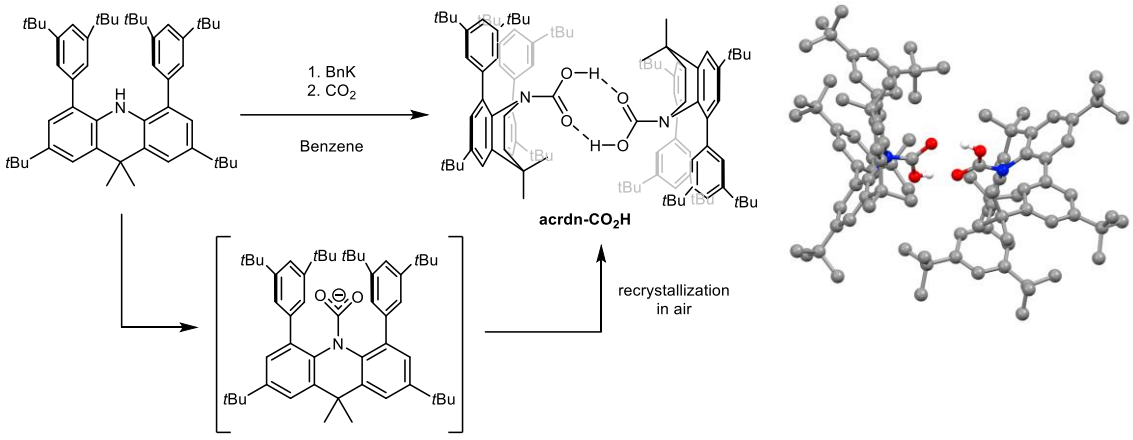

Figure 2.18 – Carbamation of **acrdn-H** with CO_2 to give **acrdn-CO_2H** and the X-ray crystal structure (hydrogen atoms except CO_2H are omitted).

2.6 Conclusion – Key Differences in Bulky Amine Scaffolds and Potential Future Applications

Overall, the synthesis, characterization, and functionalization of four bulky amine scaffolds has been discussed. With exception to the first scaffold, each of these scaffolds contain flanking di-*tert*-butylphenyl groups that serve to sterically protect an ensuing functional group such as a phosphinidene, borylene, or nitrene. The subtle differences in the tricyclic backbones of **carb-H**, **phenthz-H**, and **acrdn-H** influence the aryl centroid distances, and thus the degree of steric protection given by these flanking aromatic rings (Figure 2.19). This distance is notably longer in **carb-H** (6.301 Å) versus the two scaffolds featuring a 6-membered central ring – **phenthz-H** (4.960 Å) and **acdrn-H** (5.096 Å) which have a negligible difference of 2.70%.

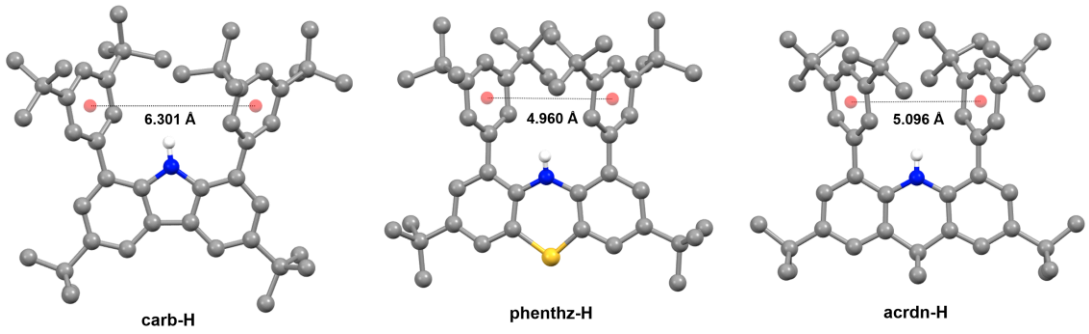

Figure 2.19 – X-ray crystal structures of **carb-H**, **phenthz-H**, and **acrdn-H** with centroid distances between flanking aryl groups.

Among these scaffolds, **phenthz-H** is a suitable choice of ligand in the absence of oxidizing/Lewis acidic species due to the incompatibility of phenothiazine derivatives with oxidants. However, we found **acrdn-H** to be the most robust candidate to stabilize species that are reactive but will not undergo aryl C-H activation. Although we found that even the *N*-functionalized **acrdn-H** has the tendency to undergo a butterfly fold leading to the puckering of the functional group, simple DFT calculations indicate that such a conformation is surprisingly disfavored for heavier p-block elements such as germanium, tin, antimony and bismuth. We believe that this is likely due to the stronger coordination of the π-electrons from the flanking aromatic rings with larger atoms. Furthermore, in the event of a butterfly fold, the resulting dimerization of species such as a germylyne radical or stibinidene has a strong probability of being reversible due to the steric repulsion of the bulky substituents (Figure 2.20).

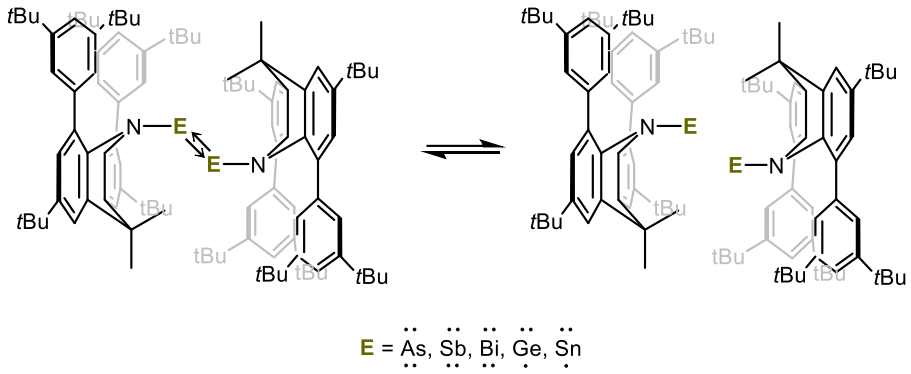

Figure 2.20 – Theorized reversible dimerization of **acrdn-E** subvalent species.

Finally, although these bulky amine scaffolds have only been discussed in the context of electronic stabilizers for main-group subvalent species, the potential for these large scaffolds may be seen in their use as ancillary amide ligands for transition metal catalysts.[68] The use of extremely bulky secondary amines as X-type ligands in catalysis is a critical area in organometallic chemistry and homogeneous catalysis. These ligands, particularly the deprotonated **phenthz-H** and **acrdn-H**, offer a wall of dendritic shielding, along with the desired electronic properties that secondary amines offer. These designs are especially attractive given their modular synthesis, allowing ease of tunability of steric bulk attached to the flanking aromatic rings.

2.7 Acknowledgements

I would like to thank Prof. Erik Romero for guidance and use of his GC-MS instrument. I would like to thank Francois Vermersch for the use of compound **pyrrol-H**. Lastly, I thank Glen Junor for his guidance with DFT calculations.

2.8 Experimental

2.8.1 General Considerations

All manipulations were performed using standard glovebox and Schlenk techniques unless otherwise noted. Glassware was dried in an oven overnight at 150 °C or flame-dried. Solvents were dried and degassed prior to use. Benzene, THF, diethyl ether, and n-pentane were freshly distilled over Na metal. Hexanes, dichloromethane, and chloroform were freshly distilled over CaH_2.

NMR Characterization: Deuterium-labeled solvents were purchased from Cambridge Isotope Laboratories. Multinuclear NMR data were recorded on a Varian INOVA 500 MHz, JEOL 400 MHz, or Bruker Avance 300 MHz at UCSD. Chemical shifts (δ) are reported in parts per million (ppm) and are referenced to residual solvent signals (^{1}H, ^{13}C). Coupling constants J are given in hertz (Hz). NMR multiplicities are abbreviated as follows: s = singlet, d = doublet, t = triplet, q = quartet, sext = sextet, sept = septet, m = multiplet, br = broad. All spectra were recorded at 298 K unless otherwise noted.

High-resolution mass spectrometry measurements were performed at the UC San Diego Mass Spectrometry Laboratory on an Agilent 6230 Accurate-Mass TOFMS spectrometer. Single crystal X-ray diffraction data were collected on Bruker Apex diffractometers using Mo-Kα radiation (λ = 0.71073 Å) or Cu-Kα radiation (λ = 1.54178 Å) at the UC San Diego Crystallography Facility. Absorption spectra were recorded on a JASCO V-630 spectrophotometer at ambient temperature.

2.8.2 Experimental Procedures

Synthesis of **pyrrol-PBr$_2$**

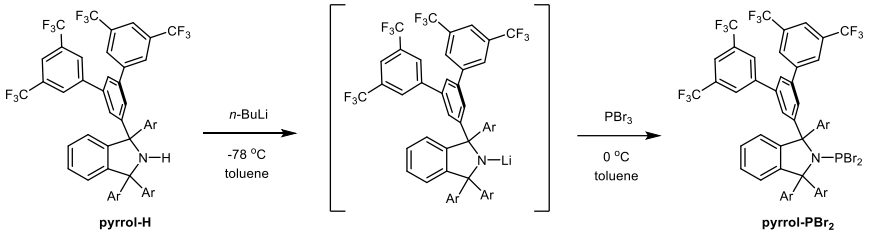

In a 50-mL Schlenk flask, **Pyrrol-H** (977 mg; 0.461 mmol; 1 equiv.) was dissolved in 15 mL of toluene and cooled to -78 ^{o}C. While stirring, 2.5 M *n*-butyllithium (0.20 mL; 0.507 mmol; 1.1 equiv.) in hexane was added dropwise. The cold bath was removed, and the reaction proceeded for another 6 hours as it warmed to room temperature and developed a dark brown color. The reaction was again cooled to 0 ^{o}C. A 0.79 M solution of PBr_3 (0.70 mL; 0.553 mmol; 1.2 equiv.) in benzene was slowly added. The cold bath was removed, and the reaction proceeded overnight, to give an orange murky suspension. Volatiles were removed and the product was dissolved in 15 mL DCM, leaving a clear precipitate. The suspension was filtered, and the product was extracted two more times with DCM. Upon removing volatiles and drying under vacuum, the product was afforded as an orange solid **pyrrol-PBr$_2$** (743 mg; 69.8% yield).

Reduction of **pyrrol-PBr$_2$**

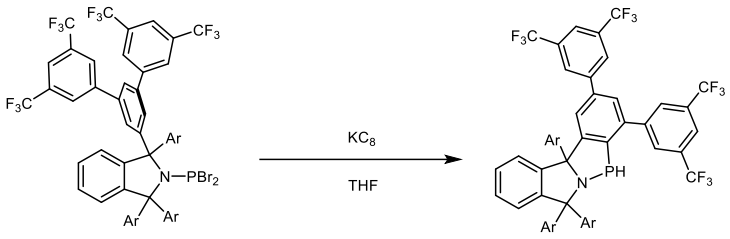

To a suspension of **pyrrol-PBr$_2$** (80 mg; 0.035 mmol; 1 equiv.) in THF was added solid KC_8 (13.5 mg; 0.10 mmol; 2.8 equiv.) in a J-Young NMR tube. The tube was inverted and placed into the NMR spectrometer, showing full conversion to **pyrrol-PH**. Yields were not calculated.

Synthesis of 3,6-di-*tert*-butylcarbazole

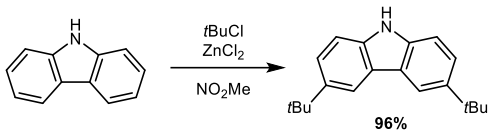

In a 250-mL Schlenk flask equipped with a stirrer bar, carbazole (3.30 g; 19.7 mmol; 1.0 equiv.) was dissolved in 10 mL nitromethane. Zinc dichloride (8.10 g; 56.0 mmol; 3 equiv.) was added as a slurry in 90 mL of nitromethane to give a tan pale brown slurry. The flask was purged with argon. Liquid *tert*-butyl chloride (6.5 mL; 56.0 mmol; 3 equiv.) was added over the course of about 5 minutes. The slurry was stirred at room temperature overnight. The next day, 100 mL of water was added, and the product was extracted with 60 mL of DCM three times. The combined extracts were washed once with water. The organic solution was dried with magnesium sulfate and filtered through a short bed of celite. Upon removal of volatiles, the product was afforded as a yellow powder (5.28 g; 95.7% yield).

Synthesis of 1,8-dibromo-3,6-di-*tert*-butylcarbazole

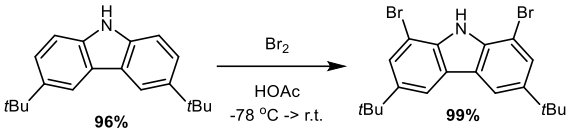

In a 250-mL RBF equipped with a stirrer bar, 3,6-di-*tert*-butylcarbazole (5.82 g; 20.8 mmol; 1 equiv.) was dissolved in 200 mL acetic acid, septum-capped, and covered with aluminum foil. The reaction contents were cooled to -78 °C. While stirring vigorously, liquid bromine (2.47 mL; 47.9 mmol; 2.3 equiv.) was slowly added through the septum with a needle. The reaction proceeded overnight at room temperature. The next day, volatiles were removed under vacuum, ensuring that the excess bromine was collected in a primary trap. The resulting yellow chalky solids were redissolved in 125 mL of ethyl acetate and washed four times with 1 M NaOH. The organic phase was dried with magnesium sulfate and filtered. Volatiles were removed under vacuum with heat to remove the residual acetic acid, affording a pale brown solid (8.97 g; 98.5% yield).

Synthesis of 3,5-di-*tert*-butylphenylboronic acid

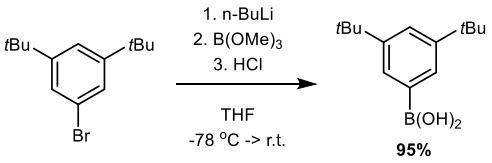

In a 250-mL Schlenk flask equipped with a stirrer bar, 3,5-di-*tert*-butylbromobenzene (5.00 g; 18.6 mmol mmol; 1 equiv.) was dissolved in 75 mL of dry THF and cooled to -78 °C. A 2.5 M solution of *n*-butyllithium (7.9 mL; 19.7 mmol; 1.06 equiv.) in hexanes was added while vigorously stirring. After 30 minutes, liquid trimethyl borate (2.2 mL; 19.7 mmol; 1.06 equiv.) was added, causing most of the precipitates to dissolve. The cold bath was removed, and the

reaction was stirred at room temperature for 2 hours. Then, 25 mL of 6M HCl was added to quench the reaction. After transferring to a separatory funnel, the product was extracted three times with diethyl ether. The combined organic phases were dried with magnesium sulfate, filtered, and evaporated until about 10 mL solvent was left. The solution was transferred to another flask via cannula filtration, leaving behind a white salt. An additional 10 mL of ether was used to extract the product through the cannula filter. Volatiles were removed from the filtrate, leaving the product as a chalky and sticky yellow solid (3.42 g; 78.6% yield). Note the purity of this product is difficult to determine as there seemed to be some oligomeric impurities that have overlapping signals in the proton NMR spectrum. Thus, when used in the next step, a significant excess was typically used.

Synthesis of **carb-H**

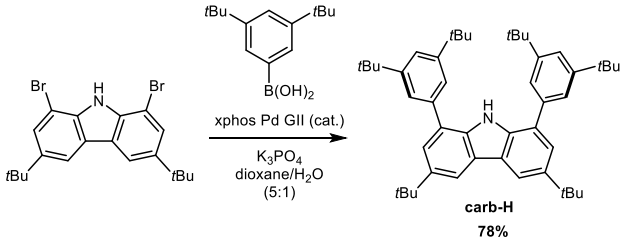

In a 100 mL RBF equipped with a stirrer bar, 1,8-dibromo-3,6-di-*tert*-butylcarbazole (13.84 g; 8.79 mmol; 1.0 equiv.), 3,5-di-*tert*-butylphenylboronic acid (8.23 g; 35.14 mmol; 4.0 equiv.), anhydrous potassium phosphate (7.52 g; 35.4 mmol; 4.0 equiv.), and xphos Pd GII catalyst (173 mg; 0.22 mmol; 0.025 equiv.) were suspended in 70 mL of a 1,4-dioxane/water (5:1) mixture which had been sparged with argon. The mixture was heated to 85 ^{o}C with stirring, leading to the dissolution of the solids into a brown solution. After 4 hours, the reaction was allowed to cool to room temperature and transferred to a separatory funnel using an additional 20 mL of diethyl ether. The aqueous layer was removed and extracted twice more with diethyl ether. The combined

organic phases were washed twice with 5 mL of water. The clearing of emulsions during these final washes took periods of up to 1.5 hours – however, this was necessary to maximize yield and purity. The organic phase was dried with magnesium sulfate and filtered. Removal of volatiles resulted in a thick brown oil which was dried overnight. Addition of 40 mL of methanol followed by sonication led to the precipitation of the product as a white solid. The product was filtered, and the sonication process was repeated with 20 mL of methanol. The product was collected and washed with methanol and dried under vacuum to give **carb-H** as an off-white powder (5.45 g; 94.5% yield).

Synthesis of **carb-PCl_2** and **carb-PBr_2**

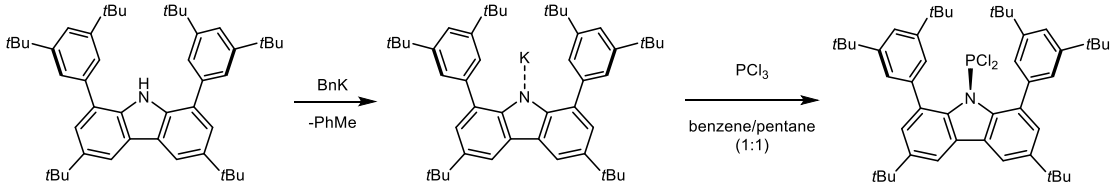

In a 25-mL Schlenk flask equipped with a stirrer bar, **carb-K** (297.5 mg; 0.4286 mmol; 1 equiv.) (prepared from the quantitative deprotonation of **carb-H**), was dissolved in 8 mL of a 1:1 ratio of pentane/benzene and cooled to -78 ^{o}C, giving a mostly frozen slurry. Liquid phosphorus trichloride (41 µL; 0.472 mmol; 1.1 equiv.) was added and the suspension was stirred overnight as it warmed to room temperature. The next day, the solids were filtered off using cannula filtration. The product was extracted three more times with pentane. Volatiles were removed and the product was dried, affording the product as a yellow solid (241.1 mg; 74.0% yield).

carb-PBr_2 was synthesized in an identical fashion and scale to **carb-PCl_2** with the only change being the use the PBr_3 instead of PCl_3, to afford the product as a yellow solid (233.6 mg; 63.9% yield).

Reduction of **carb-PCl_2**

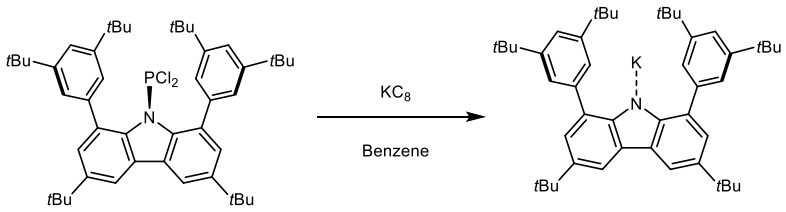

carb-PCl_2 (108 mg; 0.142 mmol; 1 equiv.) was dissolved in 1 mL of C_6D_6. Solid KC_8 (43.2 mg; 0.320 mmol; 2.25 equiv.) was added and the slurry was swirled for 10 minutes. Leftover KC_8 and remaining solids were filtered through a fritted pipet, into an NMR tube, as a deep fluorescent green solution – matching the color of **carb-K**. The formation of **carb-K** was confirmed by ^{1}H NMR.

Alternatively, **carb-PCl_2** (40 mg; 0.053 mmol) was eluted through a column of KC_8 (radius = 2 mm; height = 2 cm) with C_6D_6 into an NMR tube, again giving **carb-K** as confirmed by ^{1}H NMR.

Reaction of **carb-PCl_2** with TMS-N_3

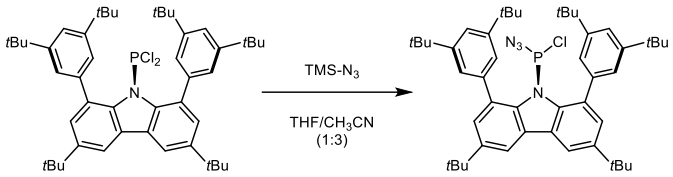

In a J-Young NMR tube, **carb-PCl_2** (77 mg; 0.102 mmol; 1 equiv.) and trimethylsilyl azide (30 µL; 0.23 mmol; 2.24 equiv.) was dissolved in 4 mL of a mixture of THF/acetonitrile (1:3). The contents were sonicated overnight at 50 ^{o}C, revealing a new signal by ^{31}P NMR at 123 ppm.

Synthesis of 3,7-di-*tert*-butylphenothiazine

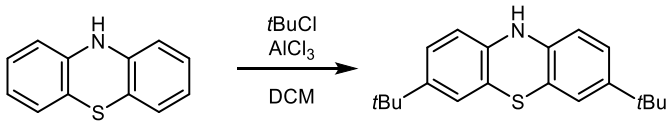

Phenothiazine (10.0 g; 50.0 mmol; 1 equiv.) and aluminum trichloride (14.05 g; 105.4 mmol; 2.1 equiv.) were placed into a 300 mL RBF with a stirrer bar. The flask was purged with argon. 150 mL of degassed DCM was added to the flask which was subsequently cooled down to 0 ^{o}C with a constant flow of argon. *Tert*-butyl chloride (23.2 g; 251.0 mmol; 5 equiv.) was slowly added to the stirred suspension over a period of 20 minutes via syringe. The reaction became a dark purple suspension. After 1 hour of stirring at room temperature, the reaction contents were poured into 1 L of water and stirred for 5 minutes. Sodium acetate (22.5 g) was added, and the product was extracted four times each with 100 mL of DCM. The organic phase was dried with sodium sulfate. After filtration and removal of volatiles, 300 mL of hexane was used to triturate the mixture, during which a pale pink/brown solid precipitated out. These solids were collected on a frit and washed with hexanes and dried in an RBF. The mixture was then triturated with methanol to remove the deep purple species. Note: this purple species gives extremely broad signals that

span the normal ^{1}H NMR range and is believed to be an oxidized byproduct of the reaction. Silica gel column chromatography was employed using a gradient from 1:6 EtOAc/hexanes to 100% EtOAc, eluting the product (R_f = 0.69) as a white solid (2.94 g; 18.9% yield).

Note: The product slowly oxidizes in air in the solid state and even more rapidly in solution to give the aforementioned purple paramagnetic species.

Synthesis of 1,9-dibromo-3,7-di-*tert*-butylphenothiazine

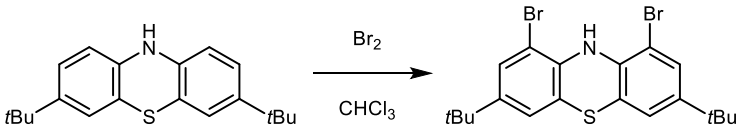

3,7-di-*tert*-butylphenothiazine (2.76 g; 8.86 mmol; 1 equiv.) was dissolved in 120 mL of dry and degassed chloroform and cooled to 0 ^{o}C. Liquid bromine (1.59 mL; 30.9 mmol; 3.49 equiv.) was slowly added while stirring. The reaction was stirred for 4 hours as it warmed to room temperature. The contents were cooled again to 0 ^{o}C and quenched with hydrazine monohydrate. The solution was washed with saturated sodium carbonate. The aqueous phase was extracted twice with 20 mL of DCM. The combined organic phases were washed once more with brine and dried over magnesium sulfate. After decantation and removal of volatiles, the product was purified via silica gel plug using hexanes, to afford the product as a tan brown solid (2.53 g; 60.7% yield).

Synthesis of **phenthz-H**

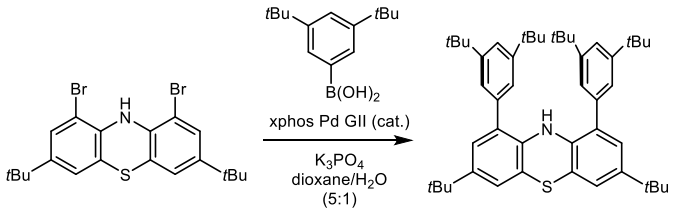

To a 100-mL Schlenk flask equipped with a stirrer bar was added 1,9-dibromo-3,7-di-*tert*-butylphenothiazine (1.94 g; 4.13 mmol; 1 equiv.), 3,5-di-*tert*-butylphenylboronic acid (3.38 g; 14.4 mmol; 3.5 equiv.), anhydrous potassium phosphate (3.07 g; 14.4 mmol; 3.5 equiv.), and xphos Pd GII catalyst (81 mg; 0.103 mmol; 0.025 equiv.). The contents were suspended in 50 mL of a degassed 1,4-dioxane/water (5:1) mixture and heated to 80 ^{o}C resulting in the dissolution of the solids concomitant with a new salt-like precipitate within 2 hours of heating. After stirring overnight, TLC revealed full conversion to a new compound with a higher R_f of 0.84 (versus 0.76 for the starting material) in 9:1 hexanes/EtOAc. This new spot absorbed both 365 and 254 nm UV light, while the starting material only absorbed 254 nm light. The mixture was suspended in 30 mL of water and extracted three times with ether. The combined ether extracts were washed once with water. The organic phase was dried with sodium sulfate, decanted, and dried under vacuum. Addition of 30 mL of methanol with sonication resulted in the precipitation of the product, which was filtered and washed with methanol. After drying under vacuum, the product was obtained as a grey powder (2.72 g; 95.9% yield). Single crystals for X-ray analysis were grown by slow evaporation from an ether solution.

Methylation of **phenthz-H**

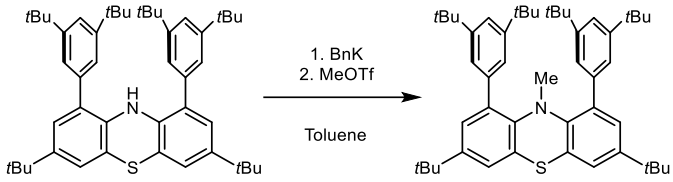

To a 25-mL Schlenk flask equipped with a stirrer bar was added **phenthz-H** (164 mg; 0.238 mmol; 1 equiv.) and benzyl potassium (47 mg; 0.36 mmol; 1.5 equiv.). The flask was cooled to -78 ^{o}C followed by the addition of 10 mL of toluene. After stirring for 4 hours at room temperature, methyl triflate (39.5 µL; 0.361 mmol; 1.5 equiv.) was added. After stirring overnight, the solution was washed twice with water and once with brine. The organic phase was dried with sodium sulfate, decanted, and dried. ^{1}H and ^{13}C NMR analysis of the crude product revealed the formation of the N-methylated product.

Synthesis of 2,7-di-*tert*-butyl-9,10-dihydro-9,9-dimethylacridine

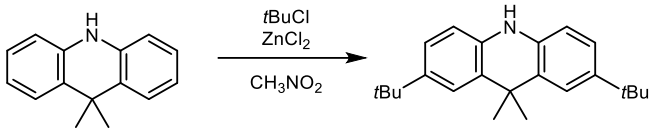

In a 50-mL Schlenk flask equipped with a stirrer bar, 9,10-dihydro-9,9-dimethylacridine (1.00 g; 4.78 mmol; 1 equiv.) and zinc dichloride (1.954 g; 14.34 mmol; 3 equiv.) were dissolved in 30 mL of nitromethane. After purging the headspace with argon, *tert*-butyl chloride (2.34 mL; 21.5 mmol; 4.5 equiv.) was added and the reaction was stirred overnight. Upon adding 35 mL of water, a green color emerged. The product was extracted three times with DCM. The extracts were dried with sodium sulfate and pushed through a short plug of silica gel using a 3:2 ratio of hexane/DCM. The product was dried under vacuum to afford a brown solid (1.42 g; 92.1% yield).

Synthesis of 4,5-dibromo-2,7-di-*tert*-butyl-9,10-dihydro-9,9-dimethylacridine

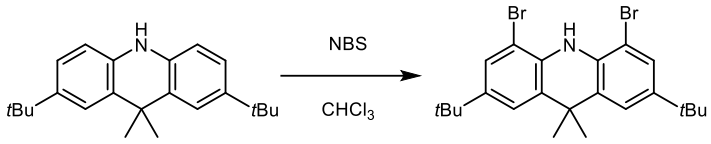

In a 100-mL Schlenk flask equipped with a stirrer bar, 2,7-di-*tert*-butyl-9,10-dihydro-9,9-dimethylacridine (1.37 g; 4.26 mmol; 1 equiv.) was dissolved in 60 mL of dry chloroform. The headspace was purged with argon for 10 minutes as it was cooled to 0 ^{o}C. With a positive pressure of argon, solid *N*-bromosuccinimide (1.59 g; 8.94 mmol; 2.1 equiv.) was added to the stirred solution. After 30 minutes, the cold bath was removed, and the reaction was stirred until the starting material and monobrominated species were consumed (monitored by TLC) – usually about 4 hours at room temperature. The reaction was then quenched with aqueous sodium thiosulfate. The product was extracted three times with DCM, and the organic phase was washed three times with water. The organic phase was dried with sodium sulfate, decanted, and evaporated. The crude product was then purified by silica gel column chromatography using a solvent gradient from pure hexane to pure EtOAc. After evaporation of solvent, the product was obtained as a white powder (1.15 g; 56.4% yield).

Synthesis of **acrdn-H**

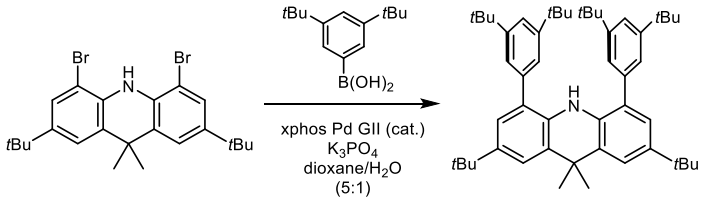

In a 50-mL RBF equipped with a stirrer bar, 4,5-dibromo-2,7-di-*tert*-butyl-9,10-dihydro-9,9-acridine (519 mg; 1.08 mmol; 1 equiv.), 3,4-di-*tert*-butylphenylboronic acid (1.04 g; 4.44 mmol; 4.1 equiv.), anhydrous potassium phosphate (920 mg; 4.33 mmol; 4 equiv.) and xphos Pd

GII catalyst (21.3 mg; 0.027 mmol; 0.025 equiv.) were suspended in 15 mL of a degassed 1,4-dioxane/water (5:1) mixture. The contents were heated to 80 ^{o}C and stirred overnight. Upon cooling to room temperature, 20 mL of water was added, and the reaction contents were extracted four times with diethyl ether. The combined organic phases were washed twice with minimal amounts of water. After drying the organic phase with sodium sulfate, volatiles were removed, and the product was precipitated with methanol via sonication. After filtration and washing with ample methanol and 0.8 mL of thawing pentane, the product was afforded as a white solid (651 mg; 86.1% yield). Single crystals for X-ray analysis were grown from slow evaporation of a pentane solution.

Synthesis of **acrdn-BCl$_2$**

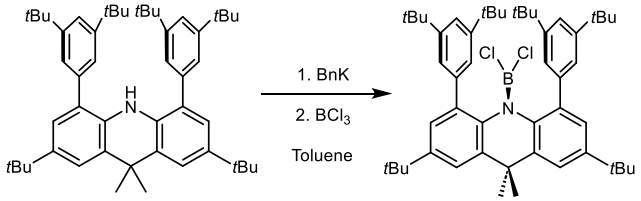

In a 50-mL pressure Schlenk equipped with a stirrer bar, **acrdn-H** (433 mg; 0.620 mmol; 1 equiv.) and benzyl potassium (95.3 mg; 0.732 mmol; 1.18 equiv.) were dissolved in 11 mL of dry toluene and stirred overnight at room temperature. The solution was then cooled to -78 ^{o}C and a 1 M solution of boron trichloride (0.81 mL; 0.81 mmol; 1.3 equiv.) in heptane was added while vigorously stirring. After stirring overnight at room temperature, the reaction produced a clear precipitate. After filtration and rinsing with hexanes, solvent was removed and the contents were dried under vacuum leaving behind the product as a white solid (289 mg; 60.0% yield).

Synthesis of **acrdn-BH_2K**

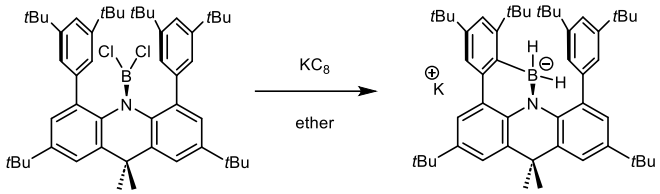

In a 50-mL pressure Schlenk equipped with a stirrer bar, **acrdn-BCl_2** (40 mg; 0.051 mmol; 1 equiv.) was dissolved in 7 mL of dry diethyl ether and cooled to -30 ^oC. Solid KC_8 (~40 mg; excess) was added and the reaction was stirred at room temperature overnight. The next day, excess KC_8 was filtered off and the deep red filtrate was collected in a J-Young tube for NMR analysis. The contents were placed in the glovebox freezer, resulting in the rapid formation of red crystals which were analyzed via X-ray crystallography.

Synthesis of **acrdn-N-O**

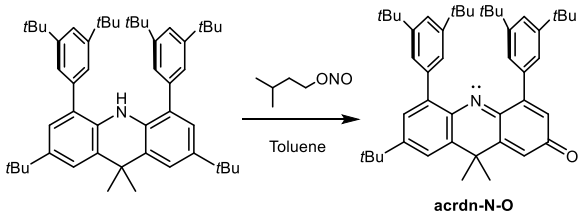

In a 50-mL pressure Schlenk equipped with a stirrer bar, **acrdn-H** (~20 mg; 0.025 mmol; 1 equiv.) was dissolved in toluene. Under a flow of argon, 6 drops (excess) of isoamyl nitrite were added. The reaction was stirred overnight at 70 ^oC. The crude product was purified via silica gel column chromatography using a solvent gradient from pure hexane to pure EtOAc, in which the product eluted with the latter solvent. After NMR analysis in deuterated benzene, orange crystals suitable for X-ray crystallography formed over the course of 11 days in the NMR tube.

Synthesis of **acrdn-CO_2H**

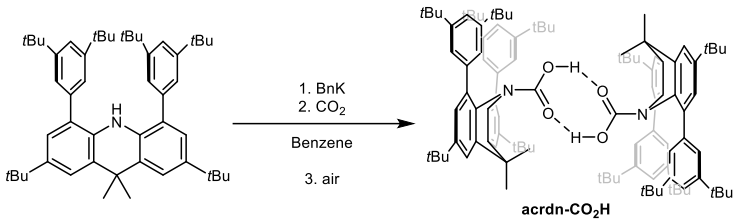

In a J-Young NMR tube, **acrdn-H** (130 mg; 0.186 mmol; 1 equiv.) and benzyl potassium (29.6 mg; 0.227 mmol; 1.2 equiv.) were dissolved in 1 mL of deuterated benzene. After 1.5 hours of sonication, the contents were frozen at -78 ^{o}C and the headspace was evacuated. The headspace was filled with dry CO_2 to a pressure of 15 psig. After two more pump/refill cycles, the reaction was thawed and allowed to sit overnight at room temperature. The contents were evaporated to near dryness and diethyl ether was added in open air before reattaching the cap with small opening. Colorless crystals suitable for X-ray crystallography formed over the course of 20 days.

2.8.3 NMR Data

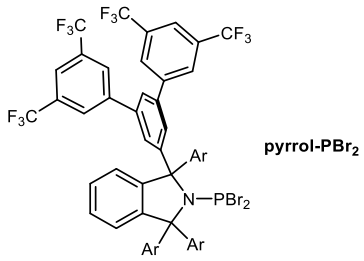

$^{31}P\{^{1}H\}$ NMR (121 MHz) in C_6D_6/DCM (1:1)

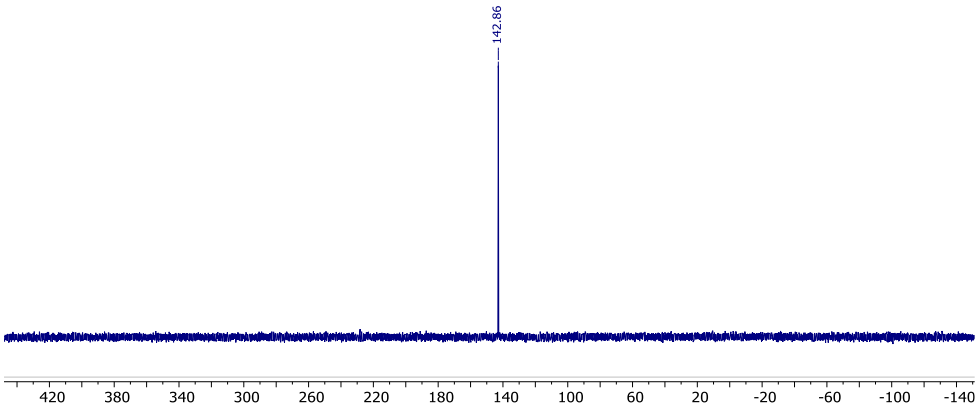

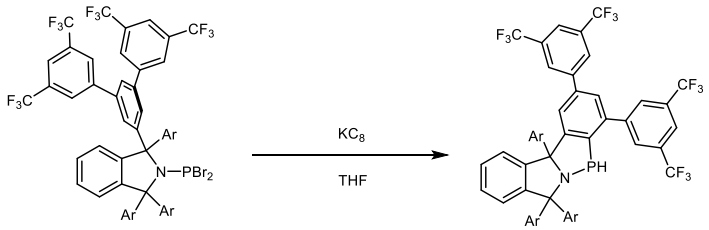

^{31}P NMR (121 MHz) in THF

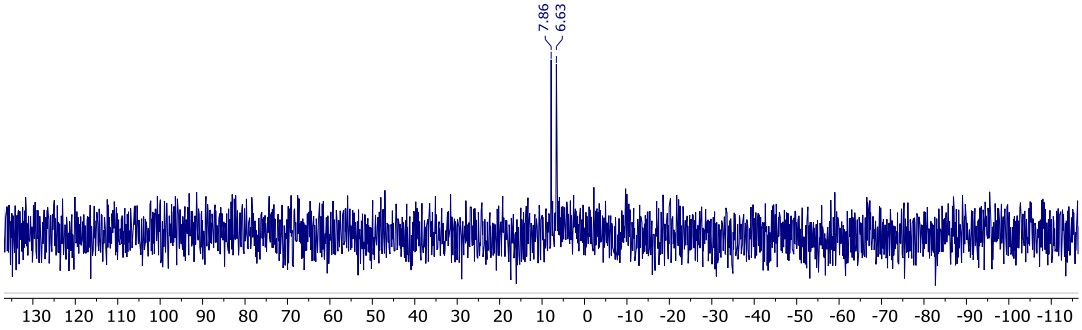

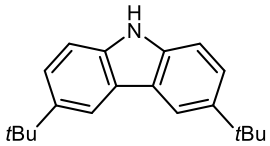

^{1}H NMR (300 MHz) in C_6D_6

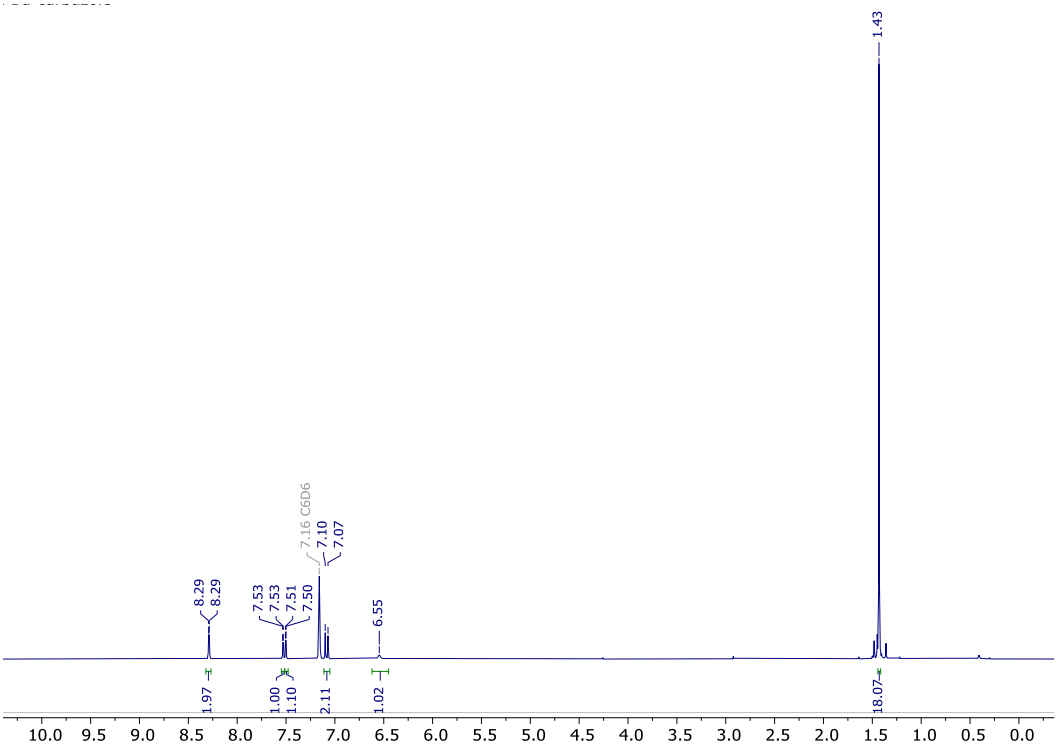

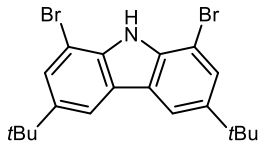

^{1}H NMR (300 MHz) in C_6D_6

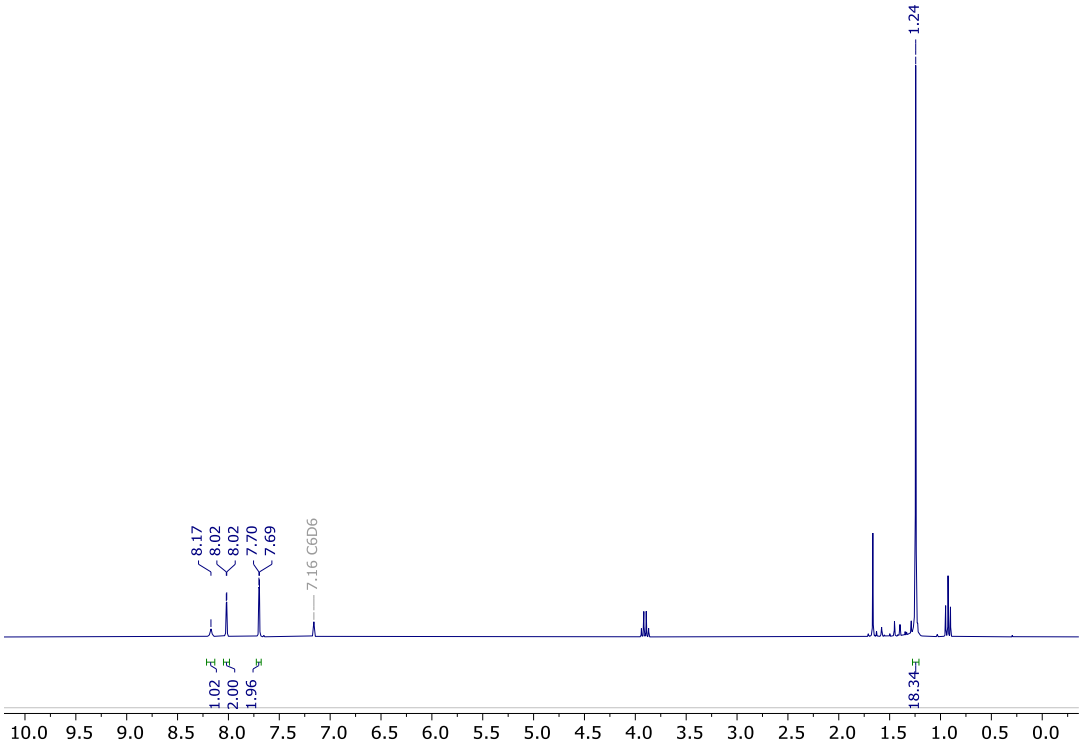

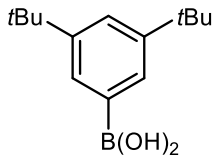

^{1}H NMR (300 MHz) in C_6D_6

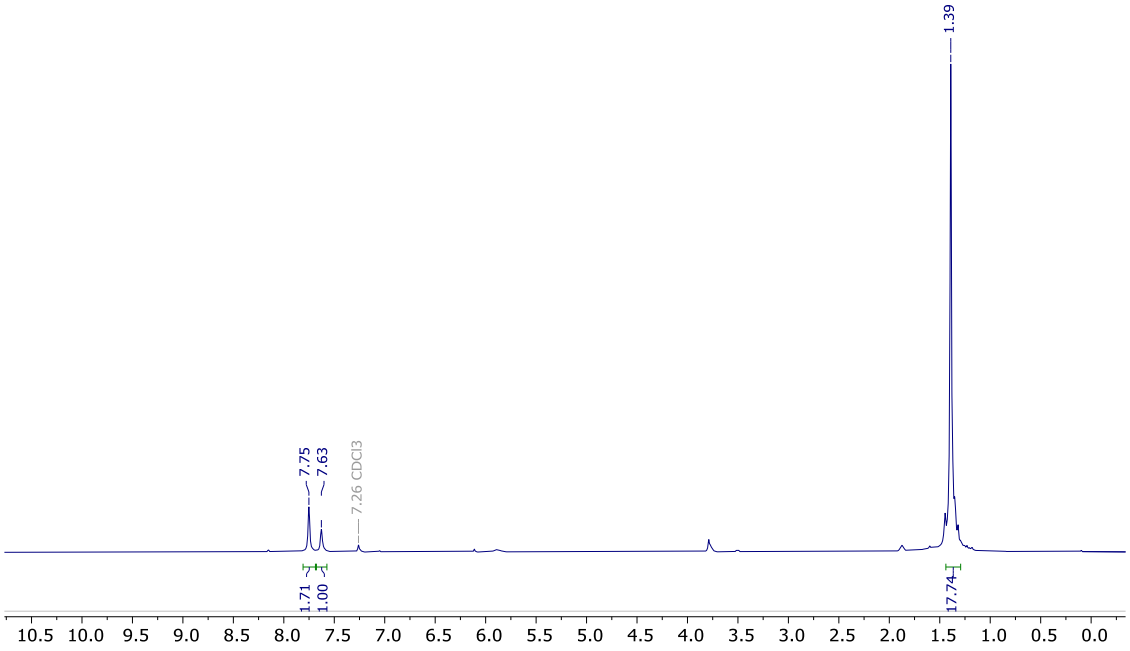

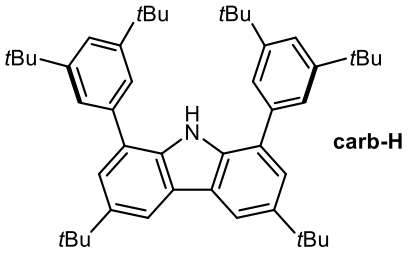

^{1}H NMR (300 MHz) in C_6D_6

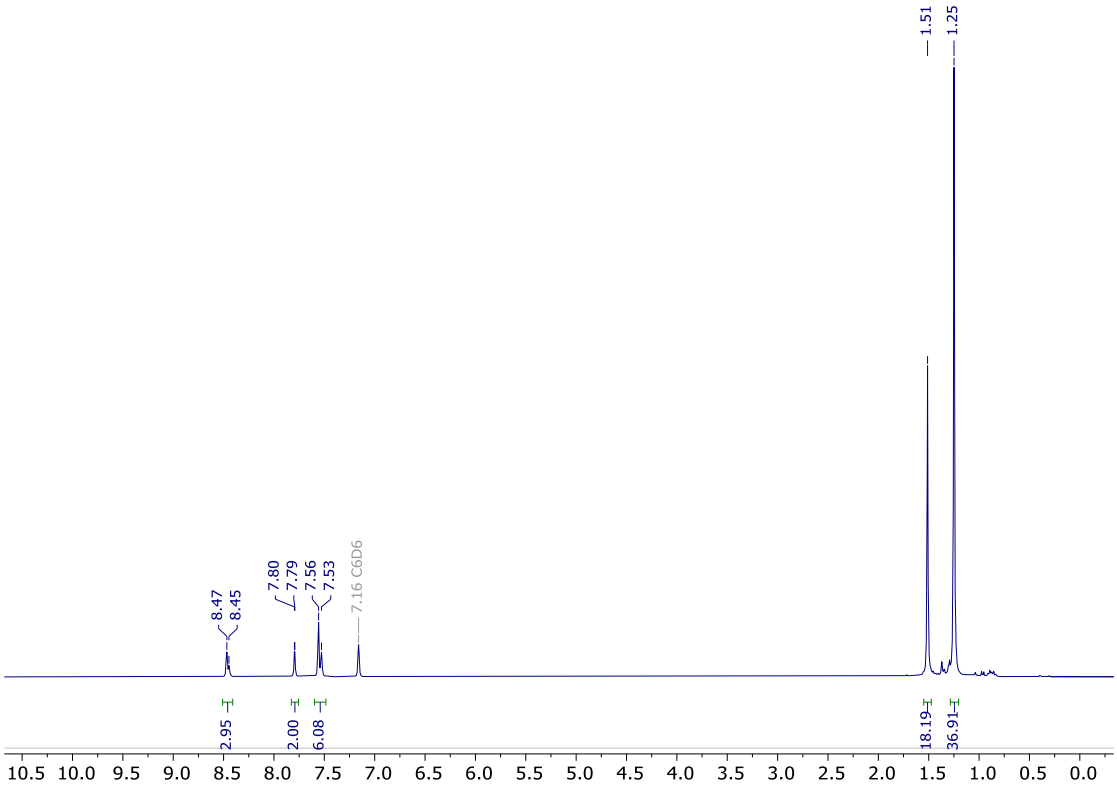

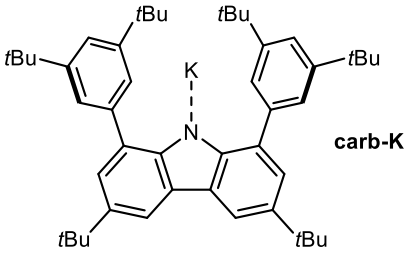

^{1}H NMR (300 MHz) in C_6D_6

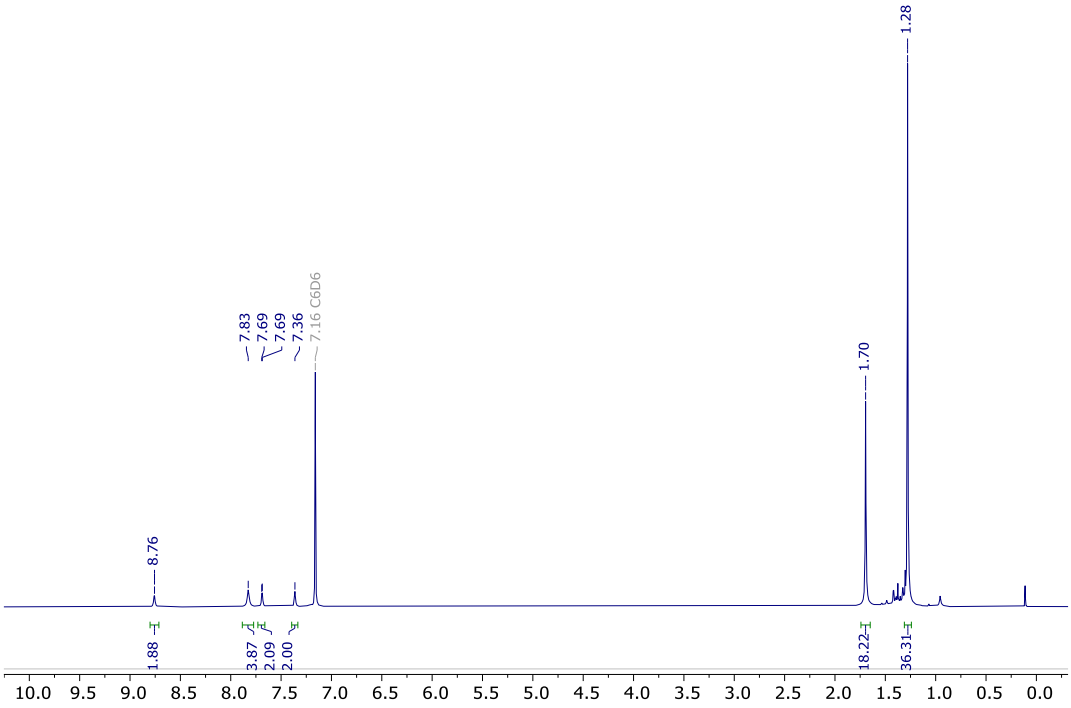

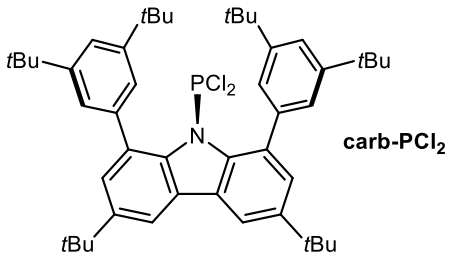

^{1}H NMR (300 MHz) in C_6D_6

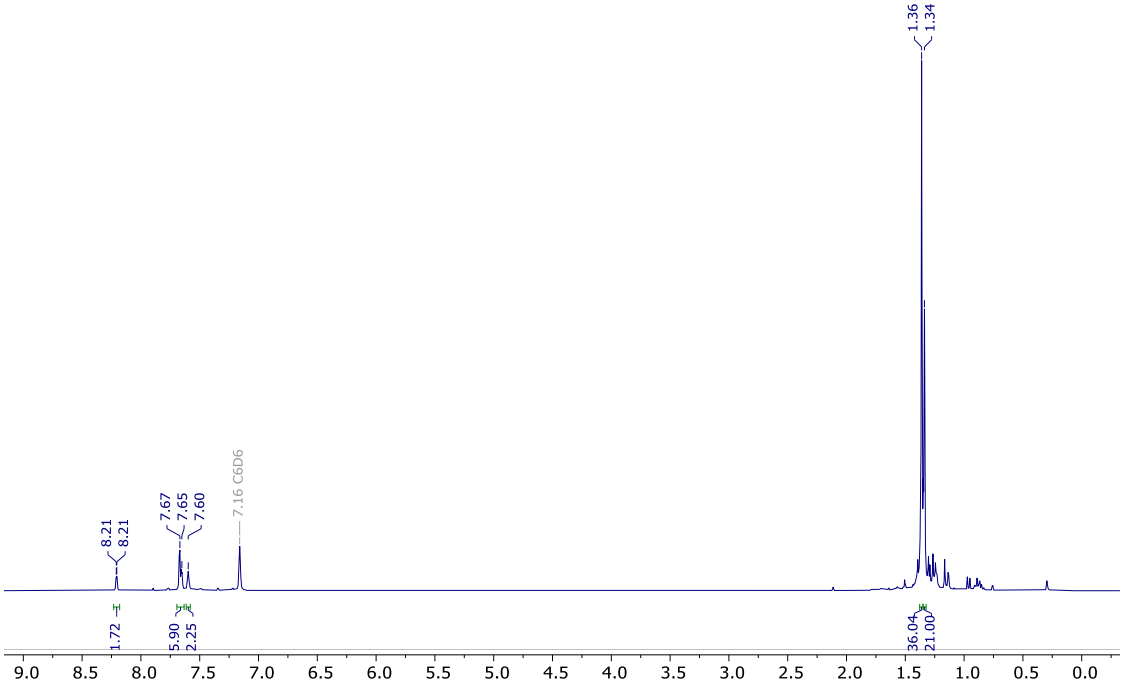

$^{31}P\{^{1}H\}$ NMR (121 MHz) in C_6D_6

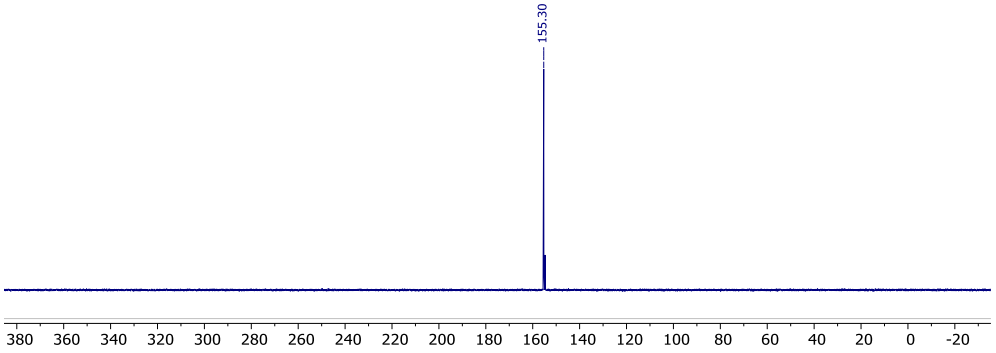

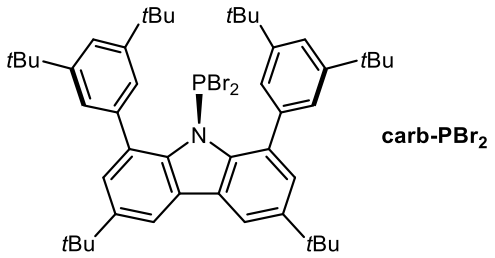

carb-PBr$_2$

^{1}H NMR (300 MHz) in C_6D_6

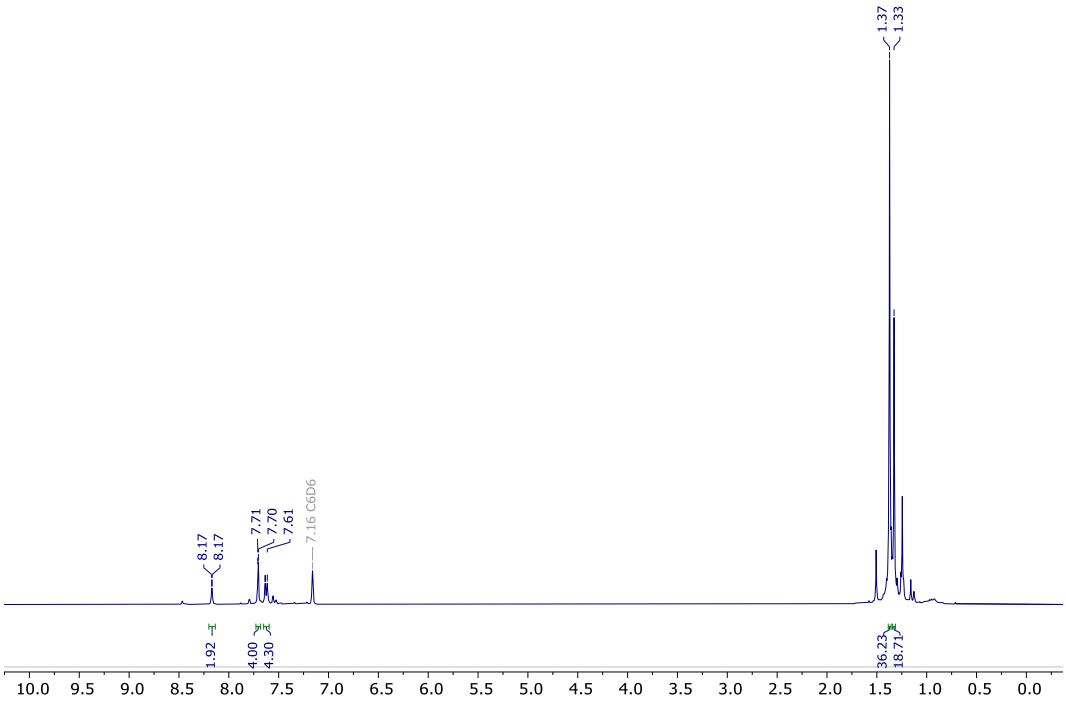

^{31}P{^{1}H} NMR (121 MHz) in C_6D_6

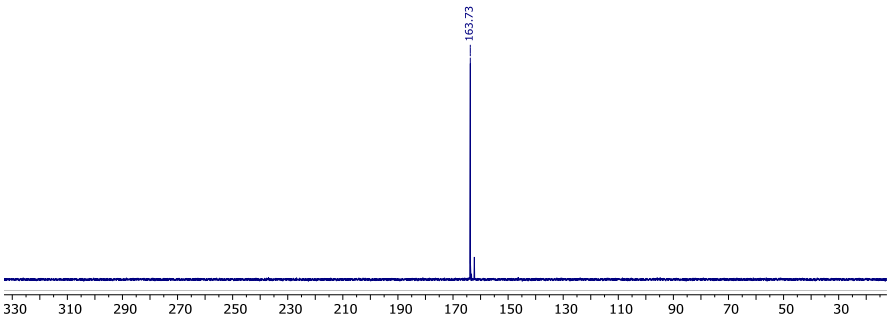

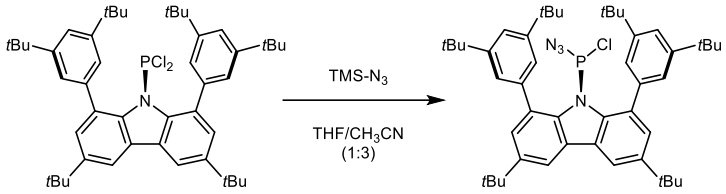

$^{31}P\{^{1}H\}$ NMR (121 MHz) in 1:3 THF/acetonitrile

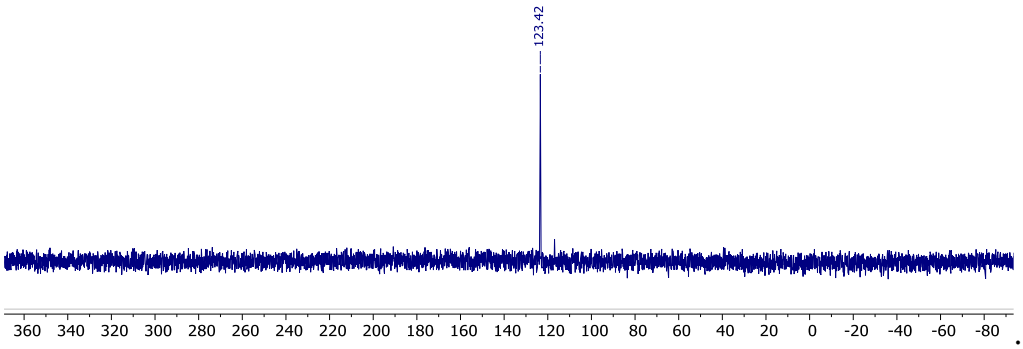

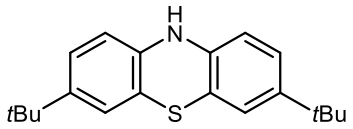

^{1}H NMR (300 MHz) in DMSO-d6

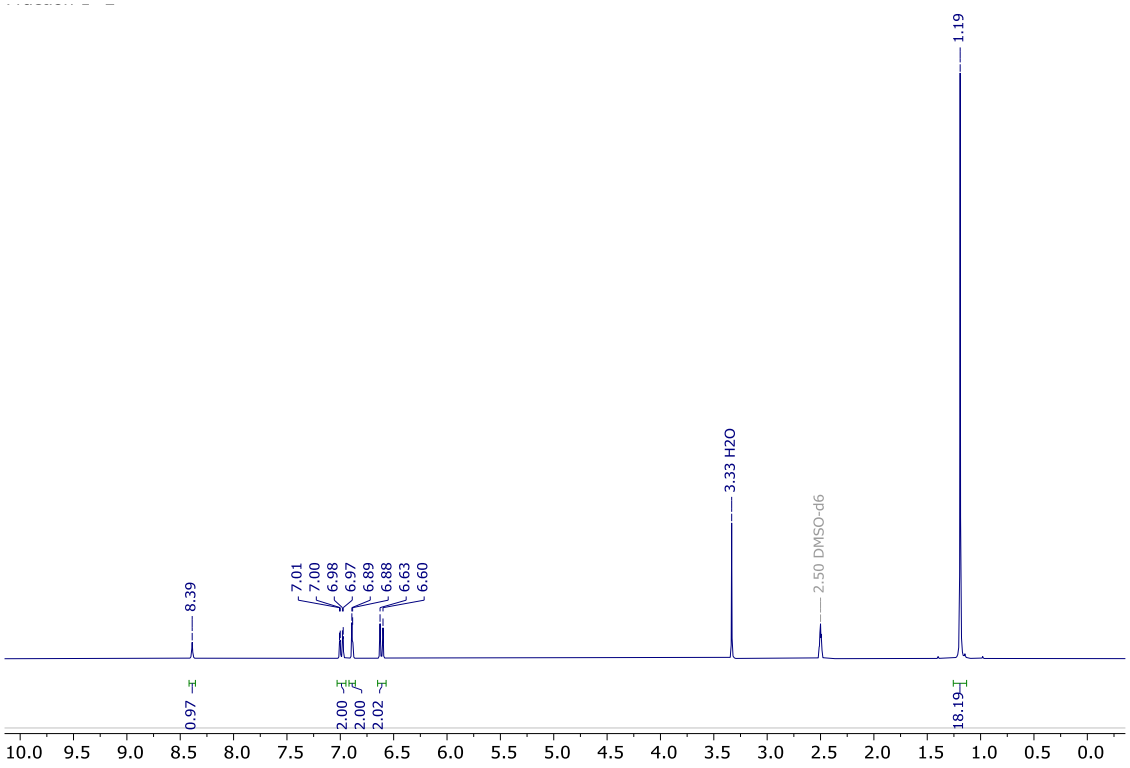

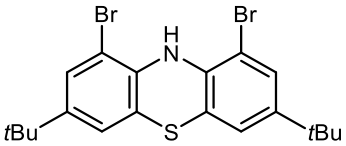

^{1}H NMR (400 MHz) in C_6D_6

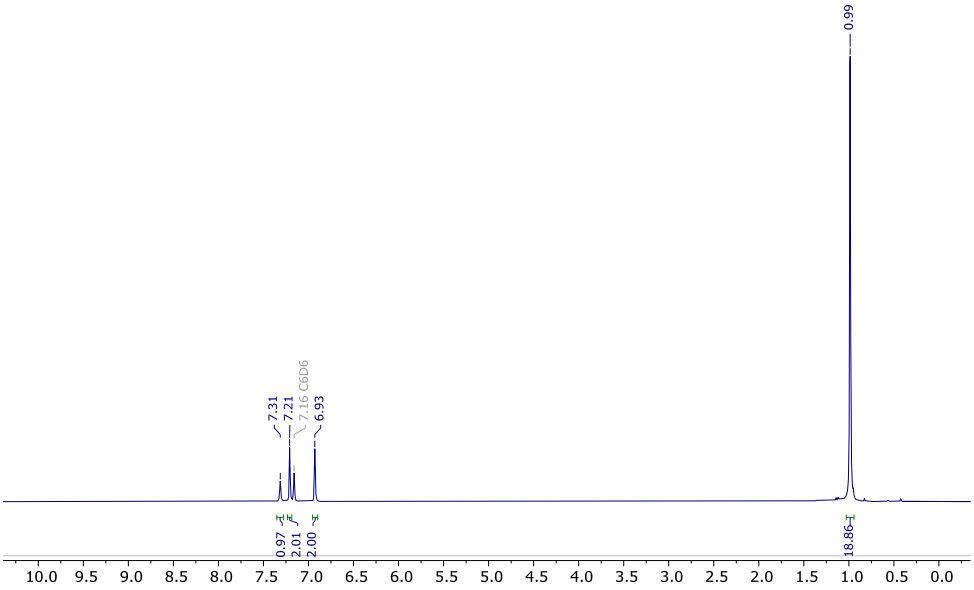

^{13}C{^{1}H} NMR (101 MHz) in C_6D_6

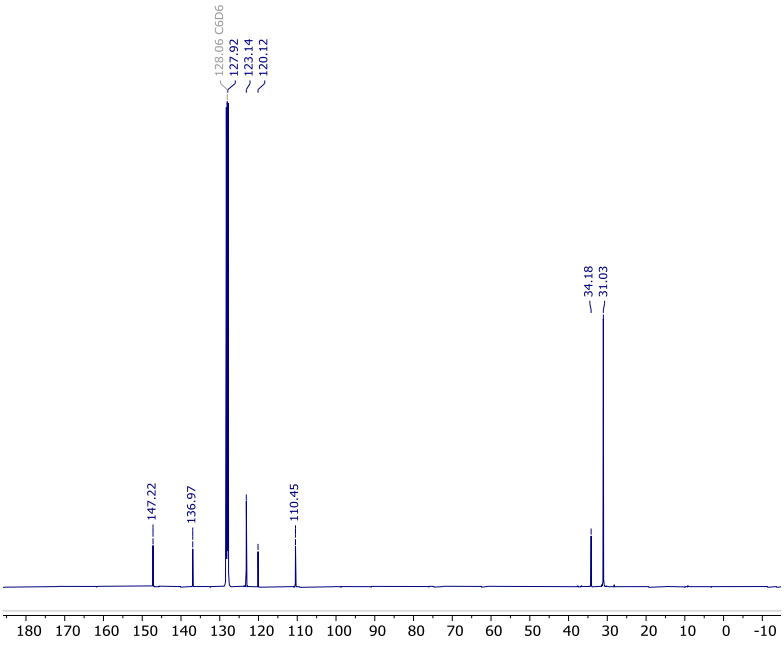

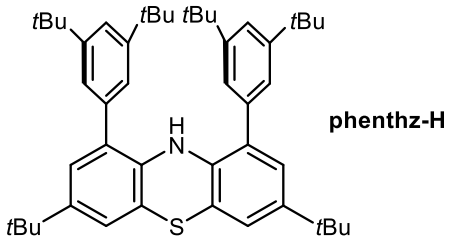

^{1}H NMR (500 MHz) in C_6D_6

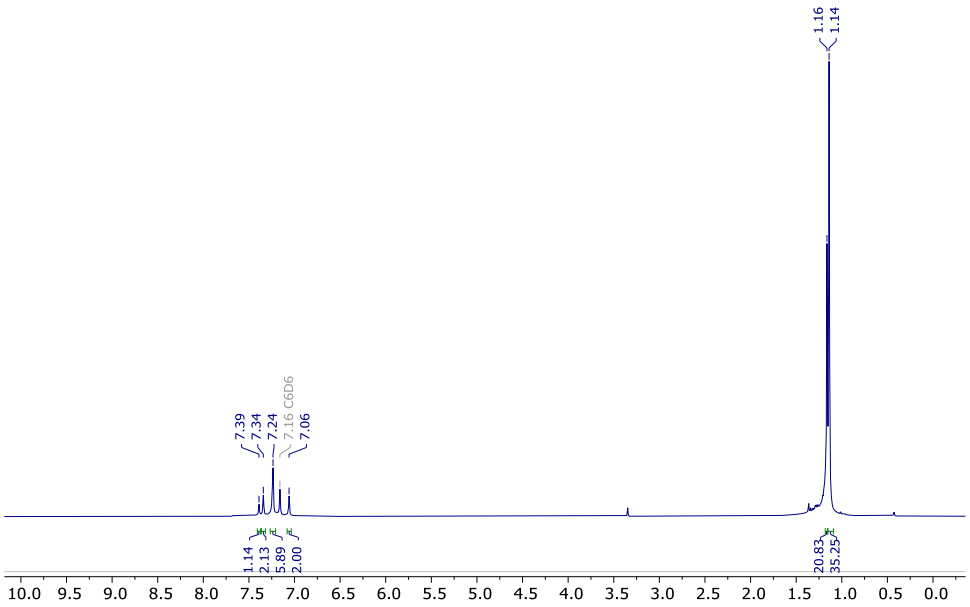

^{13}C{^{1}H} NMR (126 MHz) in C_6D_6.

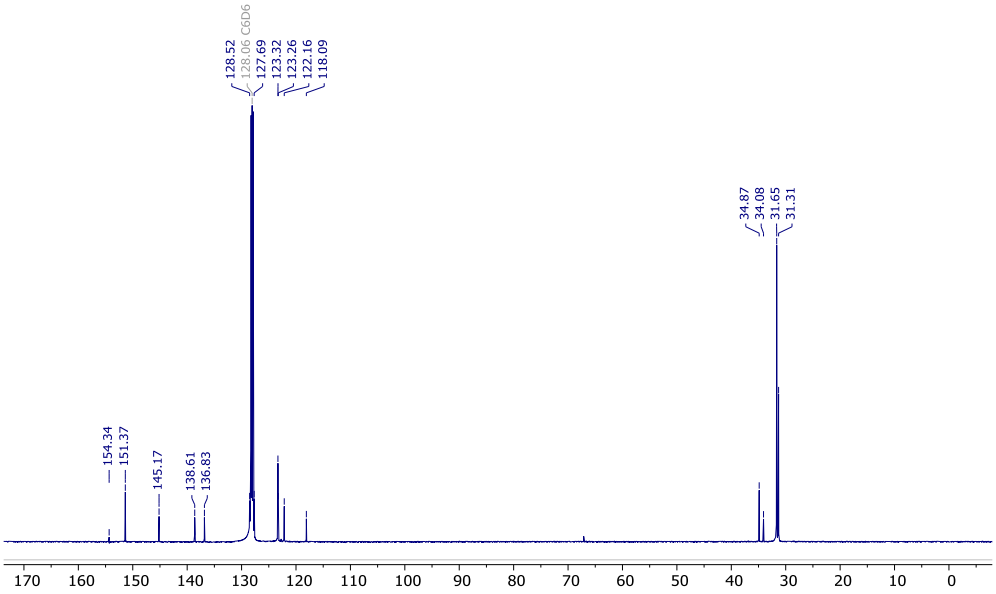

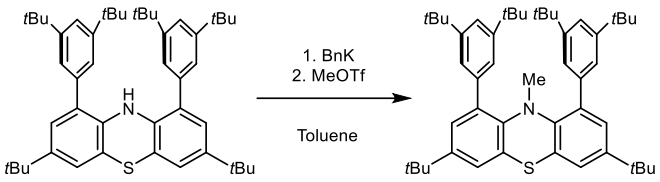

^{1}H NMR (500 MHz) in C_6D_6

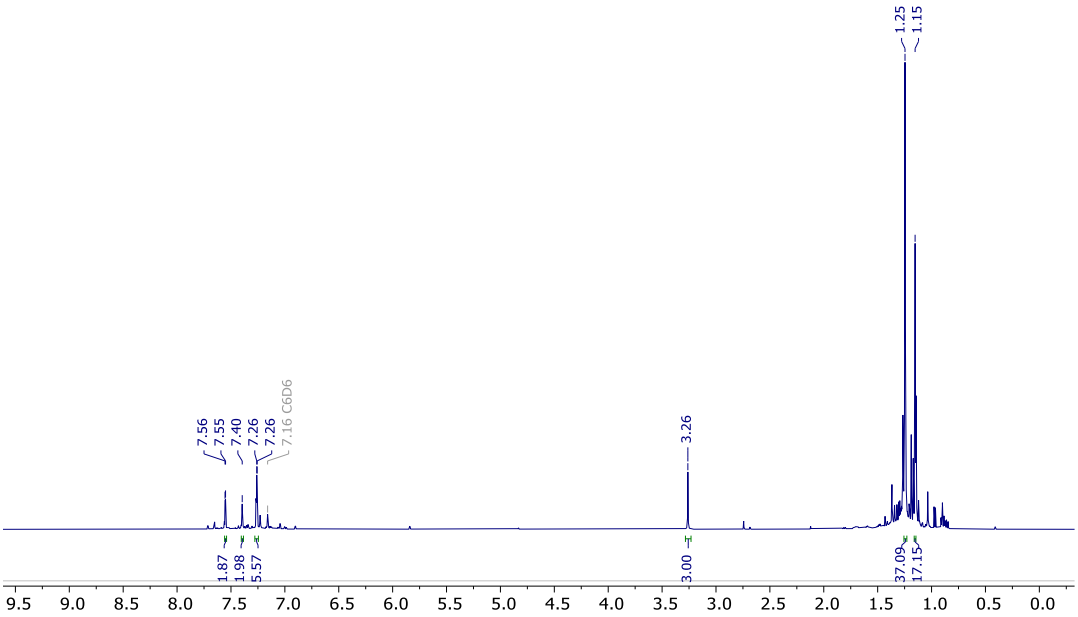

$^{13}C\{^{1}H\}$ NMR (126 MHz) in C_6D_6

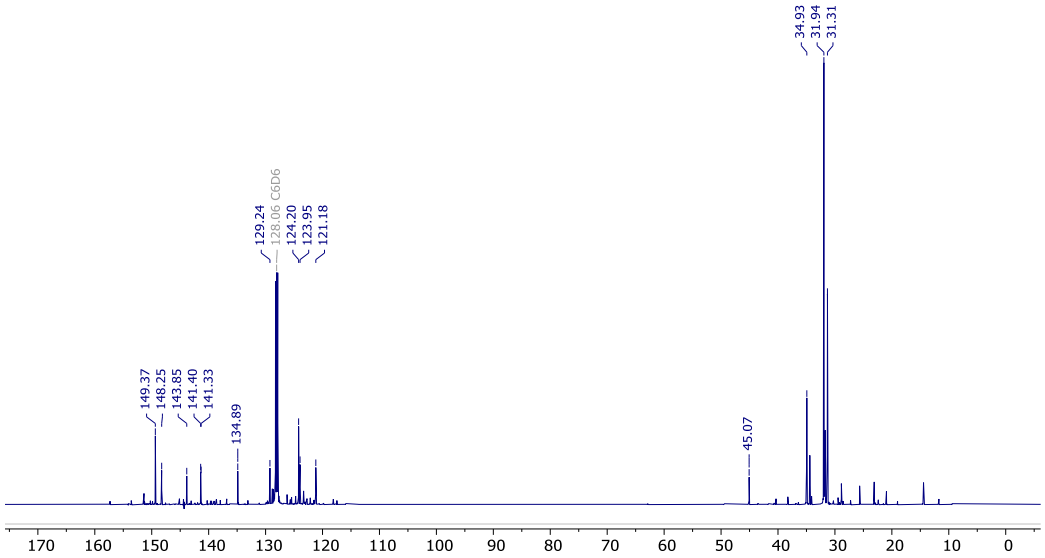

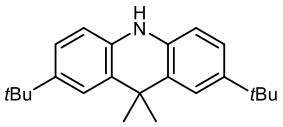

^{1}H NMR (500 MHz) in C_6D_6

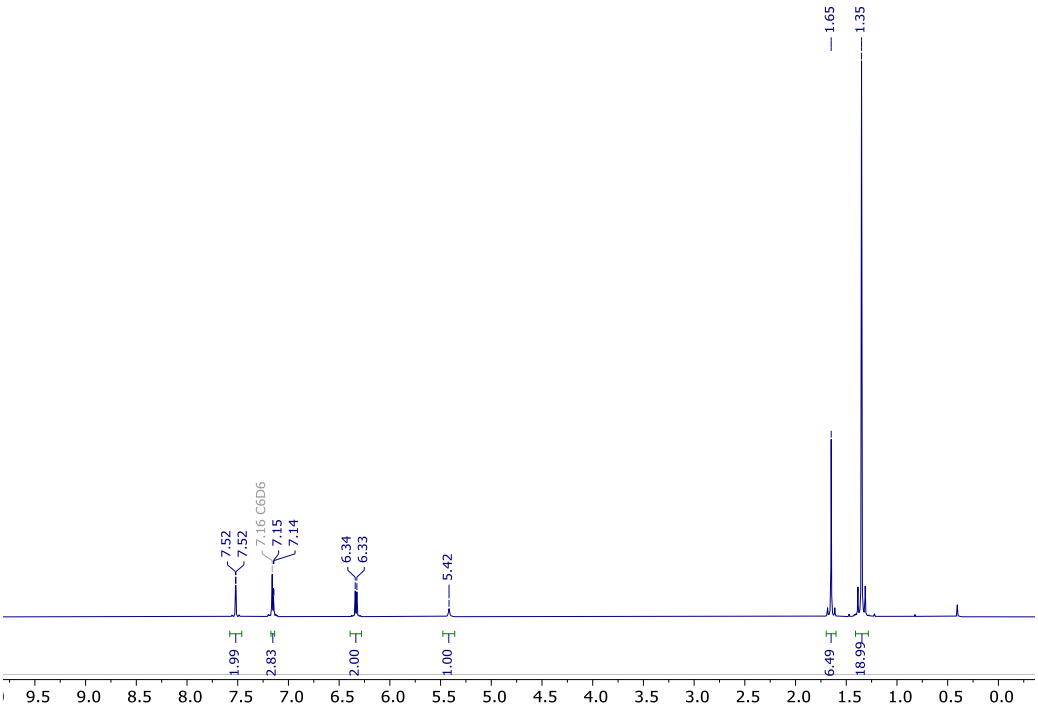

$^{13}C\{^{1}H\}$ NMR (126 MHz) in C_6D_6

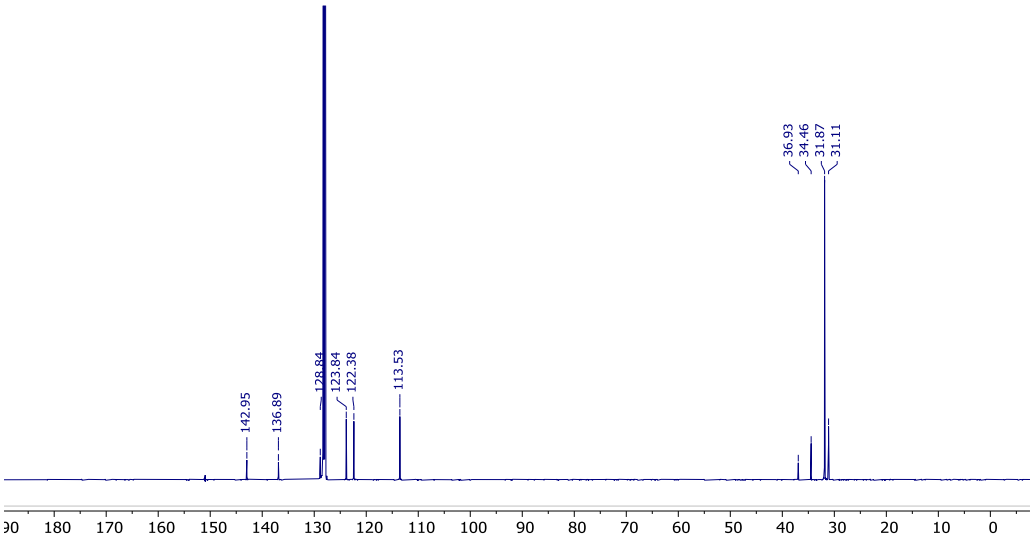

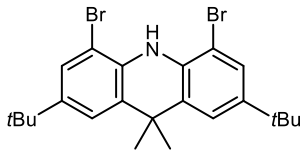

^{1}H NMR (500 MHz) in C_6D_6

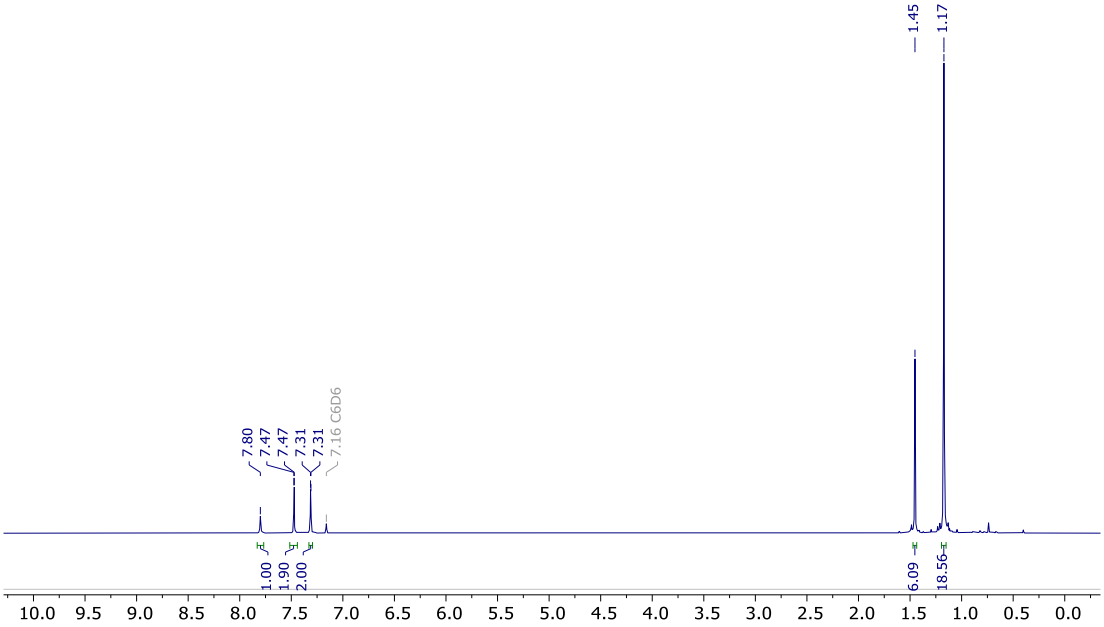

$^{13}C\{^{1}H\}$ NMR (126 MHz) in C_6D_6

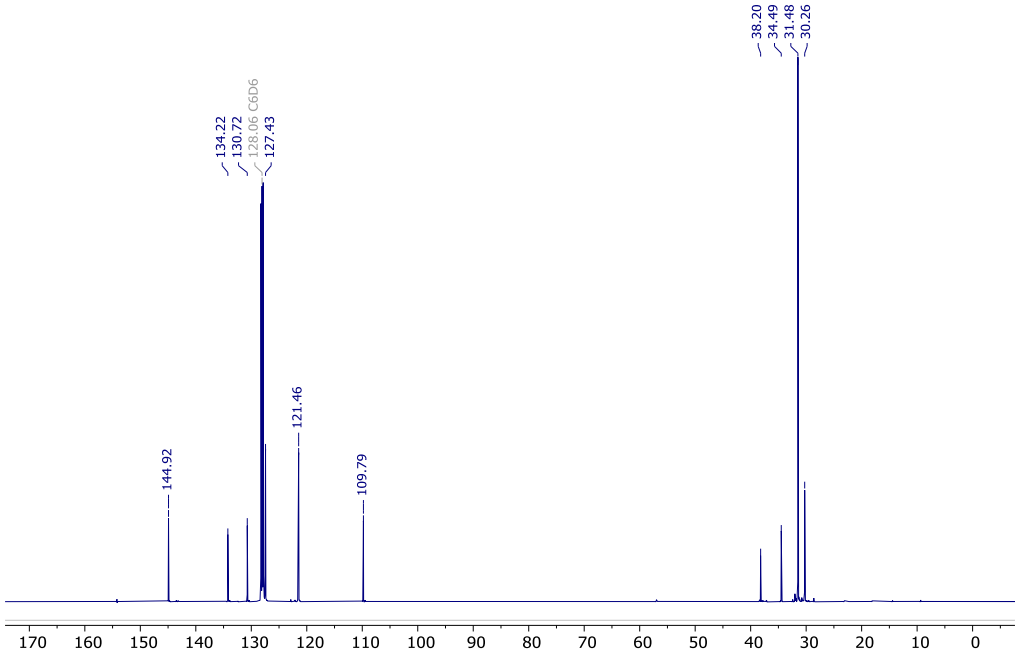

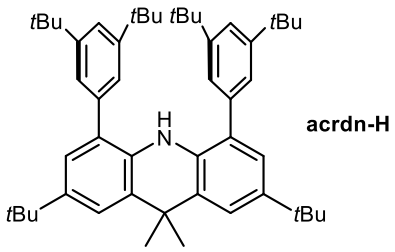

^{1}H NMR (500 MHz) in C_6D_6

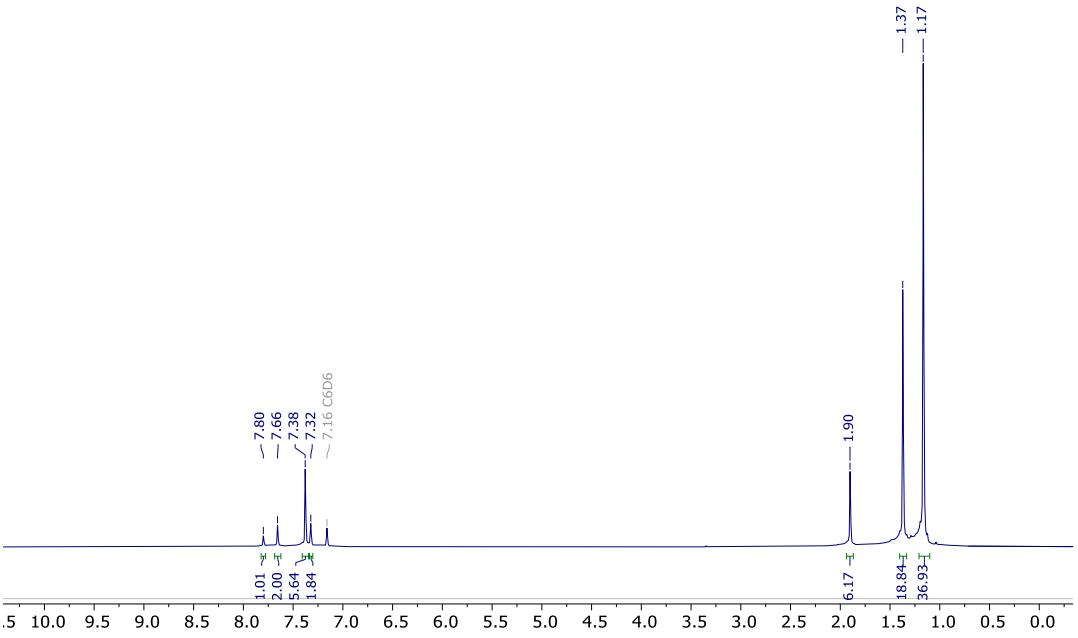

$^{13}C\{^{1}H\}$ NMR (126 MHz) in C_6D_6

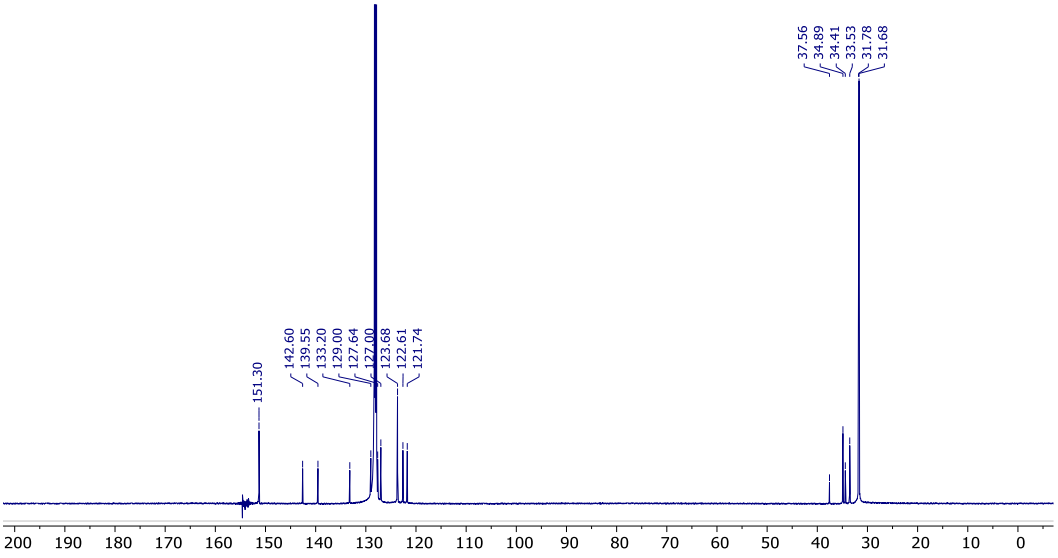

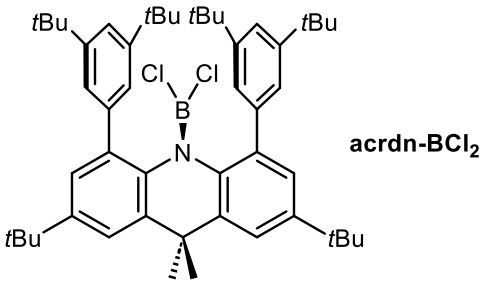

^{1}H NMR (500 MHz) in $CDCl_3$

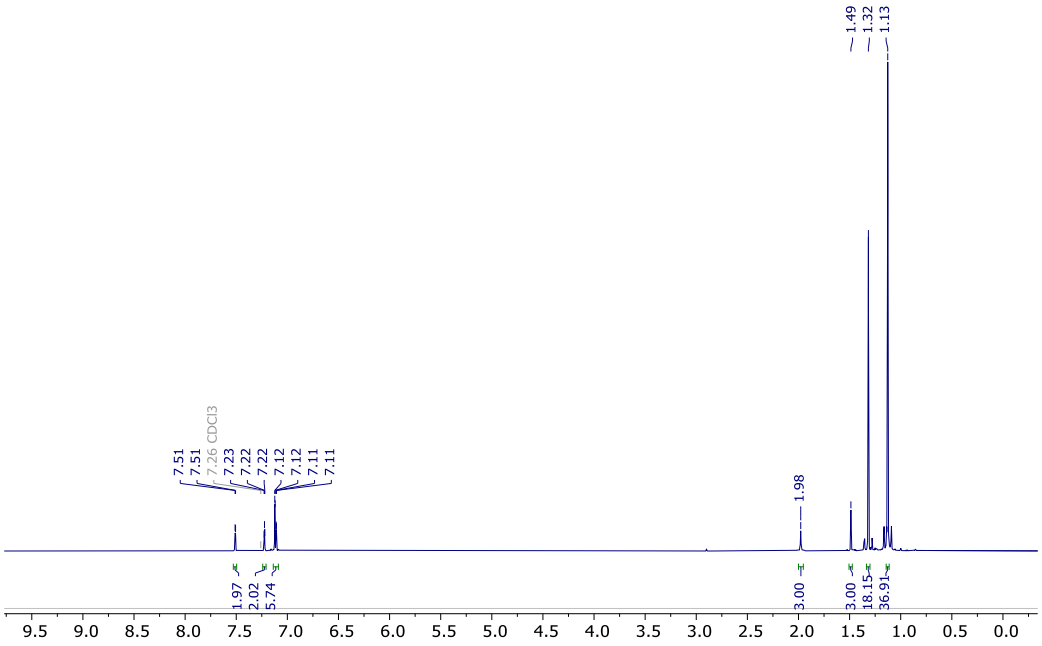

^{13}C{^{1}H} NMR (126 MHz) in $CDCl_3$

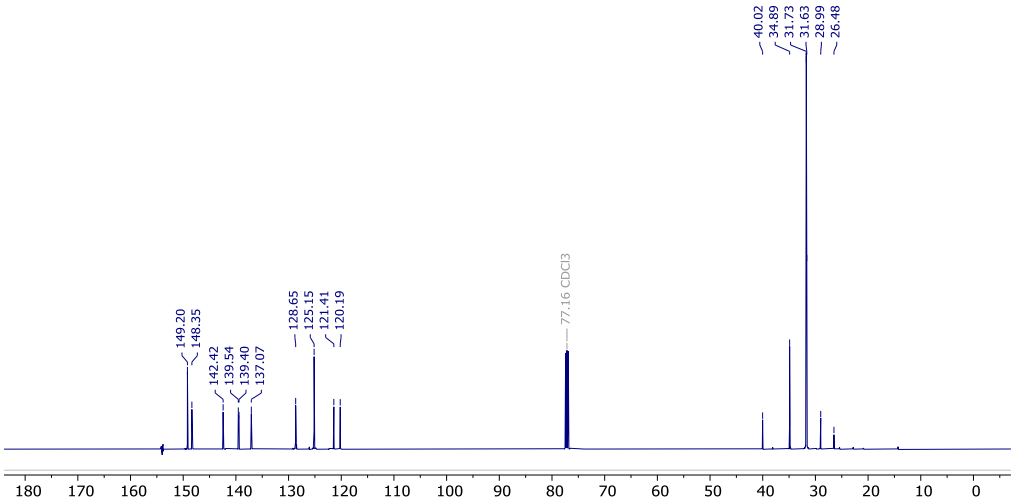

$^{11}B\{^{1}H\}$ NMR (96 MHz) in $CDCl_3$

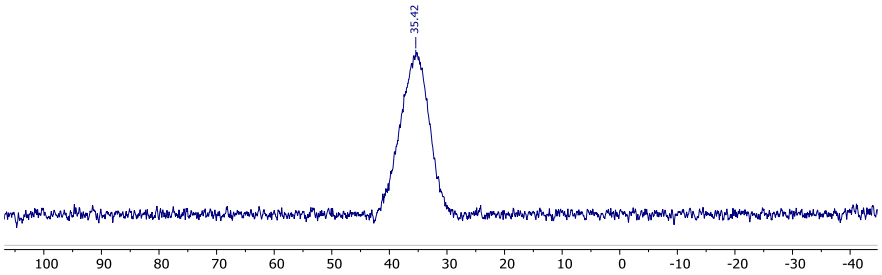

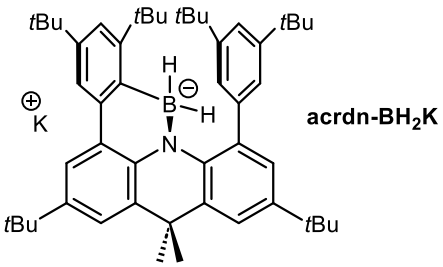

$^{11}B\{^{1}H\}$ NMR (96 MHz) in ether

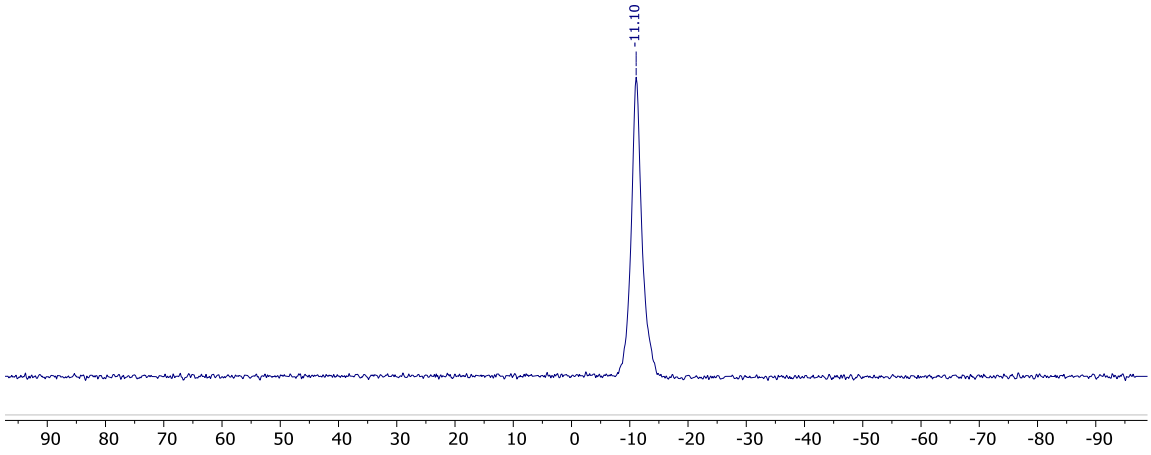

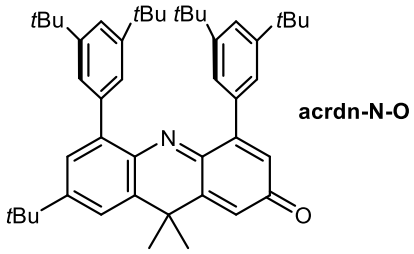

acrdn-N-O

^{1}H NMR (500 MHz) in C_6D_6

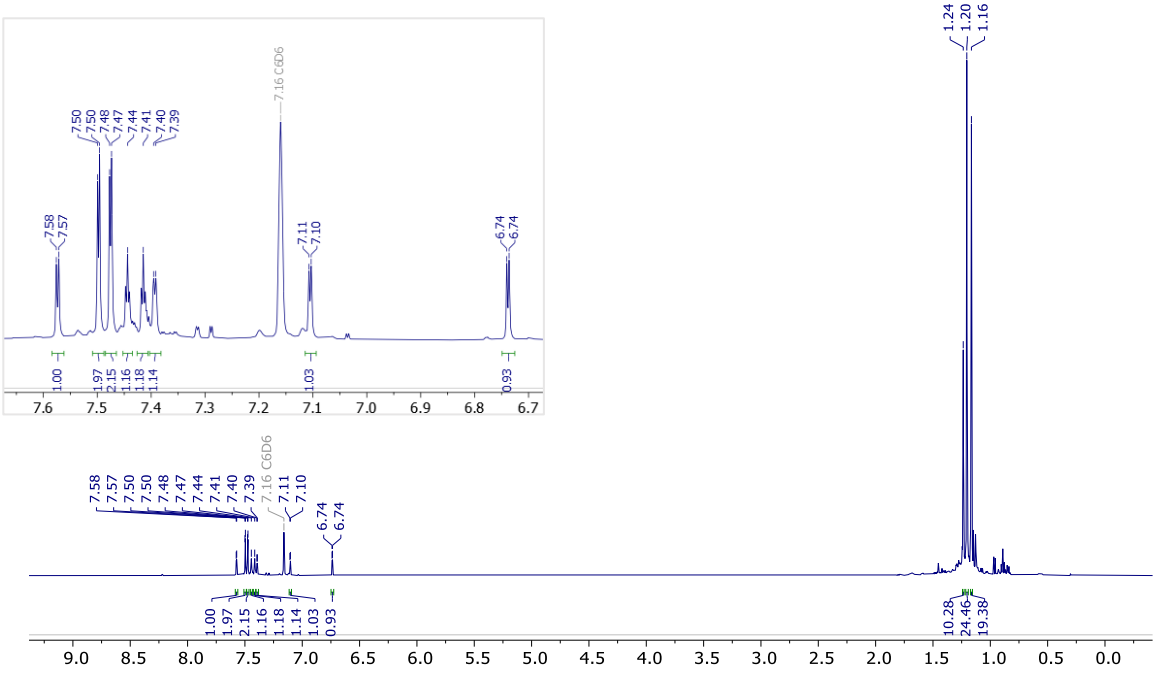

^{13}C{^{1}H} NMR (126 MHz) in C_6D_6

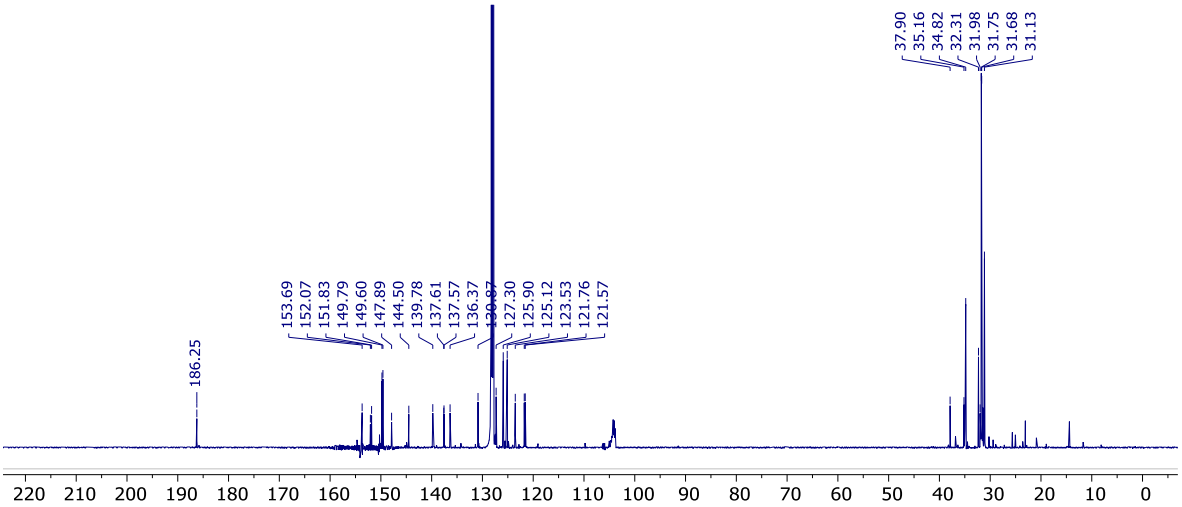

2.8.4 X-ray Crystallographic Data

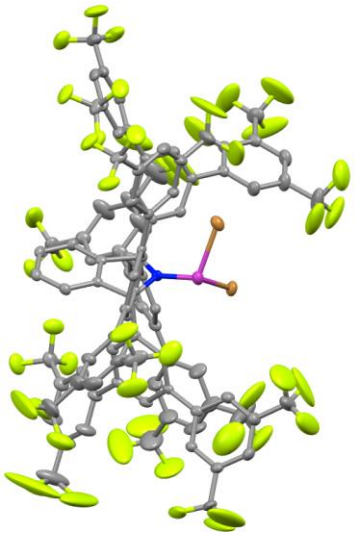

Crystal data and structure refinement for **pyrrol-PBr$_2$**

Identification code	bulky_pyrrol_CF3_PBr2	
Empirical formula	C97.50 H0.25 B0.25 Br2 Cl3 F48 Li0.25 N O0.25 P	
Formula weight	2402.81	
Temperature	100.0 K	
Wavelength	0.71073 Å	
Crystal system	Monoclinic	
Space group	P 1 21/n 1	
Unit cell dimensions	a = 20.157(8) Å	a= 90°.
	b = 23.468(13) Å	b= 99.160(13)°.
	c = 20.708(11) Å	g = 90°.
Volume	9671(8) Å^3	
Z	4	
Density (calculated)	1.650 Mg/m^3	
Absorption coefficient	1.078 mm^{-1}	
F(000)	4657	
Crystal size	? x ? x ? mm^3	
Theta range for data collection	1.992 to 25.401°.	
Index ranges	-24<=h<=24, -28<=k<=28, -24<=l<=24	
Reflections collected	156687	

Independent reflections	17750 [R(int) = 0.1133]
Completeness to theta = 25.242°	100.0 %
Absorption correction	None
Max. and min. transmission	0.6462 and 0.5321
Refinement method	Full-matrix least-squares on F^2
Data / restraints / parameters	17750 / 1301 / 1393
Goodness-of-fit on F^2	1.028
Final R indices [I>2sigma(I)]	R1 = 0.0900, wR2 = 0.2396
R indices (all data)	R1 = 0.1228, wR2 = 0.2655
Extinction coefficient	n/a
Largest diff. peak and hole	3.179 and -0.973 e.$Å^{-3}$

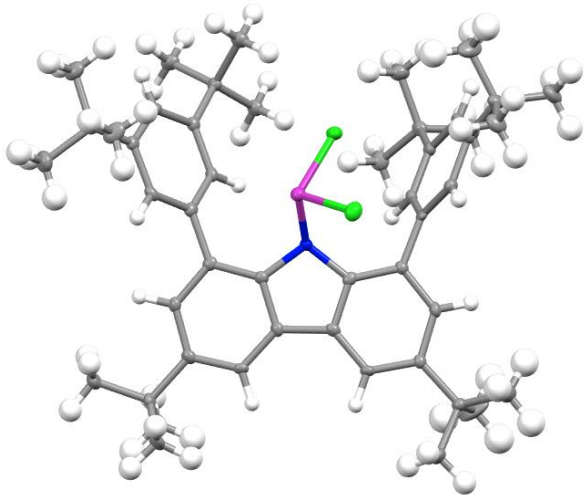

Crystal data and structure refinement for **carb-PCl_2**

Identification code	bulky_carbzl_pcl2	
Empirical formula	C48 H64 Cl2 N P	
Formula weight	756.87	
Temperature	100.00 K	
Wavelength	0.71073 Å	
Crystal system	Monoclinic	
Space group	P 1 21/c 1	
Unit cell dimensions	a = 15.2018(3) Å	a= 90°.
	b = 21.1649(4) Å	b= 117.6970(10)°.
	c = 15.4233(3) Å	g = 90°.
Volume	4393.76(15) $Å^3$	
Z	4	
Density (calculated)	1.144 Mg/m^3	
Absorption coefficient	0.216 mm^{-1}	
F(000)	1632	
Crystal size	0.25 x 0.2 x 0.15 mm^3	
Theta range for data collection	1.513 to 25.681°.	
Index ranges	-18<=h<=18, -25<=k<=25, -18<=l<=18	
Reflections collected	36618	
Independent reflections	8350 [R(int) = 0.0886]	
Completeness to theta = 25.242°	100.0 %	
Absorption correction	Semi-empirical from equivalents	

Max. and min. transmission	0.6464 and 0.6092
Refinement method	Full-matrix least-squares on F^2
Data / restraints / parameters	8350 / 0 / 487
Goodness-of-fit on F^2	1.044
Final R indices [I>2sigma(I)]	R1 = 0.0494, wR2 = 0.1027
R indices (all data)	R1 = 0.0918, wR2 = 0.1197
Extinction coefficient	n/a
Largest diff. peak and hole	0.337 and -0.355 e.$Å^{-3}$

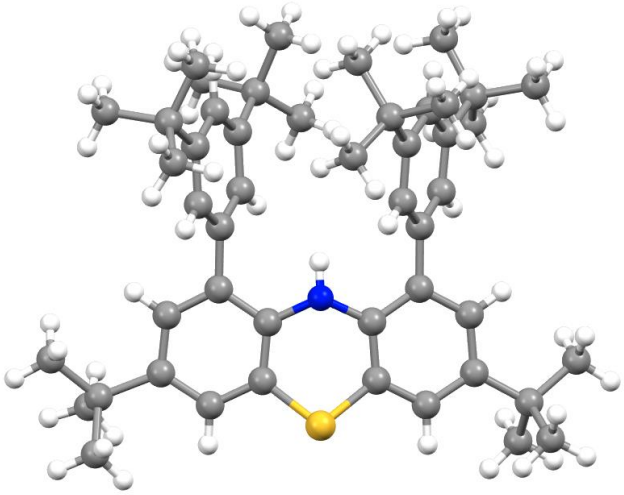

Crystal data and structure refinement for **phenthz-H**

Identification code	bulky_phenthz_nh	
Empirical formula	C54 H71 N S	
Formula weight	766.17	
Temperature	100.00 K	
Wavelength	0.71073 Å	
Crystal system	Monoclinic	
Space group	P 1 21/n 1	
Unit cell dimensions	a = 15.861(2) Å	a= 90°.
	b = 12.6692(14) Å	b= 94.930(5)°.
	c = 23.777(4) Å	g = 90°.
Volume	4760.0(11) $Å^3$	
Z	4	
Density (calculated)	1.069 Mg/m^3	
Absorption coefficient	0.102 mm^{-1}	
F(000)	1672	
Crystal size	0.04 x 0.03 x 0.03 mm^3	
Theta range for data collection	2.189 to 25.270°.	
Index ranges	-19<=h<=18, -15<=k<=15, -28<=l<=28	
Reflections collected	83171	
Independent reflections	8583 [R(int) = 0.1244]	
Completeness to theta = 25.242°	99.6 %	
Absorption correction	Semi-empirical from equivalents	

Max. and min. transmission	0.7452 and 0.6821
Refinement method	Full-matrix least-squares on F^2
Data / restraints / parameters	8583 / 145 / 587
Goodness-of-fit on F^2	1.025
Final R indices [I>2sigma(I)]	R1 = 0.0501, wR2 = 0.1151
R indices (all data)	R1 = 0.0843, wR2 = 0.1337
Extinction coefficient	n/a
Largest diff. peak and hole	0.194 and -0.342 e.$Å^{-3}$

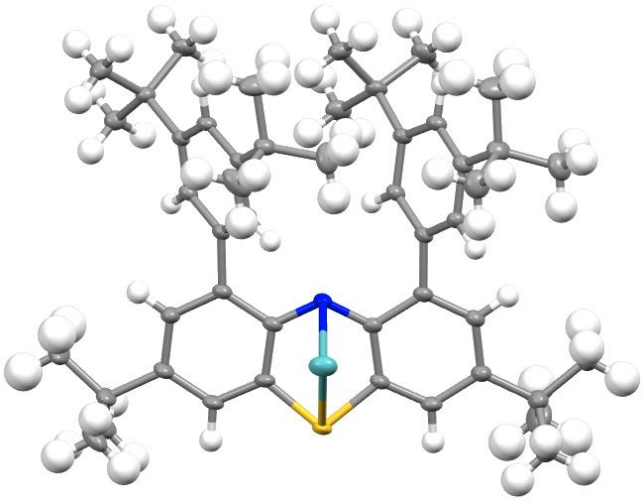

Crystal data and structure refinement for **phenthz-K**

Identification code	bulky_phenthz_nk	
Empirical formula	C69 H93 K N O2 S	
Formula weight	1039.60	
Temperature	100.15 K	
Wavelength	1.54178 Å	
Crystal system	Triclinic	
Space group	P-1	
Unit cell dimensions	a = 9.483(3) Å	a= 76.238(18)°.
	b = 14.568(6) Å	b= 79.47(2)°.
	c = 24.666(11) Å	g = 71.914(14)°.
Volume	3124(2) $Å^3$	
Z	2	
Density (calculated)	1.105 Mg/m^3	
Absorption coefficient	1.371 mm^{-1}	
F(000)	1130	
Crystal size	? x ? x ? mm^3	
Theta range for data collection	1.857 to 70.646°.	
Index ranges	-11<=h<=11, -17<=k<=17, -30<=l<=30	
Reflections collected	93461	
Independent reflections	11689 [R(int) = 0.0691]	
Completeness to theta = 67.679°	98.5 %	
Absorption correction	None	

Max. and min. transmission	0.7533 and 0.5984
Refinement method	Full-matrix least-squares on F^2
Data / restraints / parameters	11689 / 18 / 745
Goodness-of-fit on F^2	1.012
Final R indices [I>2sigma(I)]	R1 = 0.0499, wR2 = 0.1229
R indices (all data)	R1 = 0.0674, wR2 = 0.1363
Extinction coefficient	n/a
Largest diff. peak and hole	0.327 and -0.365 e.$Å^{-3}$

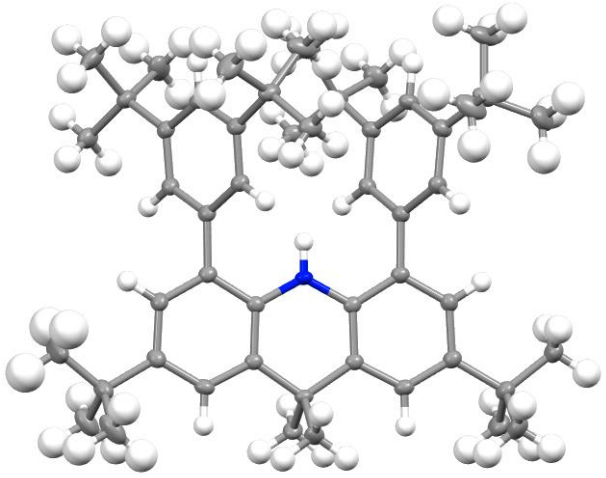

Crystal data and structure refinement for **acrdn-H**

Identification code	bulky_acrdn_nh	
Empirical formula	C57 H85 N	
Formula weight	784.25	
Temperature	100.15 K	
Wavelength	1.54178 Å	
Crystal system	Triclinic	
Space group	P-1	
Unit cell dimensions	a = 12.9044(2) Å	a= 101.7030(10)°.
	b = 13.6136(2) Å	b= 92.5900(10)°.
	c = 14.7118(2) Å	g = 96.5210(10)°.
Volume	2508.21(6) $Å^3$	
Z	2	
Density (calculated)	1.038 Mg/m^3	
Absorption coefficient	0.427 mm^{-1}	
F(000)	868	
Crystal size	0.25 x 0.25 x 0.05 mm^3	
Theta range for data collection	3.075 to 68.244°.	
Index ranges	-15<=h<=15, -14<=k<=16, -17<=l<=16	
Reflections collected	14584	
Independent reflections	8484 [R(int) = 0.0168]	
Completeness to theta = 67.679°	92.6 %	
Absorption correction	Semi-empirical from equivalents	

Max. and min. transmission	0.7533 and 0.6686
Refinement method	Full-matrix least-squares on F^2
Data / restraints / parameters	8484 / 51 / 524
Goodness-of-fit on F^2	1.062
Final R indices [I>2sigma(I)]	R1 = 0.0462, wR2 = 0.1284
R indices (all data)	R1 = 0.0508, wR2 = 0.1336
Extinction coefficient	0.00062(16)
Largest diff. peak and hole	0.333 and -0.181 e.$Å^{-3}$

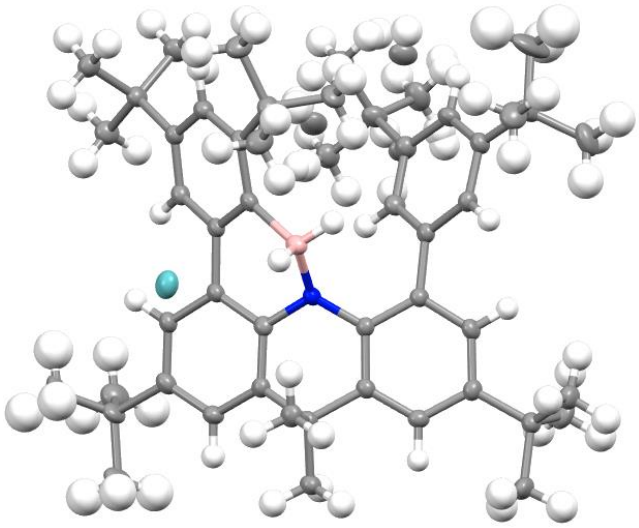

Crystal data and structure refinement for **acrdn-BH_2K**

Identification code	bulky_acrdn_bh2k	
Empirical formula	C63 H101 B K N O3	
Formula weight	970.35	
Temperature	100.00 K	
Wavelength	0.71073 Å	
Crystal system	Orthorhombic	
Space group	$Pna2_1$	
Unit cell dimensions	a = 14.0192(10) Å	a= 90°.
	b = 23.4554(14) Å	b= 90°.
	c = 18.5892(12) Å	g = 90°.
Volume	6112.6(7) $Å^3$	
Z	4	
Density (calculated)	1.054 Mg/m^3	
Absorption coefficient	0.128 mm^{-1}	
F(000)	2136	
Crystal size	0.22 x 0.2 x 0.15 mm^3	
Theta range for data collection	2.515 to 25.455°.	
Index ranges	-16<=h<=16, -28<=k<=28, -22<=l<=22	
Reflections collected	174662	
Independent reflections	11241 [R(int) = 0.1400]	
Completeness to theta = 25.242°	99.8 %	

Absorption correction	Semi-empirical from equivalents
Max. and min. transmission	0.6837 and 0.6396
Refinement method	Full-matrix least-squares on F^2
Data / restraints / parameters	11241 / 22 / 680
Goodness-of-fit on F^2	1.028
Final R indices [I>2sigma(I)]	R1 = 0.0443, wR2 = 0.1041
R indices (all data)	R1 = 0.0611, wR2 = 0.1162
Absolute structure parameter	0.00(2)
Extinction coefficient	0.0061(7)
Largest diff. peak and hole	0.268 and -0.255 e.$Å^{-3}$

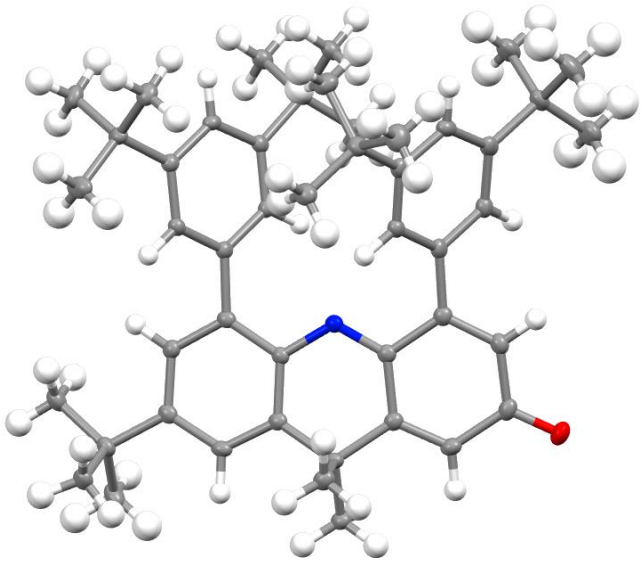

Crystal data and structure refinement for **acrdn-NO**

Identification code	bulky_acrdn_no	
Empirical formula	C47 H61 N O	
Formula weight	655.96	
Temperature	100.00 K	
Wavelength	0.71073 Å	
Crystal system	Triclinic	
Space group	P-1	
Unit cell dimensions	a = 11.8138(8) Å	a= 100.401(4)°.
	b = 18.1841(18) Å	b= 99.085(4)°.
	c = 20.2836(16) Å	g = 105.521(4)°.
Volume	4030.6(6) $Å^3$	
Z	4	
Density (calculated)	1.081 Mg/m^3	
Absorption coefficient	0.063 mm^{-1}	
F(000)	1432	
Crystal size	0.2 x 0.2 x 0.04 mm^3	
Theta range for data collection	1.195 to 25.676°.	
Index ranges	-14<=h<=14, -21<=k<=22, -23<=l<=24	
Reflections collected	71938	
Independent reflections	15301 [R(int) = 0.0473]	

Completeness to theta = 25.242°	100.0 %
Absorption correction	Semi-empirical from equivalents
Max. and min. transmission	0.5622 and 0.5127
Refinement method	Full-matrix least-squares on F^2
Data / restraints / parameters	15301 / 66 / 951
Goodness-of-fit on F^2	1.029
Final R indices [I>2sigma(I)]	R1 = 0.0492, wR2 = 0.1230
R indices (all data)	R1 = 0.0626, wR2 = 0.1332
Extinction coefficient	n/a
Largest diff. peak and hole	1.181 and -0.494 e.$Å^{-3}$

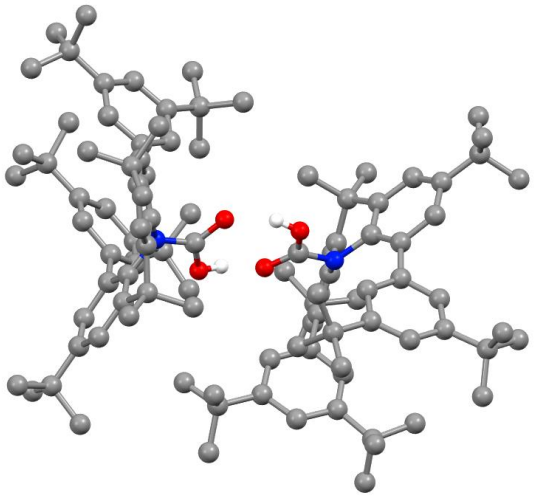

Crystal data and structure refinement for **acrdn-CO_2H**

Identification code	bulky_acrdn_co2h	
Empirical formula	C60 H91 N O4	
Formula weight	890.33	
Temperature	100.15 K	
Wavelength	1.54178 Å	
Crystal system	Orthorhombic	
Space group	$P2_12_12$	
Unit cell dimensions	a = 28.1036(18) Å	a= 90°.
	b = 30.322(2) Å	b= 90°.
	c = 12.9863(8) Å	g = 90°.
Volume	11066.5(12) $Å^3$	
Z	8	
Density (calculated)	1.069 Mg/m^3	
Absorption coefficient	0.495 mm^{-1}	
F(000)	3920	
Crystal size	0.05 x 0.03 x 0.025 mm^3	
Theta range for data collection	2.143 to 63.683°.	
Index ranges	-31<=h<=32, -35<=k<=33, -14<=l<=15	
Reflections collected	198549	
Independent reflections	18209 [R(int) = 0.1356]	
Completeness to theta = 63.683°	100.0 %	
Absorption correction	Semi-empirical from equivalents	

Max. and min. transmission	0.9972 and 0.9219
Refinement method	Full-matrix least-squares on F^2
Data / restraints / parameters	18209 / 36 / 1064
Goodness-of-fit on F^2	1.008
Final R indices [I>2sigma(I)]	R1 = 0.0578, wR2 = 0.1402
R indices (all data)	R1 = 0.0908, wR2 = 0.1607
Absolute structure parameter	0.00(12)
Extinction coefficient	n/a
Largest diff. peak and hole	0.298 and -0.221 e.$Å^{-3}$

Chapter 3 Carbene-stabilized Diphosphorus – A Triple-Bonded Diphosphorus (P≡P) and Bis-Phosphinidene (P-P) Transfer Agent

Diphosphorus surrogates that can release P_2 in solution and under mild conditions are coveted by synthetic chemists. While there have been reports of triple-bonded P_2 surrogates, there has yet to be an instance of a P_2 transfer agent that behaves also as a single-bonded P_2 source – or a bis-phosphinidene. In this chapter we report the serendipitous discovery of a unique diphospha-urea species that can photolytically lose carbon monoxide to give a diphosphorus unit capped by monosubstituted (amino)carbenes. This bis(carbene)-P_2 adduct behaves as a surrogate of P_2 as a triple-bonded diphosphorus and bis-phosphinidene source. We demonstrate the first example of ligand exchange at P_2. Finally, this new species shows promise as a P^- transfer agent under the right conditions.

3.1 Introduction

Elemental phosphorus exists primarily in two allotropic forms: polymeric red phosphorus and tetrameric white phosphorus (P_4). Unlike dinitrogen, phosphorus does not form discrete diphosphorus (P_2) units due to its low bond-dissociation energy.[69] Diatomic P_2 has only been spectroscopically characterized both at high temperatures (>1100 K)[70] and in matrices at a few Kelvin.[71] P_2 is also widely seen in the coordination sphere of transition metals.[72] Given the instability of P_2, precursors that can generate P_2 in solution and under mild conditions are highly desirable to make this species synthetically useful.

The accession of P_2 as a reagent has only been achieved by Cummins *et al.*[73] and by Wolf and Goicoechea *et al.*[74] who were able to induce Diels-Alder reactions between transient P_2 and

dienes (Figure 3.1 – left). In 2008, Robinson showed that P_2 can be stabilized by using N-heterocyclic carbenes (NHCs) to coordinate each phosphorus atom (Figure 3.1 – right).[75] This was achieved by the potassium graphite reduction of the NHC-PCl_3 adduct in a THF solution, followed by dimerization to give **bis(NHC)P$_2$**. A year later, our group demonstrated that P_4 can be fragmented and subsequently stabilized by cyclic (alkyl)(amino)carbenes (CAACs) to form, among other oligomers, **bis(CAAC)P$_2$** – a feature that is usually exhibited by transition metals.[76]

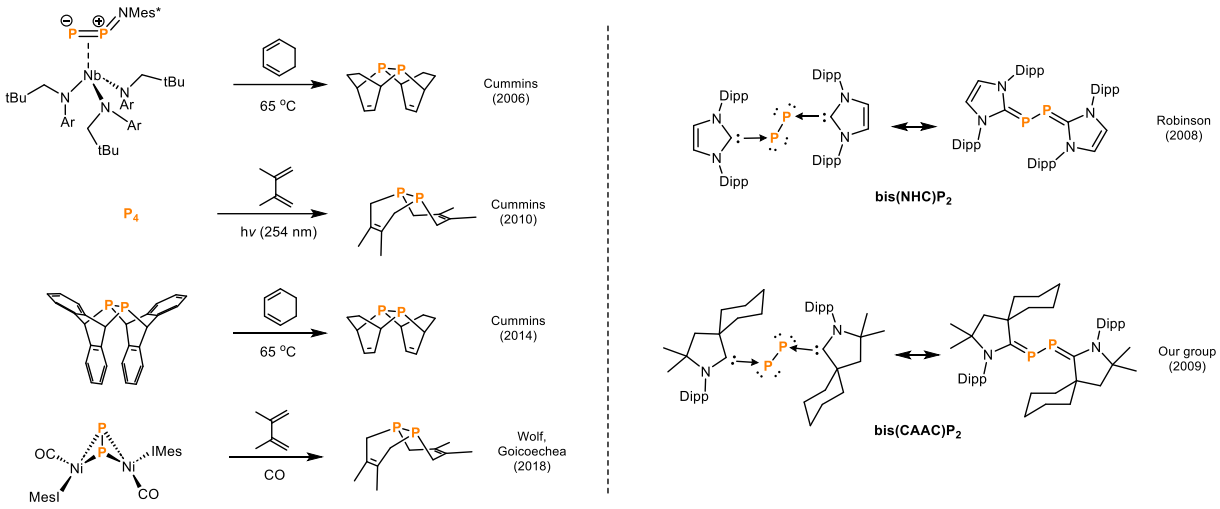

Figure 3.1 – (Left) Previously reported examples of generation and trapping of P_2. (Right) bis(NHC) and bis(CAAC) adducts of P_2.

In each of these cases, the use of stable singlet carbenes was necessary for their syntheses. Consequently, there has not been an instance where P_2 has been capped by non-isolable. While these bis(carbene)P_2 adducts were highly novel in themselves, the P_2 unit has not been successfully sequestered from the carbene units. This may in part be due to the bulkiness of the carbenes and the strength of the carbene-phosphorus interaction (particularly in the case of CAAC).

This project was initially conceived with the intention of developing a novel route to an amino phosphaalkyne. In 2016, our lab discovered that phosphaketenes are the direct precursor to

phosphinidenes via the loss of carbon monoxide (CO).[77] Based on this insight, we envisaged that the deprotonation of iminium phosphaketenes, followed by the loss of CO, would lead to an amino phosphaalkyne, a type of compound hardly available by known methods (Figure 3.2).[78] To this day, the preparation of amino phosphaalkynes are low-yielding and requires the use of harsh reagents such as CF_3PH_2. Such species are important in the formation of P-heterocycles, as they undergo various [n+2] cyclization reactions.[79,80,81] Therefore, our original aim for this project was to pursue an alternative route to access these uncommon species.

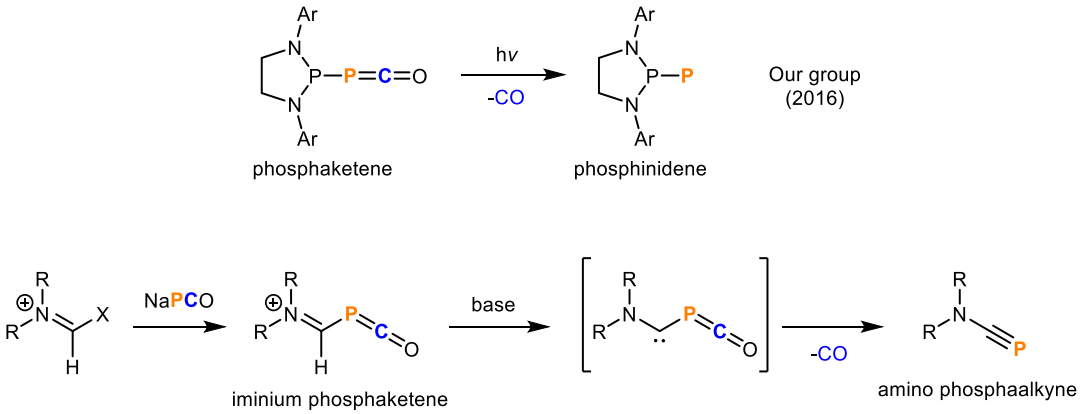

Figure 3.2 – (Top) Phosphaketenes as precursors to phosphinidenes. (Bottom) Iminium phosphaketenes as potential precursors to amino phosphaalkynes.

To pursue this goal, we synthesized sodium phosphaethynolate (NaPCO), a dual-site nucleophile known for its rich chemistry and various modes of reactivity.[82] However, early unexpected results compelled us to redirect the project in a direction that centered on the taming of P_2 as a reagent.

3.2 Synthesis and Characterization of a Novel Diphospha-urea

In our attempts to prepare an iminium phosphaketene, we first needed to prepare a haloiminium salt. We chose to prepare *N*,*N*-diisopropyl bromoiminium bromide **1** which was prepared quantitatively via the Vilsmeier-Haack reaction between *N*,*N*-diisopropyl formamide and oxalyl bromide. Due to the extremely low solubility of **1** in inert solvents (e.g. THF, chloroform, DCM, benzene, diethyl ether), the triflate salt was prepared and characterized (see NMR section). With our bromoiminium salt in hand, we expected that the addition of nucleophilic NaPCO would simply displace the bromide to give the iminium phosphaketenes. However, when we added one equivalent of NaPCO (complex of 1,4-dioxane) to **1**, we observed the surprising formation of the bench-stable cationic species **P+**, featuring a ^{31}P NMR chemical shift of 51 ppm and a characteristic doublet in the ^{1}H NMR spectrum at 12.1 ppm ($J_{P\text{-}H}$ = 9.0 Hz) (Figure 3.3). Such a species is similar to the known tetramethyl analog that was prepared from the addition of $P(SiMe_3)_3$ to *N*,*N*-dimethyl chloroiminium chloride.[83] To a greater surprise, when we added 2 equivalents of NaPCO in toluene to **1**, we observed the clean formation of diphospha-urea **2**, showing a characteristic ^{31}P NMR shift at 89 ppm.

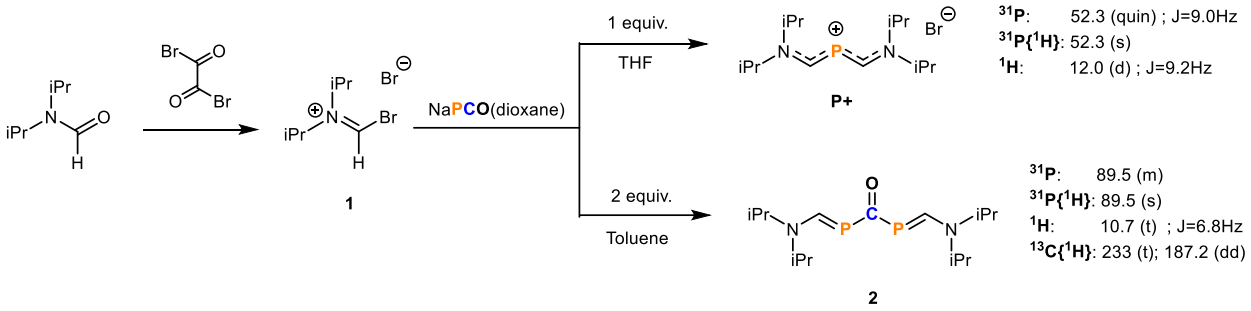

Figure 3.3 – Synthesis of **1** and subsequent addition of 1 and 2 equivalents of NaPCO to give **P+** and **2**, respectively.

To determine whether **2** can be obtained from **P+**, we added NaPCO incrementally to the bromoiminium salt **1**, and found that **P+** is indeed an intermediate to **2**. This evidence, showing that one phosphorus atom is first joined by two formamide fragments before the addition of the second phosphorus atom, led to the proposed mechanism for the formation of **2**, shown in Figure 3.4. First, nucleophilic NaPCO reacts with bromoiminium **1**, to form intermediate **i**, our targeted phosphaalkyne precursor. Due to its instability, this is quickly followed by loss of CO along with a two-electron reduction, giving a new nucleophile **ii** along with the oxidized $(PCO)_2$ dimer. This oxidized $(PCO)_2$ dimer has been previously reported to form a tetrameric $(PCO)_4^{2-}$ byproduct (which we observed traces of) in the presence of excess PCO^-.[84] Intermediate **ii** then nucleophilically attacks another bromoiminium **1** to form the cationic intermediate, **P+**. The phosphonium salt **P+** then undergoes a [2+2] cycloaddition with another PCO^- ion, which gives **2** upon elimination. Overall, this requires a 1:2 ratio of bromoiminium **1** to NaPCO.

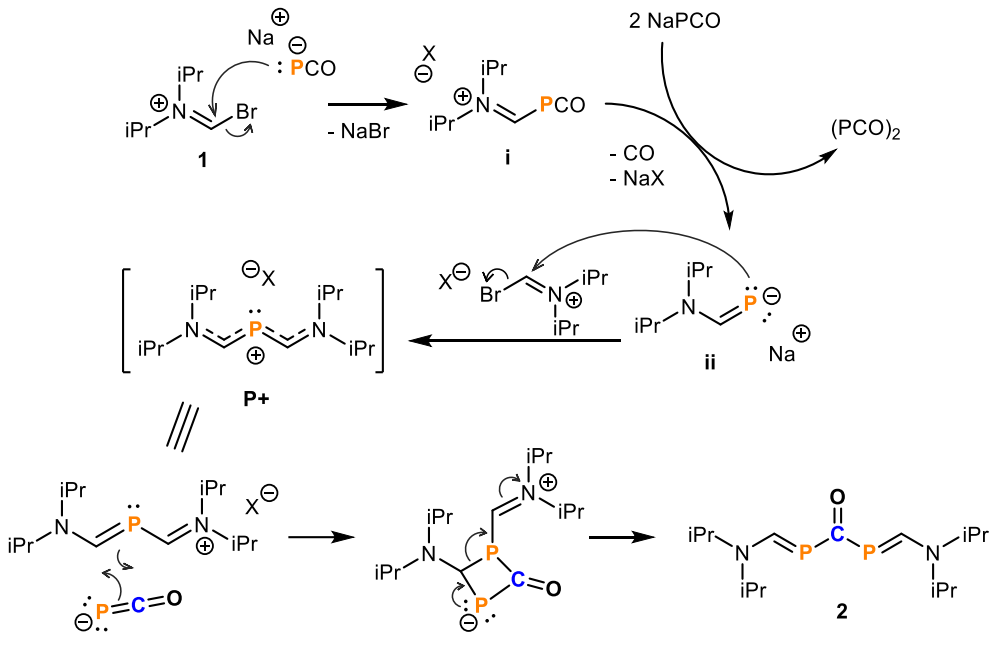

Figure 3.4 – Proposed mechanism for the formation of **2**.

While neither **P+** nor **2** matched our anticipated amino phosphaalkyne precursor, we were nonetheless intrigued by their formation – particularly the isolation of diphospha-urea **2**. Thus, we decided to investigate the properties and reactivity of **2**.

3.3 Characterization and Reactivity of 2

First, we noted that **2** slowly hydrolyzes in air to give **P+** and *N*,*N*-diisopropyl formamide. The counterion could not be determined, as there was only one compound visible in the ^{31}P NMR spectrum, leading us to believe that the counterion may either be OH^- or P^{3-}, the latter of which was proposed in the bis(cyclopropenylidene) derivative of $\mathbf{P}^+$.[85]

Next, we investigated the possibility of liberating carbon monoxide from **2**, as the decarbonylation of diphospha-ureas [$R_2P(CO)PR_2$] has much literature precedent.[86] When heated to 70 °C under vacuum, we did not observe any change. We then attempted the photolytic decarbonylation using 450 nm (blue light), as the UV-Vis spectrum of **2** shows a maximum absorbance at 425 nm. Irradiating a solution of **2** in $CDCl_3$ cleanly led to the full conversion to **P+** with a chloride anion, as ascertained by X-ray crystallography (Figure 3.5). It is worth noting that this species is somewhat of a thermodynamic sink for this phosphorus system, as it will be seen many more times in this chapter.

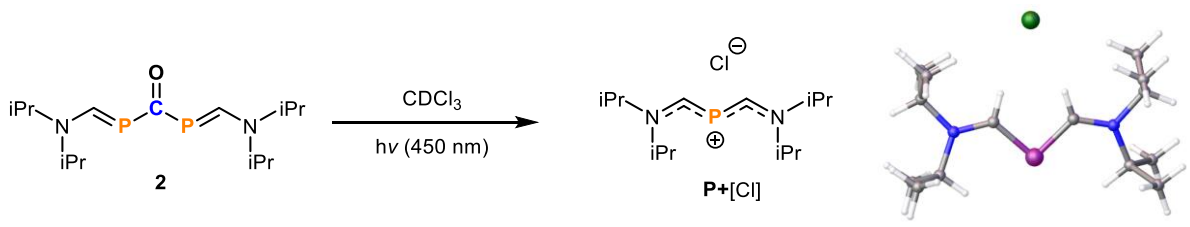

Figure 3.5 – Photolysis of **2** in $CDCl_3$ and X-ray structure of the resulting product.

The formation of **P+** indicated that carbon monoxide was, indeed, liberated. However, the decarbonylation event may have quickly been followed by oxidation with the concomitant abstraction of a chloride anion to give **P+**. With no other chloride source than the chloroform solvent, we wondered if changing the solvent would give us the simple decarbonylation product. Gratifyingly, when the irradiation was repeated using benzene or THF solvent, we observed the diminishing of the starting material ^{31}P NMR signal at 89 ppm, and the appearance of a new signal at 78 ppm (Figure 3.6). In the ^{13}C NMR, the doublet-of-doublets of the starting material N(*C*H)P at 187 ppm was converted to a new doublet-of-doublets at 182 ppm. Most tellingly, we also observed free carbon monoxide as a singlet at 184 ppm, indicating the loss of free CO.

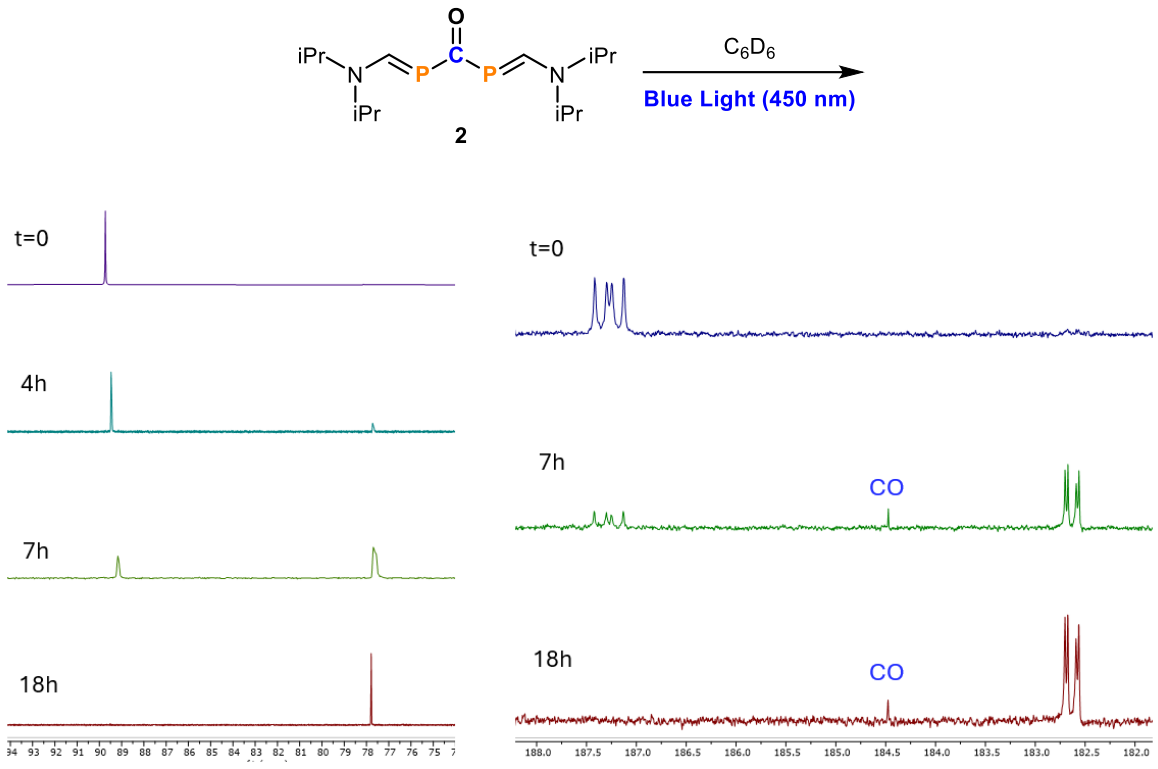

Figure 3.6 – NMR (^{31}P left; ^{13}C right) monitoring of the photolysis of **2** in benzene.

From these findings, we determined the structure of the product to be **3** (Figure 3.7), resulting from the loss of CO from **2**. The structure of **2** was unambiguously confirmed by single crystal X-ray crystallographic analysis and HR-MS.

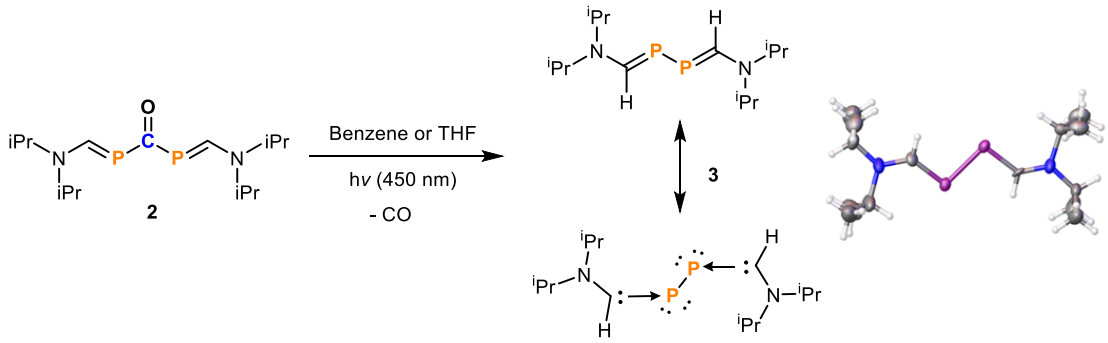

Figure 3.7 – Photolysis of **2** in benzene or THF to give **3**. Two canonical forms of **3** and X-ray crystal structure.

The kinetics of the conversion from **2** to **3** was studied using UV-Vis spectroscopy. The maximum absorbance of **2** (λ_{max} = 425 nm) is more red-shifted compared to **3** (λ_{max} = 349 nm), with an isosbestic point at 378 nm. We monitored the conversion of **2** to **3** over several time intervals by measuring the absorbance at 425 nm (Figure 3.8) and found that this decarbonylation occurs via first-order kinetics. This eliminates the possibility of a bimolecular mechanism.

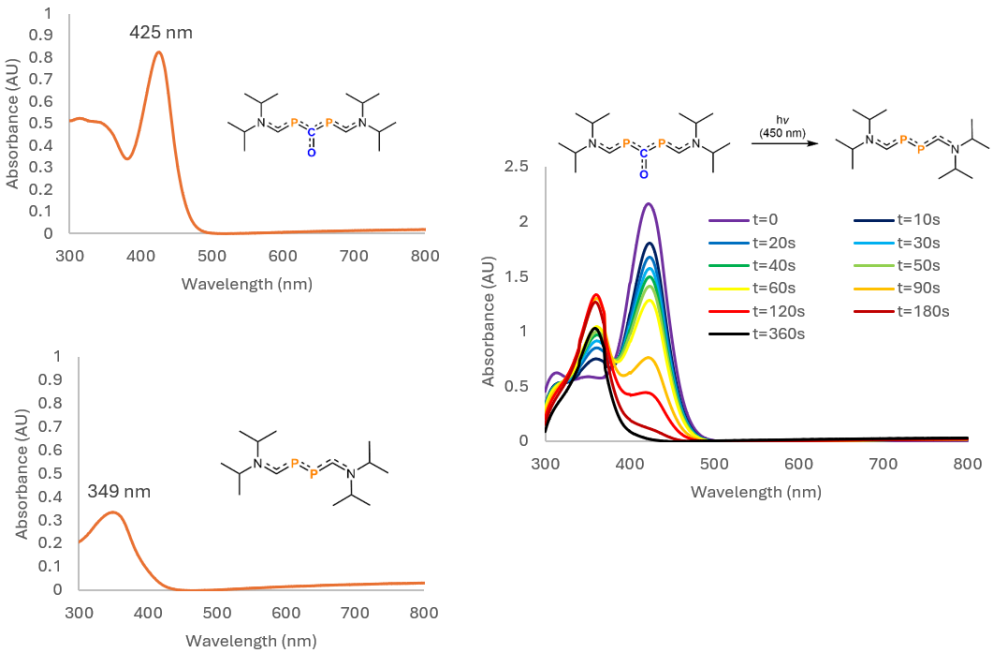

Figure 3.8 – UV-Vis spectra of **2** (0.1 mM in THF) (top left), **3** (0.1 mM in THF) (bottom left), and spectra at different moments of the photo-conversion of **2** into **3** (right).

3.4 Carbene-stabilized Diphosphorus – a Source of Triple-bonded Diphosphorus (P≡P) and (Bis)phosphinidene (P-P)

Compound **3** can be illustrated as either a diphosphabutadiene or P_2 stabilized by two monosubstituted (amino)carbenes. The latter is reminiscent of Robinson's **bis(NHC)P₂** adduct,[87] as well as **bis(CAAC)P₂** adduct previously reported by our group (Figure 3.9).[88] Robinson's **bis(NHC)P₂** adduct exhibits a considerably more shielded ^{31}P NMR signal at -52.4 ppm while the **bis(CAAC)P₂** adduct shows a downfield signal at +59.4 ppm, more akin to **3**. This is, in part, due to the weaker electrophilicity of NHCs versus CAACs and monosubstituted (amino)carbenes. The P-P bond distance in **3** (2.179 Å) is very similar to those observed for **bis(NHC)P₂** (2.205 Å) and **bis(CAAC)P₂** (2.184 Å), while the C-P bond length in **3** (1.710 Å) is comparable to that of **bis(CAAC)P₂** (1.719 Å) but shorter than in **bis(NHC)P₂** (1.750 Å). The X-ray crystal structure of

3 also reveals that the two carbene units are coplanar – indicative of a high degree of conjugation across the N-C-P-P-C-N framework. This is in contrast with the analogous NHC and CAAC adducts of P_2, for which the bulky carbene units are forced to adopt a twisted conformation to accommodate the steric congestion. These data collectively indicate that the diphosphabutadiene resonance structure is significant in **3** as it is in **bis(CAAC)P_2**.

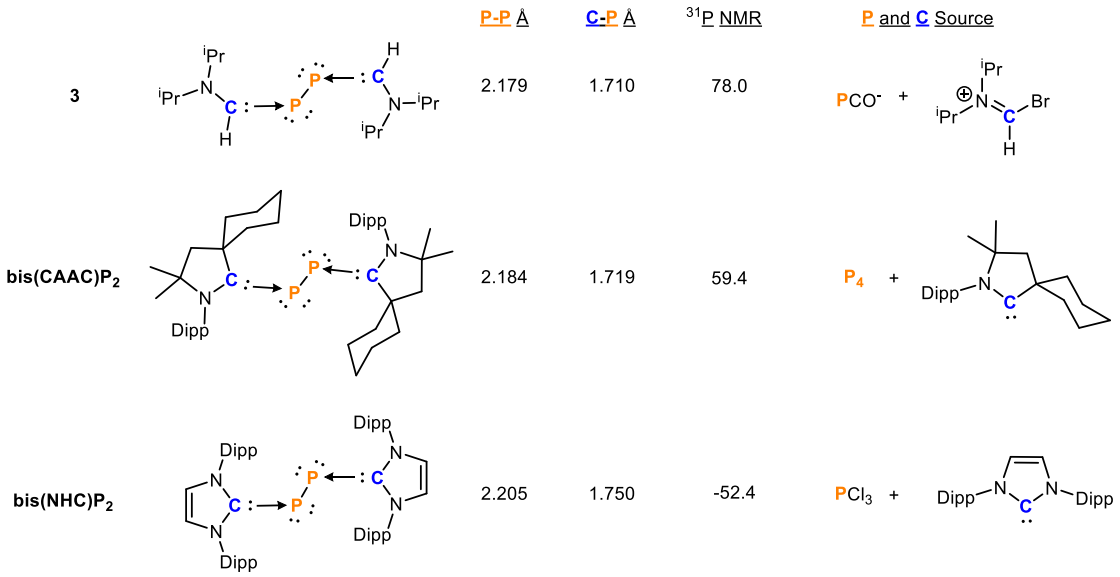

Figure 3.9 – Properties of bis(carbene)P_2 adducts and their respective sources.

Despite not having a strong bis(carbene)P_2 character, we wondered if the carbene units of **3** could be released, thereby generating free P_2. Upon heating **3** at 80 °C for 6 hours, no reaction was observed. However, upon irradiating a C_6D_6 solution of **3** (λ_{max} = 349 nm) with 365 nm light, we observed the formation of the carbene dimer, namely the 1,2-bis(diisopropylamino)ethylene **4** as a cis/trans mixture, along with P_4 and a red precipitate indicative of red phosphorus (Figure 3.10). This was the first evidence for the transient formation of P_2, which is known to spontaneously dimerize and polymerize to white and red phosphorus, respectively.[89]

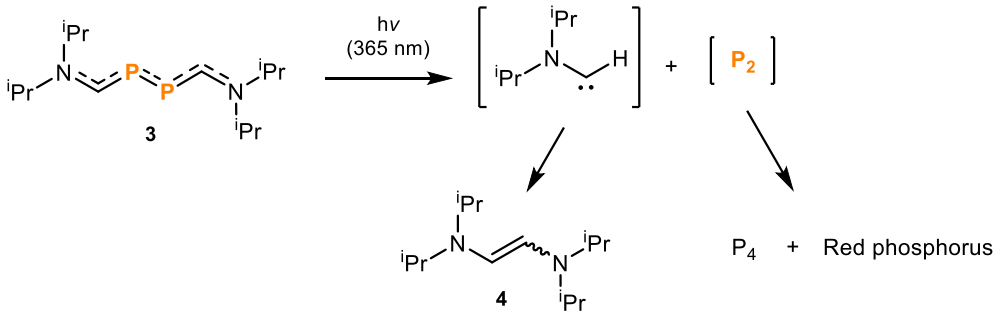

Figure 3.10 – The photolytic cleavage of carbene units from **3**.

Based on this encouraging result, we investigated the possibility of intercepting P_2 using a 1,3-diene – a rection well-established in the literature.[90] Upon adding a stoichiometric amount 1,3-cyclohexadiene to a THF solution of **3**, no reaction was observed – even upon heating to 70 °C overnight. However, when we irradiated a solution of **3** with 1,3-cyclohexadiene as solvent, we observed the clean formation of the expected double Diels-Alder product with a ^{31}P NMR shift of -80.5 ppm along with the carbene dimer **4**.

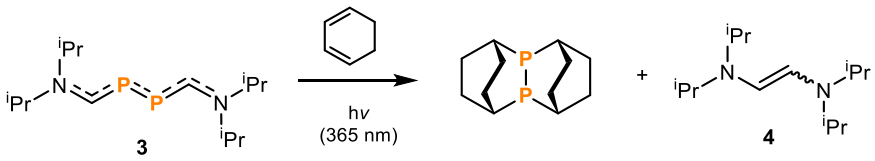

Figure 3.11 – Trapping P_2 using 1,3-cyclohexadiene to give the double Diels-Alder adduct.

When we conducted the same reaction using 2,3-dimethylbutadiene, we were surprised by the results. We observed the formation of two phosphorus containing products with ^{31}P NMR chemical shifts at -49.0 ppm (minor) and -54.4 ppm (major) ppm, along with a small signal at -41.8 ppm. The major phosphorus compound **5** (Figure 3.12) was quickly recognized as the usual

product observed by Cummins *et al*. and by Wolf and Goicoechea *et al*., namely the double Diels-Alder adduct of triple-bonded diphosphorus. The identity of the minor product **7** was first deduced by HR-MS analysis. Observation of trace amounts of **6** indicated that **7** is formed as a result of the insertion of alkene **4** into the P-P bond of **6**. Note that the reaction of phosphinidenes and phosphinidene metal complexes with dienes giving the corresponding phospholenes have precedents,[91] as well as the insertion of alkenes into diphosphines.[92] To further confirm the structure of **7**, bis(diisopropylamino)ethylene **4** and bis(phospholene) **6** were independently synthesized and allowed to react under identical conditions, giving compound **7**.

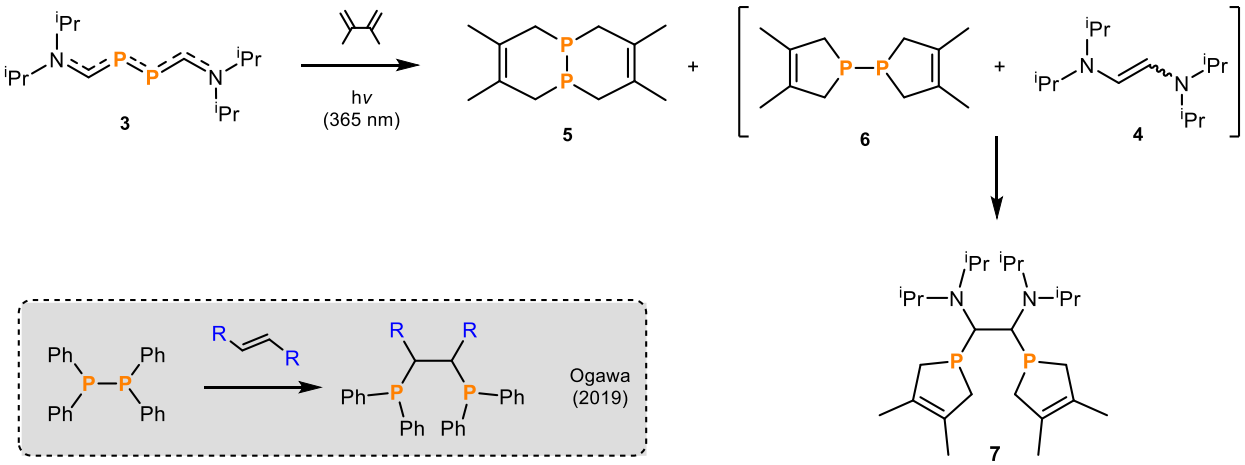

Figure 3.12 – Trapping of diphosphorus with 2,3-dimethylbutadiene to give double Diels-Alder product **5** and (bis)phosphinidene products **6** and **7**.

The formation of bis(phospholine) **6** is intriguing as it is formally derived from the trapping of single-bonded diphosphorus, or a (bis)phosphinidene. Furthermore, it indicates that the elimination of the (amino)carbenes occurs stepwise. The first step leads to the hitherto unknown diphosphorus analogue **9** of a diazo compound, which is trapped by a [4+1] reaction with

dimethylbutadiene to give **10** (Figure 3.13). Then a second carbene elimination gives a transient phosphinidene, which also reacts with the diene to afford the (bis)phospholine **6**.

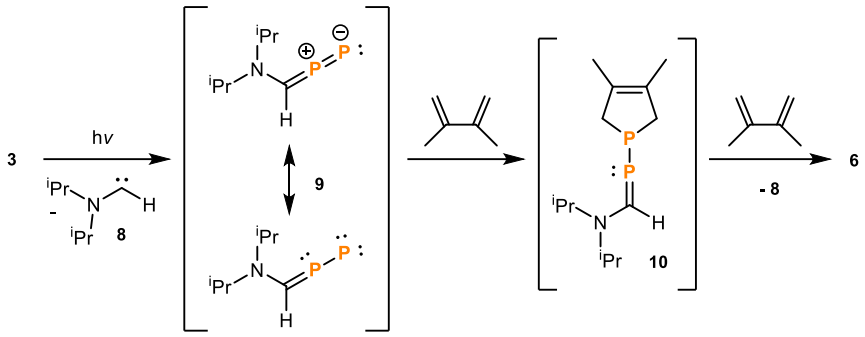

Figure 3.13 – Proposed intermediates in the formation of **6**, via stepwise elimination of carbene fragments from **3**.

To see if this P_2 generation approach is generalizable to other bis(carbene)P_2 adducts, we attempted the thermal and photolytic trapping of P_2 with 2,3-dimethylbutadiene using **bis(NHC)P$_2$** and **bis(CAAC)P$_2$**. Despite exploring a range of conditions, we found that neither of these adducts behave as P_2 surrogates.

3.5 Carbene-exchange at P_2

Based on these results showing that the carbene fragments can be cleaved from P_2, we wondered if we could substitute the (amino)carbenes with other ligands. We attempted to use triphenyl phosphine and NHC (:C{N(2,6-*i*Pr$_2$C$_6$H$_3$)CH}$_2$) for this substitution. Of course, the product that would ensue from the double substitution with NHC would be Robinson's **bis(NHC)P$_2$** adduct. However, neither of these ligands were unable to accomplish this exchange (Figure 3.14).

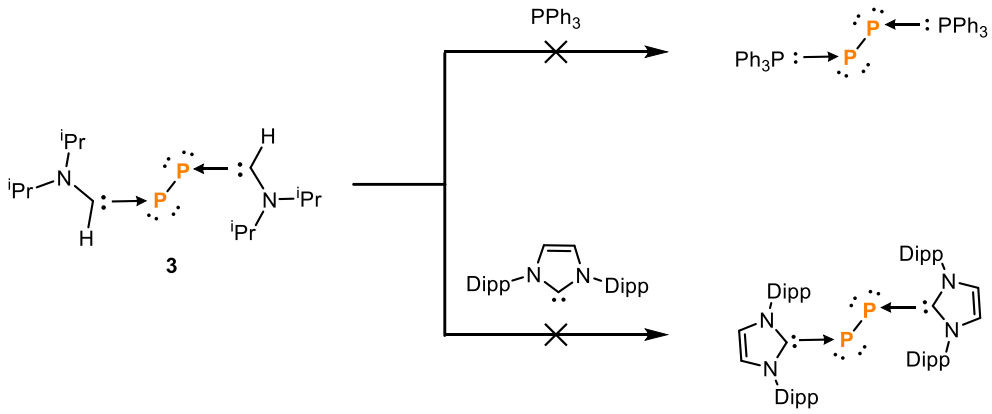

Figure 3.14 – Attempts to exchange (amino)carbenes with triphenyl phosphine and NHC.

We thought perhaps that a more ambiphilic carbene such as CAAC, may be a better candidate for this substitution. To our surprise, without any irradiation, the addition of 2 equivalents of CAAC to **3** gave rise to a new compound containing two doublets in the $^{31}P\{^{1}H\}$ NMR spectrum, along with the mixed carbene dimer **11** (Figure 3.15). This desymmetrization of the phosphorus atoms was indicative that one of the monosubstituted (amino)carbenes was replaced with CAAC. Furthermore, in the proton-coupled ^{31}P NMR spectrum, one of these doublets exhibited coupling to a proton, while the other signal did not. With these coupling patterns it was apparent that one of these signals corresponds to the phosphorus coordinated by the (amino)carbene while the other phosphorus atom is coordinated by the CAAC. It is worth mentioning that we did not observe any traces of the alkene **4** resulting from the self-dimerization of the monosubstituted (amino)carbene. Addition of another 3 equivalents of CAAC led to the doubly substituted **bis(CAAC)P_2** adduct.

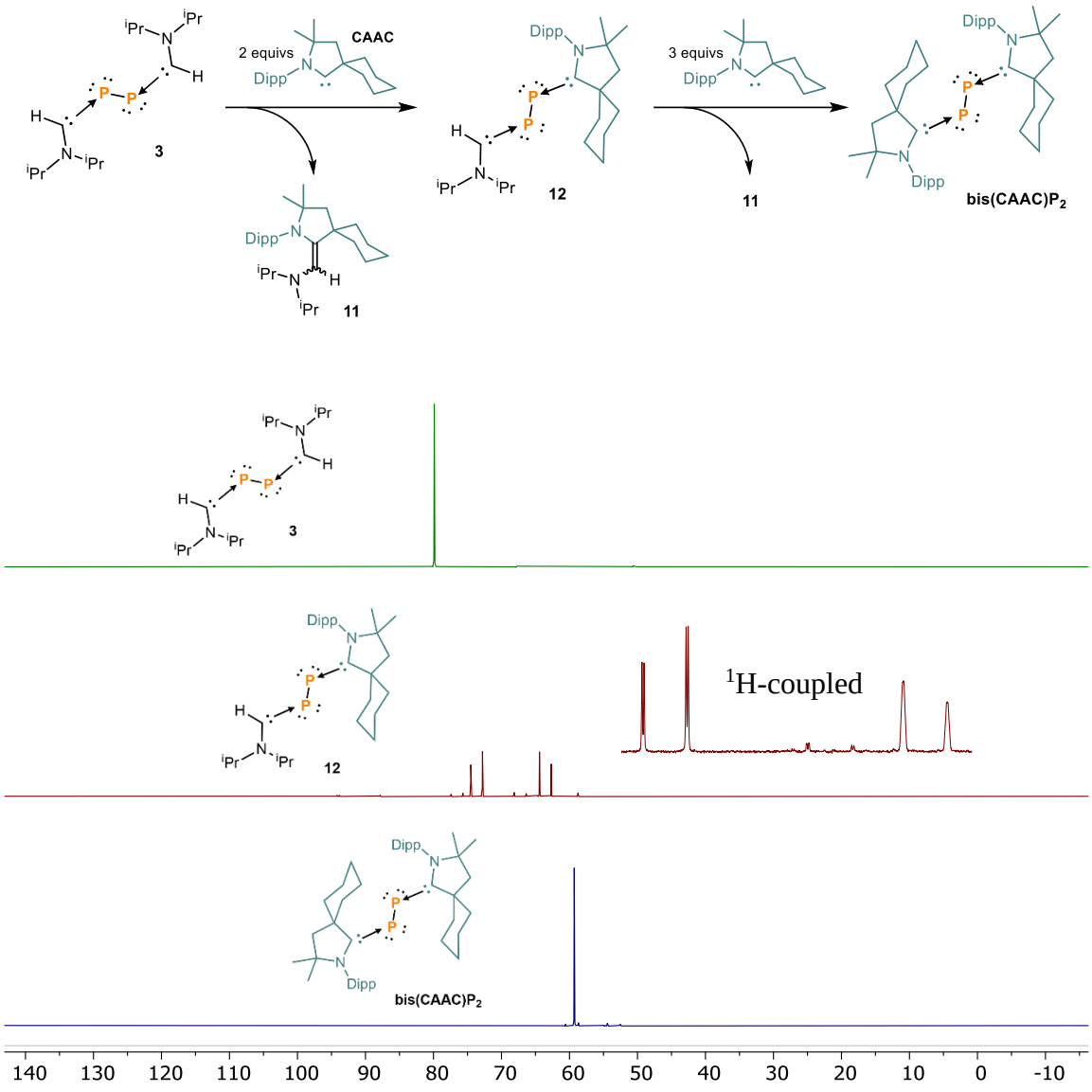

Figure 3.15 – Stepwise exchange of (amino)carbene with CAAC and the $^{31}P\{^{1}H\}$ NMR (162 MHz) spectra in THF-d8 of **3** (green), **12** (red), and **bis(CAAC)P$_2$** (blue).

Given that we did not observe any traces of 1,2-bis(diisopropylamino)ethylene **4**, we ruled out a dissociative mechanism for this substitution process. Furthermore, a dissociative mechanism is highly unlikely in that **3** would be unstable on its own if the carbene fragments dissociate spontaneously in solution. Therefore, it seems likely that this mechanism is associative in nature. These carbene-carbene exchange reactions are akin to those observed with the stable

phosphinidene, for which DFT calculations also predicted an associative mechanism.[93] In the case of carbene exchange on **3**, we propose that the first CAAC ligand undergoes a [2+1] cycloaddition to give a highly strained 3-membered phosphirane intermediate **3-CAAC**. The phosphirane then undergoes retro-[2+1] to eliminate alkene **11**, resulting in intermediate **9** which is quickly trapped by a second equivalent of CAAC. This process occurs once more on the other phosphorus atom to form the doubly substituted **bis(CAAC)P$_2$**. Intermediate **9** can be regarded as the phosphorus analog of a diazo compound. Such species have not been reported, however, can be expected to react quite differently than diazo compounds due to the favorable extrusion of dinitrogen versus diphosphorus from carbenes.

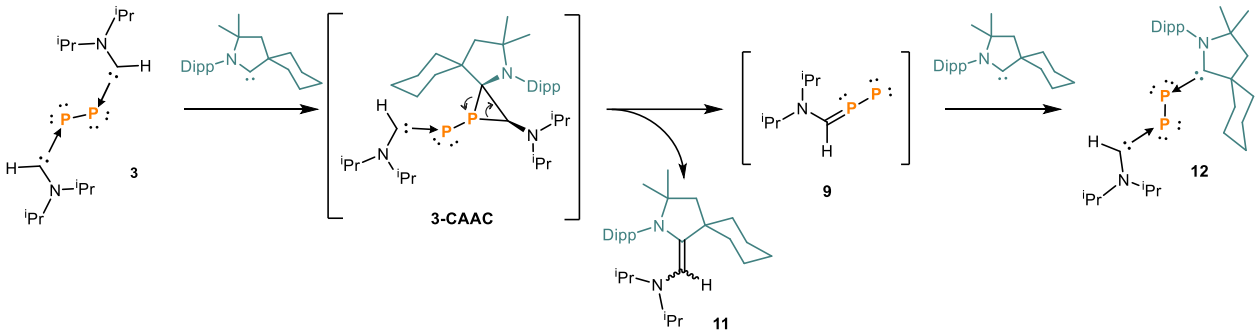

Figure 3.16 – Proposed intermediates in the substitution of (amino)carbene with CAAC.

Phosphirane intermediate **3-CAAC** was not observed likely due to the propensity for the alkene **11** to be quickly eliminated by steric compulsion. This made us wonder if a 4-membered phosphetane intermediate, stemming from a [2+2] cycloaddition with an alkene substrate, would be stable enough to be isolated. To test this, we would need to react **3** with an alkene. Given the electron-rich nature of **3**, we decided to use the electron-poor dimethyl fumarate as our alkene substrate. To our delight, one equivalent of dimethyl fumarate reacted cleanly and quantitatively

with **3** to give the cycloaddition product **13** (Figure 3.17) which is stable at room temperature. To ensure that this was not light-mediated, we obtained the same result when the experiment was repeated in the dark. The formation of **13** is yet another piece of evidence that supports an associative mechanism for the aforementioned carbene exchange reactions. The addition of excess dimethyl fumarate did not yield further reaction. Attempts to photolytically remove the carbene moiety led to a complex mixture containing many different phosphorus NMR signals.

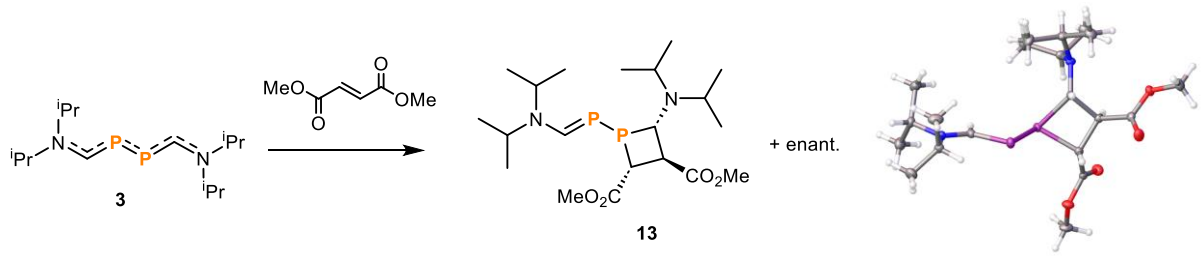

Figure 3.17 – Addition of dimethyl fumarate to **3** to give 4-membered phosphetane **13** and the X-ray crystal structure.

The final indication that the carbene-exchange reaction mechanism is associative is that the alkene **11** is initially in the *Z* configuration when produced from the reaction. This stereochemistry is retained at lower temperatures, which is presumably the reason that the crystals grown at -38 ^{o}C were purely in the *Z* isomer. Only after several days in solution at room temperature is the alkene completely converted to the more thermodynamically stable *E* isomer. If the substitution was of a dissociative nature, with both free carbenes existing in solution, we would expect to see a mixture of alkene **11** that is enriched in the *E* isomer, and perhaps even some of alkene **4**, resulting in the homo-dimerization of the monosubstituted (amino)carbene.

We believe the main driving force behind this reaction to be the "dimerization" of (amino)carbene **8** with CAAC to give **11** which is only possible due to the fact that **8** is relatively

small. To validate this hypothesis, we attempted to exchange the NHC ligand on the **bis(NHC)P$_2$** adduct with CAAC. The **bis(NHC)P$_2$** adduct was synthesized in similar manner as reported by Robinson. With two such bulky ligands, an associative process would be highly unlikely. As we had expected, there was no reaction even with excess CAAC at elevated temperatures (Figure 3.18).

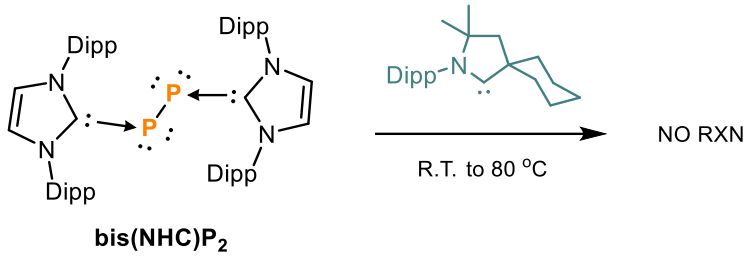

Figure 3.18 – CAAC does not substitute NHCs on P_2.

Overall, **3** was demonstrated to be a surrogate of P_2 under the classical triple-bonded form (P≡P), as well as a (bis)phosphinidene (P-P) synthetic equivalent. These findings provide new insights into the stabilization and reactivity of diphosphorus species, offering promising avenues for future synthetic applications. Our lab continues to explore carbene adducts of P_2 and their various applications.

3.6 Investigating 3 as a P$^-$ Transfer Agent

While the aforementioned results have shown **3** to be a source of P_2, we were interested by the fact that we obtained **P+** from the irradiation of **2** in chloroform solvent. While we could not identify the fate of the other phosphorus species from this reaction, we were curious to see if **3** was an intermediate. Thus, we added a super-stoichiometric amount of chloroform to a solution of **3** in

C_6D_6 and found that **P+** is obtained under irradiation (Figure 3.19). The same was true using a super-stoichiometric amount of CH_2Cl_2.

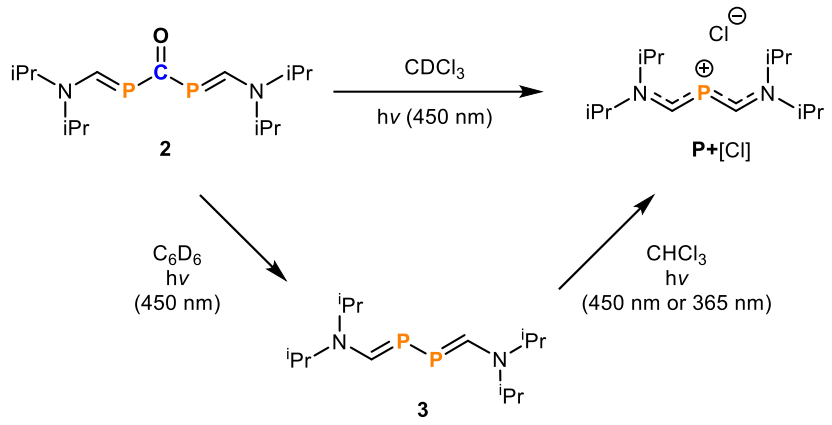

Figure 3.19 – Confirmation that **3** leads to **P+** under irradiation in the presence of chloroform.

The formation of **P+** from **3** is evidence that formally, a P^- anion must have been transferred. This result is also analogous to Driess' bis(silylene)-stabilized P_2, which was demonstrated to be a P^- anion transfer agent (Figure 3.20).[94] In his case, a series of oxidants or Lewis acids were able to accept the P^- anion. We wondered if we could obtain similar results using our simpler bis(carbene) system.

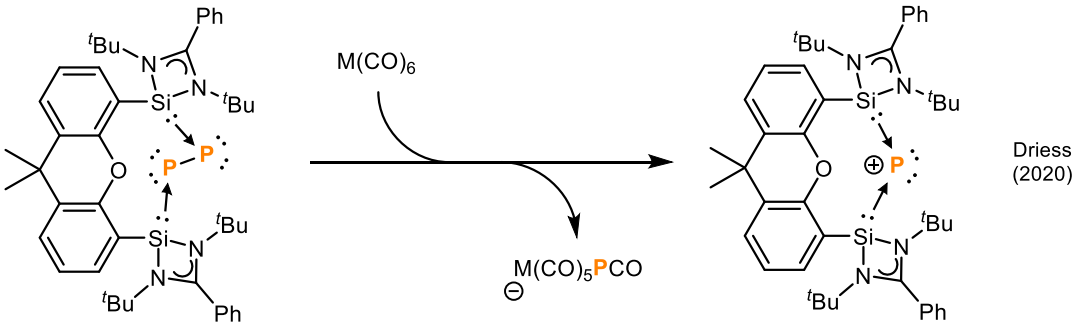

Figure 3.20 – A bis(silylene)-stabilized P_2 as a P^- transfer agent.

We first attempted to transfer P^- to a hexacarbonyl transition-metal complex. Just as in Driess' example, we expected P^- insertion into one of the metal-carbonyl bonds, whose ^{31}P NMR shows an upfield signal at -414 ppm (when M = Cr). Thus, we prepared a sample of **3** with $Cr(CO)_6$ in THF-d8 and found that no reaction was observed even at elevated temperatures. When we subjected the mixture to UV-irradiation, we observed the formation of **P+** (Figure 3.21), however, we did not observe any of the anticipated $Cr(CO)_5PCO^-$ ion. In fact, we were surprised that we did not observe any other phosphorus containing species. The same result was yielded using other metals such as molybdenum and tungsten. Since this reaction only occurred under irradiation, we believed that these conditions may have led to the degradation of the ensuing metal complex. Thus, we prepared the singly acetonitrile substituted $W(CO)_5CH_3CN$ complex to see if the more labile acetonitrile ligand could be displaced without irradiation. Upon adding **3** to the $W(CO)_5CH_3CN$ complex, however, we again did not observe any reaction.

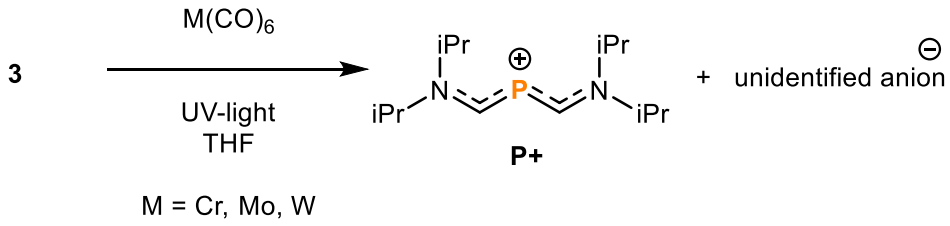

Figure 3.21 – Attempted transfer of P^- to metal-carbonyl complexes.

Since our attempts to thermally transfer anionic P^- to $M(CO)_6$ yielded no reaction and photolytic conditions seemed to have decomposed the resulting metal containing product, we tried a variety of other candidates that can act as Lewis acids (Figure 3.22) to catch the P^- anion under thermal conditions. Surprisingly, while each of these attempts gave the same cation **P+**, we were unable to identify any other phosphorus containing species. This led us to believe that while

formally, a P^- ion is being released, the transfer to another species does not occur in the expected fashion.

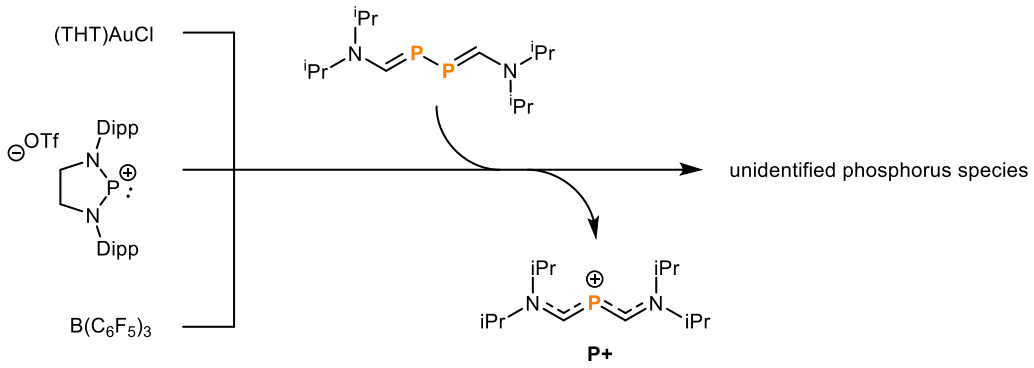

Figure 3.22 – Attempted transfer of P^- to various Lewis acids.

3.7 Exploring Other Reactivity Modes of 3

While we have previously explored **3** as a source of P_2 and P^-, we were curious to probe its functionalization, particularly in the realm of small molecule activation. We wondered if we could further functionalize **3** using CO_2. Under a high-pressure atmosphere of CO_2 gas at 50 °C, the starting material **3** remained unchanged.

In 2013, Robinson demonstrated that the **bis(NHC)P$_2$** can split molecular oxygen.[95] When we subjected **3** to oxygen, however, rapid decomposition into *N*,*N*-diisopropyl formamide and insoluble black solids occurred. The degradation of **3** with O_2 is not well understood since we were unable to observe any intermediate due to the rapidity of the reaction. Robinson reported that in the case of **bis(NHC)P$_2$**, the mechanism of triplet O_2 activation may involve a single-electron transfer. We later found (*vide infra*) that oxidation of **3** leads to the cleavage of the P-P bond, explaining why **3** does not react with O_2 in the same manner as **bis(NHC)P$_2$**. Similarly, simple

hydrolysis of **3** in air results in decomposition into the formamide along with a red precipitate (likely red phosphorus).

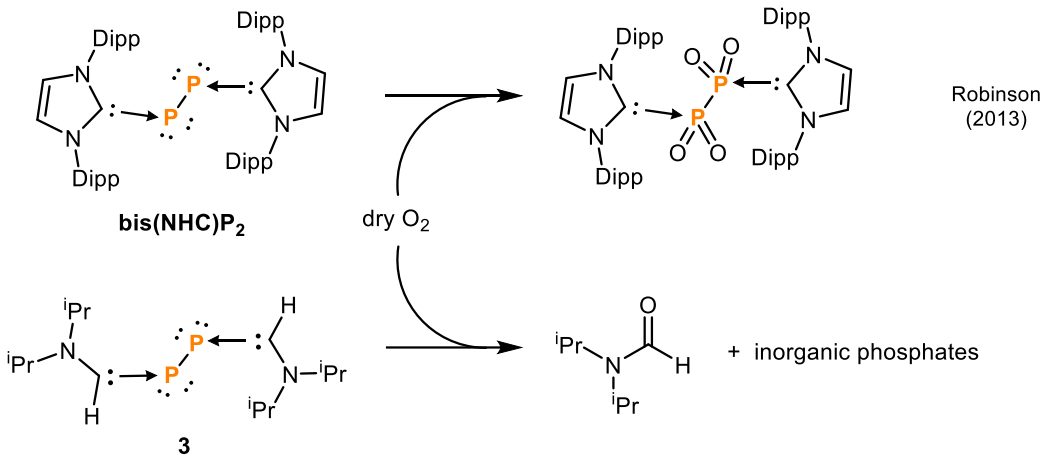

Figure 3.23 – Reactions of **bis(NHC)P2** and **3** with molecular oxygen.

We then probed into the electro-oxidation chemistry of **3**. Our group has previously shown that both **bis(NHC)P2** and **bis(CAAC)P2** adducts can undergo single-electron oxidation to give the radical cations.[96] In an attempt to attain a similar result with **3**, a stoichiometric amount of the oxidizing agent, silver hexafluoroantimonate ($AgSbF_6$), was added to our compound. The major product of this reaction was, not to our surprise, **P+** with a SbF_6^- counter anion. This [**P+**]SbF_6 ion-pair was characterized by X-ray crystallography. Cationic **P+** was also obtained using nitrosyl hexafluoroantimonate ($NOSbF_6$). This result is yet another example of the loss of P^- from **3**, which has been previously established to occur in the presence of electrophiles.

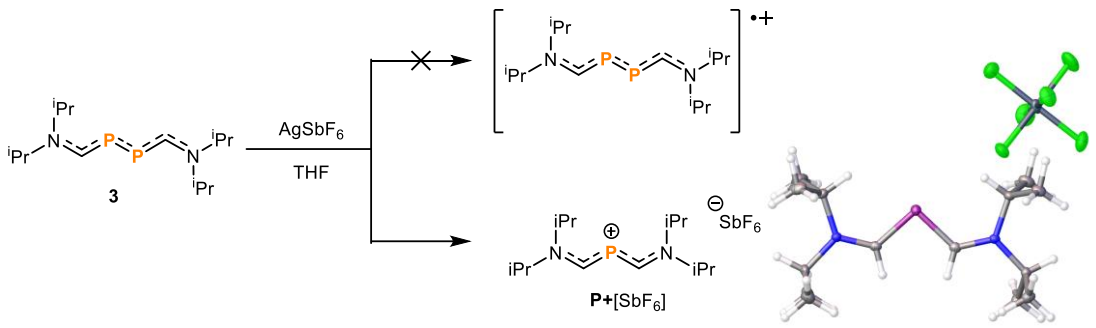

Figure 3.24 – Reaction of **3** with oxidizing $AgSbF_6$ leads to loss of P^- to give P+ with SbF_6^- anion. X-ray crystal structure of this ion-pair.

3.8 Conclusion and Outlook

In conclusion, we have discovered a unique method to synthesize a diphospha-urea derivative **2** starting from a haloiminium salt **1** and NaPCO. By photolytic decarbonylation, we showed that **2** is the precursor to diphosphabutadiene **3**, which could also be described as P_2 capped by two monosubstituted (amino)carbenes. Among the few examples of carbene-stabilized P_2 adducts, compound **3** was unique in its ability to act as a P_2 surrogate. Not only does **3** generate P_2 in the classical triple-bonded form (P≡P), but **3** also acts as a bis(phosphinidene) (P-P) synthetic equivalent. Additionally, we demonstrated the first example of stepwise exchange of ligands on P_2, underscoring the utility of **3** as a bis(phosphinidene) source. These findings provide new insights into the stabilization and reactivity of diphosphorus species, offering promising avenues for future synthetic applications. Lastly, although we have focused primarily on the reactivity of **3**, we have not given the same attention to **2** and **P+**. We believe that much can also be uncovered in the exploration of these two novel species.

3.9 Acknowledgments

I would like to thank Ying Kai Loh for his fruitful discussions that have greatly influenced the direction of this project. I also thank Rodolphe Jazzar for your insights on experimental techniques. I would like to thank Prof. Erik Romero for allowing me the use of his photolysis setup. Thank you to François Vermersch for motivating me to synthesize NaPCO.

Chapter 3 is adapted, in part, from A Carbene-Stabilized Diphosphorus: A Triple-Bonded Diphosphorus (P≡P) and a Bis(phosphinidene) (P-P) Transfer Agent. Yoon, Joseph, Abdellaoui, Mehdi; Gembicky, Milan; Bertrand, Guy. This paper is currently submitted to a journal for review. The dissertation author will be the first author of this paper.

3.10 Experimental

3.10.1 General Considerations

All reactions were performed under an atmosphere of argon by using standard Schlenk or dry box techniques. CAAC was synthesized according to the previous literature. The bis(phospholine) **6** was independently synthesized from known methods[97] with new characterization data in this document (see NMR and X-ray sections).

Materials: Solvents were dried by distillation over sodium (benzene, toluene, diethyl ether, tetrahydrofuran, pentanes) or calcium hydride (dichloromethane, chloroform, hexanes). 2,3-dimethyl-1,3-butadiene was freshly distilled over sodium borohydride and stored in a dry-box freezer over 3 Å molecular sieves. All other reagents were purchased from commercial sources and used without further purification unless otherwise noted.

Instrumentation: NMR spectra were recorded on a Varian INOVA 500 MHz or JEOL 400 MHz spectrometer. Chemical shift values for ^{1}H are referenced to the residual protio-solvent (^{1}H) resonance of C_6D_6 (δ: 7.16), $CDCl_3$ (δ: 7.26), THF-d8 (δ:3.58, 1.73). Chemical shift values for ^{13}C are referenced to the solvent (^{13}C) resonance of C_6D_6 (δ: 128.1), $CDCl_3$ (δ: 77.2), THF-d8 (δ:67.6, 25.4). Chemical shifts are quoted in δ (ppm) and coupling constants in J (Hz) and multiplicities are abbreviated as follows: s = singlet, d = doublet, t = triplet, sept = septet, m = multiplet, brs = broad signal. High-resolution mass spectrometry measurements were performed at the UC San Diego Mass Spectrometry Laboratory on an Agilent 6230 Accurate-Mass TOFMS spectrometer. Single crystal X-ray diffraction data were collected on Bruker Apex diffractometers using Mo-Kα

radiation ($\lambda = 0.71073$ Å) or Cu-Kα radiation ($\lambda = 1.54178$ Å) at the UC San Diego Crystallography Facility. Absorption spectra were recorded on a JASCO V-630 spectrophotometer at ambient temperature.

3.10.2 Experimental Procedures

Preparation of **1-Br** and **1-OTf**

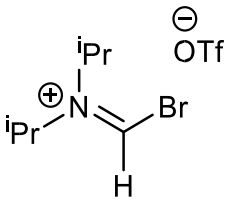

1-OTf

Preparation of bromide salt: A solution of *N*,*N*-diisopropyl formamide (3.0 mL; 10.35 mmol) in toluene (100 mL) was cooled to -78 ^{o}C. Providing a gentle flow of argon, oxalyl bromide (2.9 mL; 10.35 mmol) was slowly added over the course of 1 minute with vigorous stirring. The cold bath was removed, and a snow-white solid precipitated within several minutes. After 2 hours, the slurry was filtered leaving behind a snow-white solid. The bromide salt was washed three times with diethyl ether (about 20 mL per wash) and dried under vacuum to afford **1-Br** (5.75g; quantitative) which was used without further purification or characterization.

Counter anion exchange to triflate: **1-Br** (3.18g; 11.7 mmol) was resuspended in dichloromethane and cooled to -78 ^{o}C followed by the slow addition of trimethylsilyl triflate (4.2 mL; 23.3 mmol). The cold bath was removed, and the reaction proceeded for 2 hours at room temperature. The volatiles were removed under vacuum. The resulting brown residue was triturated with benzene (25 mL), inducing the precipitation of a tan solid. The product was filtered, washed three times with hexane (about 10 mL per wash), and dried to afford **1-OTf** (3.60g; 90.1% yield) as an off-white powder.

^{1}H NMR (500 MHz, $CDCl_3$) δ = 10.46 (s, 1H), 5.06 (sept, $^{3}J_{HH}$ = 6.7 Hz, 1H, C*H*$(CH_3)_2$), 4.63 (sept, $^{3}J_{HH}$ = 6.7 Hz, 1H, C*H*$(CH_3)_2$), 1.62 (d, $^{3}J_{HH}$ = 6.7 Hz, 6H, CH(C*H*$_3)_2$), 1.56 (d, $^{3}J_{HH}$ = 6.7 Hz, 6H, CH(C*H*$_3)_2$).

^{13}C{^{1}H} NMR (126 MHz, $CDCl_3$) δ = 162.28, 120.65 (q, $^{1}J_{CF}$ = 320.0 Hz), 62.07, 61.67, 23.15, 19.17.

^{19}F NMR (376 MHz, $CDCl_3$) δ = -78.17.

Preparation of **2**

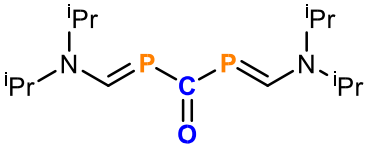

2

From **1-Br**: A solid mixture of **1-Br** (1.1 g; 4.03 mmol) and [Na(PCO)(dioxane)$_{3.5}$] (3.9 g; 9.91 mmol) was cooled to 0 ^{o}C and wrapped with aluminum foil. Under a gentle flow of argon, toluene (45 mL) was added. A vent needle to an oil bubbler was attached to prevent buildup of pressure, and the reaction was allowed to warm to room temperature overnight with stirring. The solution was filtered, and the product was extracted twice with DCM, and finally once more with toluene. Volatiles were evaporated under vacuum at 35 ^{o}C. The resulting orange solid was washed three times with cold diethyl ether and dried under vacuum to afford **2** (0.94 g; 74% yield).

From **1-OTf**: The above procedure was repeated starting with a solid mixture of **1-OTf** (0.8 g; 2.34 mmol) and [Na(PCO)(dioxane)$_{3.5}$] (2.27 g; 5.61 mmol) to afford **2** (0.22 g; 60% yield).

^{1}H NMR (500 MHz, C_6D_6) δ = 10.73 (t, $^{2}J_{HP}$ = 7.0 Hz, 2H, NC*H*P), 4.00 (m, 2H, C*H*$(CH_3)_2$), 2.89 (sept, $^{3}J_{HH}$ = 6.4 Hz, 2H, C*H*$(CH_3)_2$), 0.79 (d, $^{3}J_{HH}$ = 6.7 Hz, 12Hz, CH(C*H*$_3)_2$), 0.74 (d, $^{3}J_{HH}$ = 6.7 Hz, 12H, CH(C*H*$_3)_2$).

^{13}C{^{1}H} NMR (126 MHz, C_6D_6) δ = 236.4 (t, $^{1}J_{CP}$ = 81.6 Hz, P*C*(O)P), 187.3 (dd, $^{1}J_{CP}$ = 21.6 Hz, $^{3}J_{CP}$ = 14.8 Hz, N*C*HP), 55.8 (t, $^{3}J_{CP}$ = 8.5 Hz, *C*H$(CH_3)_2$), 48.9 (*C*H$(CH_3)_2$), 23.1 (CH(*C*H$_3)_2$), 18.6 (CH(*C*H$_3)_2$).

^{31}P{^{1}H} NMR (121 MHz, $CDCl_3$) δ = 84.0 (s).

^{31}P NMR (121 MHz, $CDCl_3$) δ = 84.0 (broad s).

HRMS (ESI+): calcd. for **2** $[M+H]^+$ $[C_{15}H_{31}N_2OP_2]^+$ m/z: 317.1906, found 317.1909.

Preparation of **3**

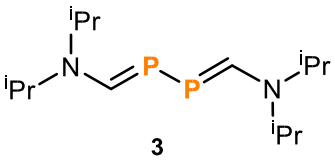

3

In a skinny pressure-sealed Schlenk flask, **2** (90 mg; 0.285 mmol) was dissolved in THF (15 mL). The resulting yellow solution was irradiated for 1 hour with 450 nm light while maintaining an internal temperature between 35-40 ^{o}C using a fan. The volatiles were removed under vacuum. The resulting orange solids were resuspended in pentane and cooled down to -35 ^{o}C. The product was filtered, washed with cold pentane, and dried under vacuum to give **3** (62 mg; 76% yield).

NOTE: For each experiment, the progression of conversion from **2** to **3** was monitored by ^{31}P NMR. The typical time required for full conversion varied by experiment, ranging between 50 to 70 minutes.

^{1}H NMR (400 MHz, THF-d_8) δ = 8.97 (s, 2H, NC*H*P), 3.99 (broad, 4H, C*H*$(CH_3)_2$), 1.17 (d, $^{3}J_{HH}$ = 6.8 Hz, 24H, CH(C*H*$_3)_2$).

$^{13}C\{^1H\}$ NMR (101 MHz, THF-d_8) δ = 182.5 (dd, $^1J_{CP}$ = 12.6 Hz, $^2J_{CP}$ = 4.2 Hz, N*C*HP), 50.0 (*C*H(CH_3)$_2$), 21.5 (CH(*C*H_3)$_2$).

$^{31}P\{^1H\}$ NMR (162 MHz, THF-d_8) δ = 79.9 (s).

^{31}P NMR (162 MHz, THF-d_8) δ = 79.9 (s).

HRMS (ESI+): calcd. For **3** $[M+H]^+$ $[C_{14}H_{31}N_2P_2]^+$ m/z: 289.1957, found 289.1957.

Photochemical degradation of **3**

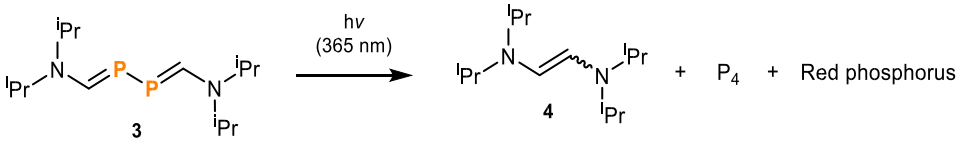

In a J-young NMR tube, **2** (53 mg; 0.17 mmol) was dissolved in C_6D_6 (0.6 mL) and irradiated with 450 nm light until full conversion to **3** was observed by ^{31}P NMR. This solution was then irradiated with 365 nm light overnight, resulting in the precipitation of a red solid. The resulting ^1H and ^{13}C NMR spectra confirmed the formation of carbene dimer, 1,2-bis(diisopropylamino)ethylene, as a *cis*/*trans* mixture (see NMR spectra section) accompanied by the disappearance of the starting material signals by ^{31}P NMR and the appearance of a singlet at -520 ppm (P_4). The identity of 1,2-bis(diisopropylamino)ethylene was also confirmed by mass spectroscopic analysis (calcd. For **4** $[M+H]^+$ $[C_{14}H_{31}N_2]^+$ m/z: 227.2482, found 227.2478.)

Photolysis of **3** with 2,3-dimethylbutadiene

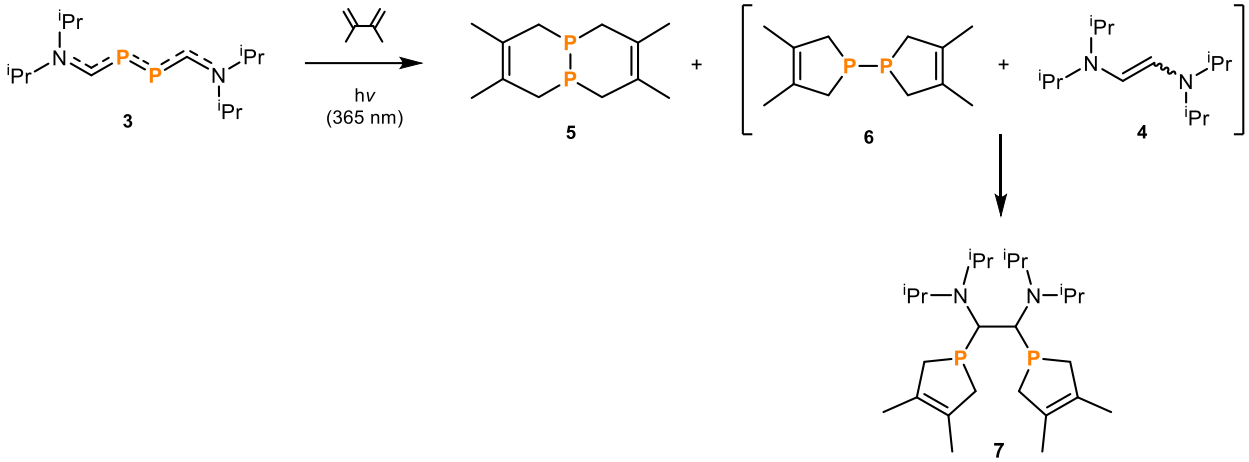

In a skinny pressure-sealed flask, **3** (75 mg; 0.26 mmol) was dissolved in a 1:1 (v/v) solution of THF and 2,3-dimethyl-1,3-butadiene (5 mL). With vigorous stirring, the solution was irradiated with 365 nm light overnight, while maintaining a temperature between 35-40 ^{o}C in the photolysis chamber using a fan. Volatiles were removed under vacuum at room temperature. Using a minimal amount of THF, the mixture was transferred to a sublimator, where the volatiles were slowly removed under vacuum at room temperature. A water-cooled (0 ^{o}C) cold finger was attached, and the mixture was heated to 110 ^{o}C under strong vacuum, resulting in the deposition of white solids onto the cold finger. Inside a glovebox, the solids were extracted from the cold finger with pentane. The product was dried under vacuum, leaving behind a mixture of **4**, **5**, and **7**, along with a trace of **6** (calc. for **5/6** $[M+H]^+$ $[C_{12}H_{21}P_2]^+$ m/z: 227.1113, found 227.1115; calc. for **7** $[M+H]^+$ $[C_{26}H_{51}N_2P_2]^+$ m/z: 453.3522, found 453.3528).

Reaction of **4** and **6** to form **7**

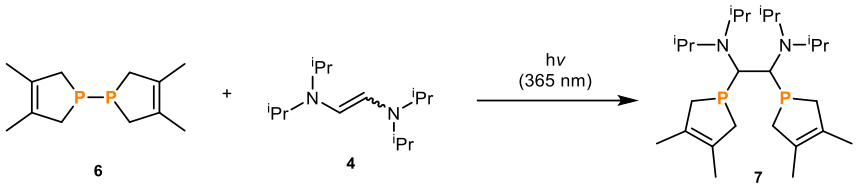

[Note: Compound **4** was prepared by the photolytic degradation of **3** with 365 nm light]. Solids **4** (ca. 1 mmol) and **7** (170 mg; 0.75 mmol) were placed in a pressure-sealed flask and dissolved in 15 mL THF showing the bis(phospholine) ^{31}P NMR shift of -41.9 ppm. The contents were irradiated with 365 nm light overnight, resulting in the full conversion to **6** with a ^{31}P NMR shift of -48.6 ppm (see NMR section).

Synthesis of **11**, **12**, and **bis(CAAC)P$_2$**

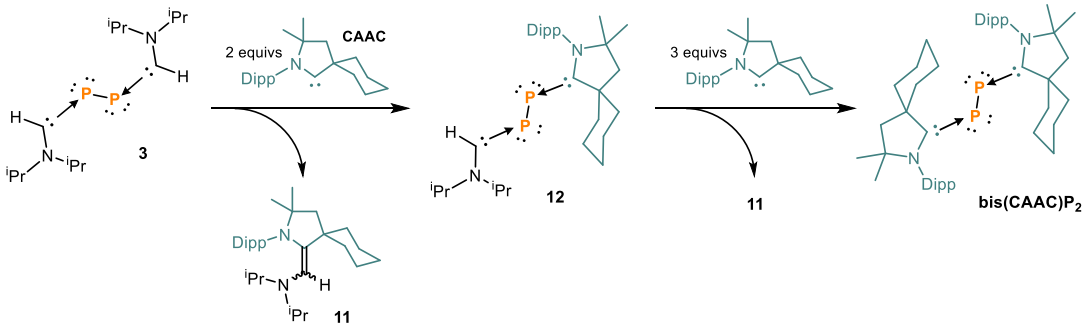

A 0.20 M solution of CAAC in THF (1.0 mL; 0.20 mmol) was added to **3** (30 mg; 0.10 mmol) in a J-young NMR tube. The reaction was monitored by ^{31}P NMR. After 2 days, **3** had been consumed and one major phosphorus containing species **12** was observed by ^{31}P NMR (see NMR spectra section). To this was added another aliquot of the 0.20 M solution of CAAC in THF (1.5 mL; 0.30 mmol), giving quantitative conversion to **bis(CAAC)P$_2$** by ^{31}P NMR. Volatiles were removed and bright orange solids were precipitated out of cold ether. The orange solid was collected and washed with cold ether and dried under vacuum to give **bis(CAAC)P$_2$** (29 mg; 41% yield) (calc. for

bis(CAAC)P$_2$ $[M+H]^+$ $[C_{46}H_{71}N_2P_2]^+$ m/z: 713.5087, found 713.5085) (see NMR spectra section). The filtrates were combined and recrystallized by evaporation at -33 ^oC to give colorless cubic crystals, which were washed with minimal cold pentane to give **11** (28 mg; 32% yield) (calc. for **11** $[M+H]^+$ $[C_{30}H_{51}N_2]^+$ m/z: 439.4047, found 439.4050) (see NMR spectra section).

Synthesis of **13**

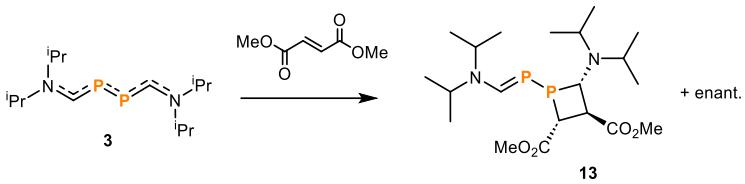

In a J-Young NMR tube, **3** (100 mg; 0.347 mmol; 1 equiv.) and dimethyl fumarate (50.0 mg; 0.347 mmol; 1 equiv.) were dissolved in THF-d8 and covered with aluminum foil. NMR measurements were acquired until the complete consumption of starting material and quantitative conversion to the product. The solvent was removed under vacuum, and the product was recrystallized by slow evaporation of a saturated ether solution in the glovebox freezer (-38 ^oC) over the course of three months to give bright yellow X-ray quality crystals.

^{1}H NMR (500 MHz, THF-d8) δ = 9.23 (t, $^2J_{HP}$ = 12.3 Hz, 1H, NC(sp^2)*H*P), 4.43 (m, 1H, C*H*(CH$_3$)$_2$), 3.77-3.65 (m, 1H, C*H*(CH$_3$)$_2$; 1H, NC(sp^3)*H*P), 3.62-3.52 (m, 1H, C(O)C(*H*CC); s, 3H, OC*H*$_3$; s, 3H, OC*H*$_3$), 3.30 (sept, 2H, C*H*(CH$_3$)$_2$), 2.95 (vt, $^2J_{HP}$ = 9.2 Hz, 1H, C(O)C(*H*CP)), 1.29-1.13 (dd, 6H, CH(C*H*$_3$)$_2$; dd, 6H, CH(C*H*$_3$)$_2$), 0.98 (dd, 12H, CH(C*H*$_3$)$_2$).

^{13}C{^{1}H} NMR (126 MHz, THF-d8) δ = 189.0 (dd, $^1J_{CP}$ = 66.5 Hz, $^2J_{CP}$ = 56.3 Hz, N*C*(sp^2)HP), 174.2 (dd, $^2J_{CP}$ = 12.6 Hz, $^3J_{CP}$ = 2.7 Hz, *C*(O)C(HCP)), 173.1 (dd, $^3J_{CP}$ = 19.3 Hz, $^4J_{CP}$ = 1.4 Hz, *C*(O)C(HCC)), 60.0 (dd, $^1J_{CP}$ = 11.8 Hz, $^2J_{CP}$ = 3.0 Hz, N*C*(sp^3)HP), 54.1 (d, $^3J_{CP}$ = 21.4 Hz,

*C*H(CH$_3$)$_2$), 51.8 (s, O*C*H$_3$), 51.5 (s, O*C*H$_3$), 49.5 (dd, $^3J_{CP}$ = 18.2 Hz, $^3J_{CP}$ = 11.0 Hz, C(O)*C*(HCC)), 49.1 (d, $^3J_{CP}$ = 2.0 Hz, *C*H(CH$_3$)$_2$), 45.5 (d, $^3J_{CP}$ = 3.9 Hz), 36.9 (dd, $^1J_{CP}$ = 13.7 Hz, $^2J_{CP}$ = 5.1 Hz, C(O)*C*(HCP)), 23.7 (s, CH(*C*H$_3$)$_2$), 23.4 (s, CH(*C*H$_3$)$_2$), 19.0 (d, $^4J_{CP}$ = 42.0 Hz, CH(*C*H$_3$)$_2$).

^{31}P{^{1}H} NMR (162 MHz, THF-d8) δ = 56.3 (d, $^1J_{PP}$ = 285.5 Hz), 39.5 (d, $^1J_{PP}$ = 285.9 Hz).

HRMS (ESI+): calcd. for **13** $[M+H]^+$ $[C_{20}H_{39}N_2O_4P_2]^+$ m/z: 433.2380, found 433.2378.

Reaction of **3** with $AgSbF_6$

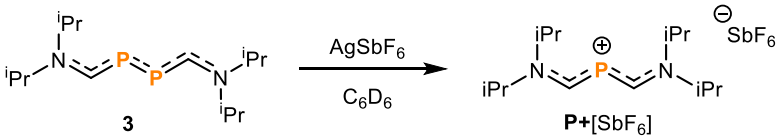

A J-Young NMR tube was charged with PP (28.8 mg; 0.1 mmol; 1 equiv.) and $AgSbF_6$ (37.8 mg; 0.11 mmol; 1.1 equiv.) in 1 mL of C_6D_6. A drop of THF was added to increase solubility. The suspension was sonicated overnight at 30 ^{o}C. After NMR analysis, the solution was filtered into a culture tube where it was slowly evaporated to give crystals suitable for X-ray analysis.

3.10.3 NMR Spectra

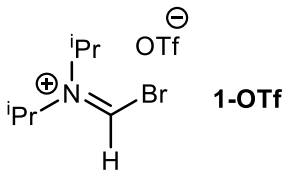

1-OTf

^{1}H (500 MHz) in $CDCl_3$

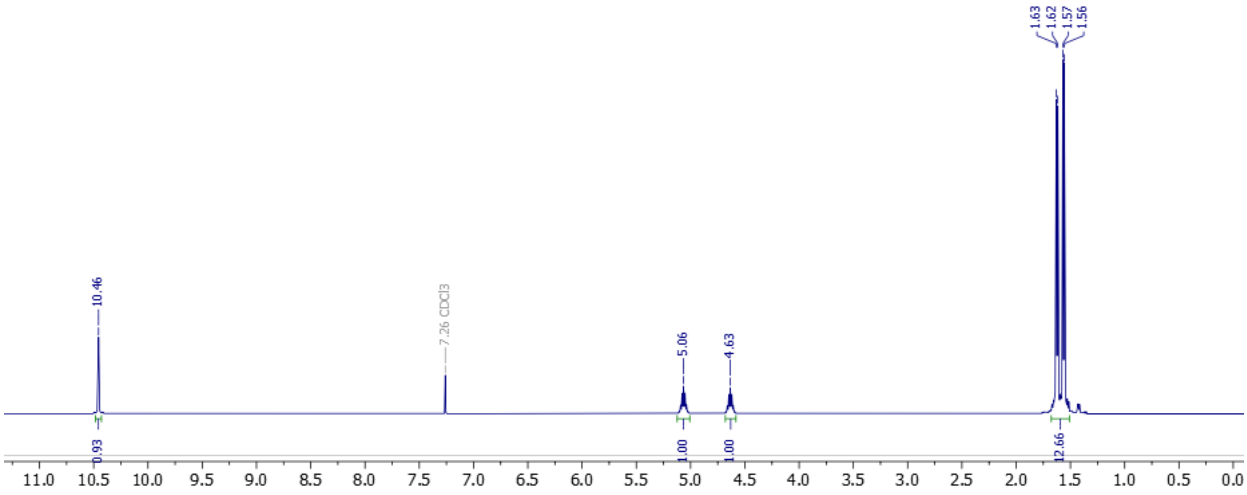

$^{13}C\{^{1}H\}$ (126 MHz) in $CDCl_3$

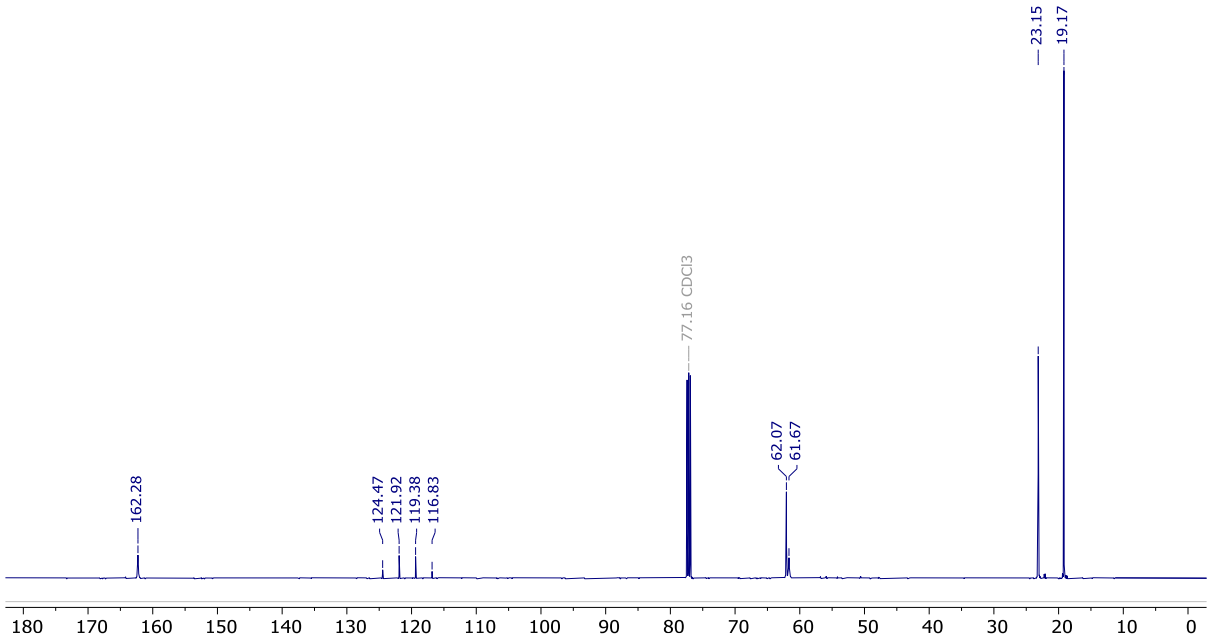

^{19}F NMR (376 MHz) in $CDCl_3$

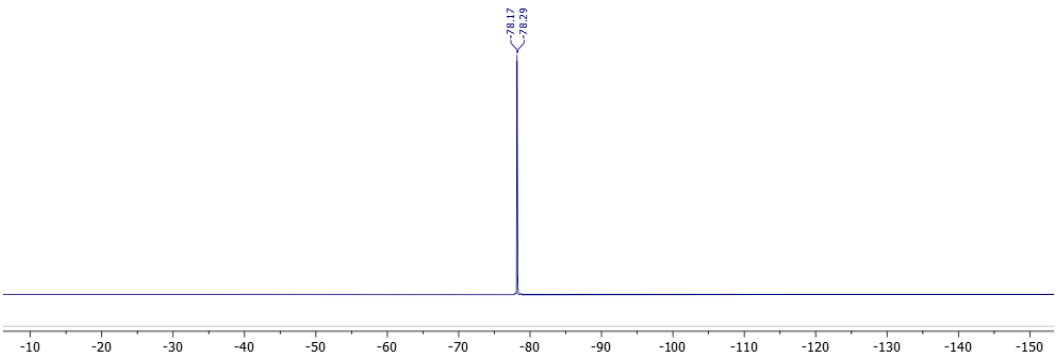

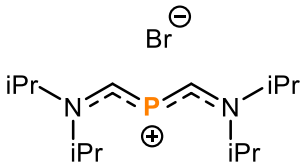

P+[Br]

^{1}H (400 MHz) in THF-d8 (and 1,4-dioxane)

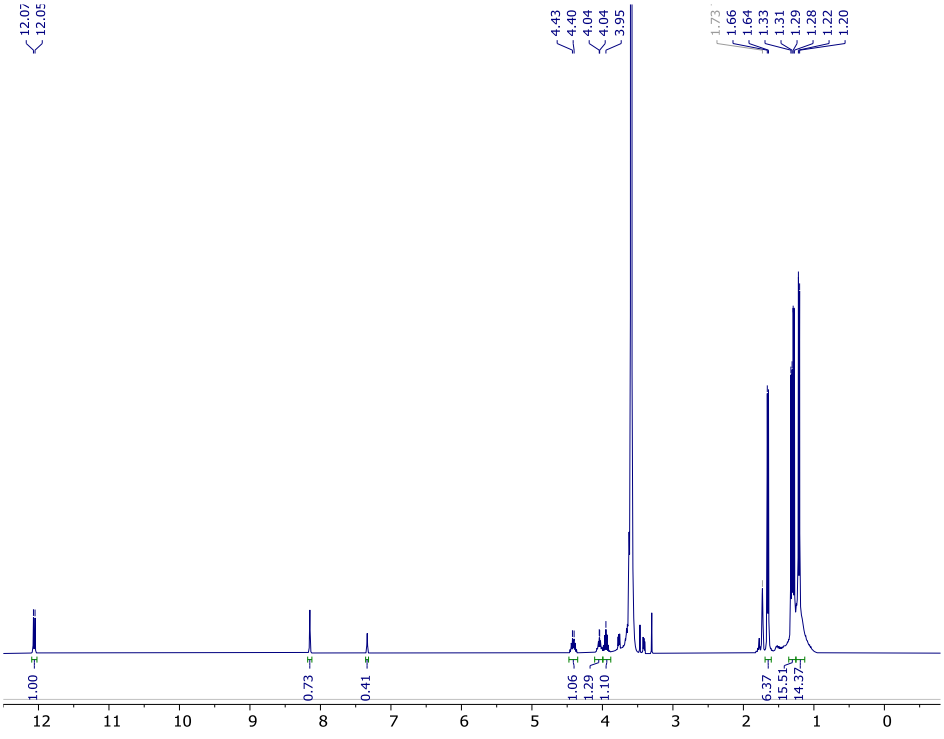

$^{31}P\{^{1}H\}$, ^{31}P (inset) (121 MHz) in $CDCl_3$

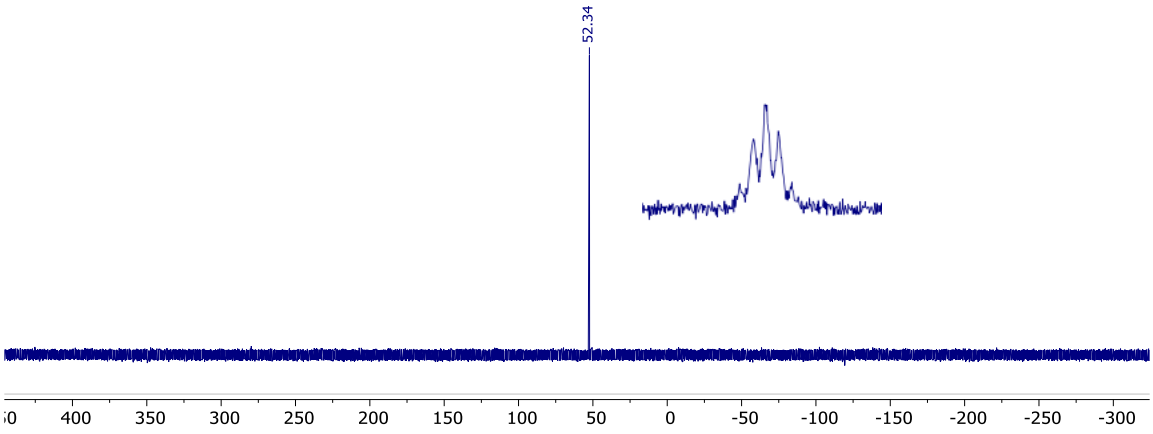

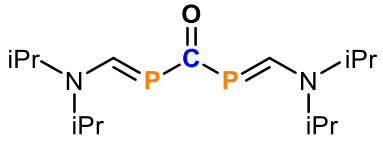

2

^{1}H (500 MHz) in C_6D_6

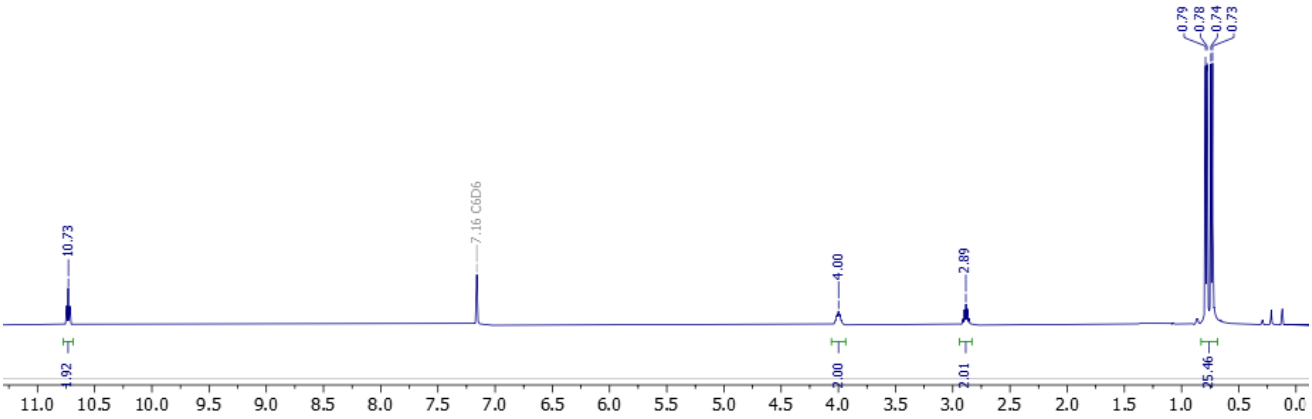

$^{13}C\{^{1}H\}$ (126 MHz) in C_6D_6

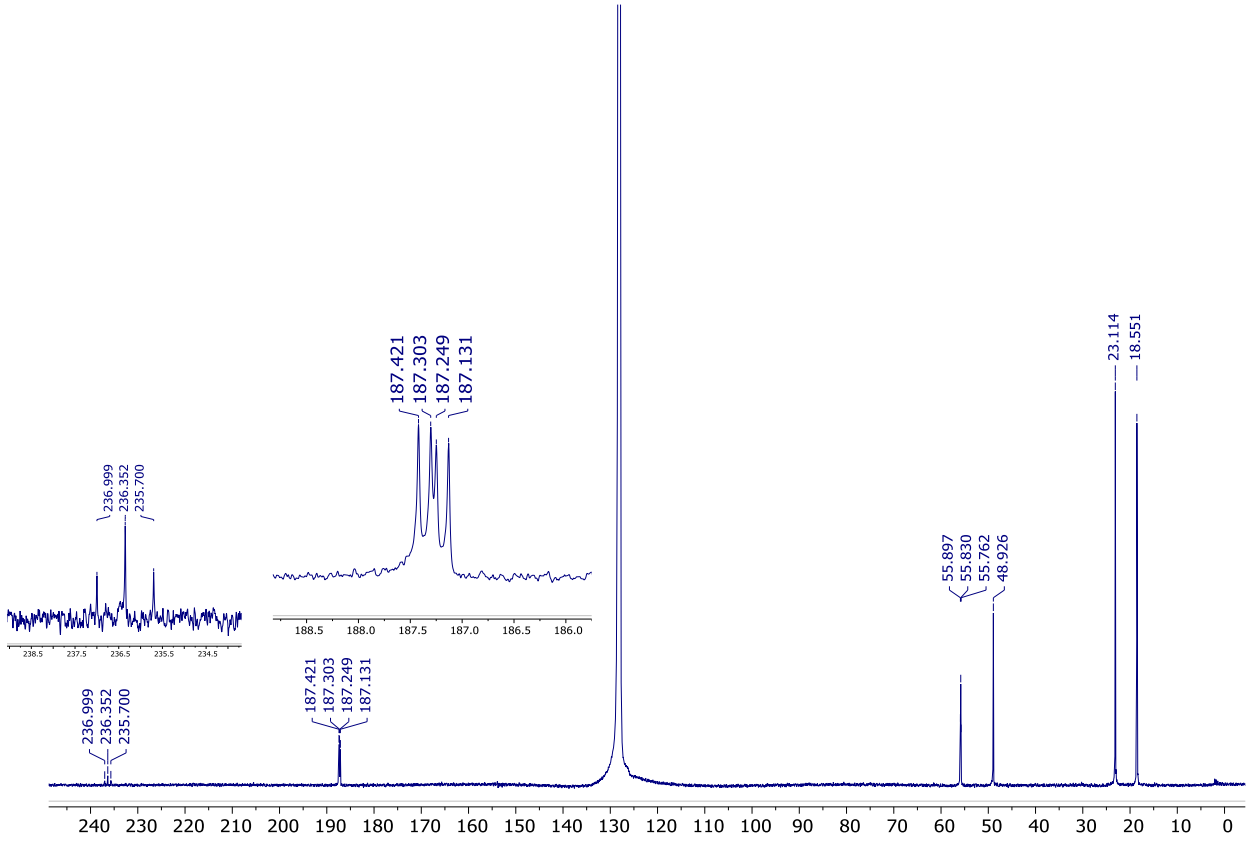

$^{31}P\{^{1}H\}$, ^{31}P (inset) (121 MHz) in $CDCl_3$.

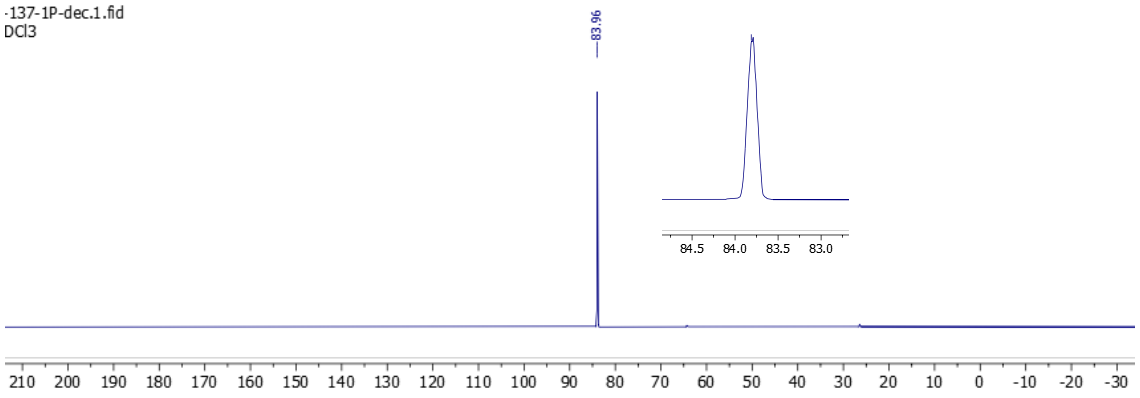

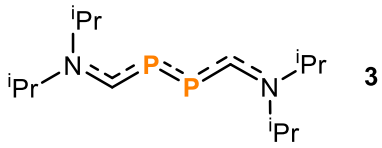

3

^{1}H (400 MHz) in THF-d8

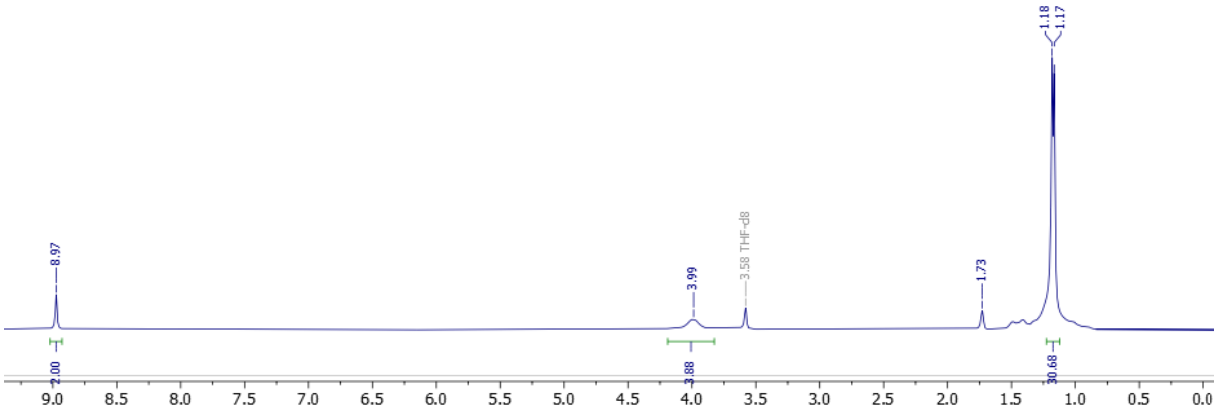

^{13}C{^{1}H} (101 MHz) in THF-d8.

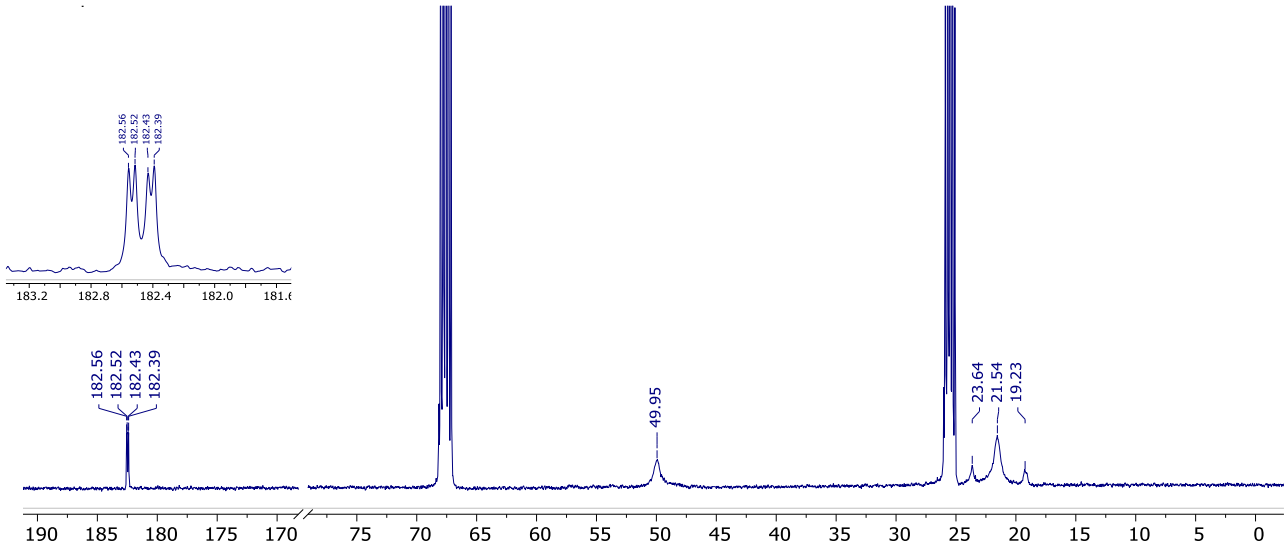

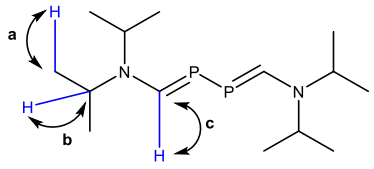

HMQC (400 MHz) in THF-d8

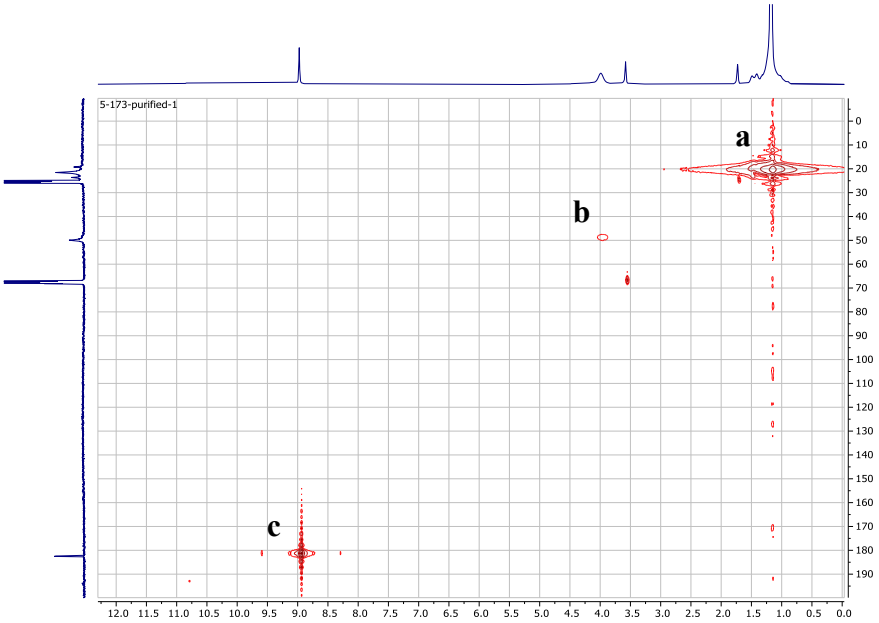

$^{31}P\{^{1}H\}$, ^{31}P (inset) (162 MHz) in THF-d8.

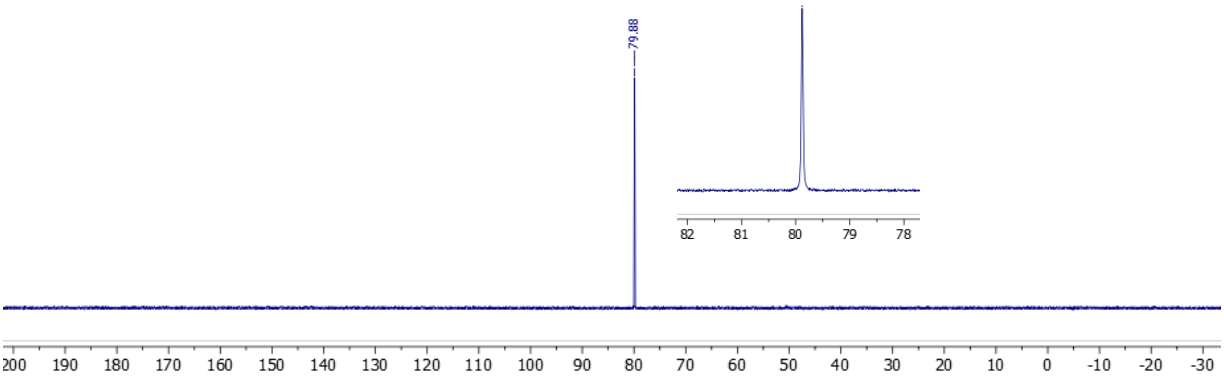

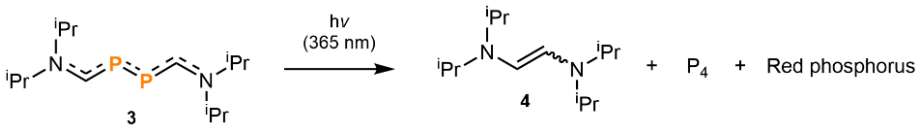

^{1}H NMR (400 MHz) spectrum in C_6D_6

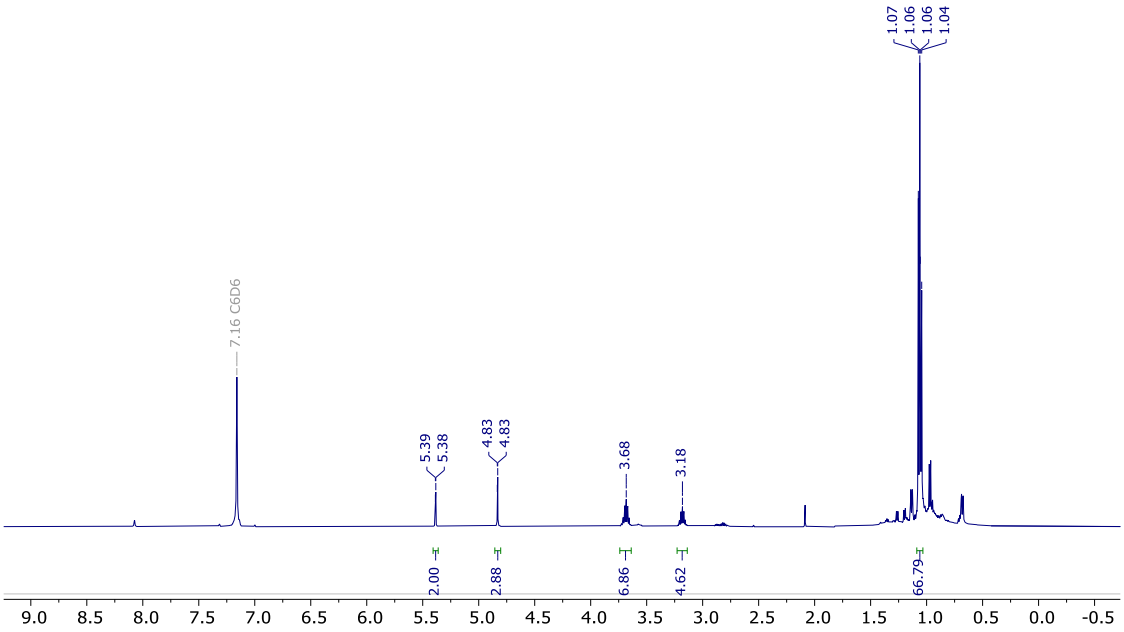

^{13}C{^{1}H} (126 MHz) spectrum in C_6D_6.

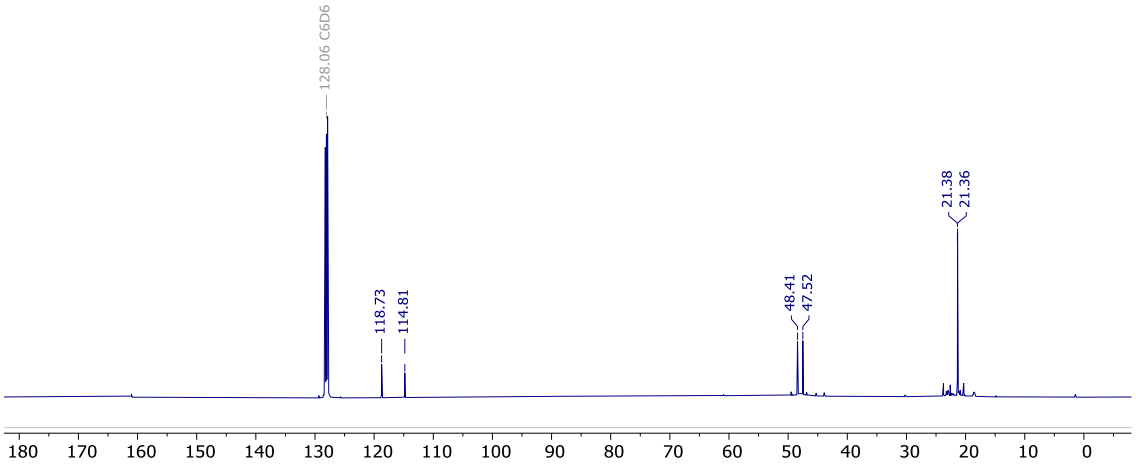

$^{31}P\{^{1}H\}$ (162 MHz) spectrum in C_6D_6.

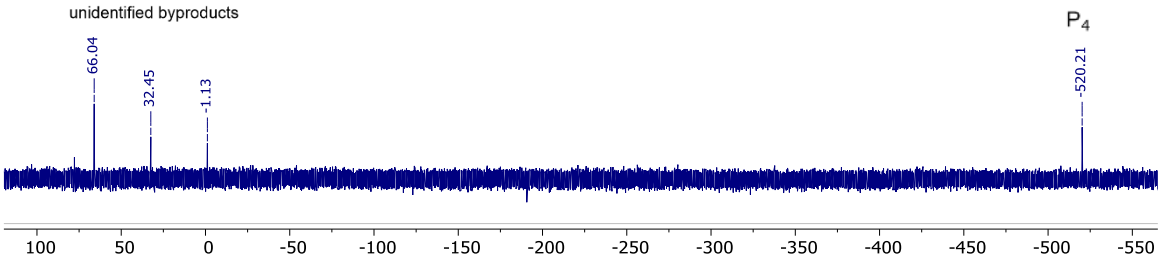

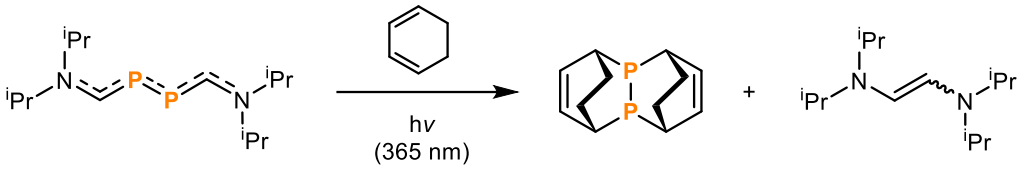

$^{31}P\{^{1}H\}$ (162 MHz) spectrum in C_6D_6.

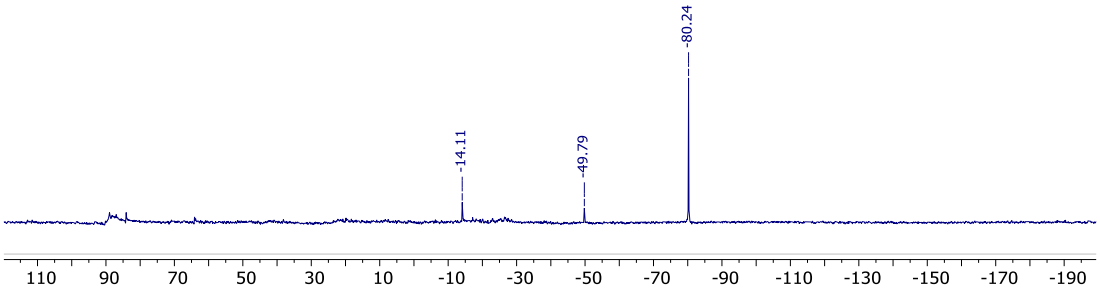

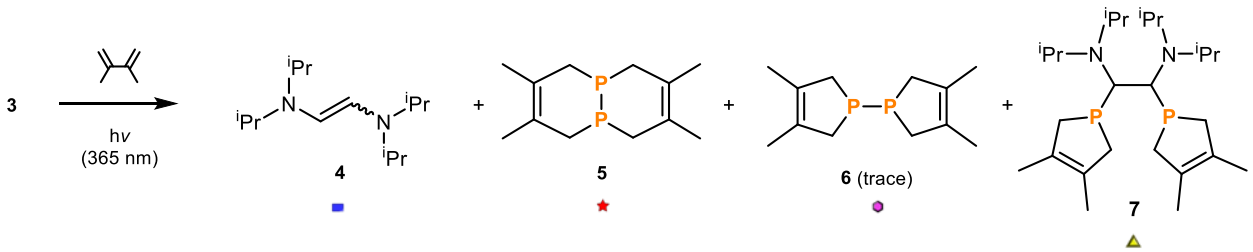

^{1}H (500 MHz) in C_6D_6.

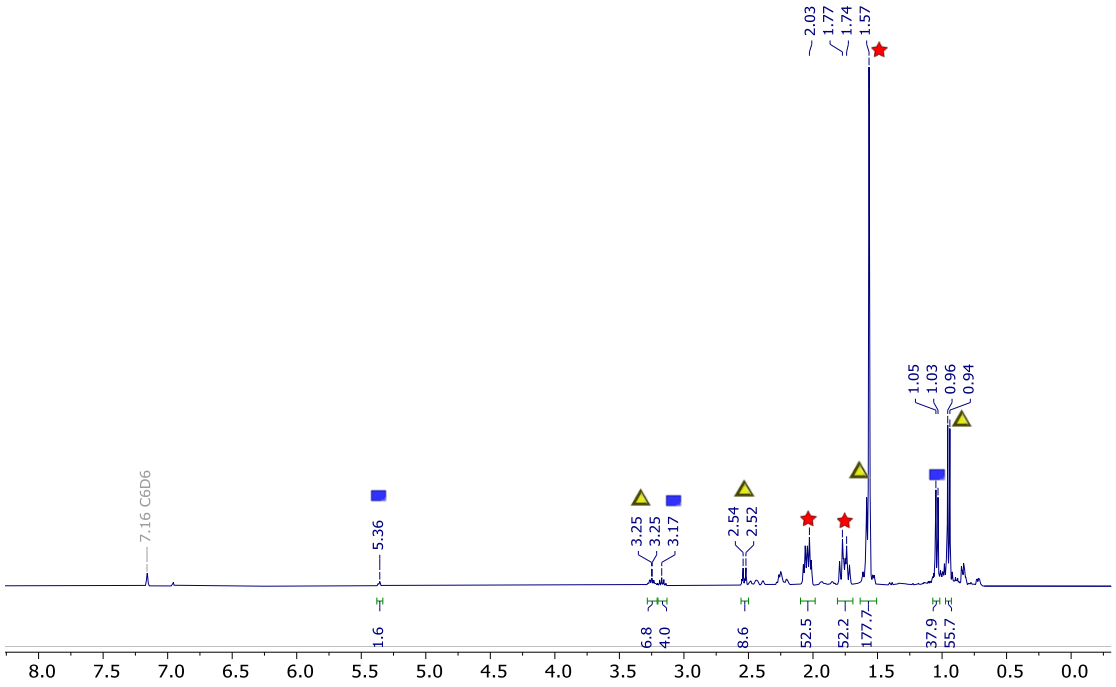

$^{13}C\{^{1}H\}$ (101 MHz) in C_6D_6.

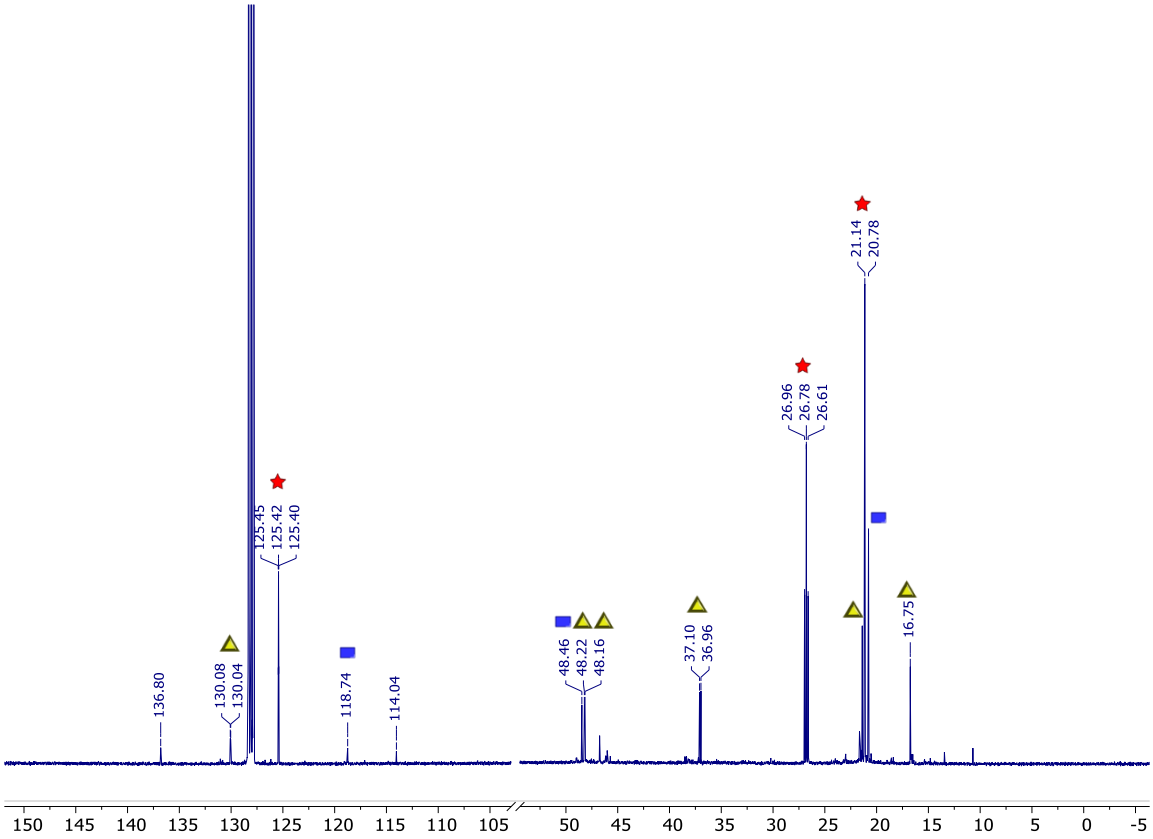

$^{31}P\{^{1}H\}$, ^{31}P (inset) (162 MHz) in C_6D_6.

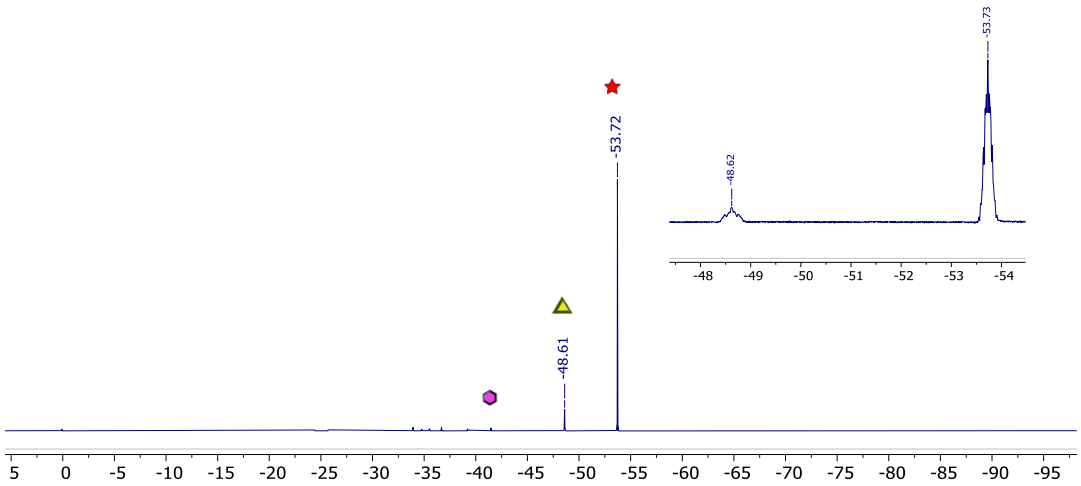

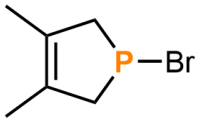

^{1}H (300 MHz) in C_6D_6

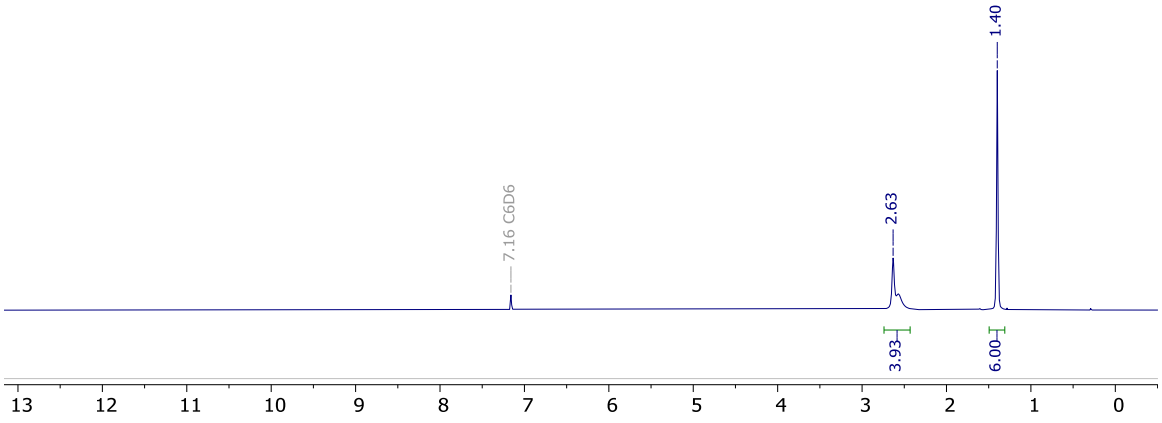

$^{13}C\{^{1}H\}$ (126 MHz) in C_6D_6.

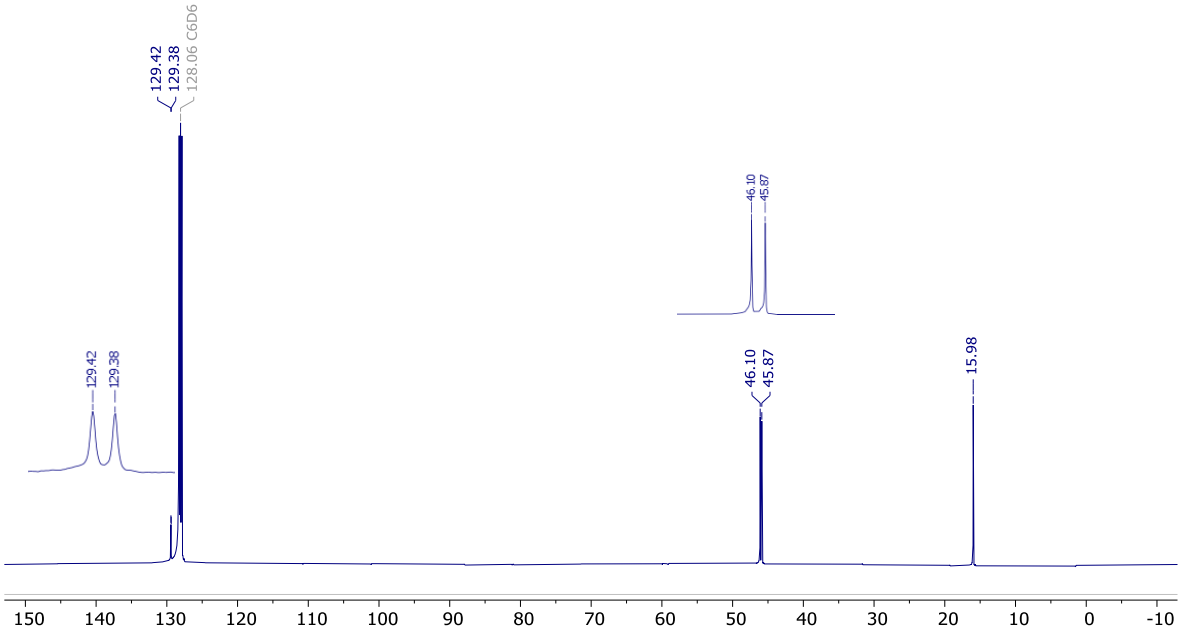

$^{31}P\{^{1}H\}$, ^{31}P (inset) (162 MHz) in C_6D_6.

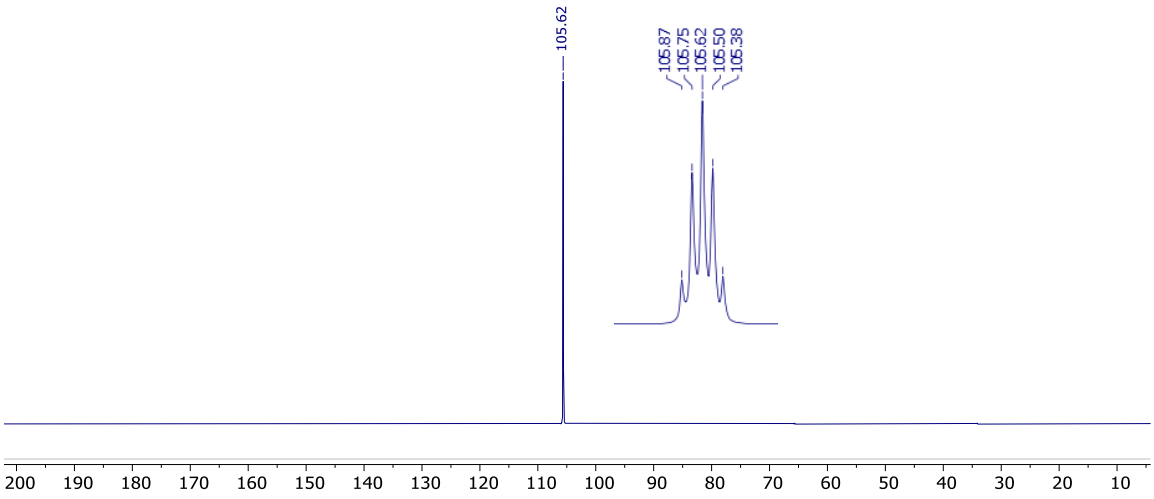

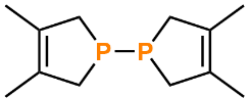

6

^{1}H (400 MHz) in C_6D_6.

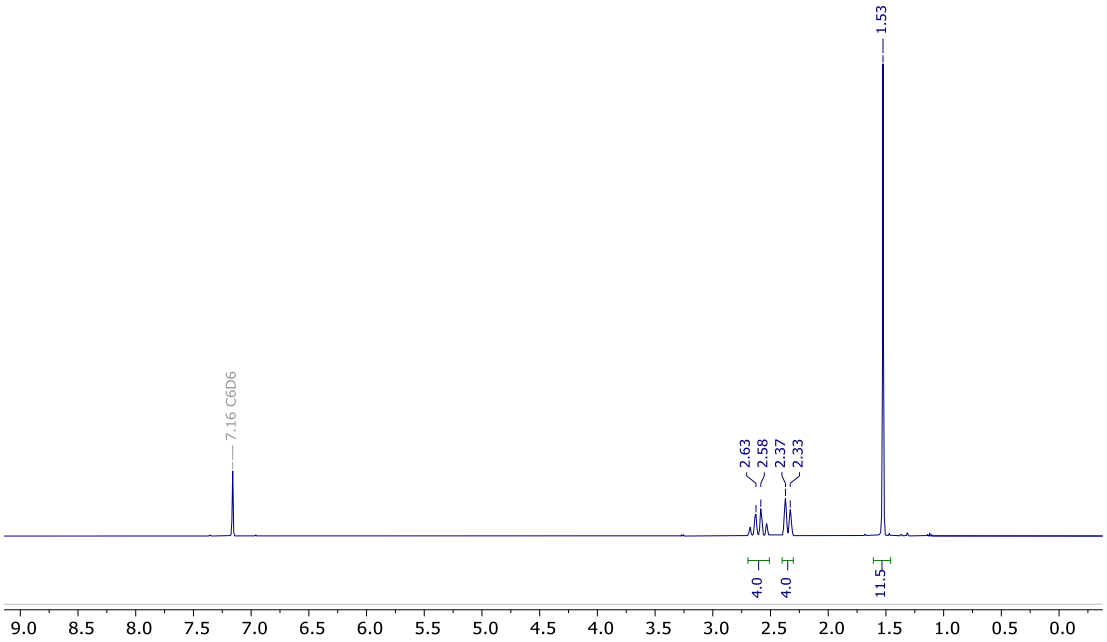

$^{13}C\{^{1}H\}$ (101 MHz) in C_6D_6.

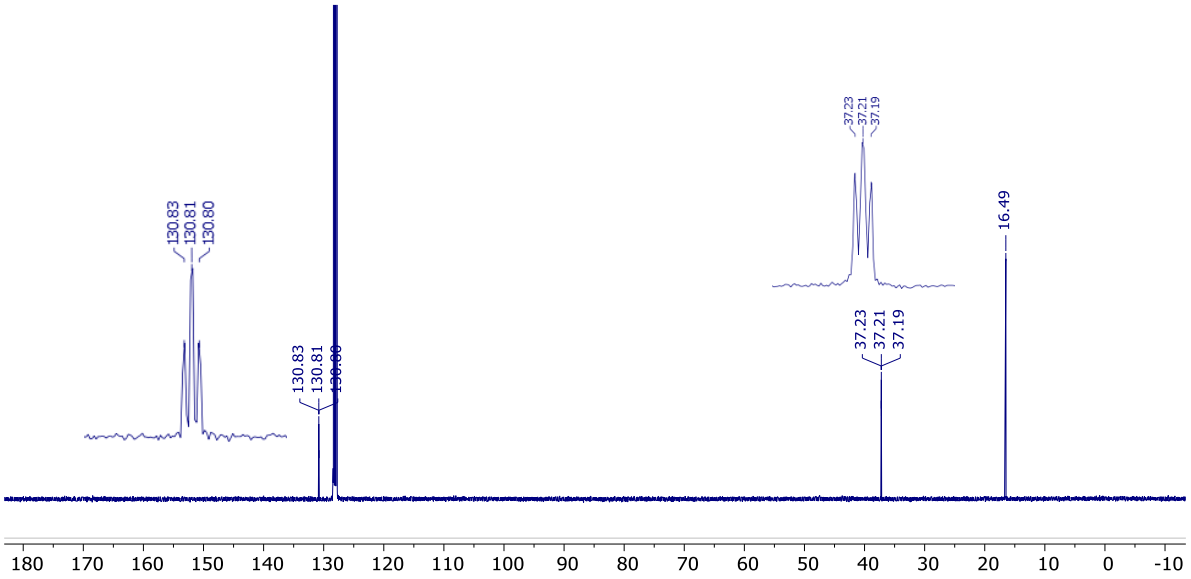

$^{31}P\{^{1}H\}$, ^{31}P (inset) (162 MHz) in C_6D_6.

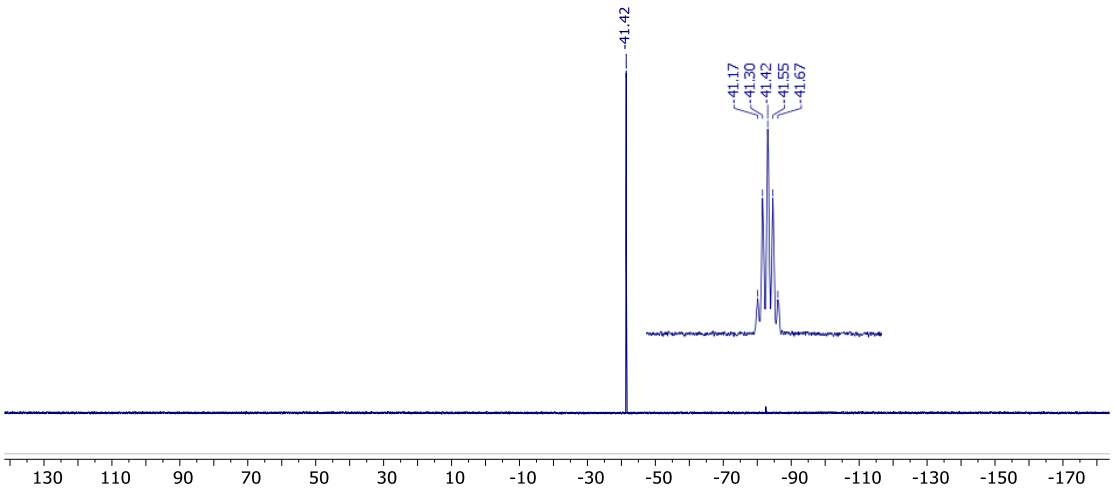

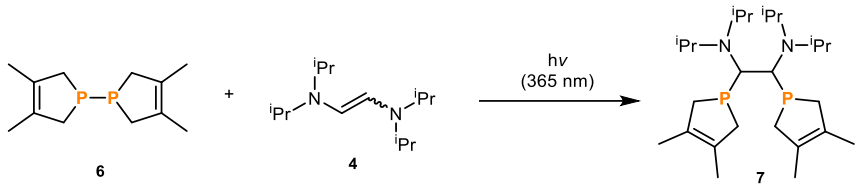

^{1}H (400 MHz) in C_6D_6

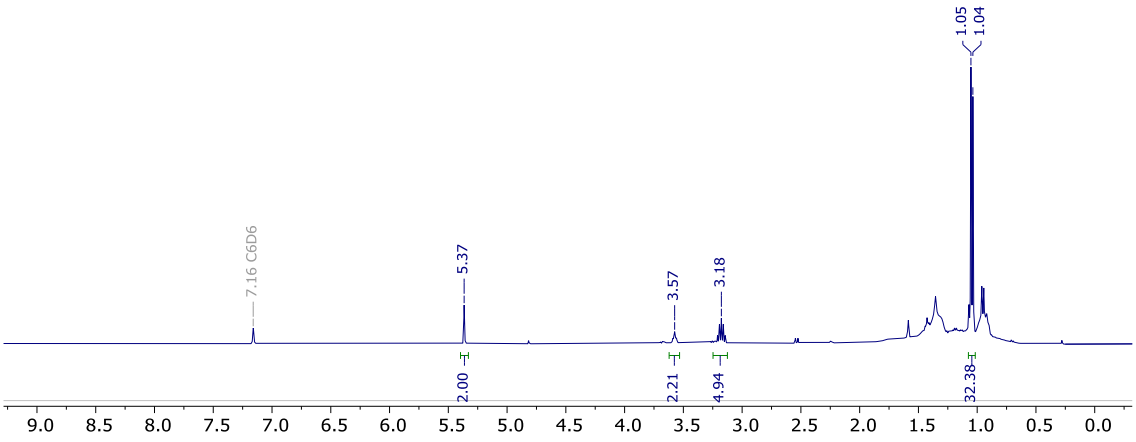

$^{13}C\{^{1}H\}$ (101 MHz) in C_6D_6.

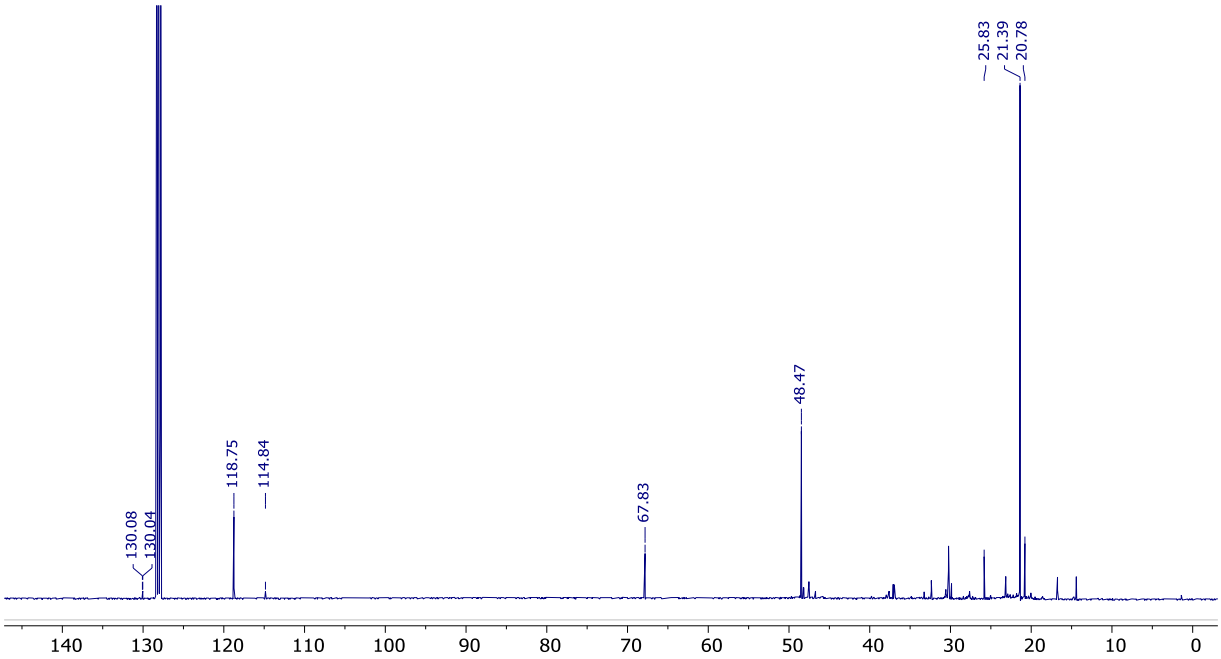

$^{31}P\{^{1}H\}$ (162 MHz) in C_6D_6.

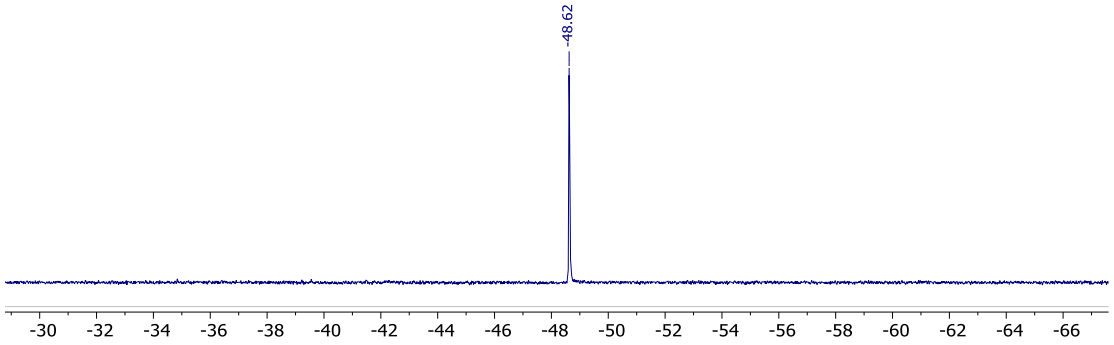

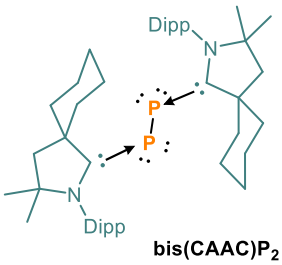

bis(CAAC)P_2

^{1}H (500 MHz) in C_6D_6

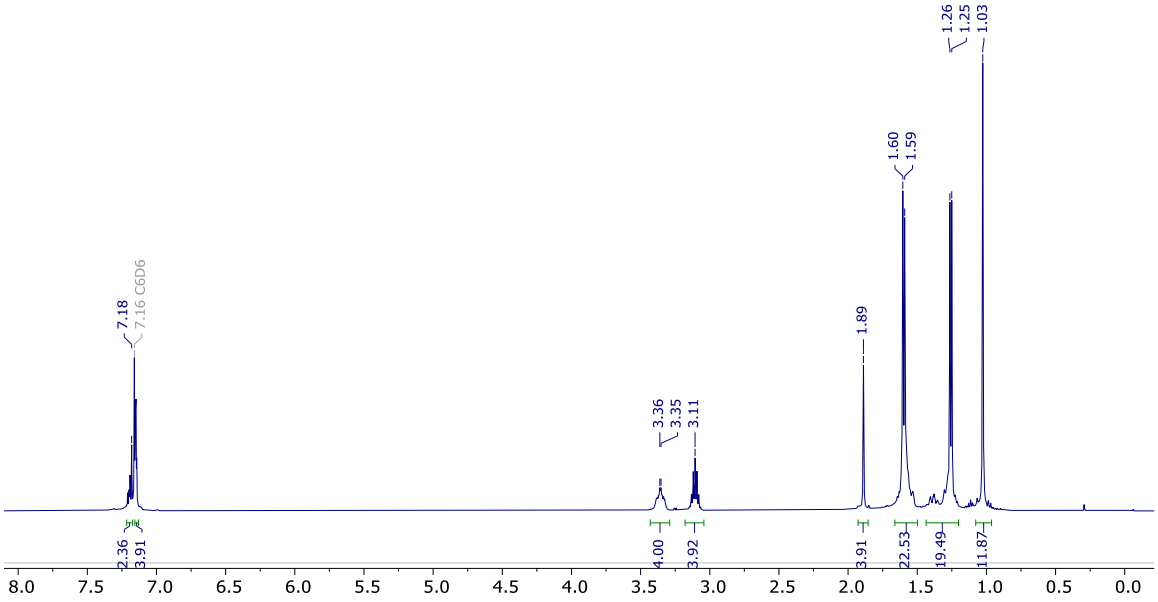

$^{13}C\{^{1}H\}$ (126 MHz) in C_6D_6.

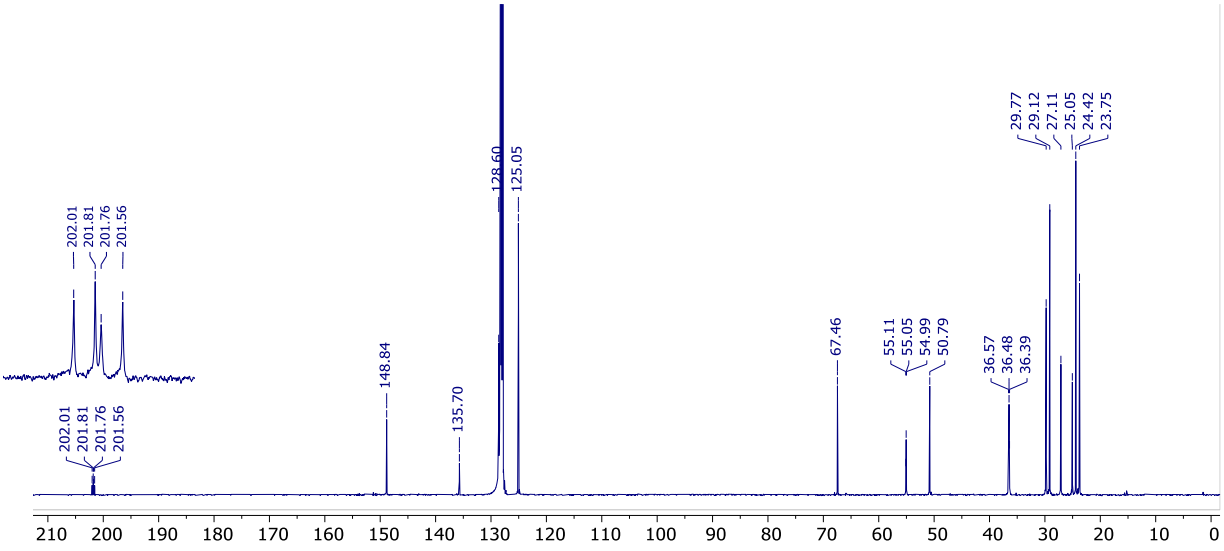

$^{31}P\{^{1}H\}$ (162 MHz) in C_6D_6.

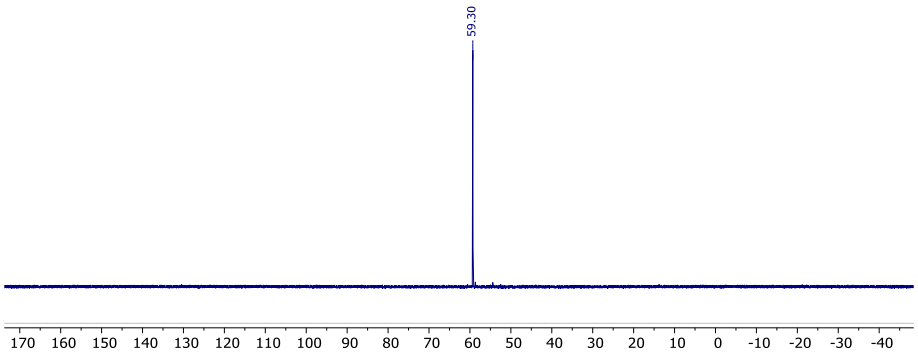

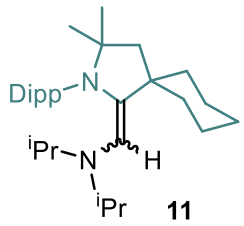

11

^{1}H (400 MHz) in C_6D_6

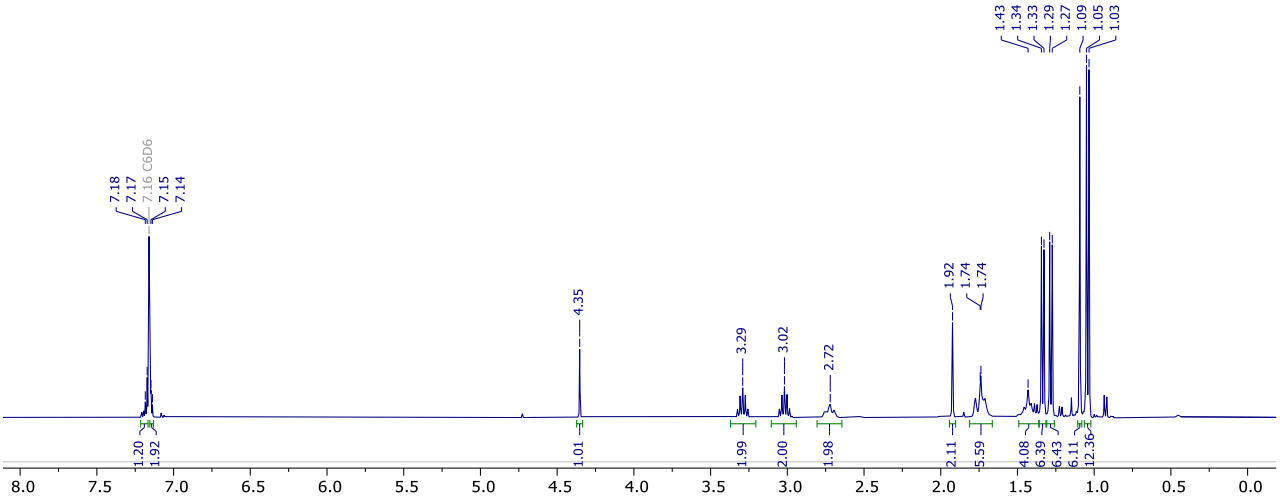

$^{13}C\{^{1}H\}$ (126 MHz) in C_6D_6

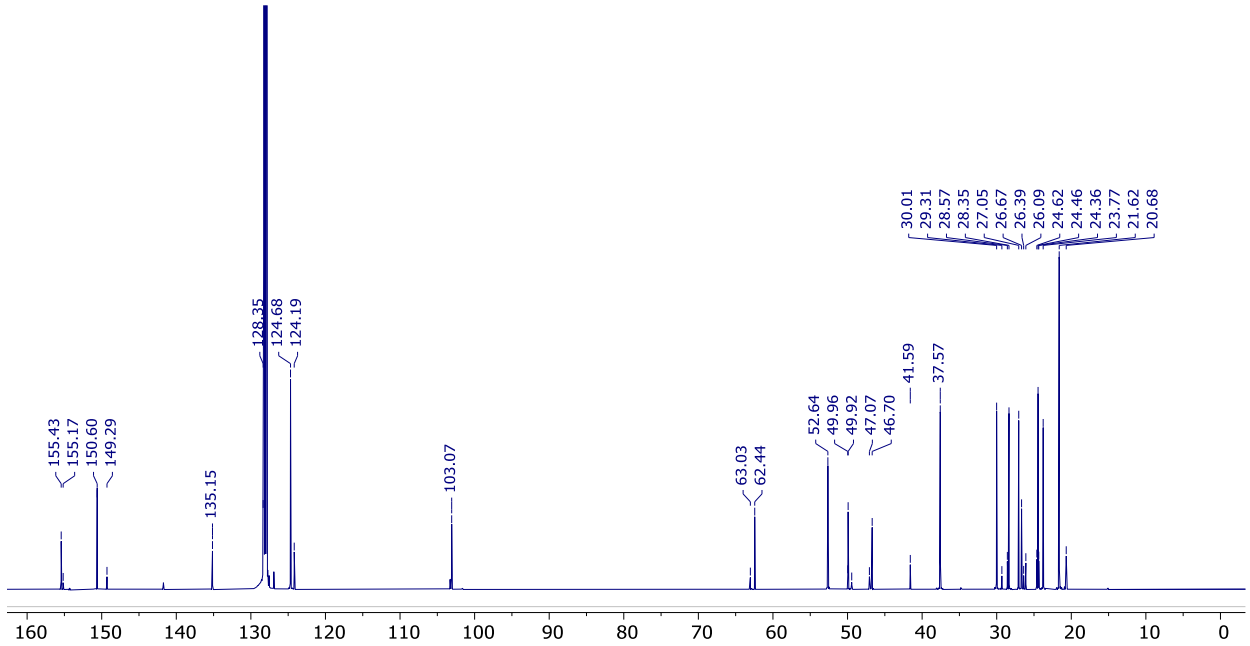

DEPT 135 (126 MHz) spectrum (yellow) and $^{13}C\{^{1}H\}$ NMR (126 MHz) in C_6D_6

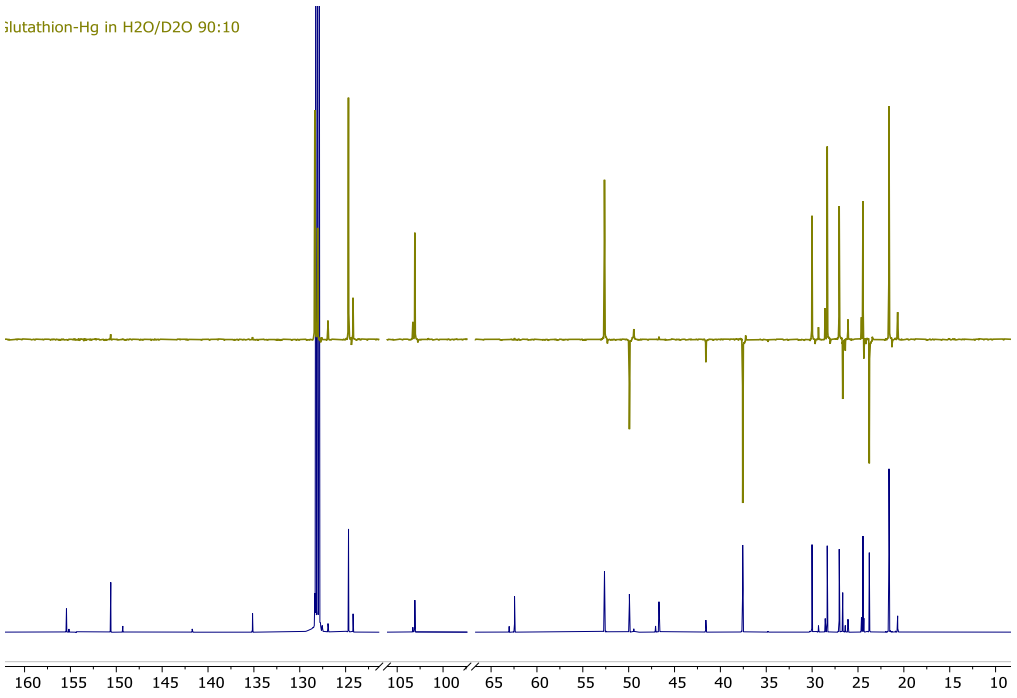

HMQC (400 MHz) in C_6D_6

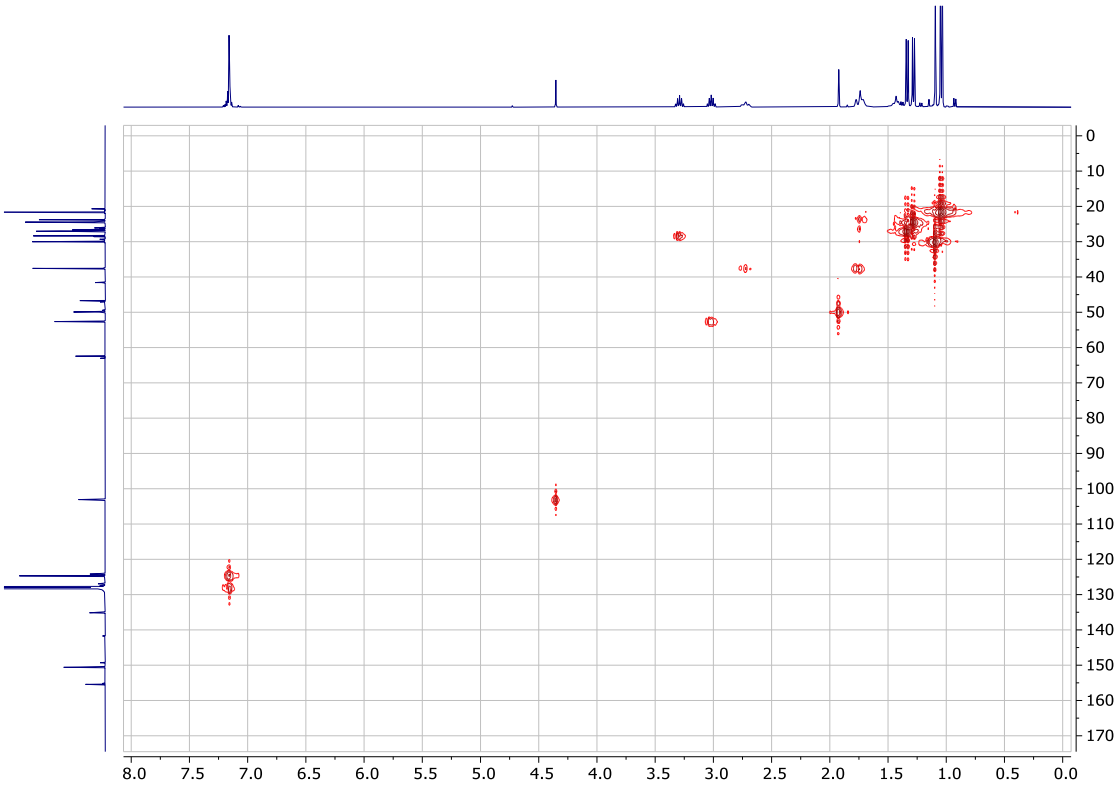

COSY (400 MHz) spectrum in C_6D_6

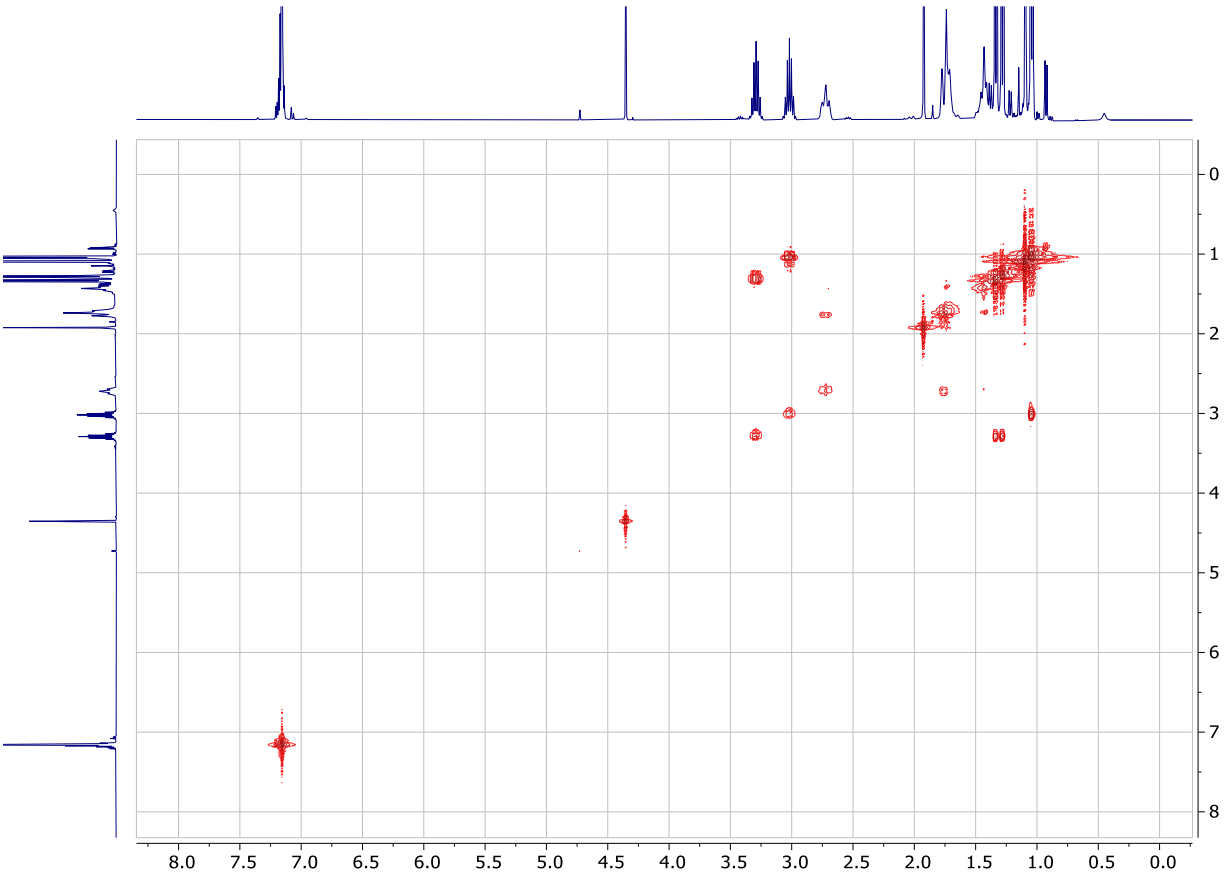

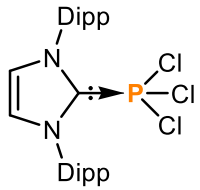

^{1}H (400 MHz) spectrum in THF-d8

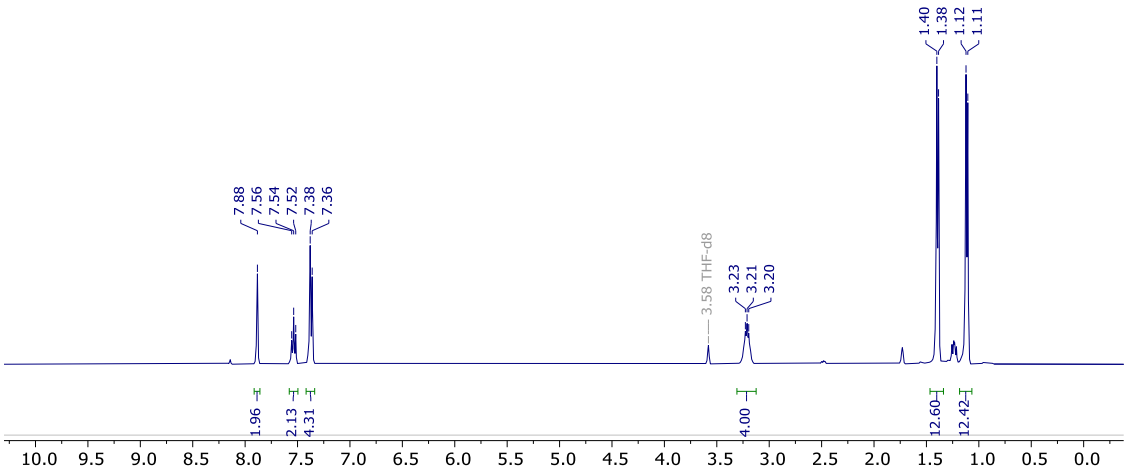

$^{13}C\{^{1}H\}$ (101 MHz) in THF-d8.

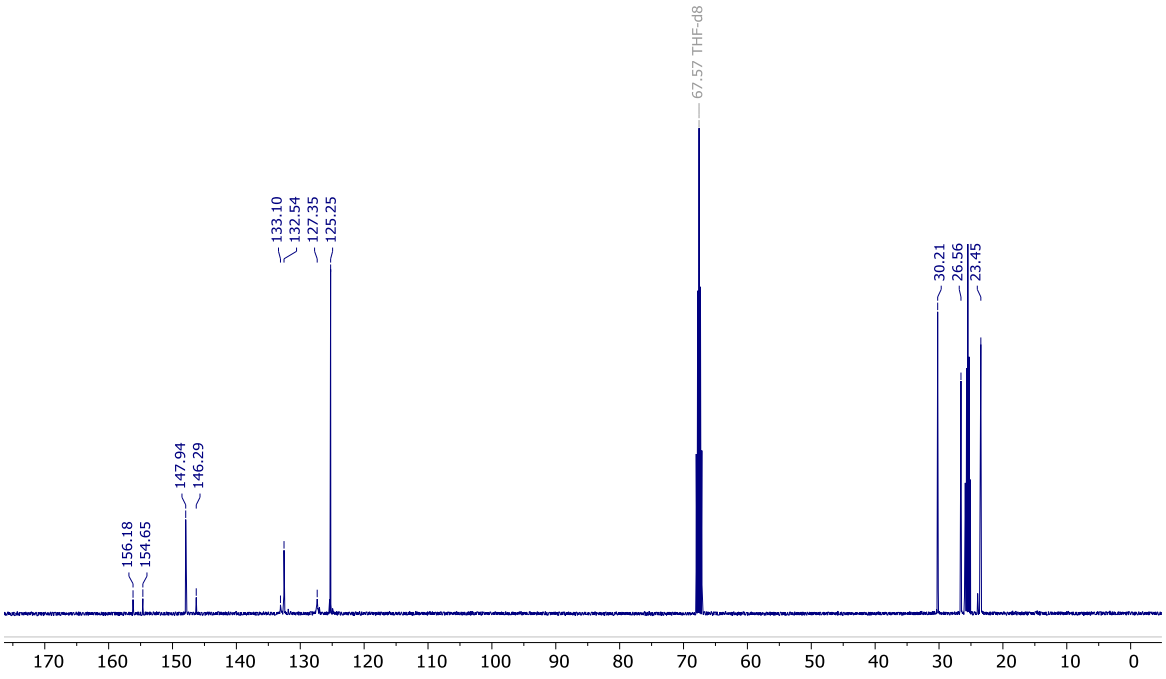

$^{31}P\{^{1}H\}$, ^{31}P (inset) (162 MHz) in THF-d8.

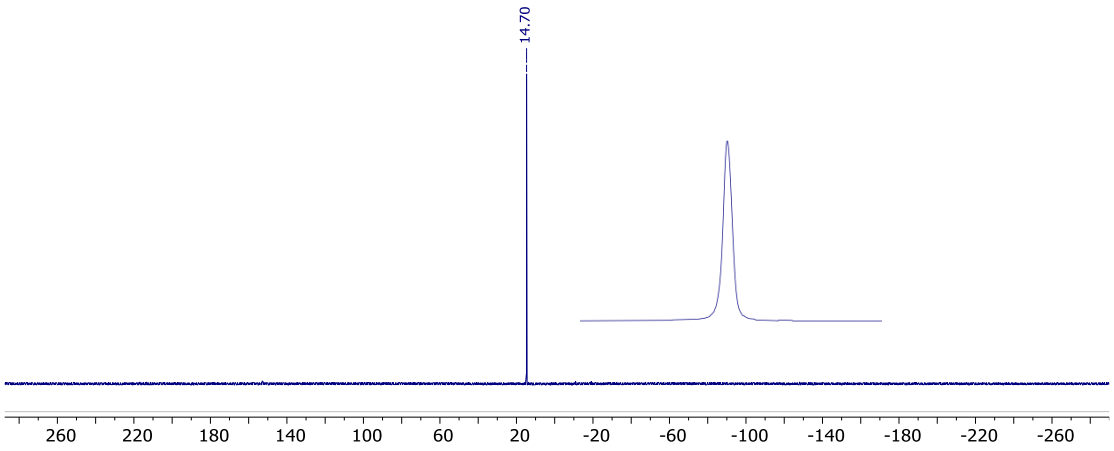

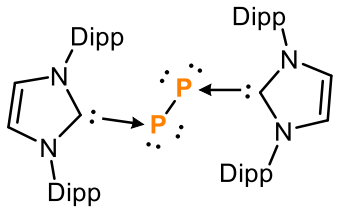

bis(NHC)P_2

^{1}H (400 MHz) in C_6D_6

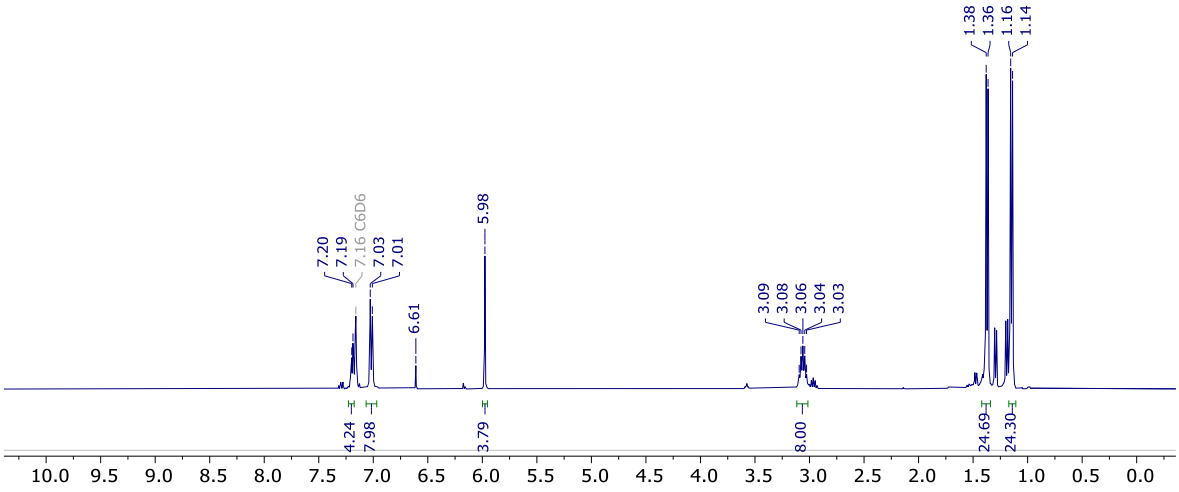

$^{13}C\{^{1}H\}$ (101 MHz) in C_6D_6

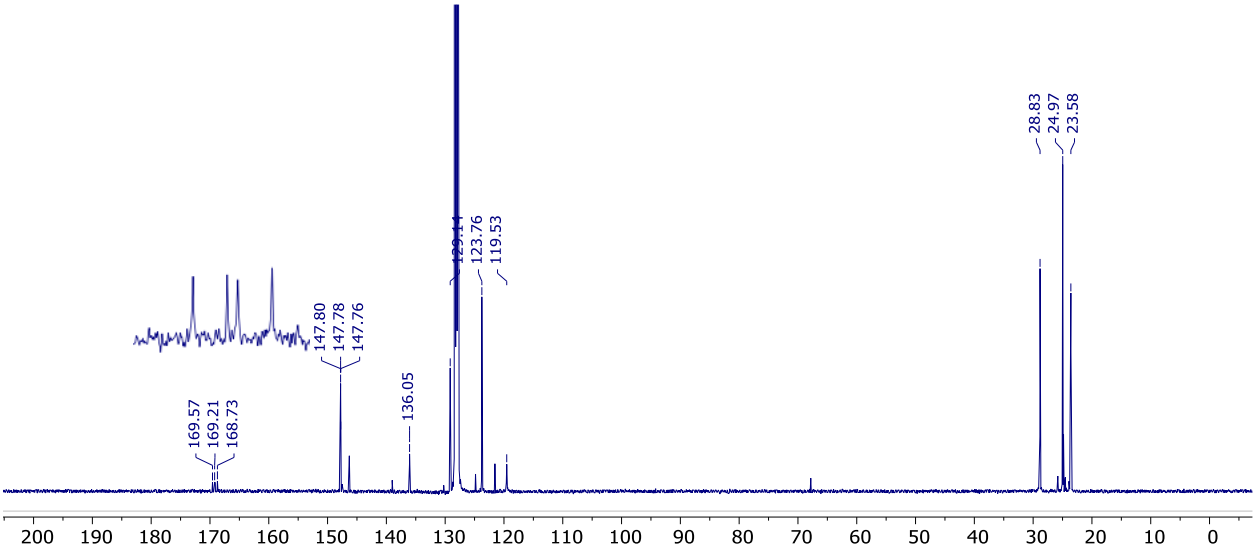

$^{31}P\{^{1}H\}$, ^{31}P (inset) (162 MHz) in C_6D_6.

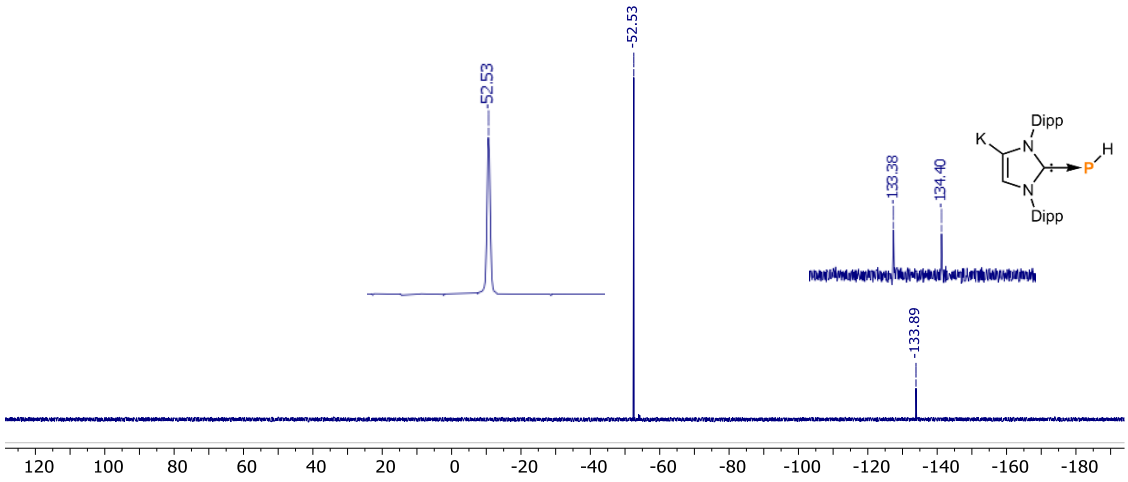

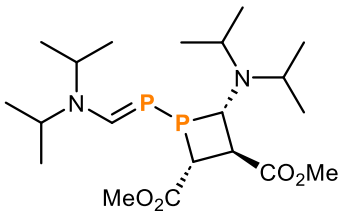

13

^{1}H NMR (400 MHz) spectrum in THF-d8

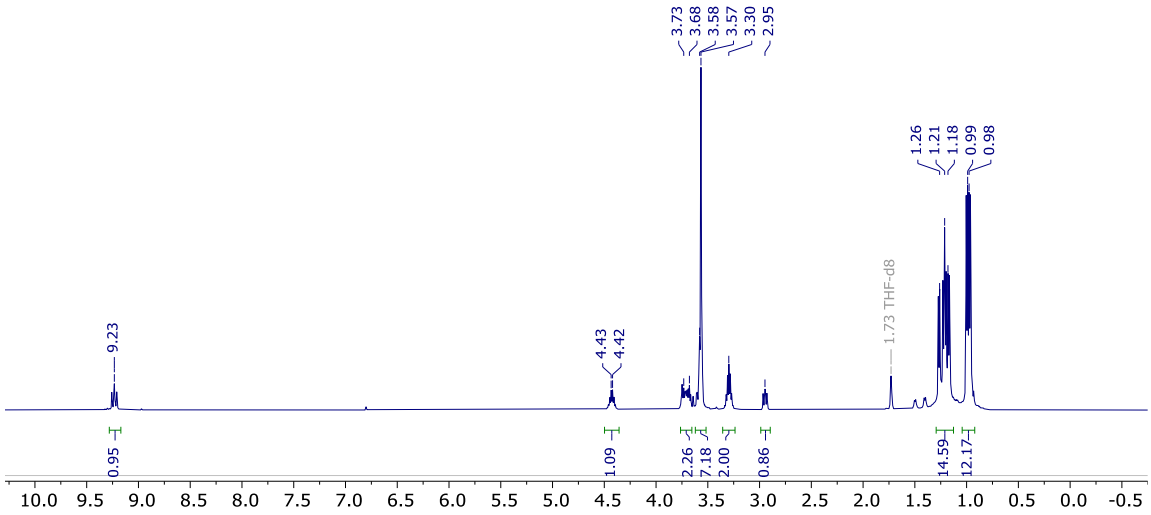

^{13}C{^{1}H} NMR (126 MHz) spectrum in THF-d8

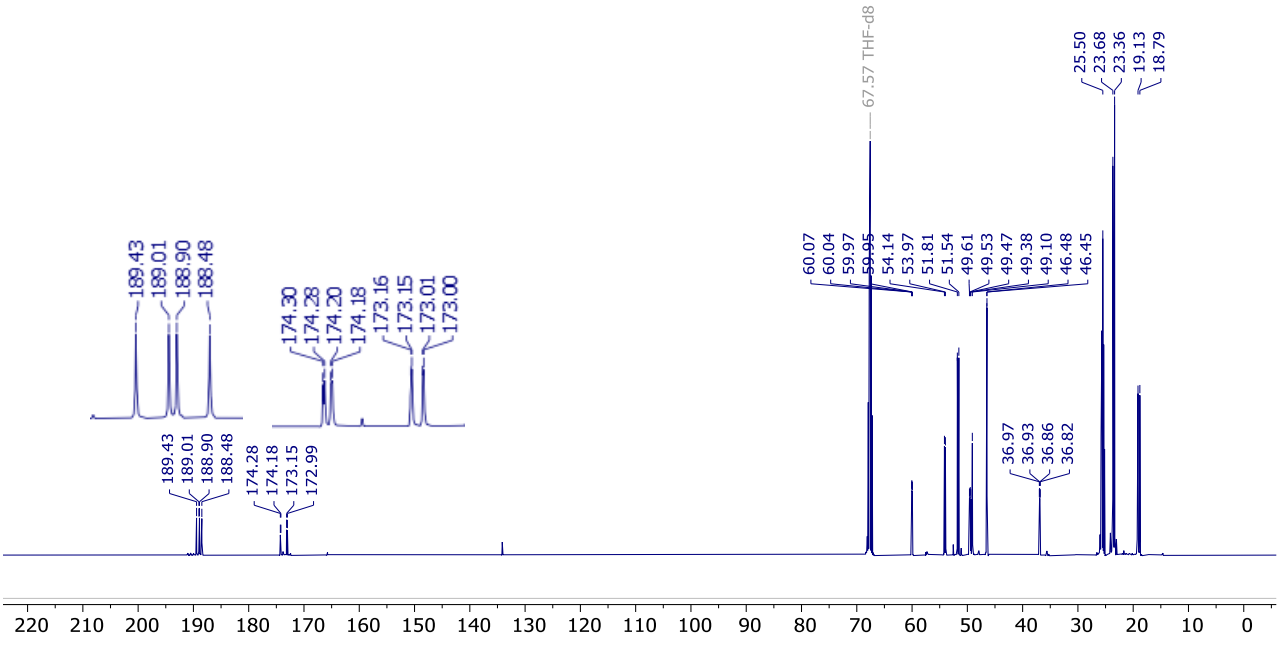

Zoomed in ^{13}C NMR (bottom) and $^{13}C\{^{1}H\}$ (top) (126 MHz) spectrum in THF-d8

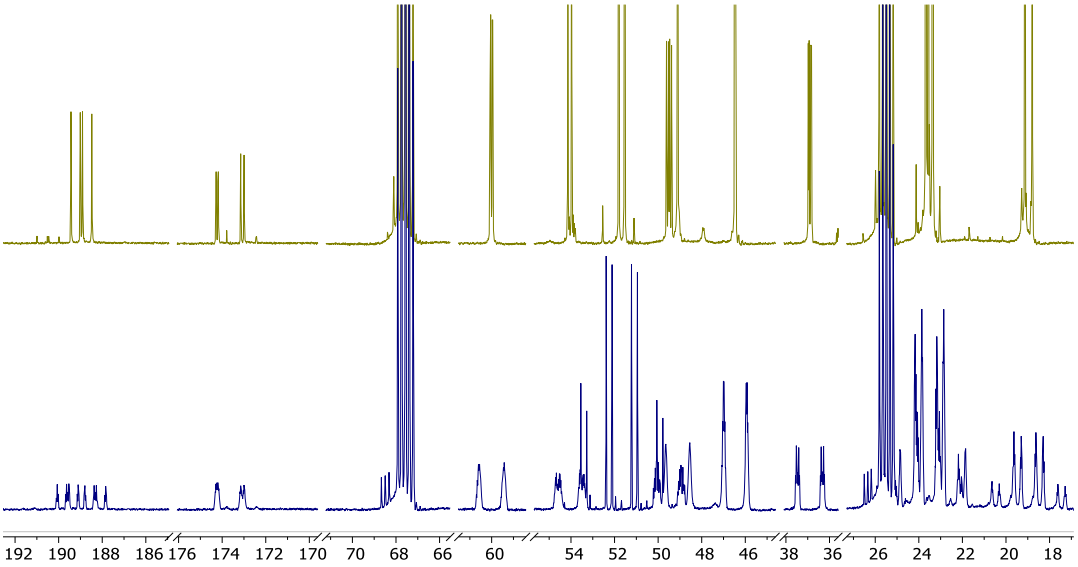

HMQC (400 MHz) spectrum in THF-d8

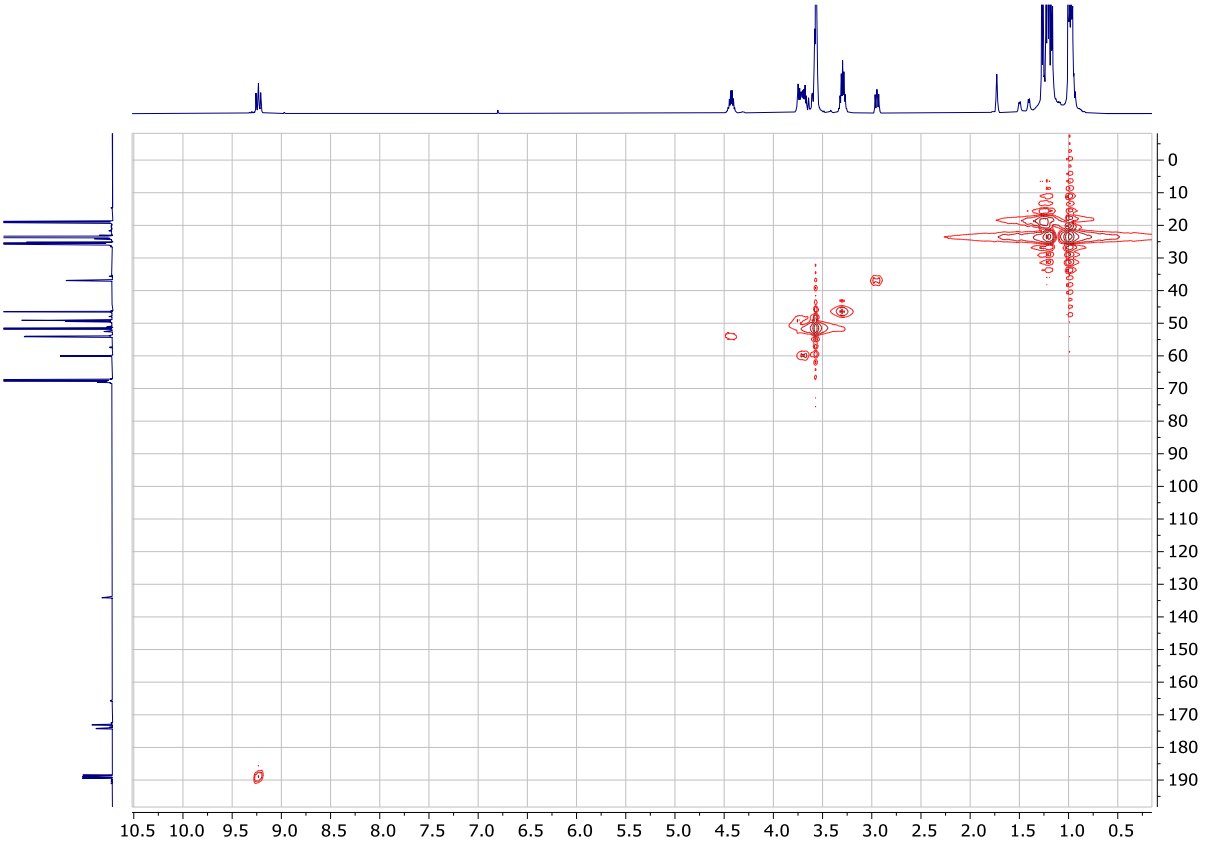

HMBC (400 MHz) spectrum in THF-d8

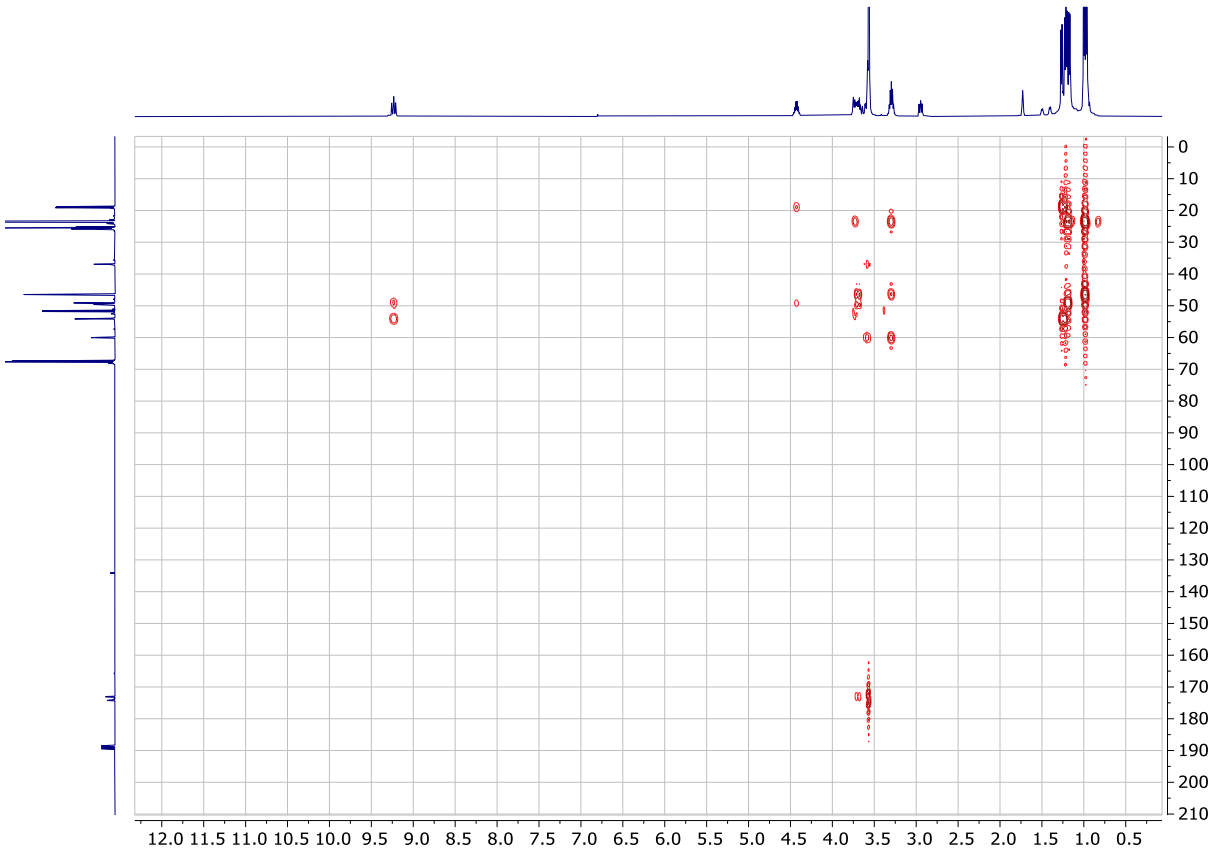

COSY (400 MHz) spectrum in THF-d8

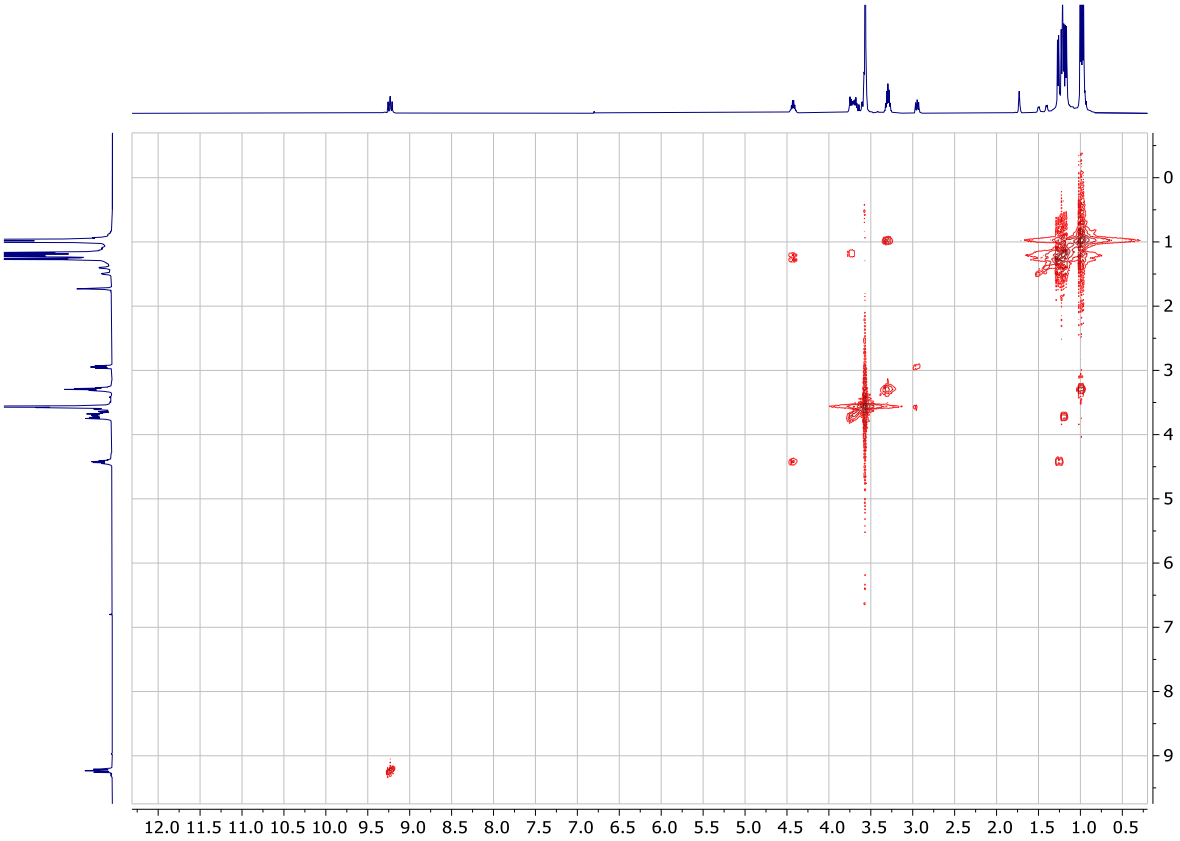

$^{31}P\{^{1}H\}$ and ^{31}P (inset) NMR (162 MHz) spectrum THF-d8

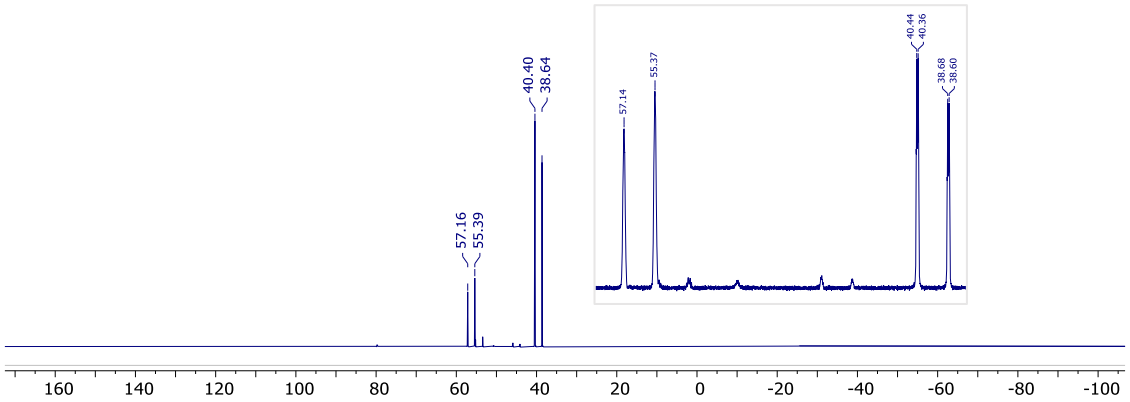

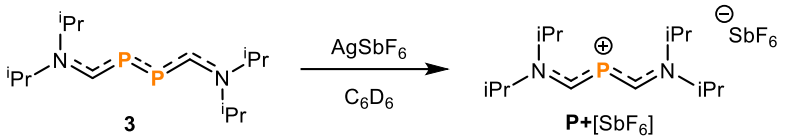

^{1}H (400 MHz) in C_6D_6

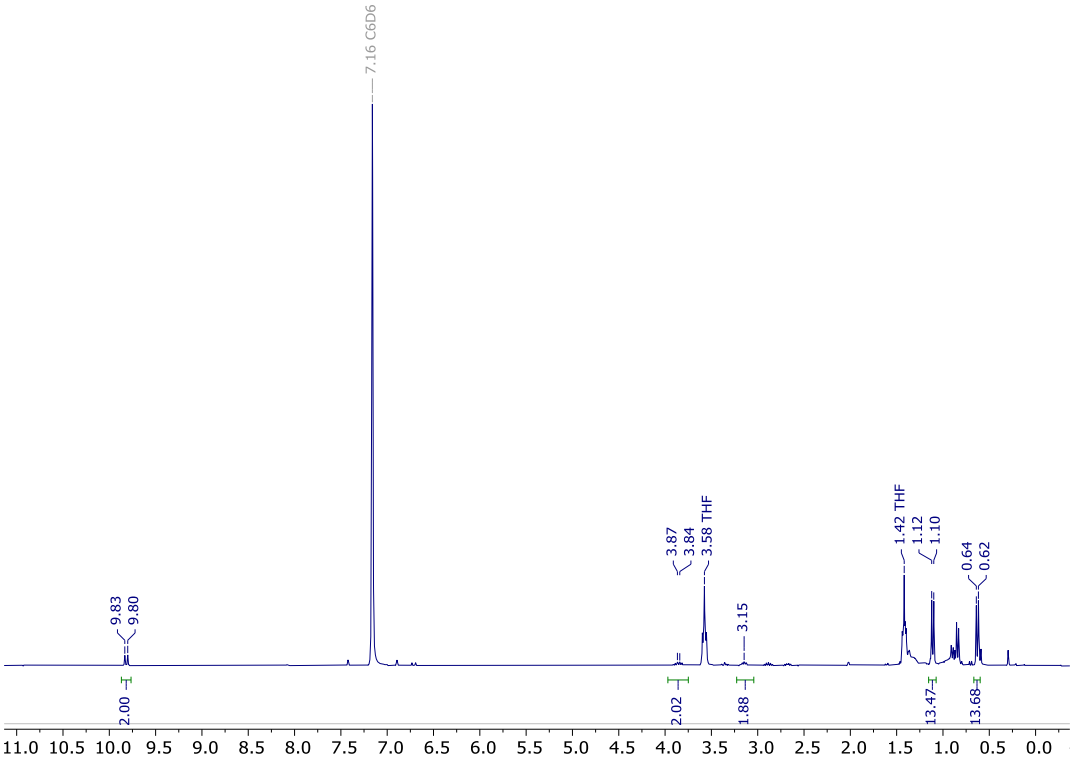

$^{31}P\{^{1}H\}$, ^{31}P (inset) (121 MHz) in C_6D_6

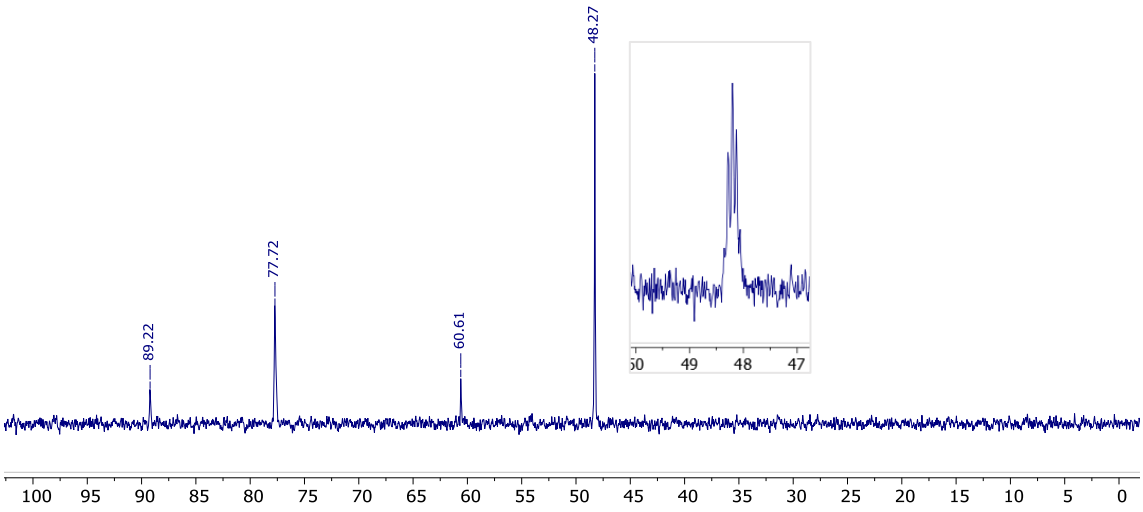

3.10.4 UV-Visible Spectroscopic Analysis

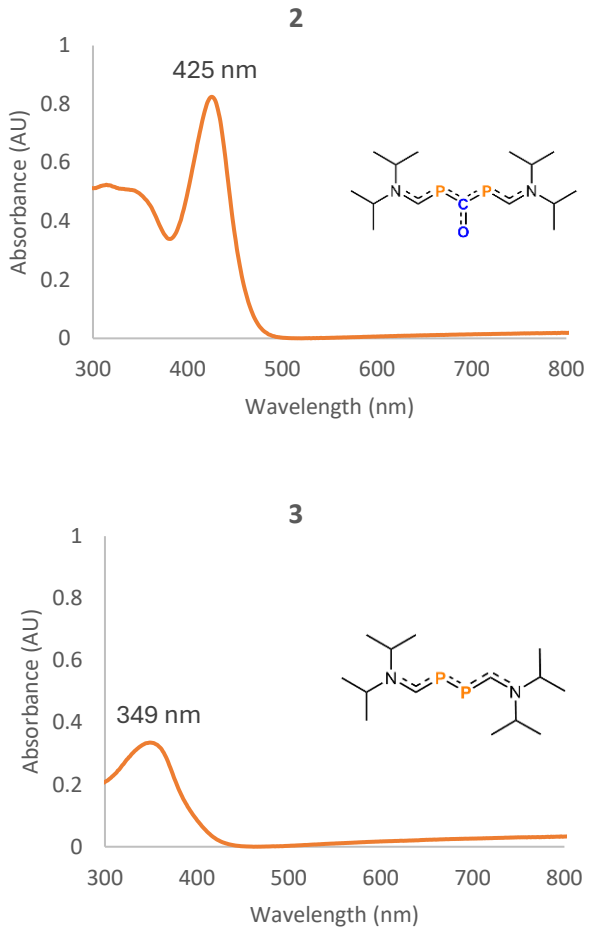

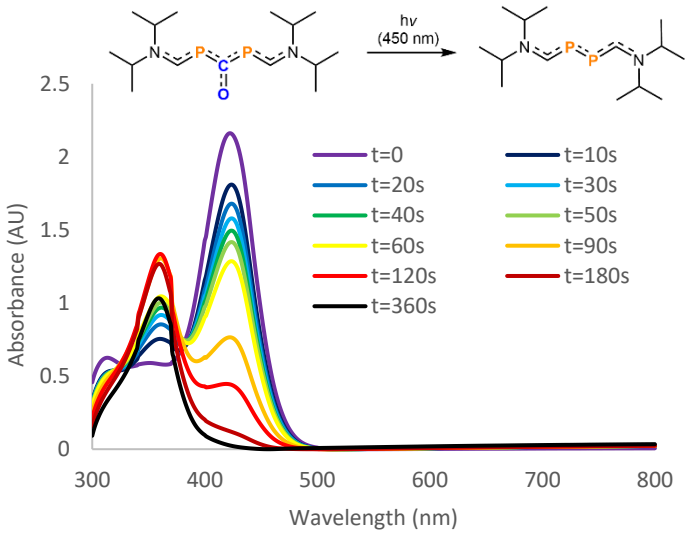

To help rationalize the photo-conversion of **2** into **3**, we monitored the absorbance of **3** during the irradiation at its maximum absorbance.

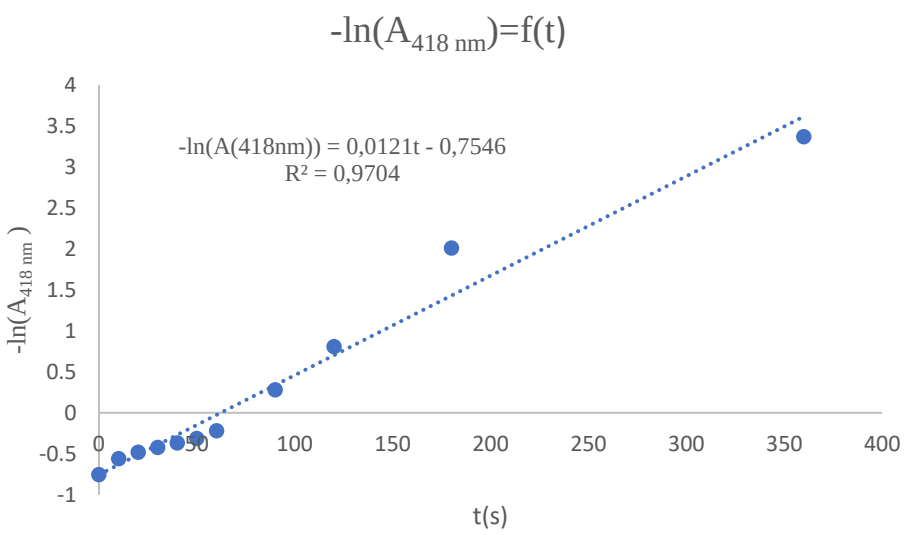

Hypothesis of a first-order kinetic:

$$-\frac{\mathrm{d}[\mathbf{2}]}{\mathrm{dt}} = k[\mathbf{2}]$$

$$Beer - Lambert\ law\colon\ A_{418\,nm} = \varepsilon(\mathbf{2})l[\mathbf{2}]$$

$$\rightarrow -\frac{\mathrm{d}A_{418\,nm}}{\mathrm{dt}} = kA_{418\,nm}$$

$$\rightarrow -\ln(A_{418\,nm}) = f(t) = kt + Constant$$

To confront our hypothesis, we realized the linear regression -ln($A_{418\ nm}$) = f(t) and obtained a constant $k(T = 298K) = 0.0121\ s^{-1}$ with an excellent correlation coefficient of R^2=0.9704 which is in line with our working hypothesis.

3.10.5 X-ray Crystallographic Data

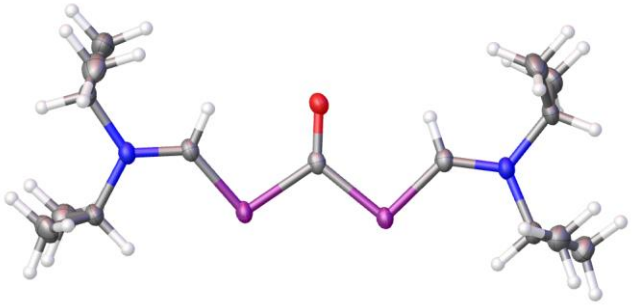

Crystal data and structure refinement for **2** (CCDC 2367862)

Identification code	p(co)p	
Empirical formula	C15 H30 N2 O P2	
Formula weight	316.35	
Temperature	100.15 K	
Wavelength	1.54178 Å	
Crystal system	Monoclinic	
Space group	P 1 21/c 1	
Unit cell dimensions	a = 12.7343(6) Å	a= 90°.
	b = 11.6579(5) Å	b= 113.366(2)°.
	c = 14.1462(6) Å	g = 90°.
Volume	1927.85(15) $Å^3$	
Z	4	
Density (calculated)	1.090 Mg/m^3	
Absorption coefficient	2.029 mm^{-1}	
F(000)	688	
Crystal size	0.2 x 0.1 x 0.1 mm^3	
Theta range for data collection	3.781 to 68.251°.	
Index ranges	-14<=h<=15, -14<=k<=14, -17<=l<=17	
Reflections collected	38129	
Independent reflections	3469 [R(int) = 0.0600]	
Completeness to theta = 67.679°	98.6 %	
Absorption correction	Semi-empirical from equivalents	
Max. and min. transmission	0.6617 and 0.5063	
Refinement method	Full-matrix least-squares on F^2	
Data / restraints / parameters	3469 / 0 / 195	

Goodness-of-fit on F^2	1.049
Final R indices [I>2σ(I)]	R1 = 0.0296, wR2 = 0.0753
R indices (all data)	R1 = 0.0333, wR2 = 0.0778
Extinction coefficient	n/a
Largest diff. peak and hole	0.359 and -0.151 e.$Å^{-3}$

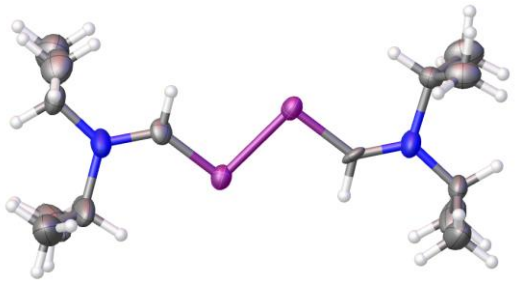

Crystal data and structure refinement for **3** (CCDC 2367863)

Identification code	bis(carbene)p2	
Empirical formula	C14 H30 N2 P2	
Formula weight	288.34	
Temperature	100 K	
Wavelength	0.71073 Å	
Crystal system	Monoclinic	
Space group	P 1 21/n 1	
Unit cell dimensions	a = 11.7119(16) Å	a= 90°.
	b = 11.7054(15) Å	b= 113.731(4)°.
	c = 14.533(2) Å	g = 90°.
Volume	1824.0(4) $Å^3$	
Z	4	
Density (calculated)	1.050 Mg/m^3	
Absorption coefficient	0.228 mm^{-1}	
F(000)	632	
Crystal size	0.15 x 0.12 x 0.08 mm^3	
Theta range for data collection	2.576 to 25.560°.	
Index ranges	-14<=h<=14, -14<=k<=14, -17<=l<=17	
Reflections collected	79435	
Independent reflections	3363 [R(int) = 0.0771]	
Completeness to theta = 25.242°	99.9 %	
Absorption correction	Semi-empirical from equivalents	
Max. and min. transmission	0.5547 and 0.5293	
Refinement method	Full-matrix least-squares on F^2	
Data / restraints / parameters	3363 / 261 / 348	
Goodness-of-fit on F^2	1.060	
Final R indices [I>2σ(I)]	R1 = 0.0473, wR2 = 0.1110	

R indices (all data)	R1 = 0.0641, wR2 = 0.1220
Extinction coefficient	n/a
Largest diff. peak and hole	0.444 and -0.218 e.Å^{-3}

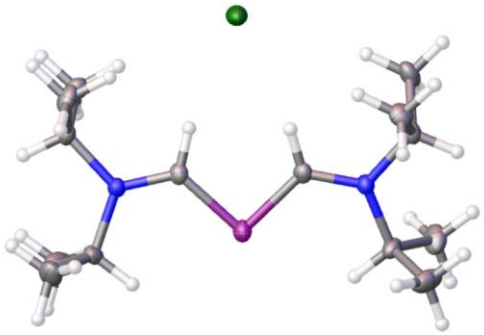

Crystal data and structure refinement for **P**+[Cl]

Identification code	ipr2nchpchnipr2-cl	
Empirical formula	C16 H30 D2 Cl7 N2 P	
Formula weight	533.57	
Temperature	100.15 K	
Wavelength	1.54178 Å	
Crystal system	Orthorhombic	
Space group	Fdd2	
Unit cell dimensions	a = 20.1819(14) Å	a= 90°.
	b = 21.8808(15) Å	b= 90°.
	c = 11.9533(8) Å	g = 90°.
Volume	5278.5(6) $Å^3$	
Z	8	
Density (calculated)	1.343 Mg/m^3	
Absorption coefficient	7.482 mm^{-1}	
F(000)	2208	
Crystal size	0.125 x 0.09 x 0.06 mm^3	
Theta range for data collection	4.751 to 70.355°.	
Index ranges	-24<=h<=24, -26<=k<=26, -14<=l<=14	
Reflections collected	22163	
Independent reflections	2520 [R(int) = 0.0459]	
Completeness to theta = 67.679°	100.0 %	
Absorption correction	Semi-empirical from equivalents	
Max. and min. transmission	0.7533 and 0.6089	
Refinement method	Full-matrix least-squares on F^2	
Data / restraints / parameters	2520 / 1 / 126	
Goodness-of-fit on F^2	1.073	

Final R indices [I>2sigma(I)]	R1 = 0.0249, wR2 = 0.0679
R indices (all data)	R1 = 0.0254, wR2 = 0.0683
Absolute structure parameter	-0.008(9)
Extinction coefficient	n/a
Largest diff. peak and hole	0.282 and -0.331 e.Å^{-3}

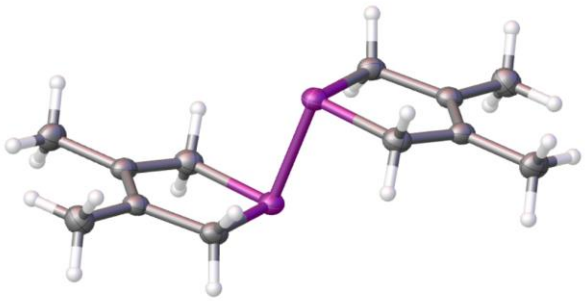

Crystal data and structure refinement for **6** (CCDC 2367864)

Identification code	bis(phospholine)	
Empirical formula	C12 H20 P2	
Formula weight	226.22	
Temperature	100.00 K	
Wavelength	0.71073 Å	
Crystal system	Triclinic	
Space group	P-1	
Unit cell dimensions	a = 5.1758(3) Å	a= 88.010(2)°.
	b = 5.3182(3) Å	b= 83.733(2)°.
	c = 11.4365(6) Å	g = 80.367(2)°.
Volume	308.46(3) $Å^3$	
Z	1	
Density (calculated)	1.218 Mg/m^3	
Absorption coefficient	0.315 mm^{-1}	
F(000)	122	
Crystal size	0.15 x 0.15 x 0.12 mm^3	
Theta range for data collection	3.585 to 25.636°.	
Index ranges	-6<=h<=6, -6<=k<=6, -13<=l<=13	
Reflections collected	2333	
Independent reflections	1167 [R(int) = 0.0482]	
Completeness to theta = 25.242°	99.8 %	
Absorption correction	None	
Refinement method	Full-matrix least-squares on F^2	
Data / restraints / parameters	1167 / 0 / 66	
Goodness-of-fit on F^2	1.142	
Final R indices [I>2σ(I)]	R1 = 0.0490, wR2 = 0.1255	

R indices (all data)	R1 = 0.0528, wR2 = 0.1272
Extinction coefficient	n/a
Largest diff. peak and hole	0.443 and -0.413 e.Å^{-3}

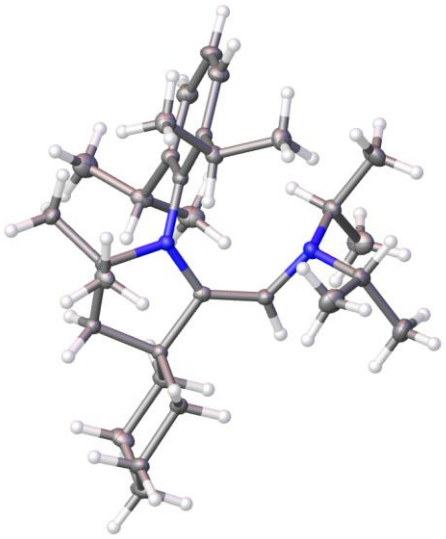

Crystal data and structure refinement for **11** (CCDC 2367865)

Identification code	dimer_aminocarbene_caac	
Empirical formula	C30 H50 N2	
Formula weight	438.72	
Temperature	100.15 K	
Wavelength	1.54178 Å	
Crystal system	Monoclinic	
Space group	P 1 21/n 1	
Unit cell dimensions	a = 10.5119(4) Å	a= 90°.
	b = 15.7592(6) Å	b= 100.3031(10)°.
	c = 16.7454(6) Å	g = 90°.
Volume	2729.30(18) $Å^3$	
Z	4	
Density (calculated)	1.068 Mg/m^3	
Absorption coefficient	0.451 mm^{-1}	
F(000)	976	
Crystal size	0.14 x 0.095 x 0.08 mm^3	
Theta range for data collection	3.881 to 68.245°.	
Index ranges	-12<=h<=12, -18<=k<=18, -17<=l<=20	
Reflections collected	34037	
Independent reflections	4985 [R(int) = 0.0394]	
Completeness to theta = 67.679°	99.9 %	
Absorption correction	Semi-empirical from equivalents	

Max. and min. transmission	0.6617 and 0.5979
Refinement method	Full-matrix least-squares on F^2
Data / restraints / parameters	4985 / 0 / 299
Goodness-of-fit on F^2	1.024
Final R indices [I>2σ(I)]	R1 = 0.0380, wR2 = 0.0971
R indices (all data)	R1 = 0.0396, wR2 = 0.0988
Extinction coefficient	n/a
Largest diff. peak and hole	0.310 and -0.204 e.$Å^{-3}$

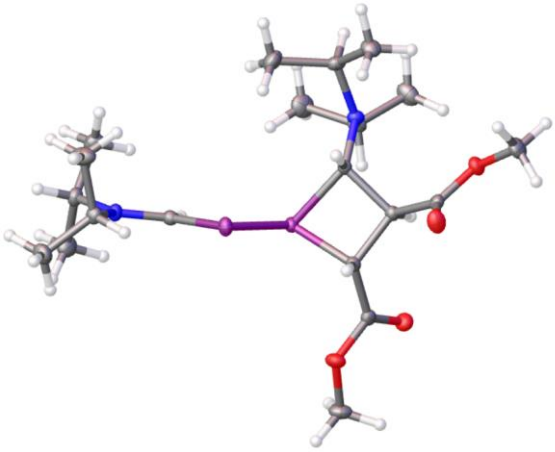

Crystal data and structure refinement for **13**

Identification code	p2-dimethylfumarate	
Empirical formula	C20 H38 N2 O4 P2	
Formula weight	432.46	
Temperature	100.00 K	
Wavelength	0.71073 Å	
Crystal system	Monoclinic	
Space group	P 1 21/n 1	
Unit cell dimensions	a = 7.8176(3) Å	a= 90°.
	b = 20.2472(9) Å	b= 104.1180(10)°.
	c = 15.9206(7) Å	g = 90°.
Volume	2443.87(18) $Å^3$	
Z	4	
Density (calculated)	1.175 Mg/m^3	
Absorption coefficient	0.203 mm^{-1}	
F(000)	936	
Crystal size	0.3 x 0.25 x 0.25 mm^3	
Theta range for data collection	2.638 to 27.538°.	
Index ranges	-10<=h<=10, -26<=k<=26, -20<=l<=20	
Reflections collected	66580	
Independent reflections	5625 [R(int) = 0.0440]	
Completeness to theta = 25.242°	99.9 %	
Absorption correction	Semi-empirical from equivalents	
Max. and min. transmission	0.7456 and 0.6842	
Refinement method	Full-matrix least-squares on F^2	

Data / restraints / parameters	5625 / 0 / 263
Goodness-of-fit on F^2	1.030
Final R indices [I>2sigma(I)]	R1 = 0.0282, wR2 = 0.0679
R indices (all data)	R1 = 0.0337, wR2 = 0.0709
Extinction coefficient	n/a
Largest diff. peak and hole	0.339 and -0.217 e.$Å^{-3}$

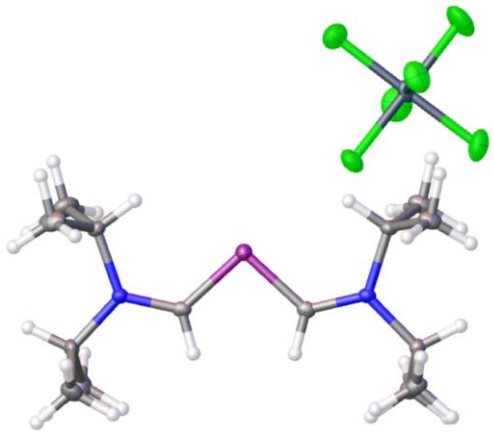

Crystal data and structure refinement for **P**+[SbF_6]

Identification code	ipr2nchpchnipr2_sbf6	
Empirical formula	C14 H30 F6 N2 P Sb	
Formula weight	493.12	
Temperature	100.00 K	
Wavelength	0.71073 Å	
Crystal system	Orthorhombic	
Space group	$Pna2_1$	
Unit cell dimensions	a = 16.8446(5) Å	a= 90°.
	b = 15.7916(4) Å	b= 90°.
	c = 7.9392(2) Å	g = 90°.
Volume	2111.85(10) $Å^3$	
Z	4	
Density (calculated)	1.551 Mg/m^3	
Absorption coefficient	1.432 mm^{-1}	
F(000)	992	
Crystal size	0.18 x 0.18 x 0.06 mm^3	
Theta range for data collection	2.580 to 26.371°.	
Index ranges	-21<=h<=21, -19<=k<=19, -9<=l<=9	
Reflections collected	36935	
Independent reflections	4307 [R(int) = 0.0389]	
Completeness to theta = 25.242°	99.9 %	
Absorption correction	Semi-empirical from equivalents	
Max. and min. transmission	0.4910 and 0.4407	
Refinement method	Full-matrix least-squares on F^2	

Data / restraints / parameters	4307 / 1 / 225
Goodness-of-fit on F^2	1.025
Final R indices [I>2sigma(I)]	R1 = 0.0152, wR2 = 0.0321
R indices (all data)	R1 = 0.0164, wR2 = 0.0325
Absolute structure parameter	-0.010(7)
Extinction coefficient	n/a
Largest diff. peak and hole	0.214 and -0.287 e.$Å^{-3}$

Chapter 4 (Side Project): Enhancing Substrate-Metal Catalyst Affinity via Hydrogen Bonding: Pd(II)-Catalyzed β-C(sp^3)-H Bromination of Free Carboxylic Acids

The achievement of sufficient substrate−metal catalyst affinity is a fundamental challenge for the development of synthetically useful C-H activation reactions of weakly coordinating native substrates. While hydrogen bonding has been harnessed to bias site selectivity in existing C(sp^2)-H activation reactions, the potential for designing catalysts with hydrogen bond donors (HBDs) to enhance catalyst-substrate affinity and, thereby, facilitate otherwise unreactive C(sp^3)-H activation remains to be demonstrated. This chapter describes the discovery of a ligand scaffold containing a remote amide motif that can form a favorable *meta*-macrocyclic hydrogen bonding interaction with the aliphatic acid substrate. The utility of this ligand scaffold is demonstrated through the development of an unprecedented C(sp^3)-H bromination of α-tertiary and α-quaternary free carboxylic acids, which proceeds in exceedingly high *mono*-selectivity. The geometric relationship between the NHAc hydrogen bond donor and the coordinating quinoline ligand is crucial for forming the *meta*-macrocyclophane-like hydrogen bonding interaction, which provides a guideline for the future design of catalysts employing secondary interactions.

4.1 Introduction

Despite significant developments in transition-metal-catalyzed C(sp^3)-H functionalization over the past decade, performing directed C-H metalation with native functional groups rather than exogenous directing groups (DGs) remains challenging.[98] In this context, the activation of alkyl C-H bonds directed by carboxylic acids on the basis of weak cation coordination has been the main platform to demonstrate the feasibility of this approach. While innovation in ligand design has

enabled a wide range of free-acid-directed C(sp^2)-C and C(sp^3)-X bond formations (X = N, O),[99] the bromination of C(sp^3)-H still requires the installation of external directing groups.[100]

Considering the broad utility of alkyl bromides as versatile intermediates in synthetic organic chemistry,[101] the invention of new methods for *mono*-selective *β*-C-H bromination of readily available carboxylic acids lags behind the wide range of enzymatic C-H halogenation reactions.[102] The unique proficiency of bidentate ligands containing internal proton acceptors, such as acetamides and pyridones, for the facilitation of a wide range of C-H bond activation reactions of free acid has been demonstrated in numerous previous reports from the Yu lab and others.[103] However, despite repeated attempts, we have found that bidentate ligands fail to promote the C−H bromination of free carboxylic acids (Figure 4.1A). Conversely, we have previously observed that monodentate pyridine-type ligands enable the C(sp^3)-H bromination of *α*-quaternary free carboxylic acid in modest yield. Unfortunately, no reactivity was observed with more challenging *α*-tertiary acids, and efforts to optimize this reactivity through routine screening have proved futile (Figure 4.1B). Intriguingly, the latter class of ligands has proved effective when the analogous transformation is directed by a more strongly coordinating electron-deficient amide instead of a free carboxylic acid, which suggests that the poor reactivity observed with free acids may be the result of insufficient affinity of the catalyst for a carboxyl group in the presence of the interfering brominating reagent.[104] In light of these results, we hypothesized that the desired transformation could be enabled through the design of a new type of monodentate pyridine ligand with an additional function: enhancement of the interaction between carboxylic acid substrates and the Pd(II) catalyst.

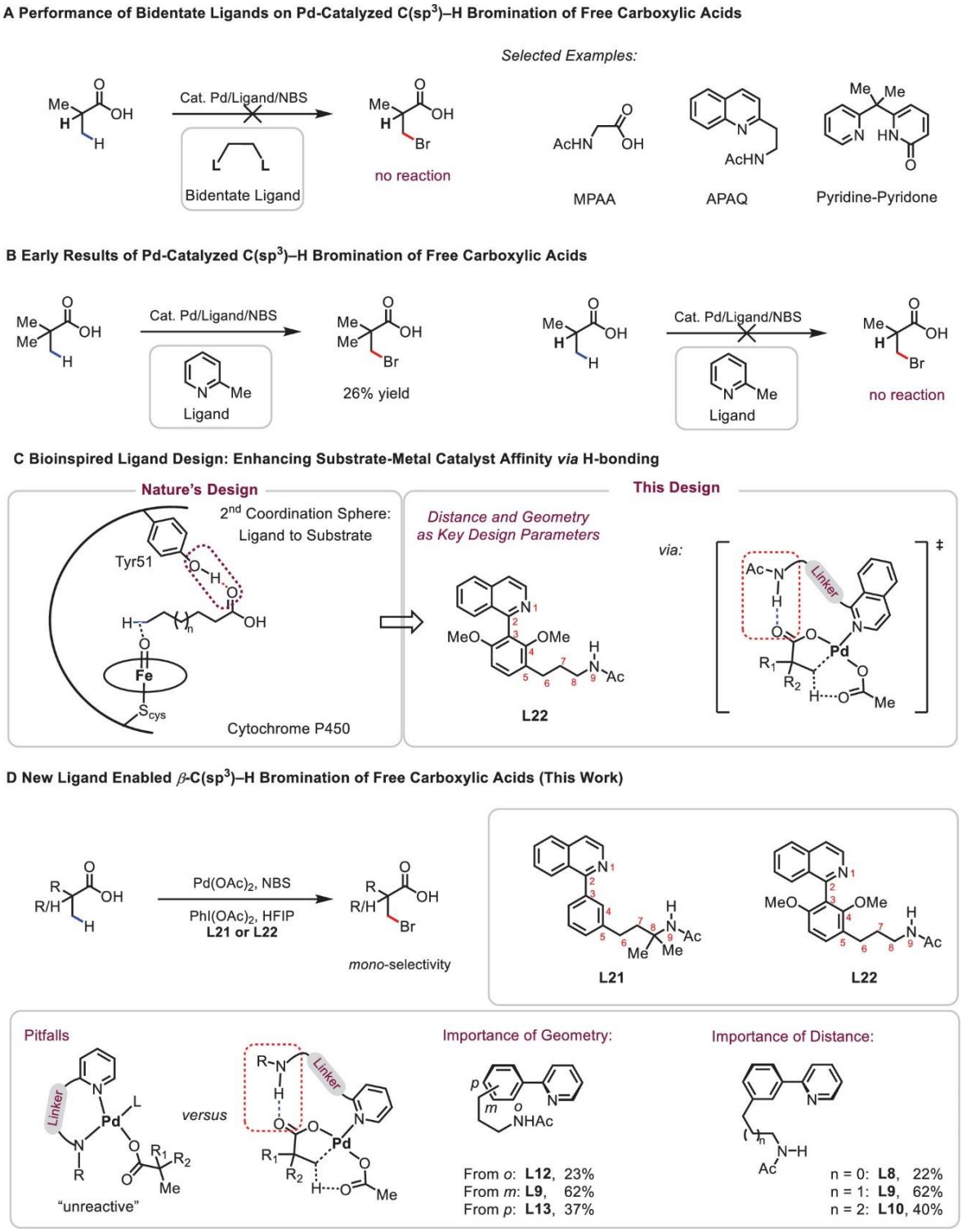

Figure 4.1 – Pd(II)-catalyzed C(sp^3)-H bromination of free aliphatic acids.

It is well established that enzymes and metalloproteins can facilitate catalysis through remote hydrogen bonding with their substrates.[105] For example, in the active site of cytochrome P450-BM3, a fatty acid hydroxylase, a hydrogen bond donor interacts with the carboxylate group of the acid substrate, thereby directing site-selective C-H bond oxidation (Figure 4.1C). Although hydrogen-bonding-directed catalysis[106] has been successfully harnessed to bias site selectivity in C-H activation,[107] the development of ligands involving a hydrogen-bonding interaction to promote the C(sp^3)-H activation of free acid by increasing the binding affinity of the carboxyl group for the metal center remains to be demonstrated. We were particularly interested in the possibility of using our established *meta*-macrocyclophane geometry[108] to assemble the hydrogen bonding interaction and help to promote the desired interaction through control over distance and geometry while suppressing undesired chelation of the hydrogen bonding donor motif to the metal center. In this chapter, we report the development of a β-C(sp^3)-H bromination and chlorination of free carboxylic acids enabled by a novel quinoline ligand bearing a pendant NHAc group that forms a hydrogen-bonding interaction with the carboxylate in a *meta*-macrocyclophane structure (Figure 4.1D).

4.2 Results and Discussion

Bearing in mind that previous efforts to achieve β-bromination of pivalic acid using a quinoline ligand only gave 40% yield, various ligands using pivalic acid **1a** as the model substrate were tested (Figure 4.2). While no product was observed in the absence of ligand, monodentate pyridine-type ligand **L1′** provided 26% yield of the desired product, which is consistent with a previous report.[109] Further screening with this ligand (**L1′**) did not improve the yield. Most importantly, **L1′** failed to show any reactivity with α-hydrogen-containing acids, thereby

highlighting the need for novel ligands. As anticipated, bidentate ligands such as *mono*-acetyl-protected aminoalkylpyridine (MPAPy) ligands (**L2**, **L3**) also gave poor yields. We next tried to extend the linker between the pyridine and the NHAc group (**L4**–**L6**) in the hope of disfavoring bidentate coordination and enabling macrocyclic hydrogen-bonding interactions to enhance the binding affinity of the substrate. Unfortunately, we did not observe any improvement, which is most likely the result of the highly flexible linker either allowing for undesired chelation by the NHAc moiety or entropically disfavoring the desired H-bonding interaction. On the basis of a previous understanding of the favorable assembly of *meta*-macrocyclophane transition states in remote C-H activation, we incorporated one phenyl ring bearing the NHAc moiety at the *meta*-position into the ligand scaffold and adjusted the ring size (**L7**–**L11**) to prevent the potential bidentate coordination. We found that **L9** significantly increased the yield to 62%. The poor performance of **L8** (eight-membered ring size) or **L10** (10-membered ring size) suggests that the precise ring size of the macrocyclophane hydrogen-bonding interaction is crucial for enabling catalysis. The poor yields observed with *ortho*- and *para*-substituted ligands **L12** and **L13** further confirmed the favorable assembly of the *meta*-cyclophane structures.

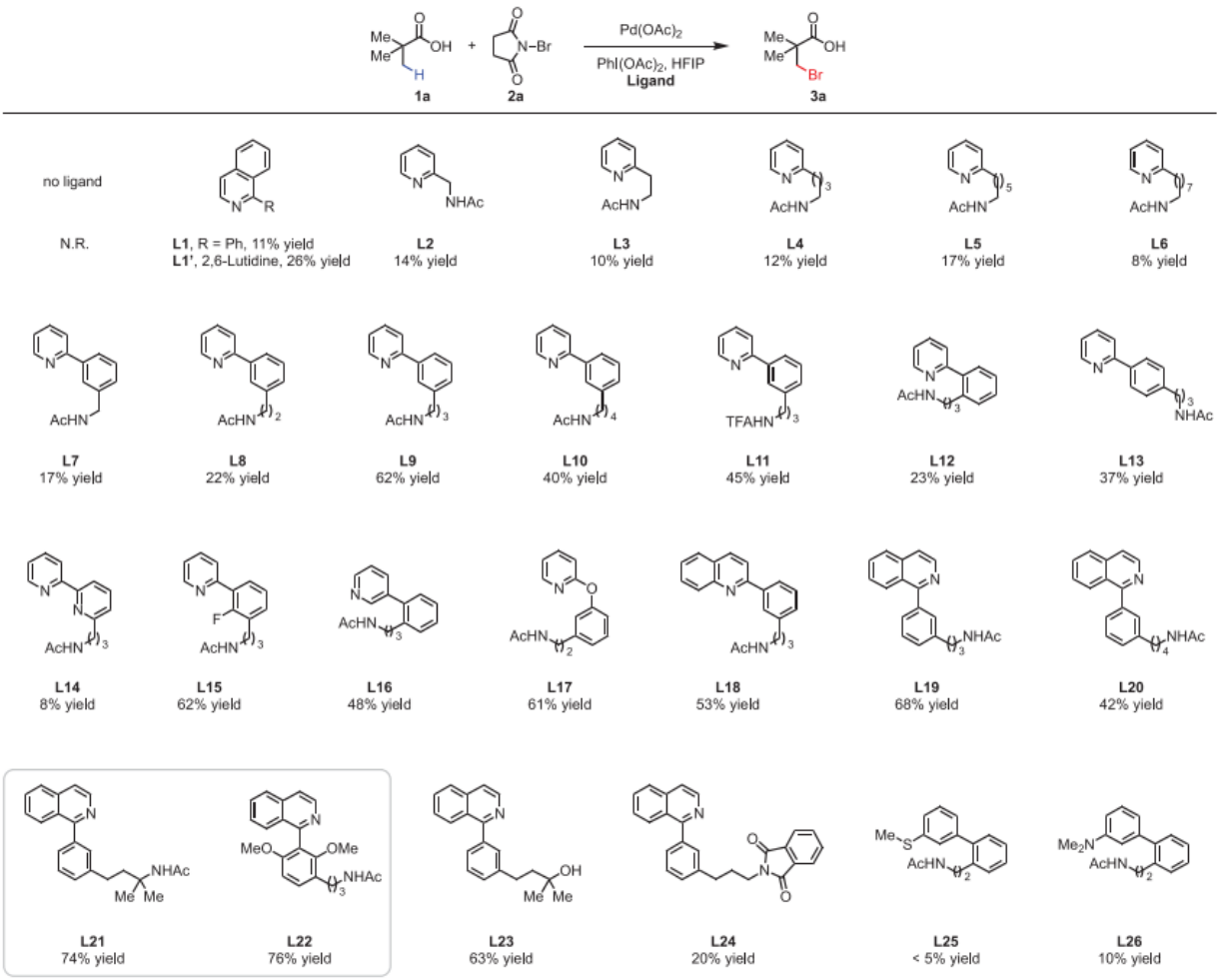

[a]Conditions: **1a** (0.1 mmol), **2a** (0.2 mmol), $Pd(OAc)_2$ (10 mol %), **ligand** (15 mol %), $PhI(OAc)_2$ (0.1 mmol), AcOH (0.1 mmol), hexafluoroisopropanol (HFIP) (1.0 mL), 100 °C, air, 24 h. ^1H NMR yields obtained using CH_2Br_2 as an internal standard.

Figure 4.2 – Scope of ligands for the β-C(sp^3)-H bromination of free aliphatic acids.

Seeking to optimize ligand **L9**, we observed that further modification of the ligand backbone (**L11**–**L18**) did not significantly improve the reactivity. Switching from pyridine to isoquinoline (**L19**) resulted in a small increase in yield of up to 68%. The comparatively poor performance of one-carbon homologated **L20** further highlighted the importance of the ring size of the macrocyclic H-bonding interactions in this system. To promote angle-compression through the Thorpe-Ingold effect, we introduced a *gem*-dimethyl in **L21**, which gratifyingly led to a modest improvement in yield. A similar result was also observed with **L22**, which might result from the

constrained environment provided by the 2,6-dimethoxy-1,1′biphenyl moiety. Importantly, the possibility that the active species is a palladacycle formed through isoquinoline-directed intramolecular C-H activation of the ligand was excluded by the high activity observed with bis-*ortho*-substituted **L22**. In support of the crucial role of the proposed hydrogen bond donor, the methylated analogue of **L18** (**L18′**) and phthalimide-protected analogue of **L19** (**L24**), both incapable of the proposed hydrogen-bonding interaction, gave poor yields similar to the simple monodentate pyridine ligand **L1**. Consistent with our hypothesis, **L23** containing a free alcohol as an alternate HBD remained highly effective, thereby affording the brominated product in 63% yield. Similarly, the importance of the pyridine or isoquinoline motif was highlighted by the failure of thiol-based ligand **L25** and aniline-based ligand **L26** to promote the reaction.

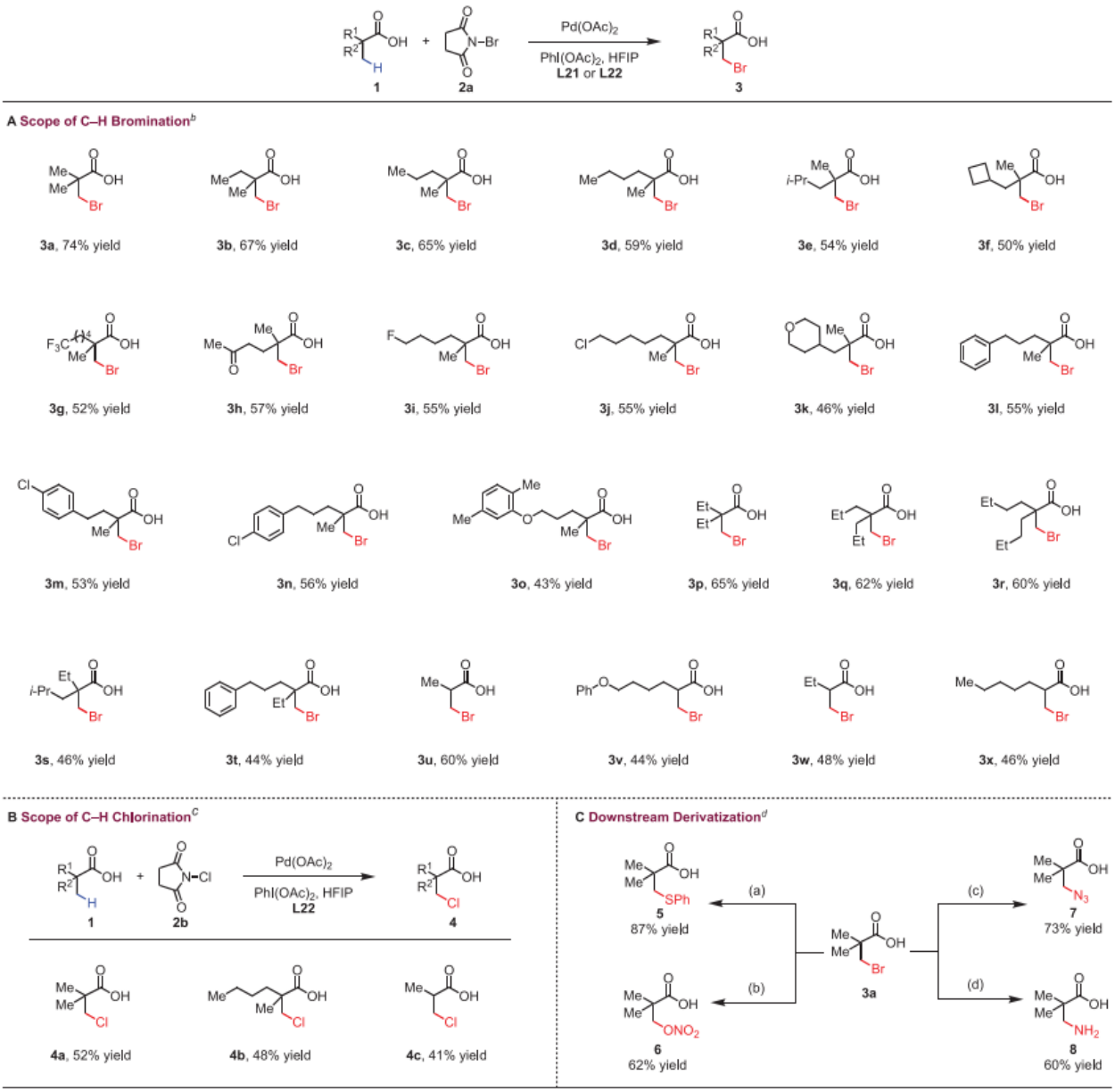

[a]**L22** was applied to **3a**, **3g**–**3k**, and **3u**–**3x**. [b]Conditions: **1** (0.1 mmol), **2a** (2.0 equiv), $Pd(OAc)_2$ (10 mol %), **ligand** (15 mol %), $PhI(OAc)_2$ (0.1 mmol), AcOH (0.1 mmol), HFIP (1.0 mL), 100 °C, air, 24 h. [c]Conditions: **1** (0.1 mmol), **2b** (2.0 equiv), $Pd(OAc)_2$ (10 mol %), **ligand** (15 mol %), $PhI(OAc)_2$ (0.1 mmol), AcOH (0.1 mmol), HFIP (1.0 mL), 100 °C, air, 24 h. [d]Conditions for derivatization: (i) PhSH (2.0 equiv), NaOH (2.0 equiv), EtOH, 40 °C, 12 h; (ii) $AgNO_3$ (2.0 equiv), EtOAc, 80 °C, 24 h; (iii) NaN_3 (4.0 equiv), MeOH, 40 °C, 24 h; (iv) NH_3H_2O (1.0 mL), 80 °C, 12 h.

Figure 4.3 – β-C(sp^3)-H halogenation of free aliphatic acids

Having identified highly reactive ligands and reaction conditions, we next sought to examine the scope of the bromination reaction (Figure 4.3A). *α-gem*-Dimethyl carboxylic acids with a range of aliphatic chains all proved compatible and afforded the *β*-brominated products in

high yields (**3a**−**3f**). A variety of functional groups, such as fluoro, chloro, trifluoromethyl, and ketone, were tolerated (**3g**−**3j**). These functionalities are useful synthetic handles for subsequent derivatization, thereby demonstrating the practicality of this methodology. Notably, in contrast with other β-C(sp^3)-H functionalization reactions, this protocol displayed exclusive selectivity for monofunctionalization despite the presence of two α-methyl groups. Aliphatic carboxylic acids bearing cyclic rings with four- and six-membered rings were tolerated (**3f**, **3k**). Phenyl groups were also compatible with these reaction conditions (**3l**−**3n**) and remained intact despite the potential for reactivity of the aryl or benzylic C-H bonds. Even electron-rich phenolic ethers (**3o** and **3v**) were compatible despite the use of NBS and phenyliodine(III) diacetate (PIDA) oxidants. Gemfibrozil, an oral drug that is used to decrease lipid levels, could be converted to the corresponding β-brominated product in useful yield (**3o**). In addition, quaternary substrates containing a single α-methyl group consistently afforded good yields (**3p**−**3t**). Likewise, α-tertiary aliphatic carboxylic acids afforded the desired monobromination products in moderate to good yield (**3u**−**3x**). These substrates are typically challenging because of the lack of a favorable Thorpe-Ingold effect, as well as the potential for side reactions, due to the acidic α-C-H bond. In addition, we examined the ability of our novel ligand to promote the Pd(II)catalyzed β-C(sp^3)-H chlorination of free carboxylic acids because of the bioactivity of alkyl halides in drug discovery (Figure 4.3B).[110] To our delight, both the quaternary carboxylic acids and α-tertiary acid substrates were chlorinated under these reaction conditions to afford the desired products in 41%−52% yields (**4a**−**4c**).

The synthetic utility of this C(sp^3)-H bromination was demonstrated by converting **3a** to a wide range of β-substituted aliphatic acids via nucleophilic substitutions (Figure 4.3C). A diverse array of chemical bonds, including C−S, C−O, and C−N bonds, were easily forged, thereby

providing straightforward access to compounds that might be challenging to access from the free acid using other methods. Notably, this methodology could be applied to the synthesis of valuable *β*-amino acid (**8**).

To probe our mechanistic hypothesis experimentally, we first looked at the complexation of **L21**, one of our optimal ligands, with $Pd(OAc)_2$ (Figure 4.4). X-ray crystallographic analysis confirmed that this ligand binds to palladium in a monodentate fashion via the quinoline nitrogen and engages in a macrocyclic intramolecular hydrogen-bonding interaction between the amide and a palladium-bound carboxylate in the solid state. To highlight the remarkable specificity of this ligand framework, we also examined **L23**, a slightly less reactive ligand bearing an alcohol HBD. In the complex formed from **L23**, we did not observe an intramolecular macrocyclic hydrogen-bonding interaction, but the alcohol instead participated in an intermolecular hydrogen-bonding interaction with a carboxylate bound to a second equivalent of palladium, which demonstrated the electronic viability of the proposed interaction. To gain additional insight into the optimal distance and geometry for the positioning of the NHAc group, we also considered **L20**, which has a longer carbon chain and lacks the *gem*-dimethyl group present in **L21**. In this case, the same macrocyclic hydrogen bonding interaction was observed as with **L21**, but structural parameters (H−O distance and N− H−O angle) suggested that the interaction was weakened, an observation consistent with the reduced yield observed with **L20** (Figure 4.2).

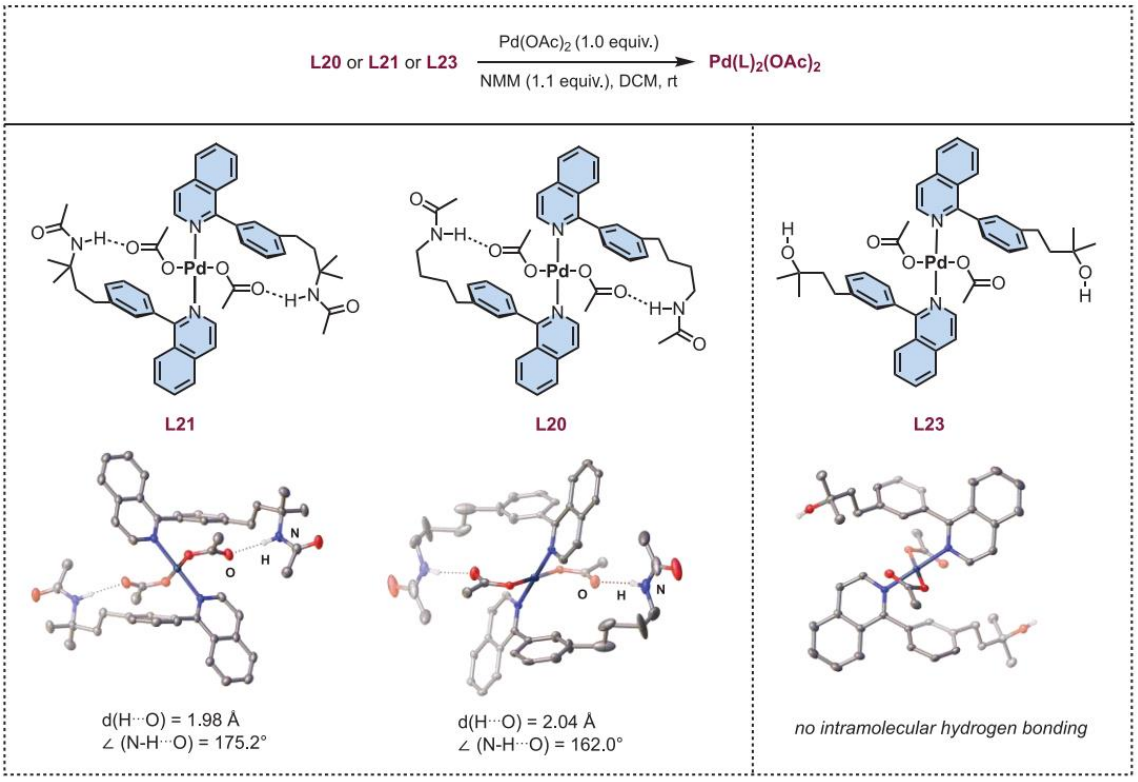

Figure 4.4 – Preparation and solid-state structures of **Pd-L20**, **Pd-L21**, and **Pd-L23** complexes (hydrogen atoms except N-H and O-H have been omitted for clarity).

To the best of our knowledge, there is no report of similar intramolecular macrocyclic distal hydrogen bonding motifs in transition metal complexes, as demonstrated by a careful search of the Cambridge Crystallographic Data Centre (CCDC). These observations and additional comparative DFT studies (detailed in the Experimental section) support our hypothesis that a hydrogen-bonding interaction between the ligand and the carboxylate directing group can be leveraged to enable increased reactivity.

4.3 Conclusion

In summary, we have discovered a new class of pyridine-based ligands containing a hydrogen bond donor that interacts with a carboxyl directing group in substrates, thereby enabling the Pd(II)-catalyzed β-C(sp^3)-H bromination and chlorination of free carboxylic acids. The broad substrate scope, as well as the ease of valuable downstream transformations of the halogenated products, demonstrates the synthetic potentiality of this strategy. Importantly, our bioinspired ligand design employing a secondary coordination sphere hydrogen-bonding interaction was the key to the success of this C(sp^3)-H halogenation. On the basis of DFT calculations, the free energy of the reaction pathway using **L21** or **L23** ligands possessing pendant hydrogen bond donors is lower than that for **L1**, a ligand incapable of hydrogen bonding. X-ray crystallographic analysis of palladium−ligand complexes provides additional support for the proposed interaction through *meta*-macrocyclophane hydrogen-bonding interaction. We expect that this new ligand design concept will be broadly applicable within the field of C-H activation and guide future ligand development efforts.

4.4 Acknowledgments

I would like to thank all the collaborators on this project: Liang Hu, Guangrong Meng, Xiangyang Chen, Jing-Ran Shan, Nikita Chekshin, Daniel Strassfeld, Tao Sheng, Zhe Zhuang, Ken Houk, and Jin-Quan Yu. Special thanks to Rodolphe Jazzar for inviting me to work on this project.

Chapter 4 is an adaptation from Enhancing Substrate-Metal Catalyst Affinity via Hydrogen Bonding: Pd(II)-Catalyzed β-C(sp3)−H Halogenation of Free Carboxylic Acids. Hu, Liang; Meng,

Guangrong; Chen, Xiangyang; Yoon, Joseph; Shan, Jing-Ran; Chekshin, Nikita; Strassfeld, Daniel; Sheng, Tao; Zhuang, Zhe; Jazzar, Rodolphe; Bertrand, Guy; Houk, Kenneth; Yu, Jin-Quan, Journal of the American Chemical Society, 2023. The dissertation author was the fourth author on this paper.

4.5 Experimental

4.5.1 General Considerations

Carboxylic acids were obtained from commercial sources or synthesized according to literature procedures. Solvents were obtained from Σ-Aldrich, Oakwood and Acros and used directly without further purification. Analytical thin layer chromatography was performed on 0.25 mm silica gel 60-F254. Visualization was carried out with UV light and Bromocresol Green Stain. ^{1}H NMR was recorded on Bruker DRX-600 instrument (600 MHz). Chemical shifts were quoted in parts per million (ppm) referenced to the literature values of tetramethylsilane. The following abbreviations (or combinations thereof) were used to explain multiplicities: s = singlet, d = doublet, t = triplet, q = quartet, p = pentet, m = multiplet, br = broad. Coupling constants, J, were reported in Hertz unit (Hz). ^{13}C NMR spectra were recorded on Bruker DRX600 instrument (150 MHz), and were fully decoupled by broad band proton decoupling. Chemical shifts were reported in ppm referenced to either the center line of a triplet at 77.0 ppm of chloroform-d or the center line of a multiplet at 29.84 ppm of acetone-d6. High-resolution mass spectra (HRMS) were recorded on an Agilent Mass spectrometer using ESI-TOF (electrospray ionization-time of flight).

4.5.2 Experimental Procedures

General procedure for synthesis of **L4**

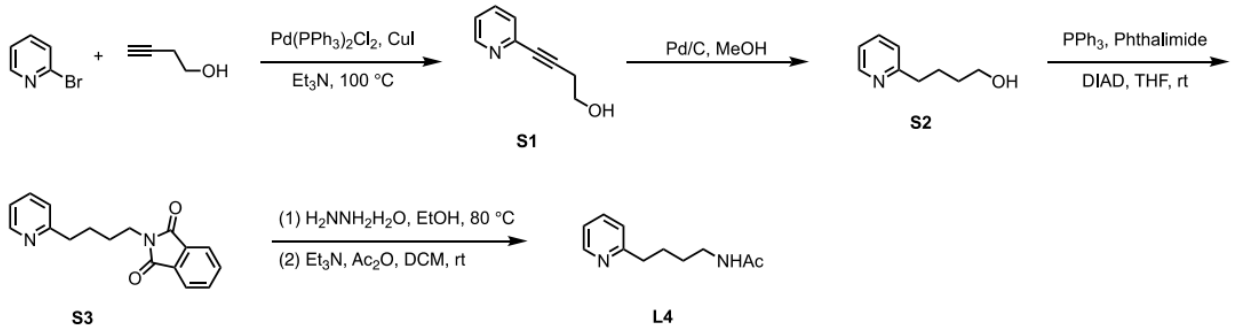

Synthesis of **S1**: To a solution of 2-bromopyridine (10 mmol), $Pd(PPh_3)_2Cl_2$ (5 mol%) and CuI (10 mol%) in Et_3N (0.25 M), 3-Butyn-1-ol (20 mmol, 2.0 equiv.) was added dropwise at room temperature under nitrogen and stirred for 10 min, then the reaction was stirred at 100 °C for 24 h. After being allowed to cool to room temperature, the crude mixture was concentrated and diluted with ethyl acetate. The mixture was passed through a pad of Celite with ethyl acetate as the eluent to remove any insoluble precipitate. The resulting solution was concentrated, and the residue was purified by column chromatography on silica gel using EtOAc/hexanes (3/7) as the eluent giving the pure product as clear oil (78 % yield).

Synthesis of **S2**: To the solution of **S1** in MeOH (20 mL) was added Pd/C 10% (0.1 g). The reaction vial was filled with H_2 (1atm), and the reaction mixture was stirred overnight. Upon completion, the crude mixture was filtered through celite, and the filtrate was concentrated in vacuo. The residue was roughly purified by column chromatography on silica gel using EtOAc/hexanes as the eluent, and the resulting crude material was used in the next step without further purification.

Synthesis of **S3**: To a solution of **S2** (5 mmol), PPh_3 (5 mmol, 1.0 equiv.), and Phthalimide (5 mmol, 1.0 equiv.) in THF (0.2 M), DIAD (5 mmol, 1.0 equiv.) was added dropwise at 0 °C. The

reaction mixture was warmed to room temperature and stirred for 20 h. Upon completion, the crude mixture was concentrated, and phosphine oxide was removed by the column chromatography on silica gel. The resulting crude material was used in the next step without further purification.

Synthesis of **L4**: To a solution of **S3** in EtOH (30 mL) was added hydrazine monohydrate (2 mL, 41 mmol) in one portion. The reaction mixture was stirred at 80 °C for 5 h. Upon completion, the white precipitate was removed by the filtration. The filtrate was concentrated and dissolved in DCM (40 ml). Triethylamine (10 mmol, 2.0 equiv.) and acetic anhydride (5 mmol, 1.0 equiv.) were added dropwise at 0 °C. The reaction mixture was warmed to room temperature and stirred overnight. Upon completion, water was added and extracted with DCM three times. The combined organic layer was dried with anhydrous Na_2SO_4, and concentrated. The residue was purified by column chromatography on silica gel using EtOAc/hexanes (4/6) as the eluent giving the pure product clear oil (42 % yield over three steps).

Note: Ligand **L5** and **L6** were prepared using the same synthetic route mentioned above.

General procedure for synthesis of **L9**

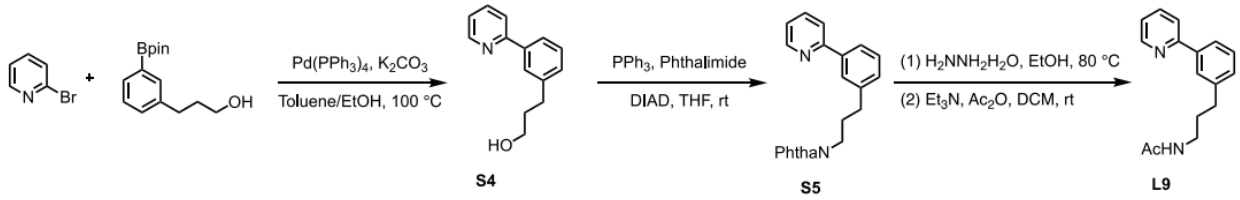

Synthesis of **S4**: A Schlenk flask containing a stir bar was charged with 2-bromopyridine (5 mmol), $Pd(PPh_3)_4$ (5 mol%), 3-(3-(4,4,5,5-tetramethyl-1,3,2-dioxaborolan-2-yl)phenyl)propan-1-ol (6 mmol, 1.2 equiv.) and K_2CO_3 (3.0 equiv.). The flask was evacuated and backfilled with nitrogen three times followed by adding EtOH (4 mL) and Toluene (20 mL). The reaction mixture

was stirred at 100°C for 24 h. After being allowed to cool to room temperature, the crude mixture was passed through a pad of Celite with ethyl acetate as the eluent to remove insoluble precipitate. The resulting solution was concentrated, and the residue was purified by column chromatography on silica gel using EtOAc/hexanes (4/6) as the eluent giving the pure product as white solid (70 % yield).

Synthesis of **S5**: To a solution of **S4** (3 mmol), PPh_3 (3 mmol, 1.0 equiv.), and Phthalimide (3 mmol, 1.0 equiv.) in THF (0.2 M), DIAD (3 mmol, 1.0 equiv.) was added dropwise at 0 °C. The reaction mixture was warmed to room temperature and stirred for 20 h. Upon completion, the crude mixture was concentrated, and phosphine oxide was removed by the column chromatography on silica gel. The resulting crude material was used in the next step without further purification.

Synthesis of **L9**: To a solution of **S5** in EtOH (20 mL) was added hydrazine monohydrate (1 mL, 20 mmol) in one portion. The reaction mixture was stirred at 80 °C for 5 h. Upon completion, the white precipitate was removed by the filtration. The filtrate was concentrated and dissolved in DCM (20 ml). Triethylamine (6 mmol, 2.0 equiv.) and acetic anhydride (3 mmol, 1.0 equiv.) were added dropwise at 0 °C. The reaction mixture was warmed to room temperature and stirred overnight. Upon completion, water was added and extracted with DCM three times. The combined organic layer was dried with anhydrous Na_2SO_4, and concentrated. The residue was purified by column chromatography on silica gel using EtOAc/methanol (96/4) as the eluent giving the pure product as white solid (50% yield over three steps).

Note: Ligands **L7**, **L8**, **L10**, **L11**, **L12**, **L13**, **L15**, **L16**, **L18**, **L19**, **L20**, **L24**, **L25** and **L26** were prepared using the same synthetic route mentioned above

General procedure for synthesis of **L14**

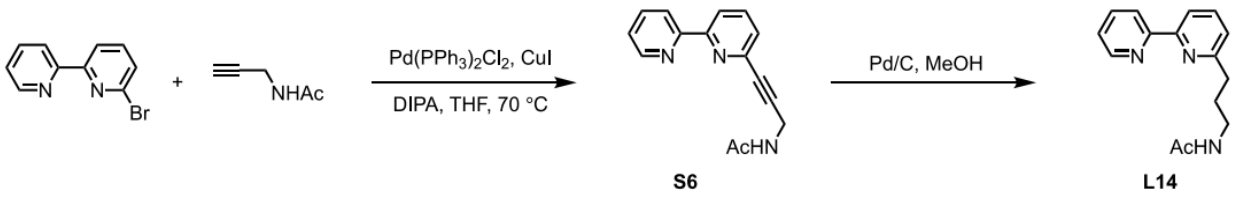

Synthesis of **S6**: A Schlenk flask containing a stir bar was charged with 6-Bromo-2,2′-bipyridine (2 mmol), CuI (2.0 equiv.), N-(prop-2-yn-1-yl)acetamide (1.0 equiv.), $Pd(PPh_3)_2Cl_2$ (5 mol%) and diisopropylamine (1.0 ml). The flask was evacuated and backfilled with nitrogen three times followed by adding THF (20 mL). The reaction mixture was stirred at 70°C for 24 h. After being allowed to cool to room temperature, the crude mixture was passed through a pad of Celite with ethyl acetate as the eluent to remove insoluble precipitate. The crude mixture was washed with water three times. The organic layer was dried with Na_2SO_4 and concentrated. The residue was purified by column chromatography on silica gel using EtOAc/MeOH (96/4) as the eluent giving the pure product as white solid (55 % yield).

Synthesis of **L14**: To the solution of **S6** in MeOH (10 mL) was added Pd/C 10% (0.05 g). The reaction vial was filled with H_2 (1 atm), and the reaction mixture was stirred overnight. Upon completion, the crude mixture was filtered through celite, and the filtrate was concentrated in vacuo. The residue was purified by column chromatography on silica gel using EtOAc/MeOH (97/3) as the eluent giving the pure product as white solid (62% yield).

General procedure for synthesis of **L17**

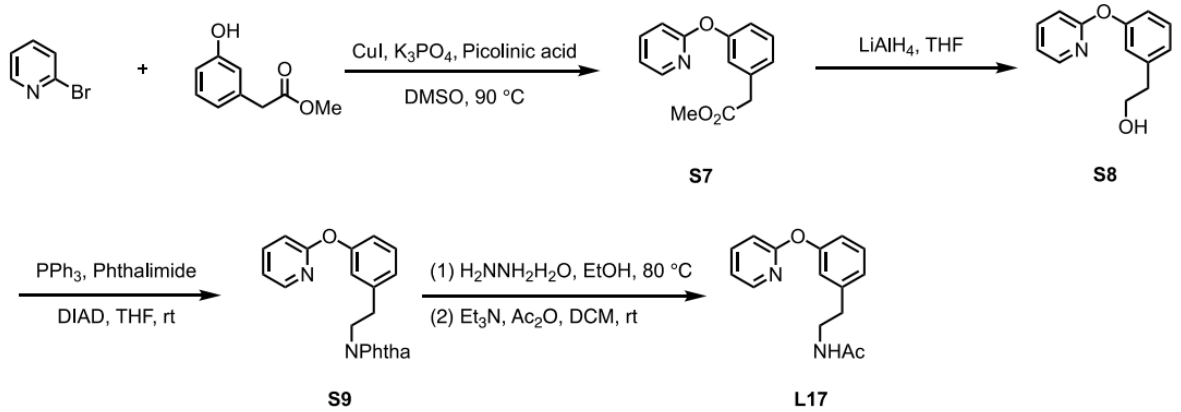

Synthesis of **S7**: A Schlenk flask containing a stir bar was charged with 2-bromopyridine (5 mmol), CuI (20 mol%), methyl 2-(3-hydroxyphenyl)acetate (1.1 equiv.), picolinic acid (1.0 equiv.) and K_3PO_4 (3.0 equiv.). The flask was evacuated and backfilled with nitrogen three times followed by adding DMSO (20 mL). The reaction mixture was stirred at 90°C for 24 h. After being allowed to cool to room temperature, the crude mixture was passed through a pad of Celite with ethyl acetate as the eluent to remove insoluble precipitate. The crude mixture was washed with water three times. The organic layer was dried with Na_2SO_4 and concentrated. The residue was purified by column chromatography on silica gel using EtOAc/hexanes (4/6) as the eluent giving the pure product as white solid (60% yield).

Synthesis of **S8**: A solution of **S7** (2.0 mmol) in THF (10 ml) was cooled to 0°C, and $LiAlH_4$ in THF (2.0 equiv.) was added slowly under nitrogen. The reaction was allowed to warm to room temperature and stirred for 6 h. Upon completion, water (5.0 ml) was added, and the crude mixture was passed through a pad of Celite with ethyl acetate as the eluent to remove insoluble precipitate. The crude mixture was dried with Na_2SO_4 and concentrated. The residue was purified by column chromatography on silica gel using EtOAc/hexanes (6/4) as the eluent giving the pure product as white solid (66% yield).

Synthesis of **S9**: To a solution of **S8** (1 mmol), PPh_3 (1 mmol, 1.0 equiv.), and Phthalimide (1 mmol, 1.0 equiv.) in THF (0.2 M), DIAD (1 mmol, 1.0 equiv.) was added dropwise at 0 °C. The reaction mixture was warmed to room temperature and stirred for 20 h. Upon completion, the crude mixture was concentrated, and phosphine oxide was removed by the column chromatography on silica gel. The resulting crude material was used in the next step without further purification.

Synthesis of **L17**: To a solution of **S9** in EtOH (10 mL) was added hydrazine monohydrate (1 mL, 20 mmol) in one portion. The reaction mixture was stirred at 80 °C for 5 h. Upon completion, the white precipitate was removed by the filtration. The filtrate was concentrated and dissolved in DCM (10 ml). Triethylamine (2 mmol, 2.0 equiv.) and acetic anhydride (1 mmol, 1.0 equiv.) were added dropwise at 0 °C. The reaction mixture was warmed to room temperature and stirred overnight. Upon completion, water was added and extracted with DCM three times. The combined organic layer was dried with anhydrous Na_2SO_4, and concentrated. The residue was purified by column chromatography on silica gel using EtOAc as the eluent giving the pure product as white solid (71% yield over three steps).

General procedure for synthesis of **L21**

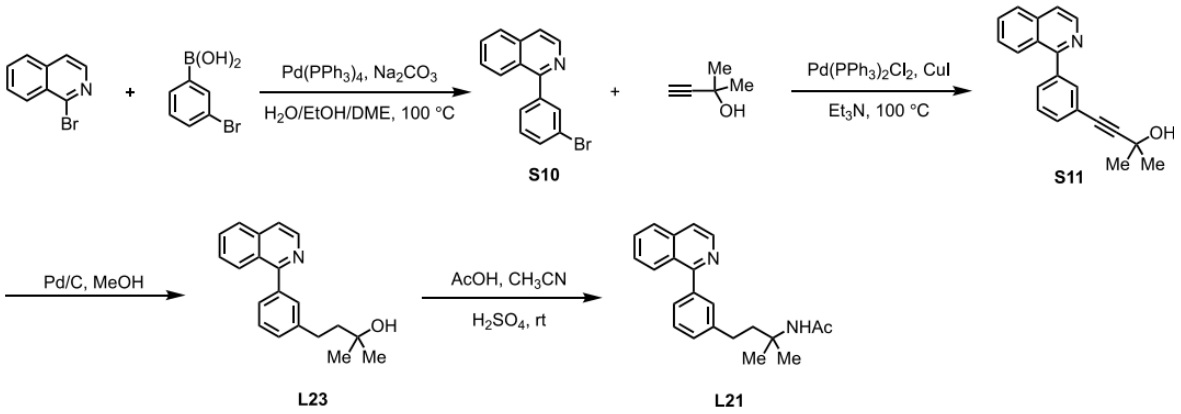

Synthesis of **S10**: A Schlenk flask containing a stir bar was charged with 1-bromoisoquinoline (5 mmol), $Pd(PPh_3)_4$ (5 mol%), (3-bromophenyl)boronic acid (6 mmol, 1.2 equiv.) and Na_2CO_3 (3.0 equiv.). The flask 9 was evacuated and backfilled with nitrogen three times followed by adding EtOH (2 mL), H_2O (1 ml) and DME (20 mL). The reaction mixture was stirred at 100°C for 24 h. After being allowed to cool to room temperature, the crude mixture was passed through a pad of Celite with ethyl acetate as the eluent to remove insoluble precipitate. The resulting solution was concentrated, and the residue was purified by column chromatography on silica gel using EtOAc/hexanes (2/8) as the eluent giving the pure product as white solid (79% yield).

Synthesis of **S11**: To a solution of **S10** (3 mmol), $Pd(PPh_3)_2Cl_2$ (5 mol%) and CuI (10 mol%) in Et_3N (0.25 M), 2-methylbut-3-yn-2-ol (6 mmol, 2.0 equiv.) was added dropwise at room temperature under nitrogen and stirred for 10 min, then the reaction was stirred at 100 °C for 24 h. After being allowed to cool to room temperature, the crude mixture was concentrated and diluted with ethyl acetate. The mixture was passed through a pad of Celite with ethyl acetate as the eluent to remove any insoluble precipitate. The resulting solution was concentrated, and the residue was

purified by column chromatography on silica gel using EtOAc/hexanes (2/8) as the eluent giving the pure product as yellow oil (80 % yield).

Synthesis of **L23**: To the solution of **S11** in MeOH (15 mL) was added Pd/C 10% (0.1 g). The reaction vial was filled with H_2 (1 atm), and the reaction mixture was stirred overnight. Upon completion, the crude mixture was filtered through celite, and the filtrate was concentrated in vacuo. The residue was purified by column chromatography on silica gel using EtOAc/hexanes (3/7) as the eluent giving the pure product as white solid (74% yield).

Synthesis of **L21**: To a solution of **L23** (2.0 mmol), AcOH (2 ml) and H_2SO_4 (1 ml) was added CH_3CN (1.0 equiv.) slowly at 0 °C. The reaction mixture was warmed to room temperature and stirred for 20 h. Upon completion, the crude mixture was poured into 100 ml ice water and neutralized with K_2CO_3. The mixture was extracted with ethyl acetate three times. The combined organic layer was dried with anhydrous Na_2SO_4, and concentrated. The residue was purified by column chromatography on silica gel using EtOAc/hexanes (4/6) as the eluent giving the pure product white solid (55% yield).

General procedure for synthesis of **L21**

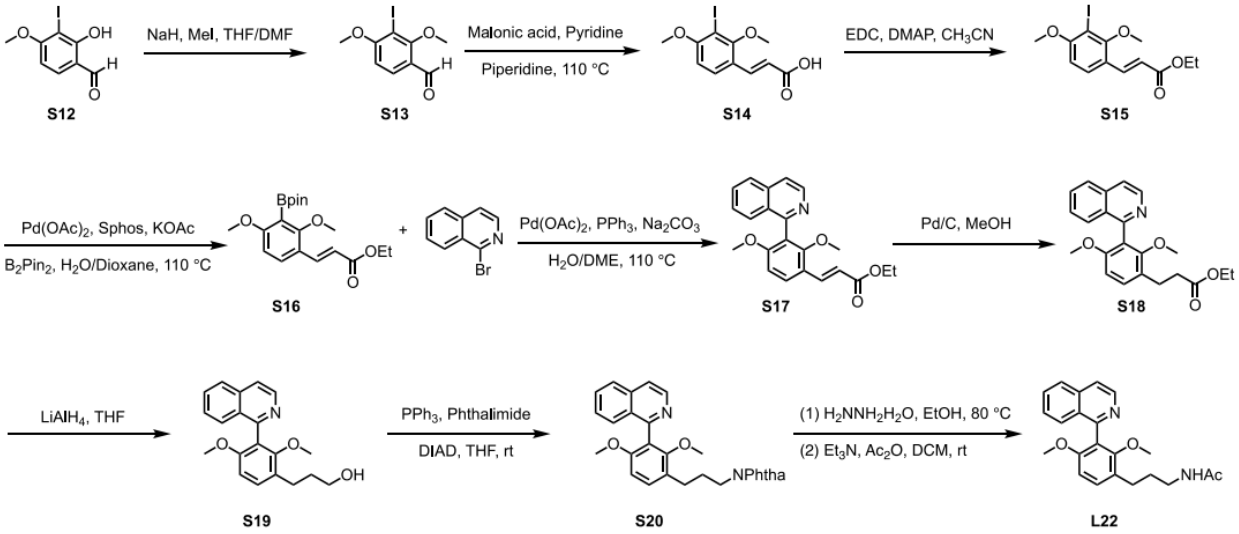

Synthesis of **S13**: To a solution of **S12** (10 mmol) in DMF (10 ml) was added NaH (3.0 equiv.) slowly at 0 °C. Then MeI (2.0 equiv.) in THF (10 ml) was added dropwise at 0 °C. The reaction mixture was warmed to room temperature and stirred for overnight. Upon completion, the crude mixture was diluted with water (10 ml) and extracted with ethyl acetate three times. The organic layer was concentrated and directly used in the next step without further purification.

Synthesis of **S14**: To a solution of **S13**, malonic acid (2.0 equiv.) in pyridine (30 ml) was added piperidine (1.0 equiv.) in one portion at 0 °C. The reaction mixture was stirred at 110 °C for overnight. Upon completion, the solvent was removed in vacuo and the residue was purified by column chromatography on silica gel using EtOAc/hexanes/AcOH (3/7/0.1) as the eluent giving the pure product as white solid (77% yield over two steps).

Synthesis of **S15**: To a solution of **S14** (6 mmol), EDC (1.0 equiv.), and DMAP (1.0 equiv.) in CH_3CN (40 ml) was added EtOH (20 equiv.) at 0 °C. The reaction mixture was stirred at 80 °C for overnight. Upon completion, the reaction mixture was filtered to remove the insoluble precipitate and concentrated in vacuo, and the residue was purified by column chromatography on

silica gel using EtOAc/hexanes (2/8) as the eluent giving the pure product as white solid (90% yield).

Synthesis of **S16**: A Schlenk flask containing a stir bar was charged with $Pd(OAc)_2$ (10 mol%), Sphos (20 mol%), **S15** (5 mmol) and B_2Pin_2 (3.0 equiv.). The flask was evacuated and backfilled with nitrogen three times followed by adding Dioxane (20 mL) and H_2O (2 ml). The reaction mixture was stirred at 110°C for 24 h. After being allowed to cool to room temperature, the crude mixture was passed through a pad of Celite with ethyl acetate as the eluent to remove insoluble precipitate. The resulting solution was concentrated, 11 and the residue was purified by column chromatography on silica gel using EtOAc/hexanes (2/8) as the eluent giving the pure product as white solid (39% yield).

Synthesis of **S17**: A Schlenk flask containing a stir bar was charged with $Pd(OAc)_2$ (10 mol%), PPh_3 (30 mol%), **S16** (2 mmol) and Na_2CO_3 (3.0 equiv.) and 1-bromoisoquinoline (2.4 mmol, 1.2 equiv.). The flask was evacuated and backfilled with nitrogen three times followed by adding DME (10 mL) and H_2O (0.2 ml). The reaction mixture was stirred at 110°C for 24 h. After being allowed to cool to room temperature, the crude mixture was passed through a pad of Celite with ethyl acetate as the eluent to remove insoluble precipitate. The resulting solution was concentrated, and the residue was purified by column chromatography on silica gel using EtOAc/hexanes (3/7) as the eluent giving the pure product as white solid (50% yield).

Synthesis of **S18**: To the solution of **S17** (1 mmol) in MeOH (15 mL) was added Pd/C 10% (0.1 g). The reaction vial was filled with H_2 (1 atm), and the reaction mixture was stirred overnight. Upon completion, the crude mixture was filtered through celite, and the filtrate was concentrated in vacuo. The resulting crude material was used in the next step without further purification.

Synthesis of **S19**: A solution of **S18** in THF (10 ml) was cooled to 0°C, and $LiAlH_4$ in THF (2.0 equiv.) was added slowly under nitrogen. The reaction was allowed to warm to room temperature and stirred for 12 h. Upon completion, water (2.0 ml) was added, and the crude mixture was passed through a pad of Celite with ethyl acetate as the eluent to remove insoluble precipitate. The crude mixture was dried with Na_2SO_4 and concentrated. The residue was purified by column chromatography on silica gel using EtOAc/hexanes (4/6) as the eluent giving the pure product as white solid (60% yield).

Synthesis of **S20**: To a solution of **S19** (0.5 mmol), PPh_3 (0.5 mmol, 1.0 equiv.), and Phthalimide (0.5 mmol, 1.0 equiv.) in THF (0.1 M), DIAD (0.5 mmol, 1.0 equiv.) was added dropwise at 0 °C. The reaction mixture was warmed to room temperature and stirred for 20 h. Upon completion, the crude mixture was concentrated, and phosphine oxide was removed by the column chromatography on silica gel. The resulting crude material was used in the next step without further purification.

Synthesis of **L22**: To a solution of **S20** in EtOH (10 mL) was added hydrazine monohydrate (0.5 mL, 10 mmol) in one portion. The reaction mixture was stirred at 80 °C for 5 h. Upon completion, the white precipitate was removed by the filtration. The filtrate was concentrated and dissolved in DCM (10 ml). Triethylamine (2.0 equiv.) and acetic anhydride (1.0 equiv.) were added dropwise at 0 °C. The reaction mixture was warmed to room temperature and stirred overnight. Upon completion, water was added and extracted with DCM three times. The combined organic layer was dried with anhydrous Na_2SO_4, and concentrated. The residue was purified by column chromatography on silica gel using EtOAc/hexanes (4/6) as the eluent giving the pure product as white solid (45% yield over three steps).

General procedure for synthesis of **L18'**

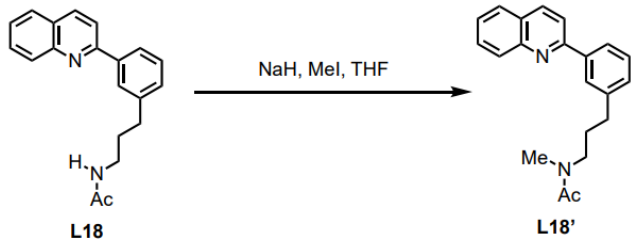

Synthesis of **L18'**: To a solution of **L18** (0.2 mmol) in THF (5 mL) was added NaH (1.0 mmol, 5.0 equiv.) in one portion. The reaction mixture was stirred at rt for 10 mins under nitrogen. MeI (1.0 mmol, 5.0 equiv.) in THF (1.0 ml) was added. The reaction was stirred at room temperature for 3 days. Upon completion, water (2.0 ml) was added and extracted with EA three times. The combined organic layer was dried with anhydrous Na_2SO_4, and concentrated. The residue was purified by column chromatography on silica gel using EtOAc/hexanes (8/2) as the eluent giving the pure product as white solid (90 % yield).

Ligand Complexation Studies

Synthesis of **$Pd(OAc)_2(L20)_2$**

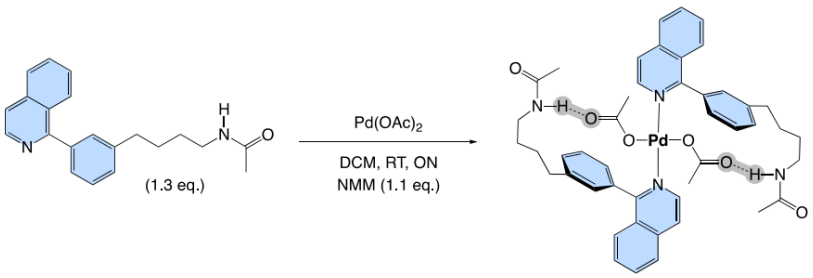

In a round-bottom Schlenk flask, $Pd(OAc)_2$ (1 eq.; 18.6 mg; 0.083 mmol), **L20** (1.3 eq. 34.9 mg; 0.110 mmol), and N-methylmorpholine (1.10 eq.; 10 µL; 0.091 mmol) were dissolved in 10 mL degassed DCM with stirring. A steady stream of argon was provided for the first 10 minutes of reaction and it was allowed to stir overnight at room temperature. The volatiles were removed

and the resulting solid was recrystallized in a culture tube by slow evaporation from a saturated solution of chloroform and ether (~1:4) with one drop of benzene to afford orange spiky crystals which were isolated in 21 mgs; 45% yield respectively to **L20**.

Synthesis of **$Pd(OAc)_2(L21)_2$**

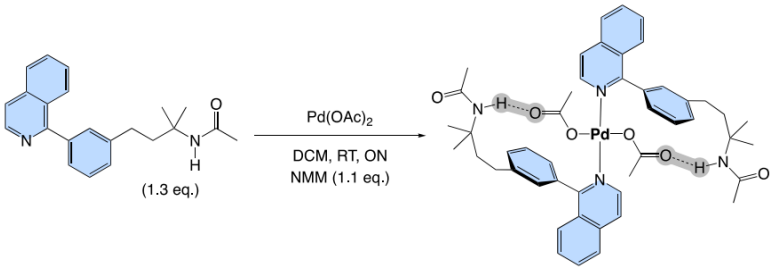

In a round-bottom Schlenk flask, $Pd(OAc)_2$ (1 eq.; 25 mg; 0.111 mmol), **L21** (1.1 eq.; 40.7 mg; 0.122 mmol) and N-methylmorpholine (1.1 eq.; 13.4 µL; 0.122 mmol) were dissolved in 5 mL degassed DCM with stirring. A steady stream of argon was provided for the first 10 minutes of reaction and it was allowed to stir overnight at room temperature. The volatiles were removed and the resulting solid was analyzed by NMR spectroscopy (in CD_2Cl_2) which showed a complex mixture. Filtration of the NMR tube content on a short plug of neutral alumina and recrystallization in a culture tube by slow vapor diffusion in hexane (~1:5) afforded the title compound as light orange crystals which were isolated in 13 mgs; 24% yield respectively to **L21**.

Synthesis of **Pd(OAc)$_2$(L23)$_2$**

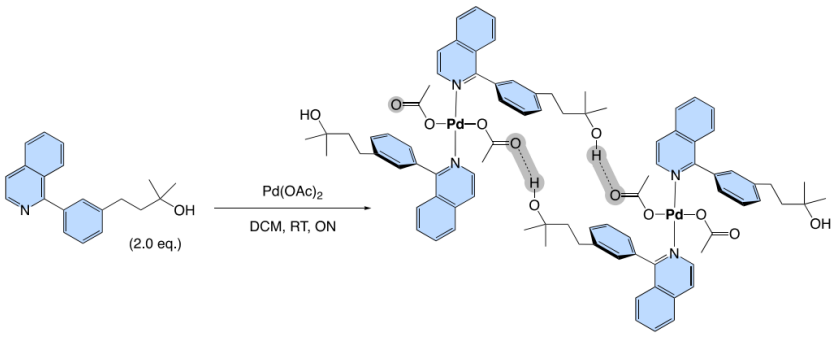

In a round-bottom Schlenk flask, $Pd(OAc)_2$ (1 eq.; 19.3 mg; 0.086 mmol) and **L23** (2 eq.; 50.0 mg; 0.172 mmol) were dissolved in 10 mL degassed DCM with stirring. A steady stream of argon was provided for the first 10 minutes of reaction and it was allowed to stir overnight at room temperature. The volatiles were removed and the resulting solid was analyzed by NMR spectroscopy (in CD_2Cl_2) which showed a complex mixture. Gratifyingly, recrystallization in a culture tube by slow evaporation from a saturated solution of DCM, layered with hexane (~1:4) afforded the title compound as light-yellow crystals which were isolated in 29 mgs; 71% yield respectively to **L23**.

4.5.3 X-ray Crystallographic Data

The X-Ray structures were collected on a Bruker diffractometer fitted with Photon 3 detector using Mo-Kα radiation (λ = 0.71073 Å). A crystal was selected under Paratone oil, mounted on nylon loops then immediately placed in a cold stream of N_2 at 100K. The space group was determined from systematic absences. The structure was solved by intrinsic phasing method using ShelXT software, in Olex1.2 environment. All non-hydrogen atoms were refined anisotropically, all CH hydrogens were placed in calculated positions with isotropic U values 1.2 times greater than U(eq) value of corresponding non-hydrogen atom.

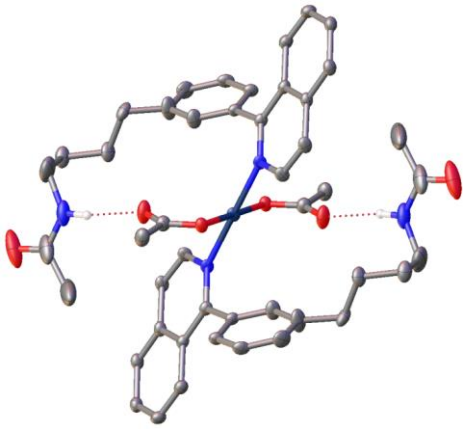

Crystal data and structure refinement for **Pd(OAc)$_2$(L20)$_2$** (CCDC 2261815)

Identification code	**Pd(OAc)$_2$(L20)$_2$**
Empirical formula	C46 H50 N4 O6 Pd
Formula weight	861.30
Temperature/K	100.00
Crystal system	triclinic
Space group	P-1
a/Å	9.6354(14)
b/Å	10.4770(15)
c/Å	12.2479(18)
α/°	104.711(6)
β/°	107.060(5)
γ/°	109.698(4)
Volume/Å^3	1023.8(3)
Z	1
ρcalcg/cm3	1.397

μ/mm^{-1}	0.507
F(000)	448.0
	MoKα (λ = 0.71073)
Radiation	3.782 to 53.526
2Θ range for data collection/°	-11 ≤ h ≤ 11, -12 ≤ k ≤ 12, -14 ≤ l ≤
Index ranges	14
Reflections collected	23638
Independent reflections	3819 [R_{int} = 0.0694, R_{σ} = 0.0452]
Data/restraints/parameters	3819/0/289
Goodness-of-fit on F^2	1.076
Final R indexes [I>=2σ (I)]	R_1 = 0.0552, wR_2 = 0.1411
Final R indexes [all data]	R_1 = 0.0616, wR_2 = 0.1465
Largest diff. peak/hole / e $Å^{-3}$	2.41/-0.84

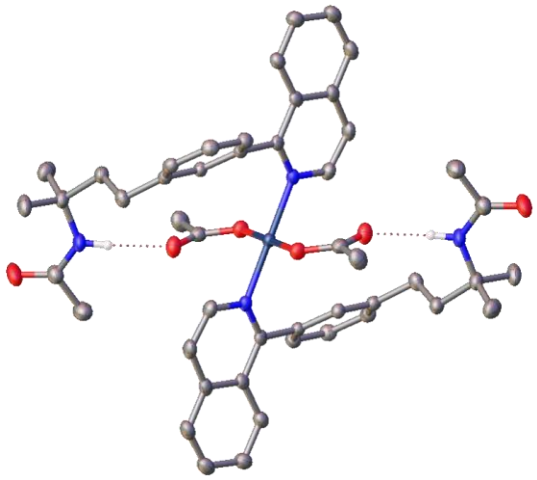

Crystal data and structure refinement for **Pd(OAc)$_2$(L21)$_2$** (CCDC 2261816)

Identification code	**Pd(OAc)$_2$(L21)$_2$**
Empirical formula	C48 H54 N4 O6 Pd
Formula weight	889.35
Temperature/K	100.00
Crystal system	monoclinic
Space group	$P2_1/c$
a/Å	13.7490(16)
b/Å	15.041(3)
c/Å	10.8286(14)
α/°	90
β/°	104.398(9)
γ/°	90
Volume/Å^3	2169.0(6)
Z	2

ρcalcg/cm3	1.362
μ/mm^{-1}	0.481
F(000)	928.0
Crystal size/mm^3	0.6 × 0.4 × 0.1
	MoKα (λ = 0.71073)
Radiation	4.086 to 52.854
2Θ range for data collection/°	-17 ≤ h ≤ 17, -18 ≤ k ≤ 18, -13 ≤ l ≤
Index ranges	13
Reflections collected	64740
Independent reflections	4448 [R_{int} = 0.0580, $R_σ$ = 0.0215]
Data/restraints/parameters	4448/1/769
Goodness-of-fit on F^2	1.084
Final R indexes [I>=2σ (I)]	R_1 = 0.0281, wR_2 = 0.0684
Final R indexes [all data]	R_1 = 0.0373, wR_2 = 0.0740
Largest diff. peak/hole / e Å^{-3}	0.53/-0.32

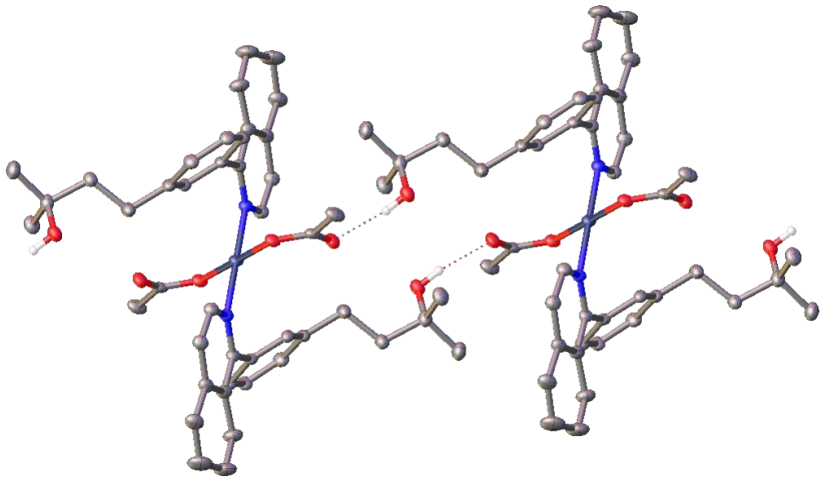

Crystal data and structure refinement for **Pd(OAc)$_2$(L23)$_2$** (CCDC 2270324)

Identification code	**Pd(OAc)$_2$(L23)$_2$**
Empirical formula	C44 H48 N2 O6 Pd
Formula weight	807.24
Temperature/K	100.00
Crystal system	monoclinic
Space group	$P2_1/c$
a/Å	10.3262(6))
b/Å	11.7906(6)
c/Å	21.1380(11)
α/°	90
β/°	101.880(2)
γ/°	90
Volume/Å^3	2518.5(2)
Z	2

ρcalcg/cm3	1.064
μ/mm^{-1}	0.407
F(000)	840.0
Crystal size/mm^3	0.2 × 0.18 × 0.075
	MoKα (λ = 0.71073)
Radiation	5.31 to 51.362
2Θ range for data collection/°	-12 ≤ h ≤ 12, -14 ≤ k ≤ 14, -25 ≤ l ≤
Index ranges	25
Reflections collected	54796
Independent reflections	4771 [R_{int} = 0.0517, $R_σ$ = 0.0221]
Data/restraints/parameters	4771/0/245
Goodness-of-fit on F^2	1.069
Final R indexes [I>=2σ (I)]	R_1 = 0.0298, wR_2 = 0.0832
Final R indexes [all data]	R_1 = 0.0362, wR_2 = 0.0875
Largest diff. peak/hole / e $Å^{-3}$	0.41/-0.49

REFERENCES

[1] Lewis, G. N. The Atom and the Molecule. *J. Am. Chem. Soc.* **1916**, *38* (4), 762-785.

[2] Langmuir, I. The Arrangement of Electrons in Atoms and Molecules. *J. Am. Chem. Soc.* **1919**, *41* (6), 868-934.

[3] Gomberg, M. An Instance of Trivalent Carbon: Triphenylmethyl. *J. Am. Chem. Soc.* **1900**, *20*, 757–771. https://doi.org/10.1021/ja02049a006.

[4] Igau, A.; Grützmacher, H.; Baceiredo, A.; Bertrand, G. Analogous α, α′-Bis-Carbenoid, Triply Bonded Species: Synthesis of a Stable λ^3-Phosphinocarbene-λ^5-Phosphaacetylene. *J. Am. Chem. Soc.* **1988**, *110*, 6463– 6466. https://doi.org/10.1021/ja00227a028

[5] Arduengo, A. J., III; Harlow, R. L.; Kline, M. A stable crystalline carbene. *J. Am. Chem. Soc.* **1991**, ***113***(1), 361-363.

[6] Scholl, M., Ding, S., Lee, C., Grubbs, R. H. Synthesis and Activity of a New Generation of Ruthenium-Based Olefin Metathesis Catalysts Coordinated with 1,3-Dimesityl-4,5-dihydroimidazol-2-ylidene Ligands. *Org. Lett.* **1999**, *1*, 6, 953-956.

[7] Herrmann, W. A.; Schwarz, J.; Gardiner, M. G. High-Yield Syntheses of Sterically Demanding Bis(N-heterocyclic carbene) Complexes of Palladium. *Organometallics* **1999**, *18*, 20, 4082-4089.

[8] Fischer, C., Smith, S., Powell, D., Fu, G. Umpolung of Michael Acceptors Catalyzed by *N*-Heterocyclic Carbenes. *J. Am. Chem. Soc.* **2006**, *128*(5) 1472-1473.

[9] Ryan, S., Candish, L., Lupton, D. *N*-Heterocyclic Carbene-Catalyzed Generation of α,β-Unsaturated Acyl Imidazoliums: Synthesis of Dihydropyranones by their Reaction with Enolates. *J. Am. Chem. Soc.* **2009**, *131*(40), 14176–14177

[10] Liu, W.; Vianna, A.; Zhang, Z.; Huang, S.; Huang, L.; Melaimi, M.; Bertrand, G.; Yan, X. Mesoionic carbene-Breslow intermediates s super electron donors: Application to the metal-free arylacylation of alkenes. *Chem. Cat.* ***2021,*** 1, 1-11.

[11] Bourissou, D.; Guerret, O.; Gabbai, F. P.; Bertrand, G. Stable Carbenes. *Chem. Rev.* **2000**, *100*(1), 39-91.

[12] Arduengo III, A. J.; Harlow, R. L.; Kline, M. A Stable Crystalline Carbene. *J. Am. Chem. Soc.* **1991**, *113*(1), 361–363.

[13] Huynh, H. V. Electronic Properties of N-Heterocyclic Carbenes and Their Experimental Determination. *Chem. Rev.* **2018,** ***118***(19), 9457-9492.

[14] Tolman, C. A. Electron Donor-Acceptor Properties of Phosphorus Ligands. Substituent Additivity. *J. Am. Chem. Soc.* **1970**, *92*(10), 2953–2956.

[15] Back, O.; Henry-Ellinger, M.; Martin, C. D.; Martin, D.; Bertrand, G. 31P NMR Chemical Shifts of Carbene–Phosphinidene Adducts as an Indicator of the π-Accepting Properties of Carbenes. *Angew. Chem. Int. Ed.*, **2013**, **52**, 2939-2943.

[16] Vummaleti, S. V. C.; Nelson, D. J.; Poater, A.; Gómez-Suárez, A.; Cordes, D. B.; Slawin, A. M. Z.; Nolan, S. P.; Cavallo, L. What Can NMR Spectroscopy of Selenoureas and Phosphinidenes Teach Us about the π-Accepting Abilities of N-Heterocyclic Carbenes? Chem. Sci. **2015**, *6*(3), 1895–1904.

[17] Liske, A.; Verlinden, K.; Buhl, H.; Schaper, K.; Ganter, C. Determining the π-Acceptor Properties of N-Heterocyclic Carbenes by Measuring the 77Se NMR Chemical Shifts of Their Selenium Adducts. *Organometallics*, **2013**, ***32***(19), 5269-5272.

[18] Hillier, A. C.; Sommer, W. J.; Yong, B. S.; Petersen, J. L.; Cavallo, L.; Nolan, S. P. A Combined Experimental and Theoretical Study Examining the Binding of N-Heterocyclic Carbenes (NHC) to the Cp*RuCl (Cp* = H5-C5Me5) Moiety: Insight into Stereoelectronic Differences between Unsaturated and Saturated NHC Ligands. *Organometallics* **2003**, *22*(21), 4322–4326.

[19] Clavier, H.; Nolan, S. P. Percent Buried Volume for Phosphine and N-Heterocyclic Carbene Ligands: Steric Properties in Organometallic Chemistry. *Chem. Commun*. **2010**, *46*(6), 841–861.

[20] Poater, A.; Cosenza, B.; Correa, A.; Giudice, S.; Ragone, F.; Scarano, V.; Cavallo, L. SambVca: A Web Application for the Calculation of the Buried Volume of N-Heterocyclic Carbene Ligands. *Eur. J. Inorg. Chem*. **2009**, *2009*(13), 1759–1766.

[21] Falivene, L.; Credendino, R.; Poater, A.; Petta, A.; Serra, L.; Oliva, R.; Scarano, V.; Cavallo, L. SambVca2. A Web Tool for Analyzing Catalytic Pockets with Topographic Steric Maps. *Organometallics* **2016**, *35*(13), 2286–2293.

[22] Gómez-Suárez, A.; Nelson, D. J.; Nolan, S. P. Quantifying and Understanding the Steric Properties of N-Heterocyclic Carbenes. *Chem. Commun*. **2017**, *53*(18), 2650–2660.

[23] Díez-González, S.; Marion, N.; Nolan, S. P. N-Heterocyclic Carbenes in Late Transition Metal Catalysis. *Chem. Rev.* **2009**, *109* (8), 3612–3676.

[24] Roy, S.; Mondal, K. C.; Roesky, H. W. Cyclic Alkyl(Amino) Carbene Stabilized Complexes with Low Coordinate Metals of Enduring Nature. *Acc. Chem. Res.* **2016**, *49* (3), 357–369.

[25] Hansmann, M. M.; Melaimi, M.; Bertrand, G. Crystalline Monomeric Allenyl/Propargyl Radical. *J. Am. Chem. Soc.* **2017**, *139*(44), 15620–15623.

[26] Hansmann, M. M.; Melaimi, M.; Bertrand, G. Organic Mixed Valence Compounds Derived from Cyclic (Alkyl)(Amino)Carbenes. *J. Am. Chem. Soc.* **2018**, *140*(6), 2206–2213.

[27] Martin, C. D.; Soleilhavoup, M.; Bertrand, G. Carbene-Stabilized Main Group Radicals and Radical Ions. *Chem. Sci.* **2013**, *4* (8), 3020–3030.

[28] (a) Frey, G. D.; Lavallo, V.; Donnadieu, B.; Schoeller W. W.; Bertrand, G. Facile Splitting of Hydrogen and Ammonia by Nucleophilic Activation at a Single Carbon Center. *J. Am. Chem. Soc.* **2007**, *129*(13), 439-441. (b) Henkel, S., Sander, W. Activation of Molecular Hydrogen by a Singlet Carbene through Quantum Mechanical Tunneling. *Angew. Chem. Int. Ed.*, **2015**, ***54***, 4603-4607.

[29] Smith, C. A.; Narouz, M. R.; Lummis, P. A.; Singh, I.; Nazemi, A.; Li, C.-H.; Crudden, C. M. N-Heterocyclic Carbenes in Materials Chemistry. *Chem. Rev.* **2019**, ***119***(8), 4986-5056.

[30] Zhang, T.; Khomane, S. B.; Singh, I.; Crudden, C. M.; McBreen, P. H. Functionalization of Metal-Supported Graphene by an N-Heterocyclic Carbene. *J. Phys. Chem. C* **2022**, *126*(34), 14430-14440.

[31] Hamze, R.; Peltier, J. L.; Sylvinson, D.; Jung, M.; Cardenas, J.; Haiges, R.; Soleilhavoup, M.; Jazzar, R.; Djurovich, P. I.; Bertrand, G.; Thompson, M. E.; et al. Eliminating nonradiative decay in Cu(I) emitters: >99% quantum efficiency and microsecond lifetime. *Science* **2019, *363***(6427), 601-606.

[32] Lammertsma, K. Phosphinidenes. *Top. Curr. Chem.* **2003**, *229*, 95–119.

[33] Hinsberg, W. D., III; Dervan, P. B. Synthesis and direct spectroscopic observation of a 1,1-dialkyldiazene. Infrared and electronic spectrum of N-(2,2,6,6-tetramethylpiperidyl)nitrene. *J. Am. Chem. Soc.* **1978**, *100*(5), 1608-1610.

[34] Dielmann, F.; Back, O.; Henry-Ellinger, M.; Jerabek, P.; Frenking, G.; Bertrand, G. A Crystalline Singlet Phosphinonitrene: A Nitrogen Atom–Transfer Agent. *Science*, **2012**, *337*(6101), 1526-1528.

[35] Janssen, M.; Frederichs, T.; Olaru, M.; Lork, E.; Hupf, E.; Beckmann, J. Synthesis of a stable crystalline nitrene. *Science,* **2024**, *First Release*.

[36] Liu, L.; Ruiz, D. A.; Munz, D.; Bertrand, G. A Singlet Phosphinidene Stable at Room Temperature. *Chem*, **2016**, ***1***(1), 147-153.

[37] Dahcheh, F.; Marin, D.; Stephan, D. W.; Bertrand, G. Synthesis and Reactivity of a CAAC–Aminoborylene Adduct: A Hetero-Allene or an Organoboron Isoelectronic with Singlet Carbenes. *Angew. Chem. In. Ed.* **2014**, *53*, 13159-13163.

[38] Legare, M.; Belanger-Chabot, G.; Dewhurst, R.; Welz, E.; Krummenacher, I.; Engels, B.; Braunschweig, H. Nitrogen fixation and reduction at boron. *Science* **2018**, *359*(6378), 893-900.

[39] Kong, L.; Lu, W.; Yongxin, L.; Ganguly, R.; Kinjo, R. Formation of Boron–Main-Group Element Bonds by Reactions with a Tricoordinate Organoboron L2PhB: (L = Oxazol-2-ylidene). *Inorg. Chem.* **2017**, *56*(10), 5586-5593.

[40] Pachaly, B.; West, R. Photochemical Generation of Triphenylsilylboranediyl (C6H5)3SiB(C6H5)3SiB(C6H5)3SiB: from Organosilylboranes. *Angew. Chem. In. Ed.* **1984**, ***23***(6), 454-455.

[41] Maringgele, W.; Dielkus, S.; Herbst-Irmer, R.; Michaelsen, H.; Meller, A. Reaktion von konjugierten Doppelbindungssystemen mit Dihalogen(diorganylamino)boranen und Na/K-Legierung. *J. Organomet. Chem.*, **1994**, ***470***(1-2), 23-29.

[42] (a) Regitz, M.; Scherer, O. J. Multiple Bonds and Low Coordination in Phosphorus Chemistry (Thieme, Stuttgart, Germany, **1990**); (b) Dillon, K. B.; Mathey, F.; Nixon, J. F. Phosphorus: The Carbon Copy (Wiley, Chichester, UK, **1998**).

[43] Wang, P.; Gong, S.; Li, Y.; Mo, Y. Bond dissociation energy of N_2 measured by state-to-state resolved threshold fragment yield spectra. *J. Chem. Phys.* **2024**, *160*, 014304.

[44] (a) Scherer, O. J.; Sitzmann, H.; Wolmershäuser, G. $Cp_2Mo_2(CO)_2P_2$ as Complex Ligand. *Angew. Chem. Int. Ed. Engl*. **1984**, *23*, 968-969; (b) Grant, L. N.; Pinter, B.; Manor, B. C.; Suter, R.; Grützmacher, H.; Mindiola, D. J. A Planer Ti_2P_2 Core Assembled by Reductive Decarbonylation of PCO^- and P-P Radical Coupling. *Chem. Eur. J.* **2017**, *23*, 6272–6276. (c) Wang, S.; Sear, J. D.; Moore, C. E.; Rheingold, A. L.; Neidig, M. L.; Figueroa, J. S. Side-on coordination of diphosphorus to a mononuclear iron center. *Science* **2022**, *375*, 1393-1397; (d) Peresypkina, E.; Virovets, A.; Scheer, M. Organometallic polyphosphorus complexes as diversified building blocks in coordination chemistry. *Coord. Chem. Rev.* **2021**, *446*, 213995; (e) Cossairt, B. M.; Piro, N. A.; Cummins, C. C. Early-Transition-Metal-Mediated Activation and Transformation of White Phosphorus. *Chem. Rev.* **2010**, *110*, 4164–4177; (f) Caporali, M.; Gonsalvi, L.; Rossin, A.; Peruzzini, M. P_4 Activation by Late-Transition Metal Complexes. *Chem. Rev.* **2010**, *110*, 4178–4235.

[45] Michaelis, A.; Gimborn, H. V. Ueber das Betaïn und Cholin des Triphenylphosphins. *Ber. Dtsch. Chem. Ges.* **1894**, *27*, 272.

[46] Wittig, G.; Schöllkopf, U. Über Triphenyl-phosphin-methylene als olefinbildende Reagenzien I. *Chem. Ber.* **1954**, *87*(9), 1318-1330.

[47] Herrmann, W. A.; Elison, M.; Fischer, J.; Köcher, C.; Artus, G. R. J. Metal complexes of N-heterocyclic carbenes—a new structural principle for catalysts in homogeneous catalysis. *Angew. Chem. Int. Ed.* **1995**, *34*, 2371-2374.

[48] Díez-González, S. *N-Heterocyclic Carbenes: From Laboratory Curiosities to Efficient Synthetic Tools*; Royal Society of Chemistry: **2016**.

[49] Scholl, M.; Ding, S.; Lee, C. W.; Grubbs, R. H. Synthesis and activity of a new generation of ruthenium-based olefin metathesis catalysts coordinated with 1,3-dimesityl-4,5-dihydroimidazol-2-ylidene ligands. *Org. Lett.* **1999**, *1*, 953-956.

[50] Nakano, R.; Jazzar, R.; Bertrand, G. A crystalline monosubstituted carbene. *Nat. Chem.* **2018**, *10*, 1196-1200.

[51] Hinz, A. A Mono-Substituted Silicon(II) Cation: A Crystalline "Supersilylene". *Angew. Chem. Int. Ed.* **2020**, *59*(43), 19065-19069.

[52] Kays, D. L. Extremely bulky amide ligands in main group chemistry. *Chem. Soc. Rev.* **2016**, *45*, 1004-1018.

[53] Hamze, R.; Peltier, J. L.; Sylvinson, D.; Jung, M.; Cardenas, J.; Haiges, R.; Soleilhavoup, M.; Jazzar, R.; Djurovich, P. I.; Bertrand, G.; Thompson, M. E. Eliminating nonradiative decay in Cu(I) emitters: >99% quantum efficiency and microsecond lifetime. *Science* **2019**, *363*, 601-606.

[54] (a) Coombs, N. D.; Stasch, A.; Cowley, A.; Thompson, A. L.; Aldridge, S. Bulky aryl functionalized carbazolyl ligands: amido alternatives to the 2,6-diarylphenyl ligand class? *Dalton Trans.* **2008**, 332–337; b) Ortu, F; Moxey, G. J.; Blake, A. J.; Lewis, W; Kays, D. L. Tuning Coordination in s-Block Carbazol-9-yl Complexes. *Chem. Eur. J.* **2015**, *21*, 6949–6956.

[55] Hinz, A. Pseudo-One-Coordinate Tetrylenium Salts Bearing a Bulky Carbazolyl Substituent. *Chem. Eur. J.* **2019**, *25*(13), 3267-3271.

[56] Ramsden, E. U.S. Patent 3,354,190, 1967; *Chem. Abstr.* **1968**, *68*, 114744.

[57] Saito, T.; Nishiyama, H.; Tanahashi, H.; Kawakita, K.; Tsurugi, H.; Mashima, K. 1,4-Bis(trimethylsilyl)-1,4-diaza-2,5-cyclohexadienes as Strong Salt-Free Reductants for Generating Low-Valent Early Transition Metals with Electron-Donating Ligands. *J. Am. Chem. Soc.* **2014**, *136*(13), 5161-5170.

[58] Ohlow, M. J.; Moosmann, B. Phenothiazine: the seven lives of pharmacology's first lead structure. *Drug Discov. Today* **2011**, *16*(3-4), 119-131.

[59] Fujihara, H.; Fuke, S.; Yoshihara, M.; Maeshima, T. Electron transfer processes in the reaction of phenothiazine and 10-methylphenothiazine with 2,2′-azobisisobutyronitrile. *Chem. Lett.* **1981**, *10*(9), 1271-1272.

[60] Grigsby, W. J.; Power, P. P. Isolation and Reduction of Sterically Encumbered Arylboron Dihalides: Novel Boranediyl Insertion into C−C σ-Bonds. *J. Am. Chem. Soc.* **1996**, *118*(34), 7981-7988.

[61] Braunschweig, H.; Dewhurst, R. D.; Herbst, T.; Radacki, K. Reactivity of a Terminal Chromium Borylene Complex towards Olefins: Insertion of a Borylene into a C−H Bond. *Angew. Chem. Int. Ed.* **2008**, *47*(32), 5978-5980.

[62] Liu, S.; Légaré, M.-A.; Hofmann, A.; Dellermann, T.; Braunschweig, H. Transition-metal-carbene-like intermolecular insertion of a borylene into C–H bonds. *Chem. Commun.* **2020**, *56*, 7277-7280.

[63] Krasowska, M.; Bettinger, H. F. Reactivity of Borylenes toward Ethyne, Ethene, and Methane. *J. Am. Chem. Soc.* **2012**, *134*(41), 17094-17103.

[64] Maringgele, W.; Dielkus, S.; Herbst-Irmer, R.; Michaelsen, H.; Meller, A. Reaktion von konjugierten Doppelbindungssystemen mit Dihalogen(diorganylamino)boranen und Na/K-Legierung. *J. Organomet. Chem.*, **1994**, ***470***(1-2), 23-29.

[65] Karunakaran, C.; Karuthapandia, S. ZnO-Photocatalyzed Oxidative Transformation of Diphenylamine. Synergism by TiO_2, V_2O_5, CeO_2, and ZnS. *J. Mex. Chem. Soc.* **2015**, *59*(2), 99-104.

[66] Tewari, B. B. Nickel ferrocyanide sensitized photo-oxidation of diphenylamine. *Rev. Soc. Quím. Perú* **2005**, *71*(4), 273-277.

[67] Tewari, B. B. Copper ferrocyanide photosensitized oxidation of diphenylamine. *Rev. Bol. Quím.* **2005**, *22*(1), 39-42.

[68] Hashim, I. I.; Tzouras, N. V.; Janssens, W.; Scattolin, T.; Bourda, L.; Bhandary, S.; Van Hecke, K.; Nolan, S. P.; Cazin, C. S. J. Synthesis of Carbene-Metal-Amido (CMA) Complexes and Their Use as Precatalysts for the Activator-Free, Gold-Catalyzed Addition of Carboxylic Acids to Alkynes. *Chem. Eur. J.* **2022**, *28*(47), e202201224.

[69] (a) Regitz, M.; Scherer, O. J. Multiple Bonds and Low Coordination in Phosphorus Chemistry (Thieme, Stuttgart, Germany, **1990**); (b) Dillon, K. B.; Mathey, F.; Nixon, J. F. Phosphorus: The Carbon Copy (Wiley, Chichester, UK, **1998**).

[70] Scherer, O. J. Small Neutral Pn Molecules. *Angew. Chem. Int. Ed. Engl.* **2000**, *39*, 1029-1030.

[71] Kornath, A.; Kaufmann, A.; Torheyden, M. Raman sepectroscopic studies on matrix-isolated phosphorus molecules P_4 and P_2. *J. Chem. Phys.* **2002**, *116*, 3323-3326.

[72] (a) Scherer, O. J.; Sitzmann, H.; Wolmershäuser, G. $Cp_2Mo_2(CO)_2P_2$ as Complex Ligand. *Angew. Chem. Int. Ed. Engl*. **1984**, *23*, 968-969; (b) Grant, L. N.; Pinter, B.; Manor, B. C.; Suter, R.; Grützmacher, H.; Mindiola, D. J. A Planer Ti_2P_2 Core Assembled by Reductive Decarbonylation of PCO^- and P-P Radical Coupling. *Chem. Eur. J.* **2017**, *23*, 6272–6276. (c) Wang, S.; Sear, J. D.; Moore, C. E.; Rheingold, A. L.; Neidig, M. L.; Figueroa, J. S. Side-on coordination of diphosphorus to a mononuclear iron center. *Science* **2022**, *375*, 1393-1397; (d) Peresypkina, E.; Virovets, A.; Scheer, M. Organometallic polyphosphorus complexes as diversified building blocks

in coordination chemistry. *Coord. Chem. Rev.* **2021**, *446*, 213995; (e) Cossairt, B. M.; Piro, N. A.; Cummins, C. C. Early-Transition-Metal-Mediated Activation and Transformation of White Phosphorus. *Chem. Rev.* **2010**, *110*, 4164–4177; (f) Caporali, M.; Gonsalvi, L.; Rossin, A.; Peruzzini, M. P_4 Activation by Late-Transition Metal Complexes. *Chem. Rev.* **2010**, *110*, 4178–4235.

[73] (a) Tofan, D.; Cummins, C. C. Photochemical Incorporation of Diphosphorus Units into Organic Molecules. *Angew. Chem. Int. Ed.* **2010**, *49*, 7516-7518; (b) Piro, N. A.; Figueroa, J. S.; McKellar, J. T.; Cummins, C. C. Triple-bond reactivity of diphosphorus molecules. *Science* **2006**, *313*, 1276–1279; (c) Velian, A.; Nava, M.; Temprado, M .; Zhou, Y.; Field, R. W.; Cummins, C. C. A retro Diels-Alder route to diphosphorus chemistry: molecular precursor synthesis, kinetics of P_2 transfer to 1,3-dienes, and detection of P_2 by molecular beam mass spectrometry. *J. Am. Chem. Soc.* **2014**, *136*, 13586–13589.

[74] (a) Hierlmeier, G.; Hinz, A.; Wolf, R.; Goicoechea, J. M. Synthesis and Reactivity of Nickel-Stabilised μ2:η2,η2-P2, As2 and PAs Units. *Angew. Chem. Int. Ed.* **2018**, *57*, 431–436; (b) Hierlmeier, G.; Wolf, R. Diphosphorus Release and Heterocumulene Oligomerisation by Nickel Complexes. *Eur. J. Inorg. Chem*. **2022**, *10*, e202101057.

[75] Wang, Y.; Xie, Y.; Wei, P.; King, R. B.; Schaefer, H. F., III; Schleyer, P. v. R.; Robinson, G. H. Carbene-stabilized diphosphorus. J. Am. Chem. Soc. 2008, 130, 14970– 14971

[76] Back, O., Kuchenbeiser, G., Donnadieu, B. and Bertrand, G. (2009), Nonmetal-Mediated Fragmentation of P4: Isolation of P1 and P2 Bis(carbene) Adducts. Angewandte Chemie International Edition, 48: 5530-5533.

[77] Liu, L.; Ruiz, D. A.; Munz, D.; Bertrand, G. A Singlet Phosphinidene Stable at Room Temperature. *Chem.* **2016**, *1*, 147-153.

[78] (a) R. Appel, M. Poppe, *Angew. Chem. Int. Ed. Engl.* **1989**, *28*, 53-54; (b) Grobe, J.; Le Van, D.; Lüth, B.; Hegemann, M. *Chem. Ber*. **1990**, *123*, 2317-2320; (c) Grobe, J.; Le Van, D.; Hegemann M.; Krebs, B.; Läge, M. *Chem. Ber.* **1992**, *125*, 411-414; (d) Hahn, F. E.; Le Van, D.; Moyes, M. C.; von Fehren, T.; Fröhlich, R.; Würthwein, E.-U. *Angew. Chem. Int. Ed*. **2001**, *40*, 3144-3148; (e) Regitz, M. Phosphaalkynes: new building blocks in synthetic chemistry. *Chem. Rev.* **1990**, *90*, 191-213.

[79] Aitken, R. A. 2-Functionalized alkylidenephosphines. *Science of Synthesis*. **2005**, *22*, 565-600.

[80] Binger, P.; Stutzmann, S.; Bruckmann, J.; Kruger, C.; Grobe, J.; Van, D.; Pohlmeyer, T. Novel Tetraphosphabarrelene and -semibullvalene Derivatives by Reactions of 2,4,6-Tri-tert-butyl-1,3,5-triphosphabenzene with Phosphaalkynes. *Eur. J. Inorg. Chem.* **1998**, 2071-2074.

[81] Grobe, J.; Van, D.; Immel, F.; Krebs, B.; Lage, M. Reactive E=C [p-p]π Systems. 1-Aza-3,4-diphospholenes by [3 + 2] Cycloaddition of 2-(Diisopropylamino)phosphaethyne to Diazo Derivatives R1R2C=N2. *Chem. Ber.* **1996**, *129*, 1271-1274.

[82] a) J. M. Goicoechea, H. Grutzmacher, *Angew. Chem. Int. Ed.* **2018**, *57*, 16968-16994; b) F. F. Puschmann, D. Stein, D. Heift, C. Hendriksen, Z. A. Gal, H. F. Grutzmacher, H. Grutzmacher, *Angew. Chem. Int. Ed.* **2011**, *50*, 8420-8423.

[83] Schmidpeter, A.; Willhalm, A. ^{1}H-1,2,4-Diazaphosphole über 2-Phosphaallylchloride. *Angew. Chem. Int. Ed.* **1984**, *96*(11), 901-902.

[84] (a) Becker, G.; Heckmann, G.; Hübler, K.; Schwarz, W. Über die Oxydation des Lithoxy-methylidinphosphans P=C–O–Li mit Schwefeldioxid und Iod. *Angew. Chem. Int. Ed.* **1995**, *621*(1), 34-46. (b) Alidori, S.; Heift, D.; Santiso-Quinones, G.; Benkő, Z.; Grützmacher, H.; Caporali, M.; Gonsalvi, L.; Rossin, A.; Peruzzini, M. Synthesis and Characterization of Terminal [Re(XCO)(CO)$_2$(triphos)] (X=N, P): Isocyanate versus Phosphaethynolate Complexes. *Chem. Eur. J.* **2012**, *18*(46), 14805-14811.

[85] Back, O.; Kuchenbeiser, G.; Donnadieu, B.; Bertrand, G. Nonmetal-Mediated Fragmentation of P_4: Isolation of P_1 and P_2 Bis(carbene) Adducts. *Angew. Chem. Int. Ed.* **2009**, *48*, 5530-5533

[86] (a) Szkop, K. M.; Jupp, A. R.; Razumkov, H.; Xu, M.; Stephan, D. W. Diphospha-Ureas from the Phosphaketene Ph_3GePCO. *Chem. Eur. J.* **2019**, *25*, 10084-10087; (b) Appel, R.; Paulen, W. $(tBuP)_4CO$, das erste cyclische Phosphaharnstoff-Derivat-Darstellung und Reaktionsabläufe im System *tert*-Butylbis(trimetehylsilyl)phosphan/Phosgen. *Chem. Ber.* **1983**, *116*, 109-113; (c) Plack, V.; Goerlich, J. R.; Schmutzler, R. Unusual Stability despite a P-bonded Proton: Phospha and Diphospha Ureas with the TrtP(H)-Moiety. *Z. Anorg. Allg. Chem.* **1999**, *625*, 919-922

[87] Wang, Y.; Xie, Y.; Wei, P.; King, R. B.; Schaefer, H. F.; Schleyer, P. v. R.; Robinson, G. H. Carbene-stabilized diphosphorus. *J. Am. Chem. Soc.* **2008**, *130*, 14970– 14971.

[88] Back, O.; Kuchenbeiser, G.; Donnadieu, B.; Bertrand, G. Nonmetal-Mediated Fragmentation of P_4: Isolation of P_1 and P_2 Bis(carbene) Adducts. *Angew. Chem. Int. Ed.* **2009**, *48*, 5530-5533.

[89] Melville, H. W.; Gray, S. C. The polymerization of phosphorus. *Trans. Faraday Soc*. **1936**, *32*, 271-285.

[90] (a) Tofan, D.; Cummins, C. C. Photochemical Incorporation of Diphosphorus Units into Organic Molecules. *Angew. Chem. Int. Ed.* **2010**, *49*, 7516-7518; (b) Hierlmeier, G.; Hinz, A.; Wolf, R.; Goicoechea, J. M. Synthesis and Reactivity of Nickel-Stabilised μ2:η2,η2-P2, As2 and PAs Units. *Angew. Chem. Int. Ed.* **2018**, *57*, 431–436

[91] (a) Velian, A.; Cummins, C. C. Facile Synthesis of Dibenzo-7λ^3-phosphanorbornadiene Derivatives Using Magnesium Anthracene. *J. Am. Chem. Soc.* **2012**, *134*, 13978-13981; (b) Marinetti, A.; Mathey, F.; Fischer, J.; Mitschler, A. Generation and Trapping of Terminal Phosphinidene Complexes. Synthesis and X-ray Crystal Structure of Stable Phosphirene Complexes. *J. Am. Chem. Soc.* **1982**, *104*, 4484-4485.

[92] (a) Hirano, K.; Miura, M. Recent advances in diphosphination of alkynes and alkenes. *Tetrahedron Lett.* **2017**, *58*, 4317-4322; (b) Burg, A. B. Tetramethylbiphosphine: Synthesis,

Thermal Condensation, Ethylene Addition, Borine Adducts and Conversion to Phosphinoborine Polymers. *J. Am. Chem. Soc.* **1961**, *83*, 2226-2231; (c) Sato, Y.; Kawaguchi, S.-i.; Nomoto, A.; Ogawa, A. Synthesis of Bis(phosphanyl)alkane Monosulfides by the Addition of Diphosphane Monosulfides to Alkenes under Light. *Chem. Eur. J.* **2019**, *25*, 2295-2302; (d) Morse, K. W.; Morse, J. G. Free radical reactions of tetrafluorodiphosphine. Preparation of 1,2-bis(difluorophosphino)ethane. *J. Am. Chem. Soc.* **1973**, *95*, 8469-8470; (e) Hajdók, I.; Lissner, F.; Nieger, M.; Strobel, S.; Gudat, D. Diphosphination of Electron Poor Alkenes. *Organometallics* **2009**, *28*, 1644-1651.

[93] M. M. Hansmann, G. Bertrand, *J. Am. Chem. Soc.* **2016**, *138*, 15885-15888

[94] Wang, Y.; Szilvási, T.; Yao, S.; Driess, M. A bis(silylene)-stabilized diphosphorus compound and its reactivity as a monophosphorus anion transfer reagent. *Nat. Chem.* **2020**, *12*, 801-807.

[95] Wang, Y.; Xie, Y.; Wei, P.; Schaefer, H. F., III; von Schleyer, P. R.; Robinson, G. H. Splitting Molecular Oxygen en Route to a Stable Molecule Containing Diphosphorus Tetroxide. *J. Am. Chem. Soc.* **2013**, *135*(51), 19139-19142.

[96] Back, O.; Donnadieu, B.; Parameswaran, P.; Frenking, G.; Bertrand, G. Isolation of crystalline carbene-stabilized P_2-radical cations and P_2-dications. *Nat. Chem.* **2010**, *2*, 369-373.

[97] Quin, L. D.; Szewczyk, J. The Formation of P(III) Products From Phosphinamides with Silicon Hydrides. Phosphorus and Sulfur. 1984, 21, 161-170.

[98] (a) He, J.; Wasa, M.; Chan, K. S. L.; Shao, Q.; Yu, J.-Q. Palladium-catalyzed transformations of alkyl C–H bonds. *Chem. Rev.* **2017**, *117*, 8754–8786; (b) Lyons, T. W.; Sanford, M. S. Palladium-catalyzed ligand-directed C–H functionalization reactions. *Chem. Rev.* **2010**, *110*, 1147–1169; (c) Dalton, T.; Faber, T.; Glorius, F. C–H activation: toward sustainability and applications. *ACS Cent. Sci.* **2021**, *7*, 245–261; (d) Daugulis, O.; Roane, J.; Tran, L. D. Bidentate, Monoanionic auxiliary-directed functionalization of carbon–hydrogen bonds. *Acc. Chem. Res.* **2015**, *48*, 1053–1064; (e) Rej, S.; Ano, Y.; Chatani, N. Bidentate directing groups: an efficient tool in C–H bond functionalization chemistry for the expedient construction of C–C bonds. *Chem. Rev.* **2020**, *120*, 1788–1887.

[99] (a) Giri, R.; Maugel, N.; Li, J.-J.; Wang, D.-H.; Breazzano, S. P.; Saunders, L. B.; Yu, J.-Q. Palladium-catalyzed methylation and arylation of sp^2 and sp^3 C–H bonds in simple carboxylic acids. *J. Am. Chem. Soc.* **2007**, *129*, 3510–3511; (b) Zhu, Y.; Chen, X.; Yuan, C.; Li, G.; Zhang, J.; Zhao, Y. Pd-catalyzed ligand-enabled carboxylate-directed highly regioselective arylation of aliphatic acids. *Nat. Commun.* **2017**, *8*, 14904–14911; (c) Ghiringhelli, F.; Uttry, A.; Ghosh, K. K.; van Gemmeren, M. Direct β- and γ-C(sp^3)–H alkynylation of free carboxylic acids. *Angew. Chem., Int. Ed.* **2020**, *59*, 23127– 23131; (d) Dolui, P.; Das, J.; Chandrashekar, H. B.; Anjana, S. S.; Maiti, D. Ligand-enabled Pd^{II}–catalyzed iterative γ–C(sp^3)–H arylation of free aliphatic acid. *Angew. Chem., Int. Ed.* **2019**, *58*, 13773–13777; (e) Zhuang, Z.; Yu, C.-B.; Chen, G.; Wu, Q.-F.; Hsiao, Y.; Joe, C. L.; Qiao, J. X.; Poss, M. A.; Yu, J.-Q. Ligand-enabled β-C(sp^3)–H olefination of free carboxylic acids. *J. Am. Chem. Soc.* **2018**, *140*, 10363–10367; (f) Zhuang,

Z.; Yu, J.-Q. Lactonization as a general route to β-C(sp^3)–H functionalization. *Nature* **2020**, *577*, 656–659, (g) Zhuang, Z.; Herron, A. N.; Fan, Z. L.; Yu, J.-Q. Ligand-enabled monoselective *beta*–C(sp^3)–H acyloxylation of free carboxylic acids using a practical oxidant. *J. Am. Chem. Soc.* **2020**, *142*, 6769–6776; (h) Ghosh, K. K.; Uttry, A.; Koldemir, A.; Ong, M.; van Gemmeren, M. Direct β-C(sp^3)–H acetoxylation of aliphatic carboxylic acids. *Org. Lett.* **2019**, *21*, 7154–7157; (i) Novak, P.; Correa, A.; Gallardo-Donaire, J.; Martin, R. Synergistic palladium–catalyzed C(sp^3)–H activation/C(sp^3)–O bond formation: a direct, step–economical route to benzolactones. *Angew. Chem., Int. Ed.* **2011**, *50*, 12236–12239.

[100] (a) Giri, R.; Chen, X.; Yu, J.-Q. Palladium-catalyzed asymmetric iodination of unactivated C–H bonds under mild conditions. *Angew. Chem., Int. Ed.* **2005**, *44*, 2112–2115; (b) Rit, R. K.; Yadav, M.; Ghosh, R. K.; Shankar, M.; Sahoo, A. K. Sulfoximine assisted Pd(II)-catalyzed bromination and chlorination of primary β-C(sp^3)–H bond. *Org. Lett.* **2014**, *16*, 5258–5261; (c) Yang, X.; Sun, Y.; Sun, T.-Y.; Rao, Y. Auxiliary-assisted palladium-catalyzed halogenation of unactivated C(sp^3)–H bonds at room temperature. *Chem. Commun.* **2016**, *52*, 6423–6426; (d) Zhu, R.-Y.; Saint-Denis, T. G.; Shao, Y.; He, J.; Sieber, J. D.; Senanayake, C. H.; Yu, J.-Q. Ligand-enabled Pd(II)-catalyzed bromination and iodination of C(sp^3)–H bonds. *J. Am. Chem. Soc.* **2017**, *139*, 5724–5727; (e) Wasa, M.; Yu, J.-Q. Synthesis of *β-, γ-*, and δ-lactams via Pd(II)-catalyzed C–H activation reactions. *J. Am. Chem. Soc.* **2008**, *130*, 14058–14059.

[101] (a) Kambe, N.; Iwasaki, T.; Terao, J. Pd-catalyzed cross-coupling reactions of alkyl halides. *Chem. Soc. Rev.* **2011**, *40*, 4937–4947; (b) Saikia, I.; Borah, A. J.; Phukan, P. Use of bromine and bromo-organic compounds in organic synthesis. *Chem. Rev.* **2016**, *116*, 6837–7042.

[102] (a) Vaillancourt, F. H.; Yeh, E.; Vosburg, D. A.; Garneau-Tsodikova, S.; Walsh, C. T. Nature's inventory of halogenation catalysts: oxidative strategies predominate. *Chem. Rev.* **2006**, *106*, 3364–3378; (b) Romero, E.; Jones, B. S.; Hogg, B. N.; Casamajo, A. R.; Hayes, M. A.; Flitsch, S. L.; Turner, N. J.; Schnepel, C. Enzymatic late-stage modifications: better late than never. *Angew. Chem., Int. Ed.* **2021**, *60*, 16824– 16855.

[103] (a) Shao, Q.; Wu, K.; Zhuang, Z.; Qian, S. Q.; Yu, J.-Q. From $Pd(OAc)_2$ to chiral catalysts: the discovery and development of bifunctional mono-N-protected amino acid ligands for diverse C–H functionalization reactions. *Acc. Chem. Res.* **2020**, *53*, 833–851; (b) Wang, Z.; Hu, L.; Chekshin, N.; Zhuang, Z.; Qian, S.; Qiao, J. X.; Yu, J.-Q. Ligand-controlled divergent dehydrogenative reactions of carboxylic acids via C–H activation. *Science* **2021**, *374*, 1281–1285; (c) Meng, G.; Hu, L.; Tomanik, M.; Yu, J.-Q. β- and γ-C(sp^3)–H heteroarylation of free carboxylic acids: a modular synthetic platform for diverse quaternary carbon centers. *Angew. Chem., Int. Ed.* **2023**, *62*, e202214459; (d) Hu, L.; Meng, G.; Yu, J.-Q. Ligand-enabled Pd(II)-catalyzed β-methylene C(sp^3)–H arylation of free aliphatic acids. *J. Am. Chem. Soc.* **2022**, *144*, 20550–20553; (e) Uttry, A.; Mal, S.; van Gemmeren, M. Late-stage β-C(sp^3)–H deuteration of carboxylic acids. *J. Am. Chem. Soc.* **2021**, *143*, 10895–10901.

[104] The succinimide formed in situ can work as ligand to coordinate with Pd(II), which will outcompete the binding of the carboxylic acid substrates. See: Fairlamb, I. J. S.; Kapdi, A. R.; Lee, A. F.; Sánchez, G.; López, G.; Serrano, J. L.; García, L.; Pérez, J.; Pérez, E. Mono- and binuclear

cyclometallated palladium(ii) complexes containing bridging (N,O-) and terminal (N-) imidate ligands: Air stable, thermally robust and recyclable catalysts for cross-coupling processes. *Dalton Trans* **2004**, 3970–3981.

[105] (a) Whitehouse, C. J. C.; Bell, S. G.; Wong, L.-L. $P450_{BM3}$ (CYP102A1): connecting the dots. *Chem. Soc. Rev.* **2012**, *41*, 1218–1260; (b) Li, H.; Poulos, T. L. The structure of the cytochrome p450BM-3 haem domain complexed with the fatty acid substrate, palmitoleic acid. *Nat. Struct. Biol.* **1997**, *4*, 140–146; (c) Haines, D. C.; Tomchick, D. R.; Machius, M.; Peterson, J. A. Pivotal role of water in the mechanism of P450BM-3. *Biochemistry* **2001**, *40*, 13456–13465; (d) Zilly, F. E.; Acevedo, J. P.; Augustyniak, W.; Deege, A.; Häusig, U. W.; Reetz, M. T. Tuning a P450 enzyme for methane oxidation. *Angew. Chem., Int. Ed.* **2011**, *50*, 2720–2724.

[106] (a) Reek, J. N. H.; Bruin, B. D.; Pullen, S.; Mooibroek, T. J.; Kluwer, A. M.; Caumes, X. Transition metal catalysis controlled by hydrogen bonding in the second coordination sphere. *Chem. Rev.* **2022**, *122*, 12308–12369; (b) Davis, H. J.; Phipps, R. J. Harnessing non-covalent interactions to exert control over regioselectivity and site-selectivity in catalytic reactions. *Chem. Sci.* **2017**, *8*, 864–877; (c) Knowles, R. R.; Jacobsen, E. N. Attractive noncovalent interactions in asymmetric catalysis: Links between enzymes and small molecule catalysts. *Proc. Natal. Acad. Sci.* **2010**, *107*, 20678– 20685; (d) Neel, A. J.; Hilton, M. J.; Sigman, M. S.; Toste, F. D. Exploiting non-covalent π interactions for catalyst design. *Nature* **2017**, *543*, 637–646.

[107] (a) Hoque, M. E.; Bisht, R.; Haldar, C.; Chattopadhyay, B. Noncovalent interactions in Ir-catalyzed C–H activation: L-shaped ligand for *para*-selective borylation of aromatic esters. *J. Am. Chem. Soc.* **2017**, *139*, 7745–7748; b) Das, S.; Incarvito, C. D.; Crabtree, R. H.; Brudvig, G. W. Molecular recognition in the selective oxygenation of saturated C–H bonds by a dimanganese catalyst. *Science* **2006**, *312*, 1941–1943; (c) Goswami, N.; Sinha, S. K.; Mondal, P.; Adhya, S.; Datta, A.; Maiti, D. Distal *meta*-alkenylation of formal amines enabled by catalytic use of hydrogen-bonding anionic ligands. *Chem.* **2023**, *9*, 989–1003; (d) Mondal, A.; Diaz-Ruiz, M.; Deufel, F.; Maseras, F.; van Gemmeren, M. Charge-controlled Pd catalysis enables the *meta*-C–H activation and olefination of arenes. *Chem.* **2023**, *9*, 1004–1016; (e) Li, G.; Yan, Y.; Zhang, P.; Xu, X.; Jin, Z. Palladium-catalyzed *meta*-selective C–H functionalization by noncovalent H-bonding interaction. *ACS Catal.* **2021**, *11*, 10460–10466; (f) Kuninobu, Y.; Ida, H.; Nishi, M.; Kanai, M. A meta-selective C–H borylation directed by a secondary interaction between ligand and substrate. *Nat. Chem.* **2015**, *7*, 712–717; (g) Genov, G. R.; Douthwaite, J. L.; Lahdenpera, A. S. K.; Gibson, D. C.; Phipps, R. J. Enantioselective remote C–H activation directed by a chiral cation. *Science* **2020**, *367*, 1246–1251; (h) Frost, J. R.; Huber, S. M.; Breitenlechner, S.; bannwarth, C.; Bach, T. Enantiotopos-selective C–H oxygenation catalyzed by a supramolecular ruthenium complex. *Angew. Chem., Int. Ed.* **2014**, *54*, 691–695.

[108] Meng, G.; Lam, N. Y. S.; Lucas, E. L.; Saint-Denis, T. G.; Verma, P.; Chekshin, N.; Yu, J.-Q. Achieving site-selectivity for C–H activation processes based on distance and geometry: a carpenter's approach. *J. Am. Chem. Soc.* **2020**, *142*, 10571–10591.

[109] Zhu, R.-Y.; Saint-Denis, T. G.; Shao, Y.; He, J.; Sieber, J. D.; Senanayake, C. H.; Yu, J.-Q. Ligand-enabled Pd(II)-catalyzed bromination and iodination of C(sp^3)–H bonds. *J. Am. Chem. Soc.* **2017**, *139*, 5724–5727

[110] (a) Schoepfer, J.; Jahnke, W.; Berellini, G.; Buonamici, S.; Cotesta, S.; Cowan-Jacob, S. W.; Dodd, S.; Drueckes, P.; Fabbro, D.; Gabriel, T.; Groell, J.-M.; Grotzfeld, R. M.; Hassan, A. Q.; Henry, C.; Iyer, V.; Jones, D.; Lombardo, F.; Loo, A.; Manley, P. W.; Pelle, X.; Rummel, G.; Salem, B.; Warmuth, M.; Wylie, A. A.; Zoller, T.; Marzinzik, A. L.; Furet, P. Discovery of asciminib (ABL001), an allosteric inhibitor of the tyrosine kinase activity of BCR-ABL1. *J. Med. Chem.* **2018**, *61*, 8120–8135; (b) Chiodi, D.; Ishihara, Y. Magic Chloro": profound effects of the chlorine atom in drug discovery. *J. Med. Chem.* **2023**, *66*, 5305–5331.